THESIS

MICROWAVE DIFFRACTION BY CYLINDRICAL OBSTACLES

presented by

A. W. Adey

for the Diploma of the Imperial College of Science and Technology.

August 1954.

ABSTRACT

The work reported in this thesis can conveniently be divided into two parts.

The first deals with the design, operating procedure and major inherent errors of an equipment intended for indoor measurements of the near scattering or diffracting properties of cylindrical obstacles with lateral dimensions comparable with the wavelength. The equipment consists of a parallel-plate region, suitably terminated so as to effectively simulate a region infinite in the plane of the plates. It has been designed to measure amplitude and phase, both in the shadow and on the illuminated side of the cylinders, in the 3 cm. wavelength band.

The usefulness of the instrument has been assessed by making measurements on metal, circular cylinders, whose scattering properties have been well established.

In the second part of the thesis the equipment has been applied to measurements on cylinders of circular, rectangular and square cross-section, the last two for both metal and polystyrene and for two different orientations. Structures consisting of two coaxial cylinders have also been treated.

Calculations have been made for comparison in some of the cases. The circular cylinder has been treated in detail, with respect to the diffraction resonances that occur because of the field's penetration of the cylinder material.

The far fields of the polystyrene, circular cylinder have been discussed for both plane wave and cylindrical wave incidence, and some

of the calculations repeated for comparison purposes for a material with a relative permittivity of 4.

Measurements have been made on several dielectrics, to determine the effect on the scattering of the change in the electrical properties of the material.

Acknowledgements.

The general guidance of Prof. Willis Jackson, F.R.S. and of Mr. J. Brown is gratefully acknowledged, as is the financial assistance of the Dept. of Scientific and Industrial Research.

Thanks are extended to the University of New Brunswick for the award of an Overseas Beaverbrook Scholarship and its extension and to the Canadian Defence Research Board for a subsequent study grant.

The Weissfloch test on the phase shifter was made by Dr. R. E. Collin and the 1.25 cm. spectrometer measurements by Mr. P. Sollom.

CONTENTS.

CHAPTER I.

INTRODUCTION.

The diffracting properties of cylinders have not received the attention given to those of spheres. One reason may have been the difficulty of performing experiments on cylinders in free space which was, until recently, the only technique available. Because of the experimental limitations, the work done has been confined almost exclusively to cylinders of circular cross-section, and the near fields, which would be expected to be the more complex, have been almost completely neglected. The development of microwave techniques has now made it possible to perform experiments on obstacles whose dimensions place them in the interesting transition region between those of optics and quasi-statics.

Interest in the scattering properties of a cylinder has two main practical bases. The far-scattered field gives the usual indication of its interfering or obstructing effect. The near field is of importance in determining the dielectric properties of an array of cylinders, since it determines the nature of the energy coupling between the cylinders. The dispersive properties of an array would be expected to bear some relation to those of the individual elements.

An historical introduction will now be given to indicate the scope of the previous work, as far as it is known to the writer.

A formal solution of the problem of the diffraction of a plane wave by a dielectric cylinder, considered to be infinitely long and of circular cross-section, seems to have been first given by Rayleigh. He

expanded the incident, externally-scattered and internal fields in a series of Bessel functions and solved for the amplitude coefficients of the terms of the series by matching the tangential electric and magnetic fields across the boundary of the cylinder. He dealt with both parallel and perpendicular polarizations. In a later paper he made some numerical calculations, based on the previous solution, for the following cases-

(a) ka in the range 0.4-2.4, where ka= 2π x radius/wavelength.

(b) small cylinders for which the first few terms of the series expansions of the Bessel functions sufficed.

(c) large cylinders whose index of refraction differed so little from that of the external medium that the internal field could be approximated by the incident field.

The solution for the metal cylinder was given by Thomson, but he did not give the complete Bessel function expansion for the incident field.

Seitz derived Rayleigh's solution and made some near-field calculations for small cylinders of copper, platinum and steel. He, also, considered both polarizations.

Ignatowski obtained the solution for dielectric, metal and imperfect metal cylinders, but gave no calculations.

Schaefer and Grossman used the solution for a dielectric cylinder to make calculations for a water cylinder in a glass tube (neglecting the loss of the water and the effect of the glass). Using damped waves of 24-58 cms. wavelength and a cylinder small with respect to the

wavelength they gave experimental results and calculations for the near, shadow fields and tried to explain them on the basis of the natural oscillations of the cylinder.

Zaviska treated multiple scattering by arrays of metal and dielectric cylinders, while attributing the solution in series form to Seitz and Ignatowski. In his final analysis he dealt with only far fields and small cylinders.

Kobayashi-Iwao gave a solution for the scattering of a damped wave by a dielectric cylinder and compared the calculations with the experimental results of Schaefer and Grossman.

None of the continental papers referred to the work of Rayleigh, a circumstance noted by him in his 1918 paper.

Thilo discussed the radiation pressure on a dielectric cylinder.

Lax and Feshbach gave tables of scattering and absorption coefficients.

Tamarkin gave experimental results, taken along a line transverse to the direction of incidence, for far field scattering of an acoustic wave behind a liquid-filled cylinder of polystyrene in water. The cylinder was about 5 external wavelengths in radius.

Papas, using the variational principle of Levine and Schwinger, derived an expression for the scattering cross-section of a metal cylinder of any radius.

Kodis made calculations and measurements on the near field scattering of a cylindrical wave by a metal cylinder of radius comparable

with the wavelength(1.25 cms.). Some measurements were also made on polystyrene cylinders. All the measurements were made transverse to the direction of incidence and at several distances behind the cylinder.

Montroll and Hart gave an approximate solution for scattering by a dielectric cylinder which subjects the incident field to only a small phase shift.

Franz and Depperman explained the fluctuations in the angular distribution of the field scattered by a metal cylinder as due to the interference between the geometrically reflected wave and a surface wave creeping around the cylinder.

Faran made calculations and measurements on the angular distribution of the field scattered by metal cylinders of radii up to approximately a wavelength. The results were discussed in relation to the natural acoustical vibrations of the cylinder. In a later paper he treated the influence of the curvature of the incident wave front on the far field scattered by a metal cylinder.

Miles discussed the field scattered by a small cylinder.

Bezuszka made calculations to check the experimental results of Tamarkin.

Underhill, using free-space methods at 3 cms., made measurements and calculations of the far shadow field of metal cylinders over a range of diameters extending from 1 inch to 3 feet.

Carter presented calculations for the scattering of plane and dipole fields by various configurations of cylinders.

Sinclair discussed the field of a dipole in the presence of a

conducting, elliptic cylinder.

Moullin gave the results of some calculations on scattering by a metal cylinder.

Row treated theoretically and experimentally the scattering of a 3 cm. cylindrical wave by two conducting cylinders, with the cylinder spacing and radius comparable with the wavelength.

Wiles and McLay did measurements and calculations similar to those of Kodis, but in free space and at a wavelength of 3 cms.

On the basis of the above references it would appear that the only previous attempt made to compare theory with experiment for the near field of a dielectric cylinder, under approximately equivalent conditions of calculation and measurement, was that of Schaefer and Grossman and Kobayashi-Iwao. They used damped waves, small cylinders and neglected the water loss.

No work appears to have been done on determining the properties of an array of dielectric cylinders of any cross-section or of metal cylinders for other than circular. Neither have the scattering properties of the individual cylinders of square and rectangular cross-section been measured or calculated.

The work to be described in this thesis was therefore planned to be in the following directions-

(a) to construct equipment for use in the laboratory in studying the near fields of cylindrical obstacles. Interest would be primarily in the shadow fields, and of obstacles with lateral dimensions comparable with the wavelength. The usefulness of the equipment was to be assessed by

studying the fields for the conducting cylinder, since its scattering properties have been well established.

(b) to make calculations and measurements of the near scattering by a polystyrene cylinder, since the material would be fairly easily obtainable, would machine well and have a loss small enough to be neglected in the calculations. Calculations were to be made for the far fields, for comparison, and for a curved wave front as well as a plane to show the conditions under which the plane wave incidence assumption is valid.

(c) to make measurements on other materials, with the view of observing the effect of the constants of the material on the scattering properties. The corresponding calculations would not be possible, because of the lack of tables of Bessel functions of complex argument.

(d) to make calculations and measurements on scattering from coaxial cylinders.

(e) to measure and, where possible, calculate the scattering from metal and dielectric cylinders of square and rectangular cross-section, both because of their being an example of sharp-edge diffraction and because of their possible practical use as elements in an array.

CHAPTER 2.

MEASURING EQUIPMENT AND TECHNIQUE

2.1. Introduction.

The scope of diffraction measurements has long been limited by the necessity of performing them under free space conditions, either in a large, open space or in an enclosed space where unwanted reflections are eliminated as much as possible by careful positioning of apparatus and the use of absorbing materials on the walls, etc.

In addition the calculations, in the case of obstacles with cylindrical symmetry, are based on the assumption that the obstacles are infinitely long. Since, in practice, they are always finite, they must be many wavelengths long if the assumption is to be reasonably valid. The cost of such obstacles, and the difficulty of dimensioning them to the required tolerances, limits one's choice of materials and obstacle cross-section.

As a first attempt toward improvement over the free space methods, Kodis used a single, image plane in his study of scattering by cylinders. Then independently at this Laboratory(by EL-Kharadly) and at Cruft Laboratory(by Row) the parallel-plate technique was developed to make a two-dimensional treatment of the cylindrical-symmetry problems possible. The equipment to be described in detail later was based on the general design outlined in EL-Kharadly's work, which describes a system used to study the properties of artificial dielectrics in the 10 cm.

region by, in the main, amplitude measurements only.

The method involves confining the field from the source between two parallel, metal plates, so that the source and obstacle can be considered infinite in a direction normal to the plates. The electric field is everywhere normal, also. The plate spacing is kept less than a halfwavelength, so that only a TEM wave can propagate between the plates. A region infinite in extent in the plane of the plates is simulated by matching the edge of the finite region to the external space to prevent the presence of standing waves between the plates.

Space requirements are much reduced by the method, interference of the auxiliary apparatus and the operator with the field region is eliminated and the length of obstacle required is only that of the plate spacing. A more systematic measuring programme can be carried out, compared with the usual practice with out-of-doors equipment, where weather conditions usually determine to a great extent the possible working schedule.

The arrangement of the parallel-plate region and the auxiliary equipment, the method of mounting the obstacles in the line, the measuring procedure and the major sources of error are discussed in the following sections.

2.2. Feed System.

Since it was impossible to provide a plane-wave source for the parallel-plate region, two alternatives were available. One was to use a

line source, such as a small horn, and make all the subsequent calculations on the basis of a cylindrical incident wave. The other was to provide a wave front plane over as wide a region as possible and to limit the lateral dimensions of the obstacle to that region, such as by a wide, lens-corrected horn. The former method was adopted at Cruft Laboratory, the latter here.

The primary feed comprised a wave guide section of 1/2" x 1" I.D. terminating at the throat of an H-plane sectoral horn. The latter flared to an aperture of 23 1/2", with an aperture-throat length of 25". The aperture distribution was phase-corrected by a plano-convex lens of polystyrene, of focal length 25" and maximum thickness 4.5".

The top and bottom plates of the horn were of 1/16" brass and screwed to side spacers of 1/4" x 1/2" brass, giving a plate spacing of 1/2". The aperture and throat ends of the horn were provided with 90-degree angles for fastening to the transmission line and feed wave guide respectively. The side walls of the latter were tapered to an edge where they entered the horn throat, to provide a better transition, and were soldered to the side spacers of the horn.

2.3. <u>The parallel-plate region.</u>

The overall length of the transmission line, from the horn to the far termination, was approximately 16 ft. The width was 30". The general features are shown in Plates I and II and in Fig. 2.1.

The line plates were of two general types-

(a) sections of 3/8" x 30" bakelite covered with a

PLATE I. General view of the parallel-plate equipment.

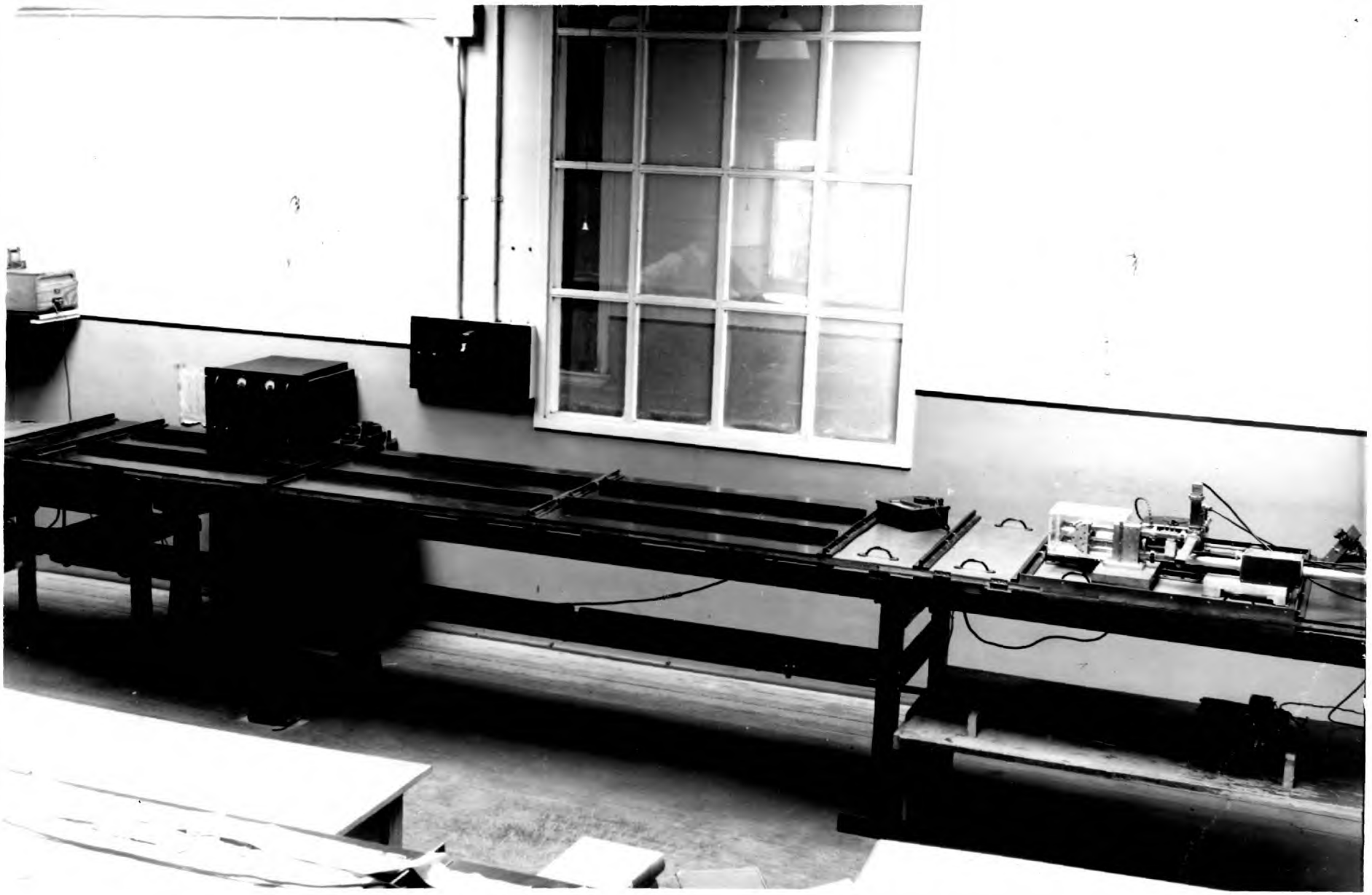

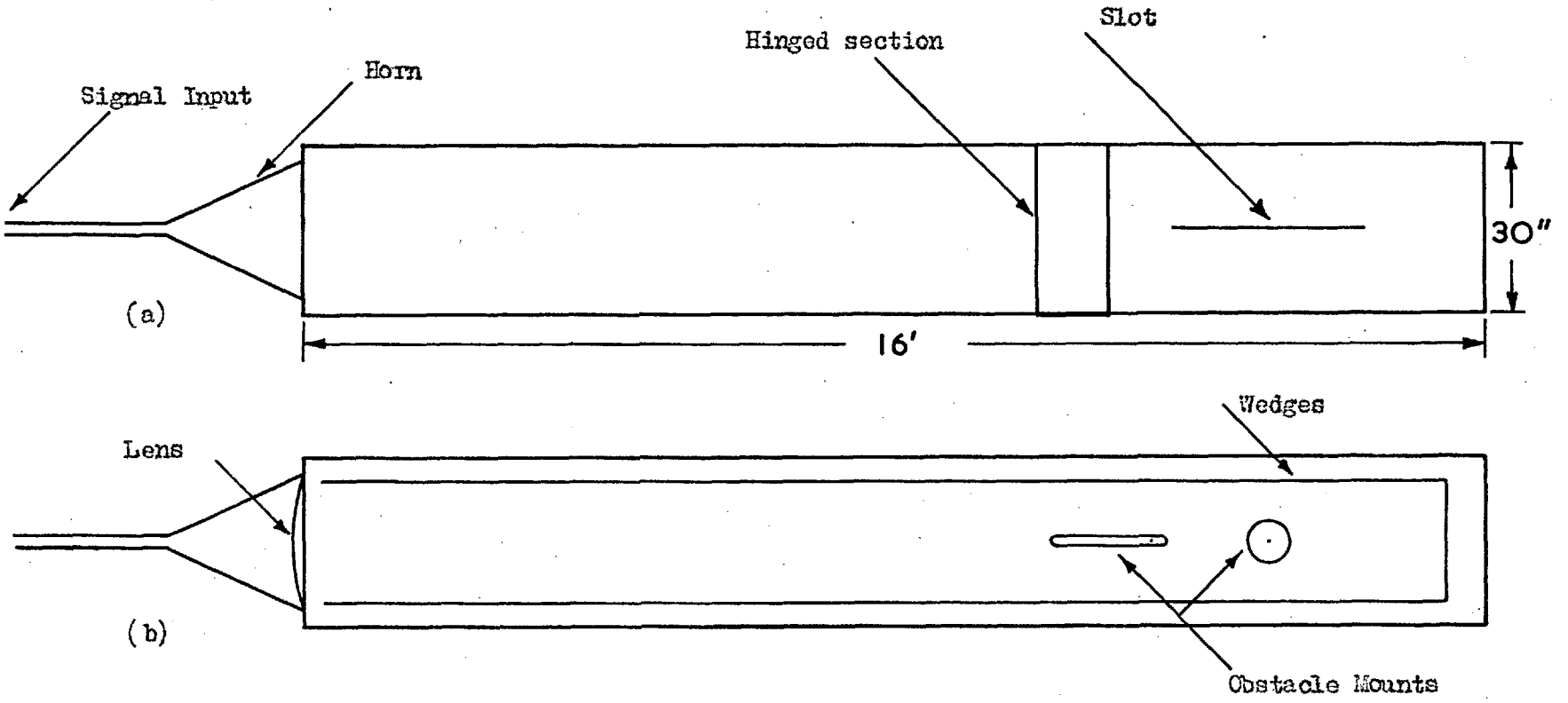

Fig. 2.1. Top view of the parallel-plate region and the feed system. (a) Top plate on. (b) Top plate removed.

PLATE II. View of the measuring end of the parallel-plate equipment, with the hinged and detector plates removed to show the arrangement of the wedges, the obstacle mount and the section angles.

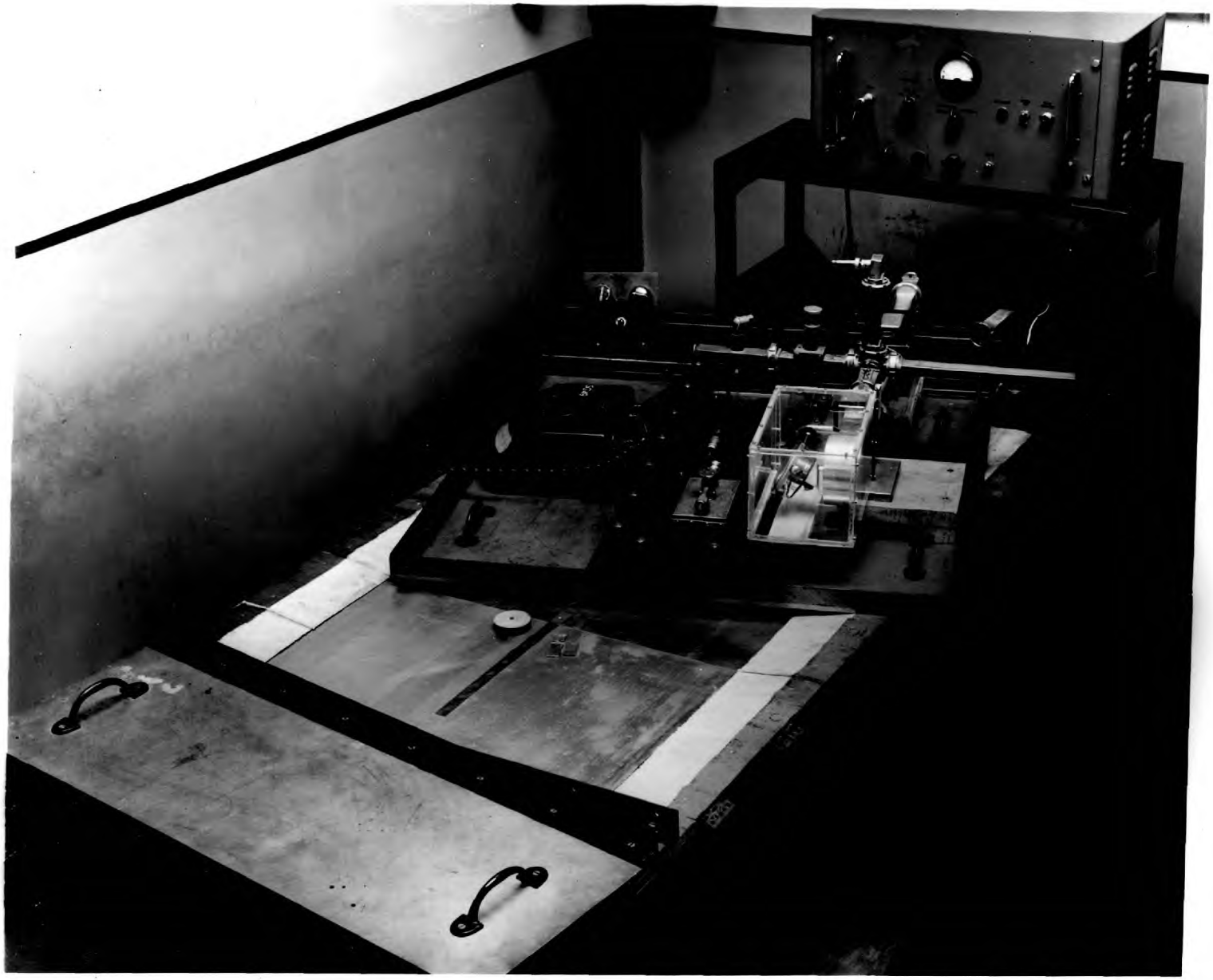

0.001" layer of tinfoil. There were 3- 40" sections and 2- 9 1/2". Each was provided with transverse 1" x 1" angles for fastening together and , in addition, each 40" section was ribbed with 2- 1" x 1 1/4" channel pieces to give them extra rigidity. The tinfoil was applied by first coating the cleaned bakelite with a thin film of a hot solution of vaseline in carbontetrachloride, allowing the latter about a half-hour to evaporate, and then pressing on the foil. The ends of the foil were extended over the edge of the angles and were clamped between the sections.

The ends of each section were machined parallel to each other after the angles had been screwed on.

(b) three brass sections, with angles as for the bakelite. Two were 1/4" x 30" x 11 3/4" long while the third, which was to serve as a combined detector and obstacle section, was of 3/8" brass and 30" square. The plates of the third section had angles on all four sides and the bottom plate had extra ribbing of the same angle material. The top plate was slotted 1/16" x 21" along a center line and was backed by a ribbing of 2" x 1" channel. The inside surfaces of the detector section and the top surface adjacent to the slot were machined flat. All the brass sections were fitted with lifting handles.

The top and bottom plates were separated, and the parallel-plate region terminated, by wooden wedges coated on their top and bottom surfaces with Aquadag(colloidal carbon). The side wedges were of oak, nominally 1/2" thick, and in pieces 7" wide. They were cut with a flat

top of 1 1/2" and a taper of 4" and gave a VSWR of less than 1.03. The end wedge was of teak, flat for 2" and tapered for 5". Its VSWR was less than 1.02.

To confine the propagating mode to the ~~lowest, or~~ TE AND TEM, the plate spacing was kept less than a half wavelength. Some drying-out of the wedges took place after the line was assembled, a later check showing a spacing of 0.480" plus or minus 0.010". At this spacing and a source wavelength of 3.275 cms., the attenuation constant for the next-highest mode was 48.9 db. per wavelength, or a reduction by a factor of about 280 per wavelength.

The choice of the width of the plates had to be governed by economy as well as by the signal available. A wider aperture would have resulted in a higher signal level at the center of the line, but necessitated an increase in the length, as will be seen.

The length had to be made sufficient to ensure a reasonable behaviour of the axial distribution of the electric field. At short distances from the aperture the field amplitude oscillates with distance along the central normal, the oscillations tending to disappear as the Fresnel region is traversed, i.e., as the number of Fresnel zones, as seen at the field point and covered by the aperture, decreases. The behaviour can be illustrated by the following spiral diagram(Fig. 2.2)-

Fig. 2.2

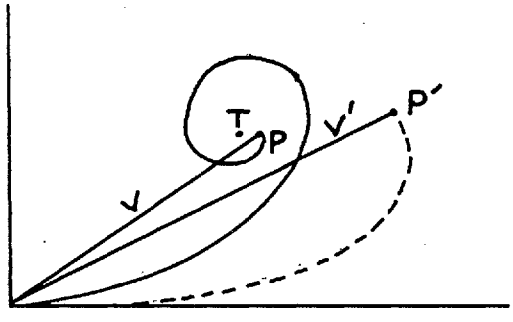

Near the aperture the terminal of the total-field vector V lies on an inner curl of the spiral. As the observation point is moved away from the aperture, P moves out along the spiral and T downward to the right. The last minimum has been passed when the aperture covers only one Fresnel zone at the field point, i.e., when the contribution from the aperture edge lags that from the center by 180 degrees.

In the present case it was anticipated that a length of line sufficient to produce an angle of approximately 120 degrees(point P') would serve as a starting point in the design. For the aperture in question this gave a line length(to the obstacle and measuring region) of approximately 13 1/2 feet.

This aperture-distance relationship corresponded to that for the equipment used by Sterns and Hamren. For their case a 30" paraboloid at a wavelength of 3.20 cms. gave an almost-flat amplitude distribution in the region of 120-180 wavelengths.

2.4. Signal source and auxiliary equipment.

The general layout of the circuit is shown in Fig. 2.3. The signal source was a CV-129 reflex klystron, operating at a wavelength of 3.275 cms., with an output of approximately 100 mw. It was supplied with power from a BTH Type 698 electronically-stabilized unit, with square-wave modulation available at 2500 cps. The unit itself was fed by way of a constant-voltage transformer which gave an additional correction to the supply-voltage fluctuations of approximately 40:1.

LEGEND FOR FIG. 2.3. OPPOSITE.

A	Selective amplifier	P	Padding attenuator
C	Crystal rectifier	PA	Probe assembly
DC	Directional coupler	PP	Parallel-plate region
F	Flap attenuator	PS	Phase shifter
HL	Horn and lens	PU	Power unit
I	To indicator	R	Rotary attenuator
K	CV-129 klystron	S	Tuning screws
M	Magic T	T	Line termination
		W	Wavemeter

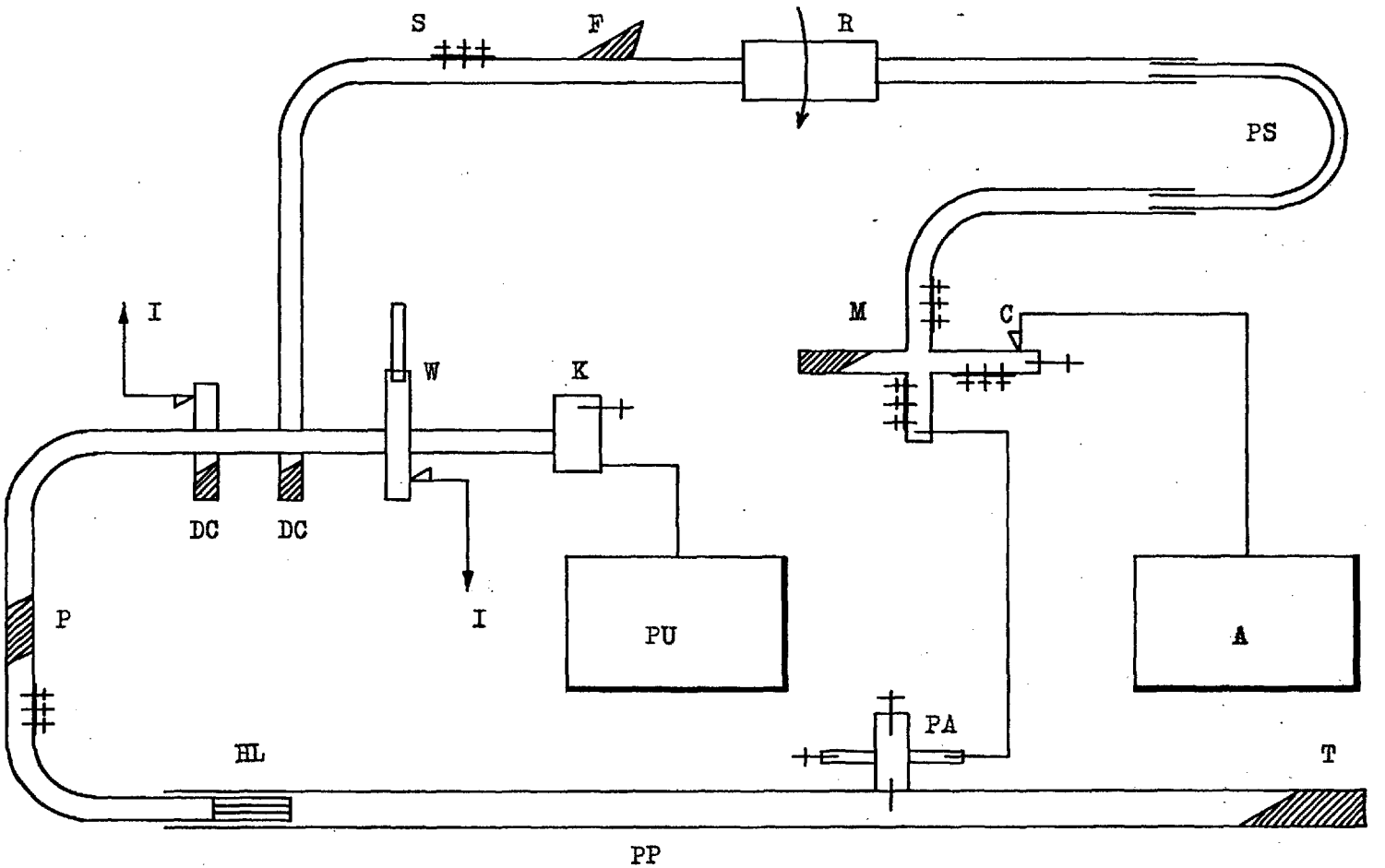

Fig. 2.3. Schematic layout of the parallel-plate region and associated equipment. The legend is given on the opposite page.

A small blower provided cooling for the klystron.

The signal was carried by standard 1" x 1/2" I.D. X-band wave guide to a directional coupler based on the cruciform design by Brewitt-Taylor and with an attenuation of 21 db. The main signal was then led by way of a padding attenuator and a screw-type tuning section to the sectoral horn.

The -21 db signal from the directional coupler- to be used as a reference signal for the phase measurements- was fed by wave guide to the far, or operating end of the line. It passed through a flap attenuator, a rotary attenuator, a phase shifter and finally another screw-tuner section to the H-arm of a Magic T. The E-arm of the T was terminated in a commercial wave guide to coaxial line transformer with tuning screws. The two side arms of the T were terminated in a matched load and a tunable crystal holder respectively. The output of the crystal, a BTH coaxial Type CV-2226, fed an amplifier-detector tuned to the 2500 cps modulation frequency. The amplifier, with its self-contained, electronically-stabilized power supply, had a gain of 140 db and was fed, as was the klystron supply, through a constant-voltage transformer. One end of a 41" length of coaxial cable terminated at the E-arm of the T, the other at a modified BTH 3 cm. probe assembly situated at the slot of the line detector section.

Frequency was monitored by a BTH Type No. 2 cavity wavemeter and power by a -21 db signal taken off the main wave guide run by a directional coupler similar to the one already described.

2.5. Probe assembly.

The probe assembly was based on a BTH design. It incorporated a probe-depth adjustment and a short-circuit plunger. The termination was modified to take either (a) a BTH Type 2226 coaxial crystal and a Belling Lee terminal or (b) a microwave terminal on the coaxial line leading from the E-arm of the Magic T.

The assembly was mounted on a 3" x 5" x 11/16" cast iron base block with a 1/16" x 3/8" x 2" tongue penetrating into the detector plate slot. The probe, of 0.007" copper, penetrated the tongue through a 0.013" hole in a polystyrene insulating sleeve pressed into a 0.055" hole in the tongue. A probe-depth range of approximately 3/16" was available. Felt wipers on each end of the base block served to protect the sliding surfaces.

2.6. Phase shifter.

The phase shifter was of the trombone type(Plate III) and was based on the circumstance that one type of X-band wave guide(0.4" x 0.9" I.D.) can, with very little manipulation of the surfaces, be made to slide smoothly in the other type(0.5" x 1.0" I.D.). The slide portion was in three parts. Two were 4" long pieces of the smaller wave guide with mounting brackets fitted to one end. The third was a U-shaped section of duralumin. It comprised two pieces, each milled with a semi-circular slot 0.4" x 0.45" with a radius of approximately 3 inches. When screwed together the two pieces formed a semi-circular piece of 0.4" x 0.9" wave guide, to

PLATE III. The phase shifter with the slide extended to show the matching steps between the two wave guide sizes.


0
10
20
30
40
50
60
70
80
90
MERCER
.01 M/M

which the 4" sections were screwed.

To match the wave guide sizes, quarter-wave steps were cut in the free end of the 4" sections of smaller guide.

The movement was controlled by a screw mechanism with a pitch of 1 mm., and the slide position indicated on a dial gauge graduated in 0.01 mm.

A thin film of vaseline on the sliding surfaces made the movement lighter and a Perspex(Lucite) housing protected them from dust and thus abrasion.

This type of phase shifter has the advantage that the total phase shift is double that corresponding to the slide movement.

2.7. Rotary attenuator.

A major problem in phase measurements is that of controlling the amplitude of the reference signal without at the same time changing its phase. The piston attenuator is sometimes used, but involves a large insertion loss- usually of the order of 25 db- if it is to operate in its constant-phase range. The phase shifter and attenuator combination using a travelling probe in a matched wave guide section, and a resonant wave guide section, respectively, is perhaps the least expensive, but involves a high loss due to the extra cables and connections required.

For this work the rotary attenuator was used(Elliott, Type B-204). The theory of its operation is given by Southworth and by Hand. It had an insertion loss of less than 1 db, a theoretically-constant phase shift with setting and a VSWR of less than 1.03.

2.8. Obstacle holders.

For all the shadow-field measurements the obstacles were inserted into the line from above. The two line sections preceding the detector section were of brass. The top plate of the section adjacent to the latter was hinged to its bottom partner at one end. It is shown unhinged in Plate II, and moved from its normally-closed position, to show the details of the line interior. The angle holes for connecting it to its neighbours were reamed and fitted with machined pins, rather than with ordinary screws, so that when closed its inner surface presented a minimum discontinuity with that of the adjacent plates. The bottom plate of the hinged section had been previously fastened to the corresponding plate of the detector section and a slot 3/32" deep x 5/8" wide x 12" long milled in the combination, extending for 5" into the detector section. This slot was then fitted with milled brass strips.

On each obstacle a short projection was machined(Plate IV) to permit locating and orientation in the line. For the circular cylinder it was 3/16" in diameter and, for the squares and rectangles, 0.200" square. There was a corresponding strip to be used for each measurement(as shown in the same Plate IV) so that, in the case of the squares and rectangles, either normal or diagonal incidence could be employed.

Inserting an obstacle then involved unpinning and raising the top hinged plate, placing the obstacle on the appropriate strip, which was then placed in the slot, sliding the combination into the detector section and finally, filling the remainder of the slot with the strips.

The hinged plate was then closed.

The obstacle was always located about 4" inside the detector section and was machined slightly long so that a positive contact would be produced between the cylinder and the plates.

The position of the locating recesses in the strips, relative to the far end of the line, was known to 0.001".

Toward the end of the programme the modification shown in Plate V was made to the bottom detector plate to enable measurements to be repeated for some of the obstacles in their standing-wave region. A 6" diameter hole was cut in the plate and a cover-plate provided, with 3/8" shoulders on the cover-plate and on the rim of the hole to ensure the cover's fitting flush with the inner surface of the main plate. The relative depths of the two rims were adjusted so as to protect the sharp edge of the cover-plate's upper surface when inserting it in the hole. Three wing clamps with thumb screws kept the plate in position during a measurement. To enable the cover-plate to be inserted smoothly, a gap of approximately 0.002" was left between it and the rim.

A shallow 3/16" hole was drilled in the center of the upper surface of the cover-plate to permit the circular cylinders to be located(these were the only ones measured). The method of inserting the cylinders in the line is obvious in this case.

The two strips seen fastened to the rim, and placed at 90 degrees relative to each other, were provided to avoid the inconvenience of removing the plate again if it had been found possible at a later

PLATE IV. Obstacles typical of the three cross-sections studied. The corresponding recessed strips for locating and orienting the obstacles are also shown.

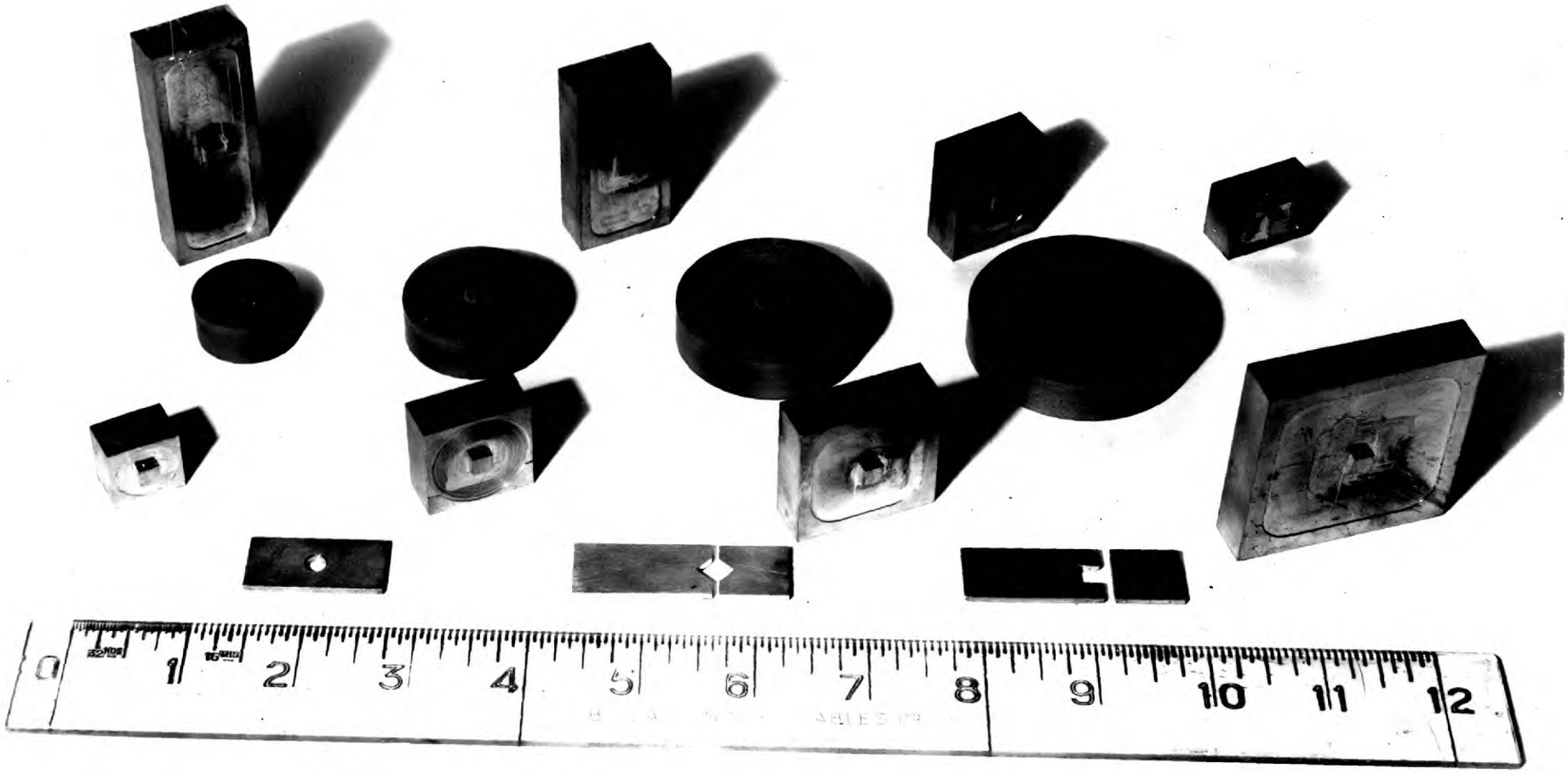
0
1
2
3
4
5
6
7
8
9
10
11
12

date to repeat some of the rectangle measurements. The corresponding strip on the cover-plate permitted repeating some of the circular cylinder measurements for two mutually-normal orientations of the cover-plate, to determine the effect of the discontinuity of the inner surface.

2.9. Line field distribution.

The transverse field distribution for the empty line in the measuring region is given in Fig. 2.4. While it is far from plane, it is flatter in phase than would have obtained with a line source. One was still safe in the assumption of plane wave excitation for the obstacle, however, since, for the largest measured, the maximum phase deviation was less than 1 degree and the amplitude variation less than 1 percent.

The transverse field was measured by turning the detector section so that the slot was normal to the line axis. Hence the reason for the square section and the angles on all four sides. A centimeter scale and associated vernier of 0.1 mm. were used to locate the position of the probe carriage. To avoid slot radiation during the measurement, brass strips were machined to fit into the slot flush with the under side and to extend under the detector base plate to the end of the tongue. They were cut to various lengths so that, as the probe carriage was moved across the line, they could be transferred from one side to the other and so keep the slot filled.

The mean value of the axial field distribution was constant to within plus or minus 1/2 percent over the obstacle and measuring region,

PLATE V. Arrangement of the hole and cover-plate in the detector section for standing-wave measurements.

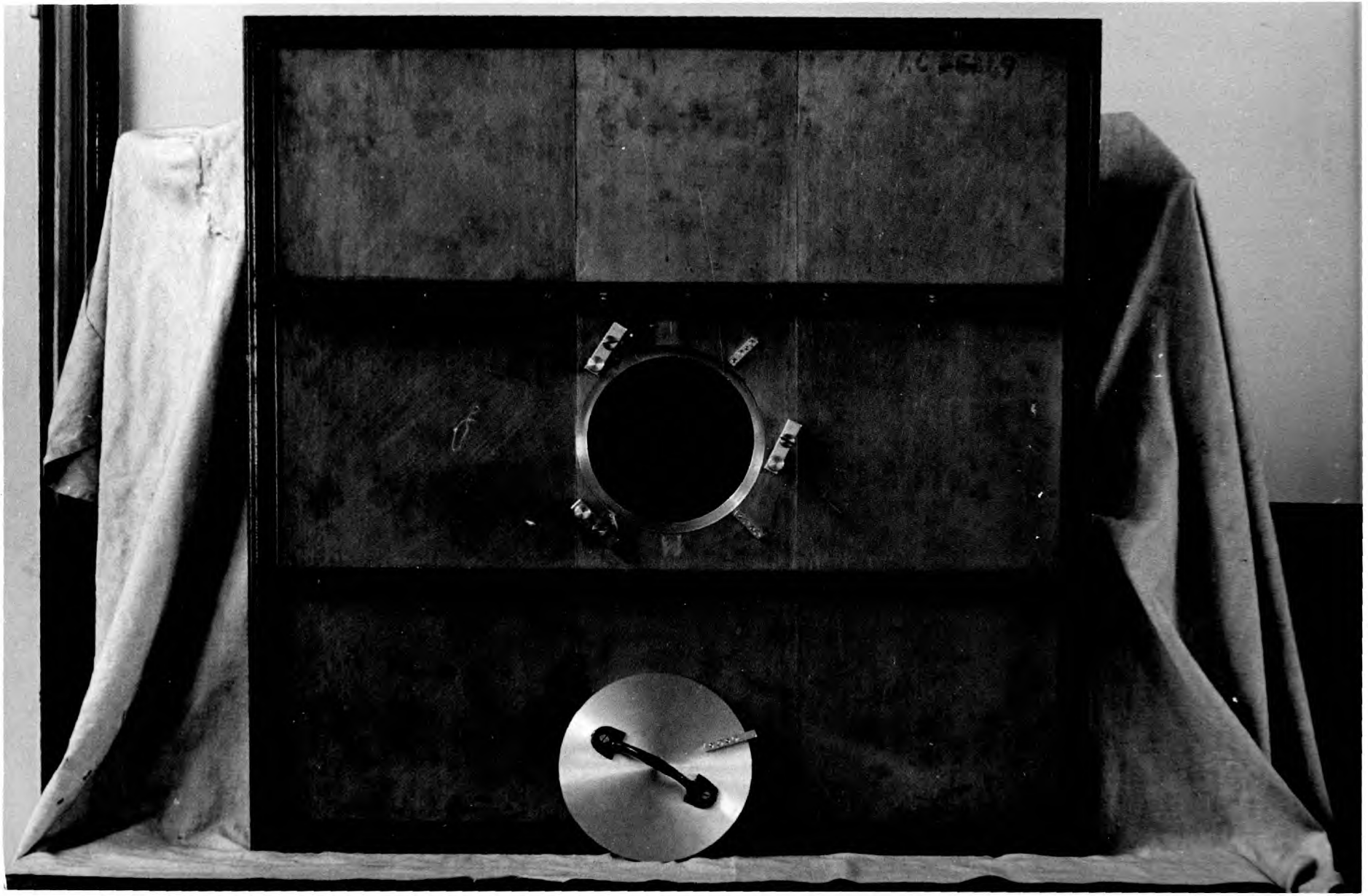

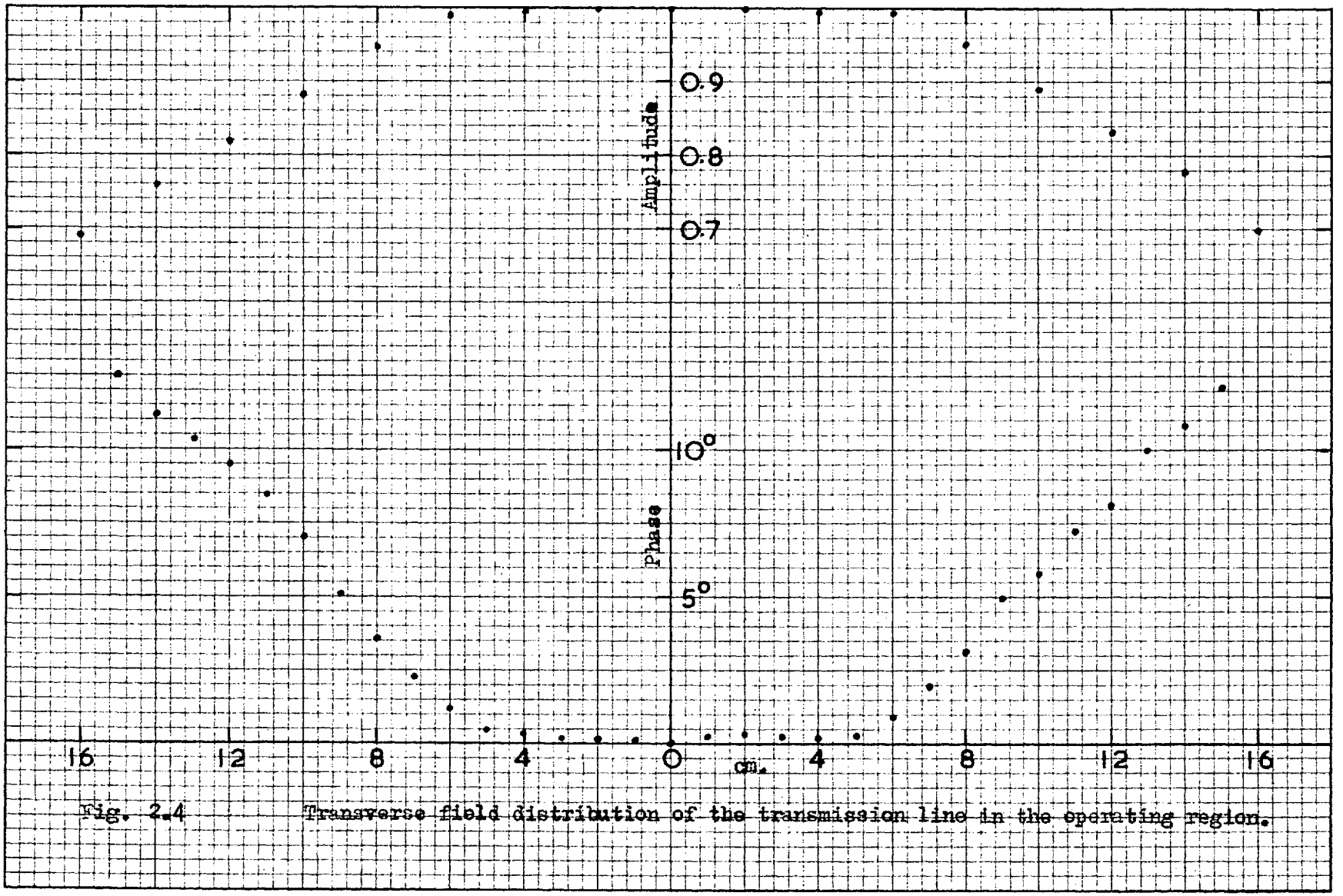

Fig. 2.4 Transverse field distribution of the transmission line in the operating region.

with the exception of a 4 cm. region at one end of the slot, where there was an increase of approximately 5 percent. The increase appeared to be too abrupt to be a Fresnel phenomenon, so it was considered to be due to either a resonance condition between the carriage tongue and the end of the slot or to a variation in the penetration of the probe. Closing a short section of the slot with a metal strip did not cause the field pattern to move down the slot a corresponding amount, so the first suggestion was ruled out. With respect to the other possible cause, on the basis of the crystal's current being proportional to the square of the probe penetration(Barlow and Cullen, p. 139) the increase in current could be accounted for by an increase in penetration of the order of 0.003". If such a change in penetration were responsible, it could be allowed for in the measurements by normalizing, at each probe position, the total field with an obstacle in the line to the incident field. This was done in the initial measurements on the metal cylinders and the difference between the measured and calculated fields appeared to justify it. Later it was found possible to measure the thickness of the detector plate along the slotted region and a decrease of the assumed value was found in the region in question. That normalizing procedure was therefore followed in all the measurements, since the small fluctuation in the field along the remainder of the measuring region could have been accounted for by variations in the plate thickness well within the tolerance possible in machining such a large surface on both sides.

Reflections from the terminating wedge produced a small standing-

wave on the main distribution. This was equivalent to a VSWR of less than 1.02 and had to be absorbed in the normalizing.

2.10. Line wavelength.

A short-circuit method was used to determine the line wavelength. To achieve greater accuracy a 0.01 mm. dial gauge as indicator was fitted to the probe carriage. The distance between adjacent minima was determined along the major part of the slot length and the average taken. The result was a value of 3.280 cm., with a scatter of approximately plus or minus 1/6 percent. Later the value was again found by using the phase shifter and the matched termination. The probe was moved a definite distance along the slot and the phase shift between the points determined. Again the result was 3.280 cm., with a scatter of plus or minus 1/4 percent. The absence of a systematic variation in the wavelength along the slot was evidenced by the results of repeating the measurement several times in both cases.

The low level of attenuation due to the finite conductivity of the plates and the tinfoil was shown during the above measurement by the absence of a tendency for the amplitude of the field at the minima positions(in this case not detectable) to rise as the probe was moved down the slot toward the short-circuiting plate.

2.11. Probe position calibration.

The probe position(for the vernier at zero on the accompanying scale) with respect to the obstacle mount was then determined by the

standard short-circuit procedure used in wave guide measurements(Barlow and Cullen, p. 125). The accuracy with which this could be found depended, of course, on the previous determination of the line wavelength. Again the initial obstacle measurements were depended on to reveal a possible discrepancy. The later measurements in the standing-wave region would have been more sensitive to an error in the wavelength than would those in the shadow, because of the more-rapid changes in the field amplitude. The results indicated that the value previously used could not have been much in error.

2.12. Effect of variation in line spacing.

As stated before the spacing was kept less than a half wavelength, to prevent modes other than the TEM AND TE from propagating. A variation in the spacing can have the effect, however, of changing the propagating wavelength, but it was considered that the magnitude- small with respect to the wavelength- and the spacing- large with respect to the wavelength- of the variations would make the change negligible(Rice).

Another effect of the variation in the spacing is the excitation of transverse and longitudinal components of field. Again, as a short calculation by Row has shown, the rate and the magnitude of the variation occuring here was not sufficient to produce a troublesome effect. Because of the attenuation of higher-mode fields, components excited by variations would not propagate to an appreciable distance, although their excitation could affect the phase distribution of the incident field.

2.13. Phase measurements.

(a) Procedure. Phase was measured by the standard interference method. This involved mixing the signal from the probe- which fed the E-arm of the Magic T- with the reference signal, which fed the H-arm through the rotary attenuator and the phase shifter. The resultant was then fed from a side arm of the T to a BTH Type 2226 crystal rectifier and thence to the amplifier-detector and the output indicator, the last being a 0-1 ma. meter built in the amplifier. The phase shifter and the attenuator were first adjusted to give a minimum signal and the phase shifter then adjusted to bridge this position and give two equal indications on the meter. The minimum position could then be determined more accurately as the average of the two positions(Montgomery, p. 593). The phase shift between different positions of the field probe could then be calculated from the constant of the phase shifter.

From the phase shifter readings with no cylinder in the line and those with it in, the phase shift due to the cylinder could be determined.

(b) Line equalization. If the phase bridge is adjusted for a minimum signal and the frequency then changed, the bridge has to be rebalanced, since the propagation constants of the several system components are not, in general, identical. To minimize this tendency for the phase to drift during measurements as the frequency inevitably fluctuates, the relative lengths of the two lines feeding the bridge can be adjusted to make the drift a second-order effect. The procedure(Montgomery, p.917) is to write an expression for the difference between the two electrical

lengths, taking into consideration the different propagation constants of the various components. One then equates to zero the first derivative of this difference with respect to the free space wavelength, and obtains a relation involving the relative lengths of the various components. Most of these lengths will be fixed by the nature of the equipment. A conveniently-adjustable one is chosen from among the remainder and values assigned to the lengths of all the other components in the system. The length of the one in question is then determined to satisfy the condition previously obtained. In the present case the length of the coaxial cable feeding the signal to the E-arm of the Magic T was adjusted to be 41". The transmission line length was taken with respect to the mid-point of the probe travel, as a compromise.

(c) Major sources of error. (1) One source of error has just been referred to- that of frequency drift. With the lines equalized the drift in phase due to the maximum frequency drift experienced was less than 1/2 degree.

(2) The constant of the phase shifter is determined by the value of the free space wavelength. In this work it was considered to be known to 0.001 cm. This corresponded to an error in the phase constant of approximately 0.05 percent, which was negligible even for the largest angles measured.

The tolerance on the larger dimension of the wave guide also enters into the calculation of the constant. This, also, would lead to a negligible error.

(3) Sharp bends introduced into coaxial cables can cause large phase errors at microwave frequencies. In this work the cable leading from the probe to the T was the only one involved. It was found possible to support it in such a position that the general curvature remained unaltered during a measurement. Deliberately distorting to the degree met in practice did not produce any detectable phase change. In this connection it may be noted that the errors due to bends in the cable are related to the standing-wave conditions on it. The importance of having the cable correctly terminated is therefore obvious.

(4) It has been stated that the attenuator used was chosen to eliminate as much as possible the phase errors due to a change of phase shift through the attenuator with setting. No change of phase could be detected over the range used in the measurements.

(5) It is very important to isolate the reference line from the signal line- with the exception of the necessity of extracting the reference signal. In this equipment the extraction of the signal through a directional coupler and the subsequent mixing in a well-matched Magic T effectively decoupled the two lines.

(6) The probe could be located to within 0.01 cm. by the scale and vernier. This corresponded to a phase uncertainty of approximately 1 degree. There was also a possible error in estimating the distance of the obstacle from the probe.

(7) The constant of the phase shifter was calculated on the basis that there was a pure travelling wave in the reference line.

Actually there was a small standing wave due to reflections from the Magic T and from the discontinuity between the two wave guide sizes. The former was eliminated as much as possible by placing matching screws between the phase shifter and the Magic T. These were adjusted, as were all the tuning sections, by placing the section to be matched in a wave guide bench behind a directional coupler and a standing-wave indicator. The reflected wave was then passed to a crystal rectifier and the output to an amplifier. The matching section was then adjusted for a minimum reflected power. At best this would indicate a match equivalent to the matching of the load on the dead arm of the directional coupler, which in the present case had a VSWR of approximately 1.01.

A previous Weissfloch test(Marcuvitz, p. 132) on the phase shifter indicated a deviation from linearity of phase with movement of approximately plus or minus 0.65 degrees, over a movement of 2.0 cm. The reflection indicated a VSWR of about 1.01 for each step.

A rigorous analysis of the error due to these reflections would be complex, but one can obtain some estimation of its magnitude by assuming a worst condition of all the reflections adding in the reference line. The phase error would then be approximately equal to the reflection coefficient(Barlow and Cullen, p. 24). With a total VSWR of 1.03 the maximum error would be approximately 0.9 degrees.

From the sources of error discussed one would be led to an estimation of a probable error of the order of 2 degrees.

2.14. Amplitude measurements.

(a) Procedure. Since the bridging method was used for the phase measurements, it was not convenient to measure the amplitude and phase simultaneously, as is sometimes done when the null method is used. Since a sensitive crystal rectifier and galvanometer were available and the former was found to have a law with no detectable departure from square, the crystal was used directly at the probe of the line and its output fed to the galvanometer. To change from a phase measurement to an amplitude, therefore, required only the disconnecting of the coaxial cable microwave terminal from the probe assembly and its replacement by the crystal and the output cable. The law of the crystal was checked, in the same circuit in which it was subsequently used, by short-circuiting the line. It was periodically checked, with no detectable change.

The amplitude for each probe position was normalized to the value with no cylinder in the line.

(b) Sources of error. (1) The crystal was checked as discussed above.

(2) For the shadow measurements the error due to the uncertainty of the probe location was not as serious as in the case of the phase measurements, because of the normally-slow variation of the field. In the later standing-wave measurements this was not so, however.

(3) Reading error would depend on the field level being dealt with. It was not serious in the present measurements. It was minimized in the few cases of low-level fields met with by doing the run in two parts, for two probe settings, and matching the results, in a manner similar to that

used in phase measurements when using a variable-phase attenuator. For continuously low level work the amplifier would be used, with the attendant more-frequent and longer calibration checks.

(4) For some of the shadow measurements- involving the larger obstacles- and for all the standing-wave measurements, the obstacle was partially in the slotted region of the line. No detectable error resulted, however, as was shown by comparing results taken with and without metal inserts in the slot over the obstacle surface. The slot in this case was narrow, and deeper than normally found in wave guide practice at this wavelength.

(5) Coupling between the obstacle and the source was negligible, because of the distance involved and the padding attenuator in the feed guide. Reflections from the lens could be neglected, both because of the low level of the scattered field reaching it(a distant obstacle radiating an essentially cylindrical wave) and because of the matching of the feed system.

Two other sources of error common, with the last two, to both the amplitude and the phase measurements, were the effect of uncertainty in the lateral dimensions of the obstacles and that of the presence of the recesses in the strips and the corresponding projections on the obstacles. In the case of the former, the obstacles could be machined very accurately and, in the case of the latter, the absence of a disturbing effect was shown by checking the field distribution in the empty line with the recessed strip in various positions in the slot,

while the field with the obstacle in the line was checked for several lengths of the projection. For the metal obstacles one would not expect the recess and projection to affect the results, because of the boundary conditions involved.

On the basis of the errors considered, a total probable error of 2 or 3 percent in the amplitude measurements seems to be a reasonable estimation.

In the next chapter the initial measurements on the equipment are discussed.

CHAPTER 3.

DIFFRACTION OF A PLANE WAVE BY A METAL CYLINDER.

3.1. To assess the overall usefulness of the diffraction equipment described in the last chapter, it was decided to study the problem of the scattering of a plane wave by a metal cylinder, the solution of which has been sufficiently well established to validate its use for equipment calibration purposes.

The problem can be formulated with reference to Fig. 3.1.

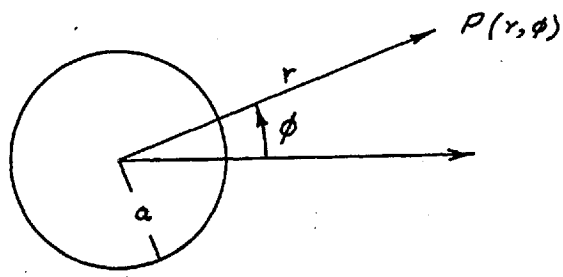

Fig. 3.1.

A plane wave, with the electric vector polarized parallel to the cylinder axis, is incident on the cylinder in the direction $\phi=0$. Since the cylinder is considered to be infinitely long, there will be no field variations in the axial direction and the problem becomes a scalar one, with only an axial component of electric field. Rationalized units will be used and the time factor $\exp(-i\omega t)$ omitted.

If the amplitude of the incident field is taken as unity, for convenience, then-

$$E_{inc}(r,\phi) = \exp(ikr\cos\phi) \qquad (3.1)$$

where k= 2π/wavelength.

By the use of the well-known relation for Bessel functions (McLachlan, p.43), (3.1) can be written as-

$$E_{inc}(r,\phi) = \sum_{o}^{\infty} \varepsilon_n (i)^n J_n(kr) \cos n\phi \qquad (3.2)$$

where $\varepsilon_o = 1$; $\varepsilon_n = 2$, $n \geq 1$, and J_n is the Bessel function of the 1st kind.

The scattered field must be of the form of an outgoing wave at large distances from the cylinder and so can be written as-

$$E_{sc}(r,\phi) = \sum_{o}^{\infty} \varepsilon_n B_n H_n^{(1)}(kr) \cos n\phi \qquad (3.3)$$

where the B_n are to be determined by the boundary conditions at the cylinder surface and the $H_n^{(1)}$ indicate the Bessel function of the third kind or the 1st Hankel function.

The corresponding magnetic fields in the incident and scattered fields can be found from the Maxwell equations-

$$H_\phi(r,\phi) = \frac{i}{\omega\mu} \frac{\partial}{\partial r} E(r,\phi) \quad ; \quad H_r(r,\phi) = \frac{i}{\omega\mu r} \frac{\partial}{\partial \phi} E(r,\phi) \qquad (3.4)$$

where w is the angular frequency and μ the permeability of the external medium. But we will not be interested in these fields, so will not consider them further.

The boundary condition that the tangential electric field(here the total electric field) shall disappear at the cylinder surface, r=a, yields the relation-

$$E_{tot}(a,\phi) = E_{sc}(a,\phi) + E_{inc}(a,\phi) = 0 \qquad (3.5)$$

By substitution in (3.5) from (3.2) and (3.3) there is obtained for each term of the expansion (3.3)-

$$B_n = -(i)^n J_n(ka)/H_n^{(1)}(ka) \qquad (3.6)$$

The scattered field then becomes, from (3.6) and (3.3)-

$$E_{sc}(r,\phi) = -\sum_{o}^{\infty} \varepsilon_m (i)^n \frac{J_m(ka)}{H_n^{(1)}(ka)} H_n^{(1)}(kr)\cos n\phi \qquad (3.7)$$

and the total field, as the sum of (3.2) and (3.7)-

$$E_{tot}(r,\phi) = \sum_{o}^{\infty} \varepsilon_m (i)^m \left(J_n(kr) - \frac{J_n(ka)}{H_n^{(1)}(ka)} H_n^{(1)}(kr) \right) \cos n\phi \qquad (3.8)$$

From (3.7) calculations have been made of the near scattered fields in the forward, backward and side directions for cylinders of ka= 2, 3, 4, 5.97 and 8, corresponding to a radius of 0.319, 0.478, 0.638, 0.950 and 1.274 wavelengths respectively. From (3.8) the corresponding total shadow field has been calculated, while the total field in the illuminated or standing-wave region has been calculated for the first three cylinders. The radius of cylinder that could be treated was limited by (a) the extent of the plane-wave portion of the incident wave front, (b) by difficulties of accurately machining large cylinders and (c) by the number of terms required in the calculations from the series solution (3.8). The first would, of course, only involve the experimental results. With respect to the second, it was found possible to turn the cylinders to a

tolerance of plus or minus 0.002" on the diameter. In the case of (c) the number of terms required is of the same order as ka. The following table indicates the number of terms used in the present calculations-

ka	2	3	4	5.97	8
Terms	6	7	8	11	14

The computations were done on a desk machine, with the help of the Bessel function Tables contained in (a) Vol. VI and X of the British Association Mathematical Tables and (b) the Tables from the Computation Laboratory of Harvard University. The Bessel function recurrence relations and the auxiliary functions from (a) were used in the case of the Y_n for the higher orders and arguments.

The total shadow field for the first 4 cylinders and the corresponding standing-wave fields for the first 3, shown in Fig. 3.2-3.11, give the amplitude and phase, for each value of kr, relative to those at the same point with no scattering cylinder present. They illustrate the deep shadow effect behind a metal cylinder, the shadow deepening with increase of the cylinder radius. The standing wave in front of the cylinder is due to the interference between the incident field and the field scattered back toward the source. The amplitude of the fluctuations decreases with distance from the cylinder, since the incident field is of constant amplitude while the scattered field decreases in amplitude with distance. No such fluctuations appear in the shadow region, however, where the incident and scattered fields(or rather, waves) travel in the same direction, with a phase difference that decreases

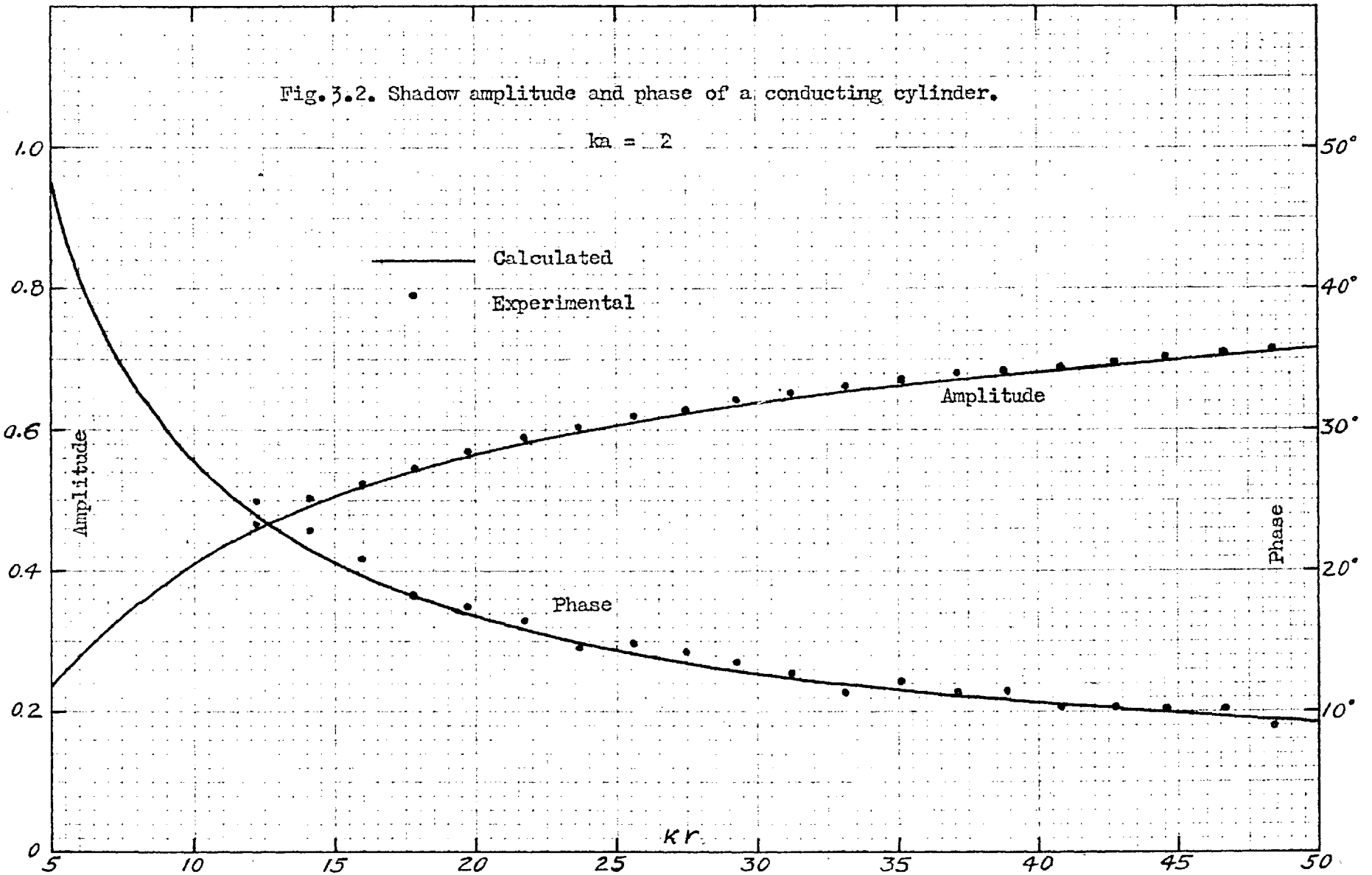

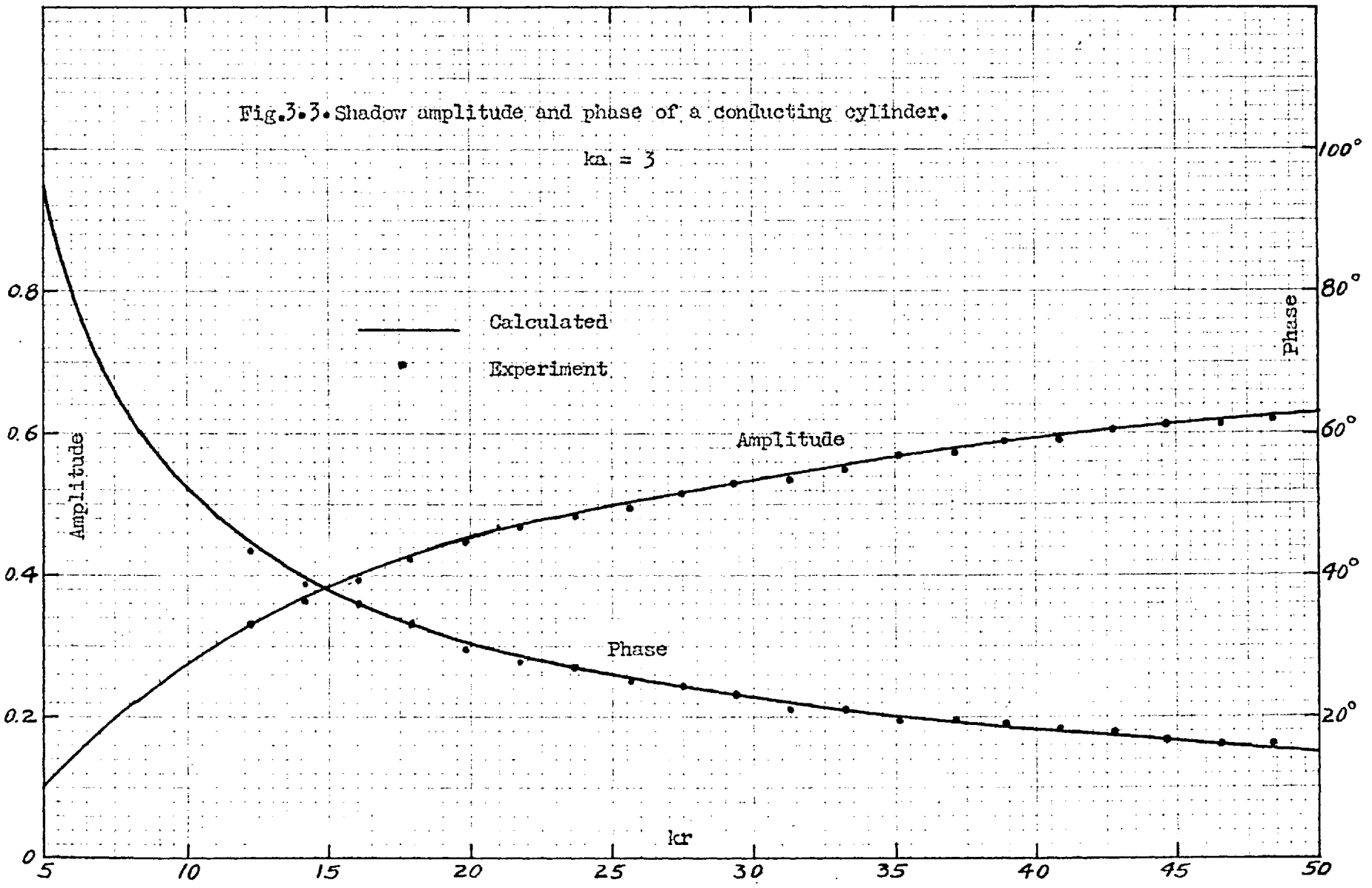

Fig.3.3. Shadow amplitude and phase of a conducting cylinder.

ka = 3

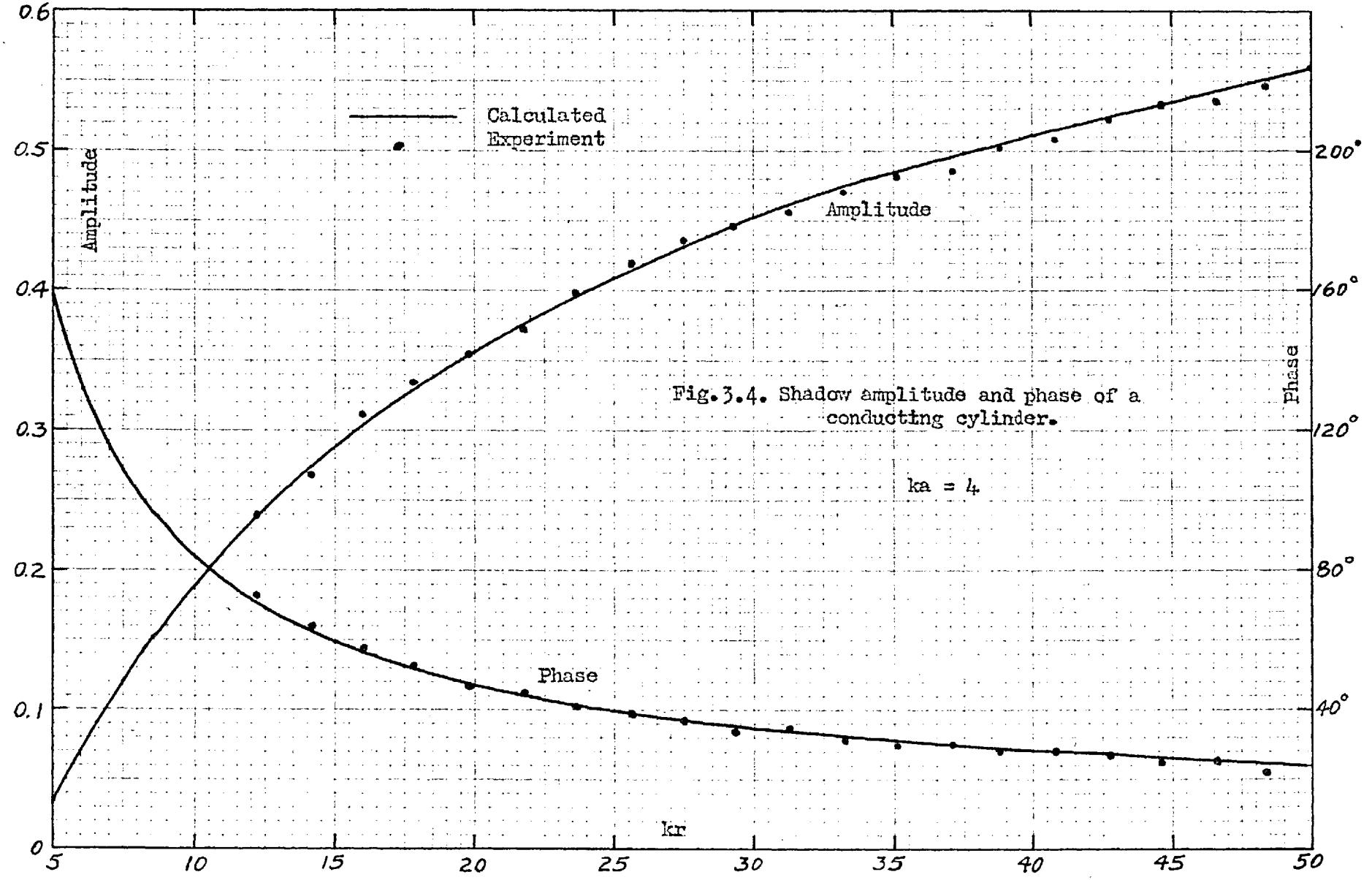

Fig.3.4. Shadow amplitude and phase of a conducting cylinder.

ka = 4

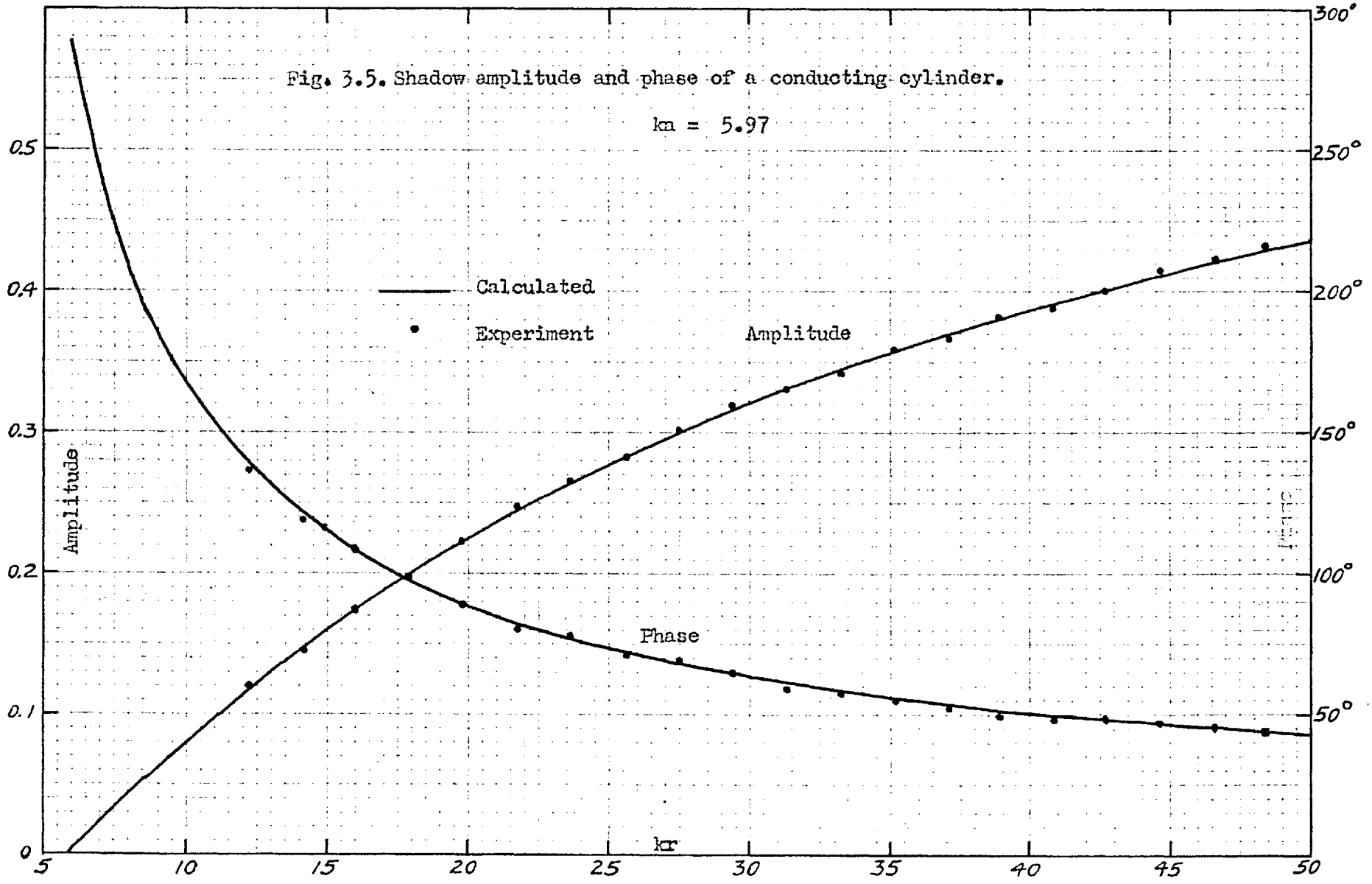

Data Sheet No. 2. 105 Divisions x 45 Divisions

Wightman Mountain Ltd.,
Artillery House, Artillery Row, Westminster, S.W.1

Fig. 3.6.

Field on the illuminated side of a conducting cylinder of ka= 2.

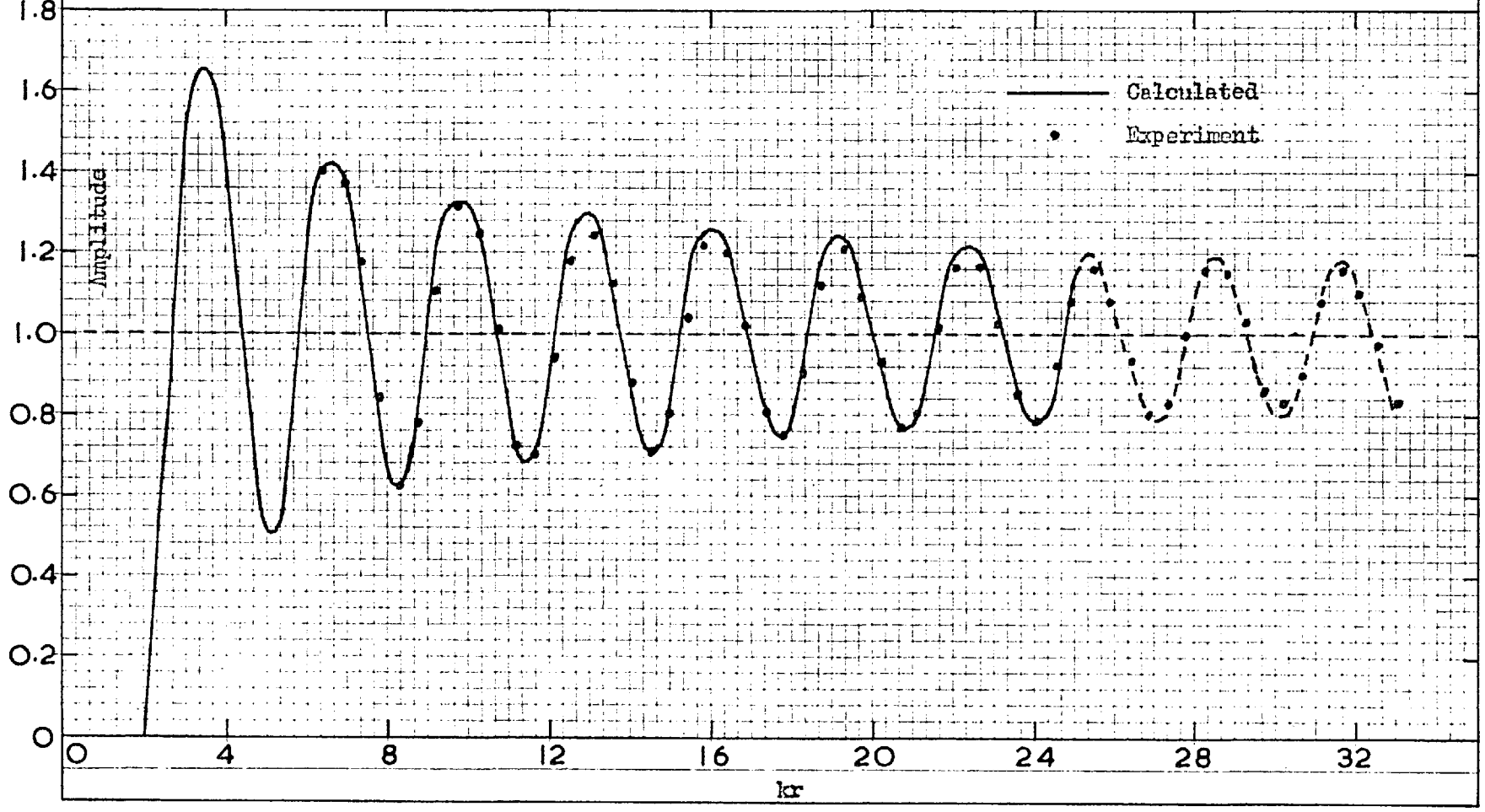

DATA SHEET NO. 2. 105 DIVISIONS × 45 DIVISIONS

WIGHTMAN MOUNTAIN LTD.,
ARTILLERY HOUSE, ARTILLERY ROW, WESTMINSTER, S.W.1

Fig. 3.7.

Amplitude of the field on the illuminated side of a conducting cylinder of ka = 3,

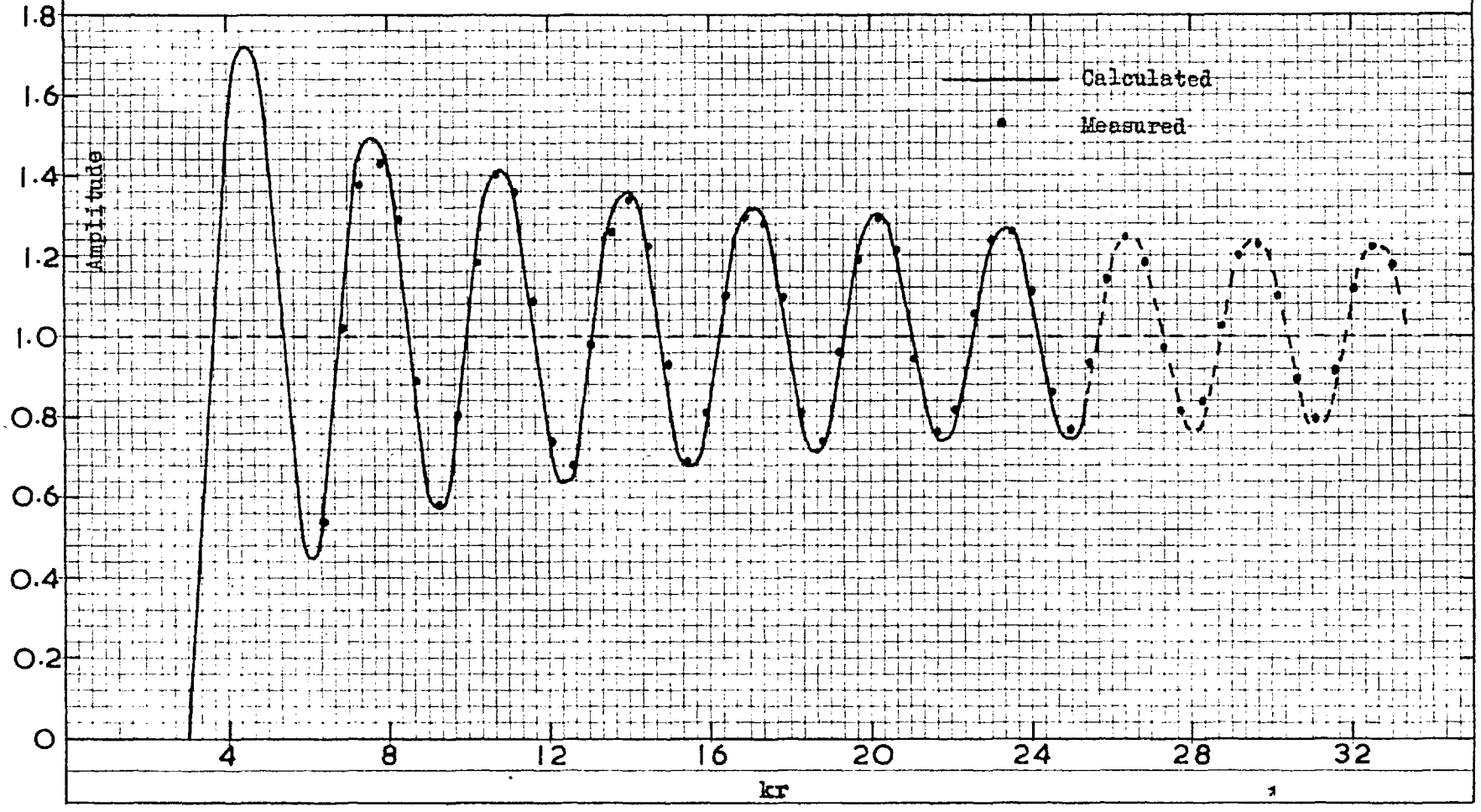

DATA SHEET NO. 2. 105 DIVISIONS × 45 DIVISIONS

WIGHTMAN MOUNTAIN LTD.,
ARTILLERY HOUSE, ARTILLERY ROW, WESTMINSTER, S.W.1

Fig. 3.8.

Amplitude of the field on the illuminated side of a conducting cylinder of ka = 4.

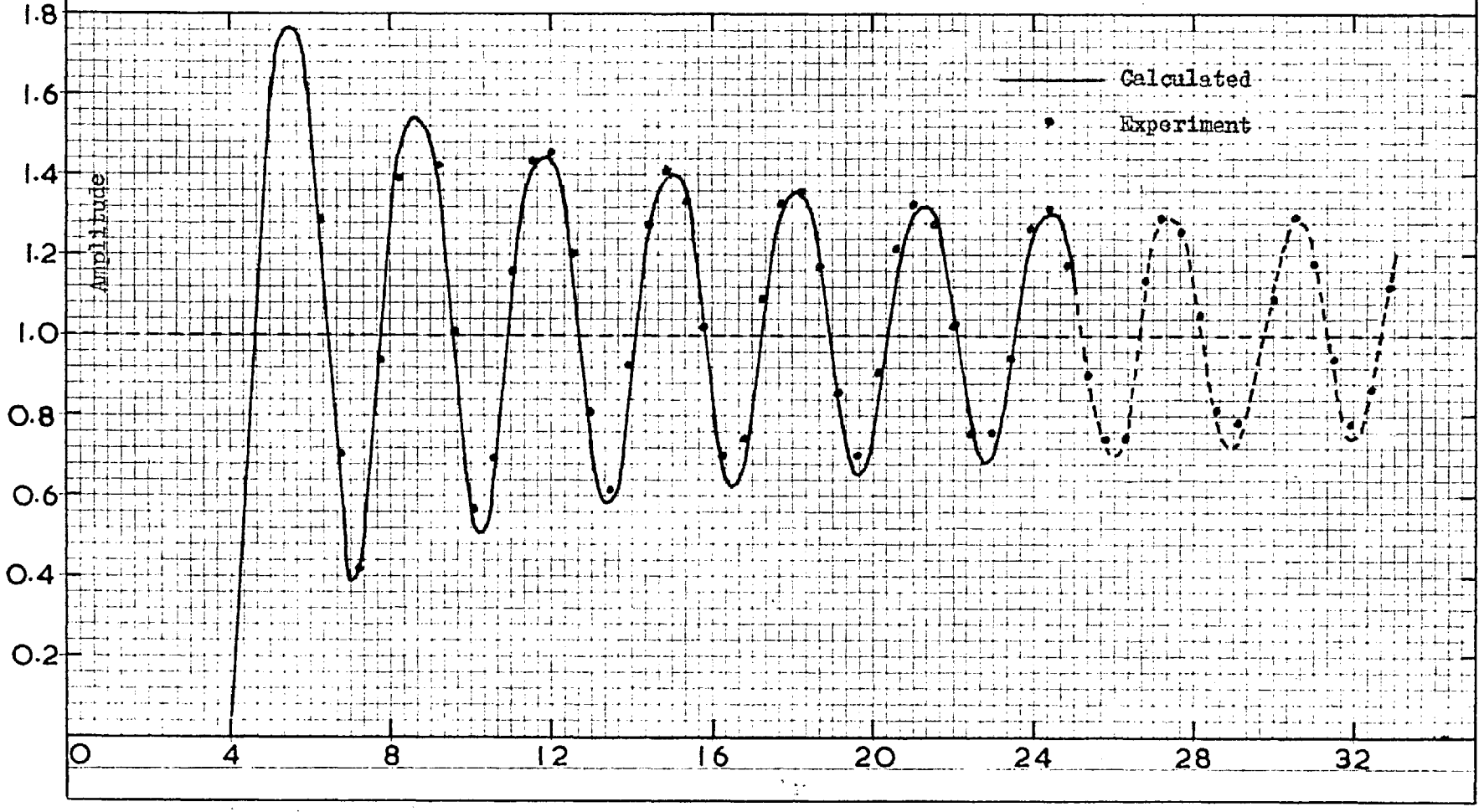

DATA SHEET No. 2. 105 DIVISIONS × 45 DIVISIONS

WIGHTMAN MOUNTAIN LTD.,
ARTILLERY HOUSE, ARTILLERY ROW, WESTMINSTER, S.W.1

Fig. 3.9.

Phase of the field on the illuminated side of a conducting cylinder of ka = 2.

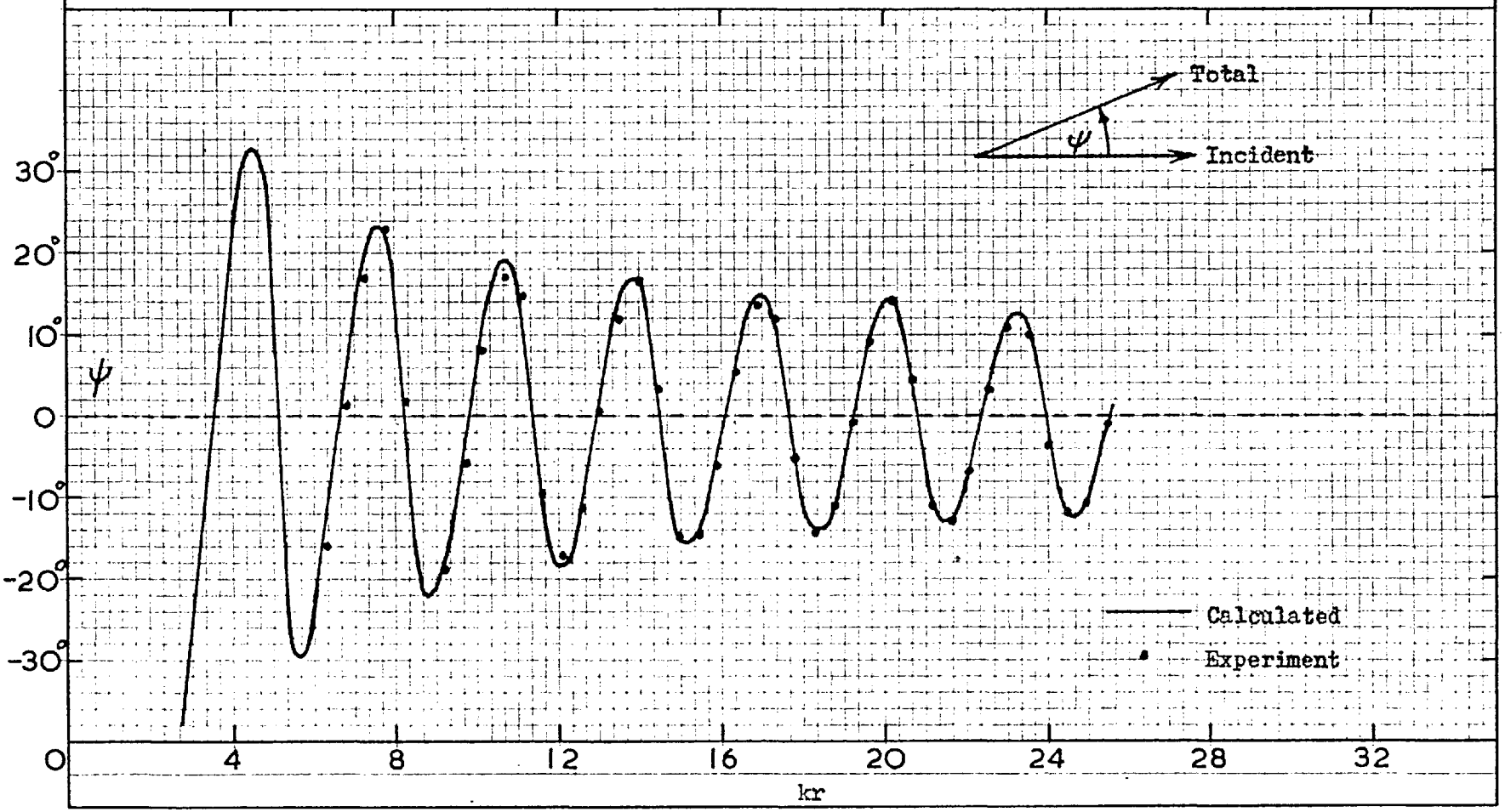

Data Sheet No. 2. 105 Divisions x 45 Divisions

Wightman Mountain Ltd.,
Artillery House, Artillery Row, Westminster, S.W.1

Fig. 3.10.

Phase of the field on the illuminated side of a conducting cylinder of ka = 3.

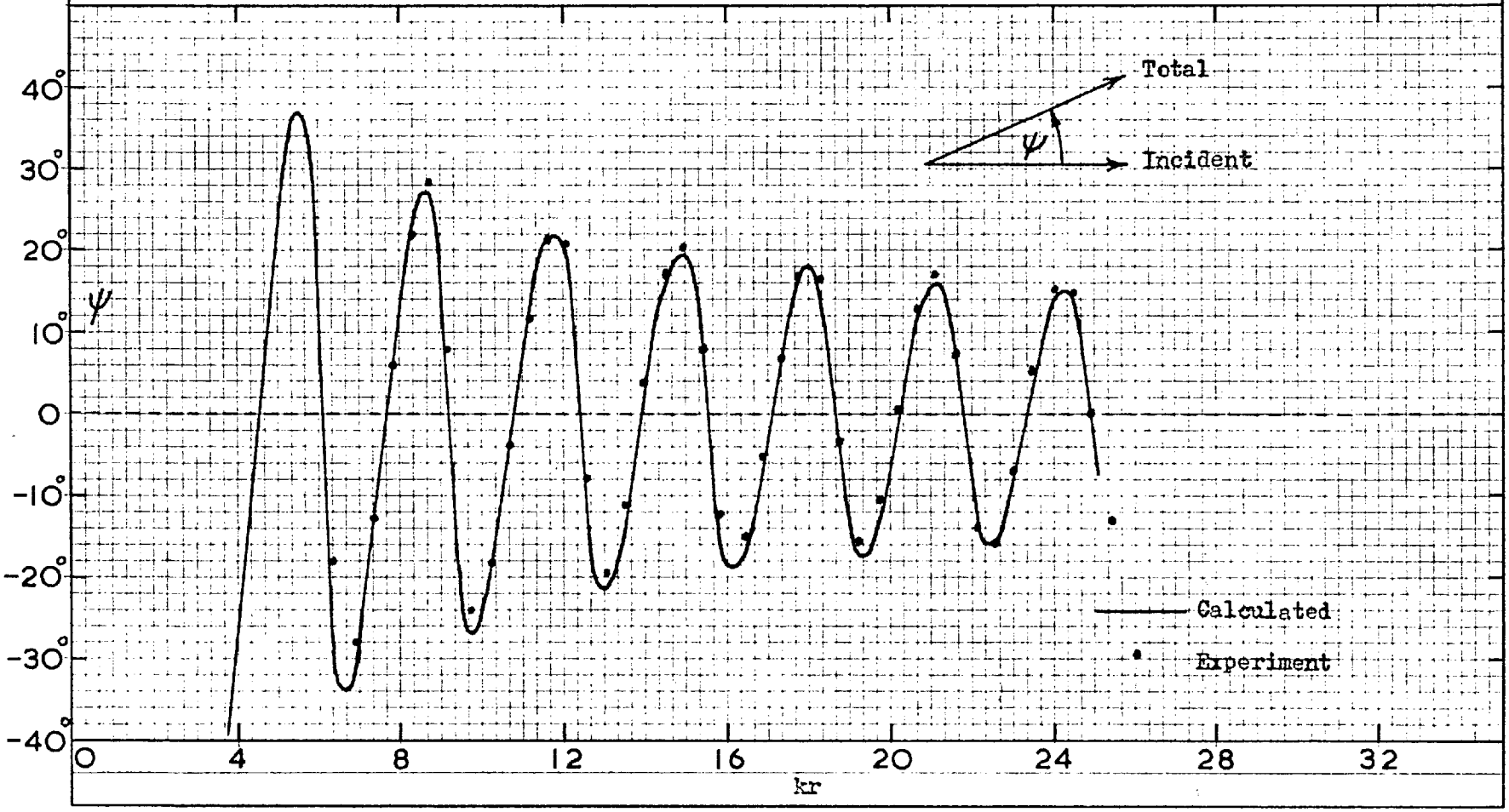

WIGHTMAN MOUNTAIN LTD.,
ARTILLERY HOUSE, ARTILLERY ROW, WESTMINSTER, S.W.1

Fig. 3.11.

Field on the illuminated side of a conducting cylinder of ka= 4.

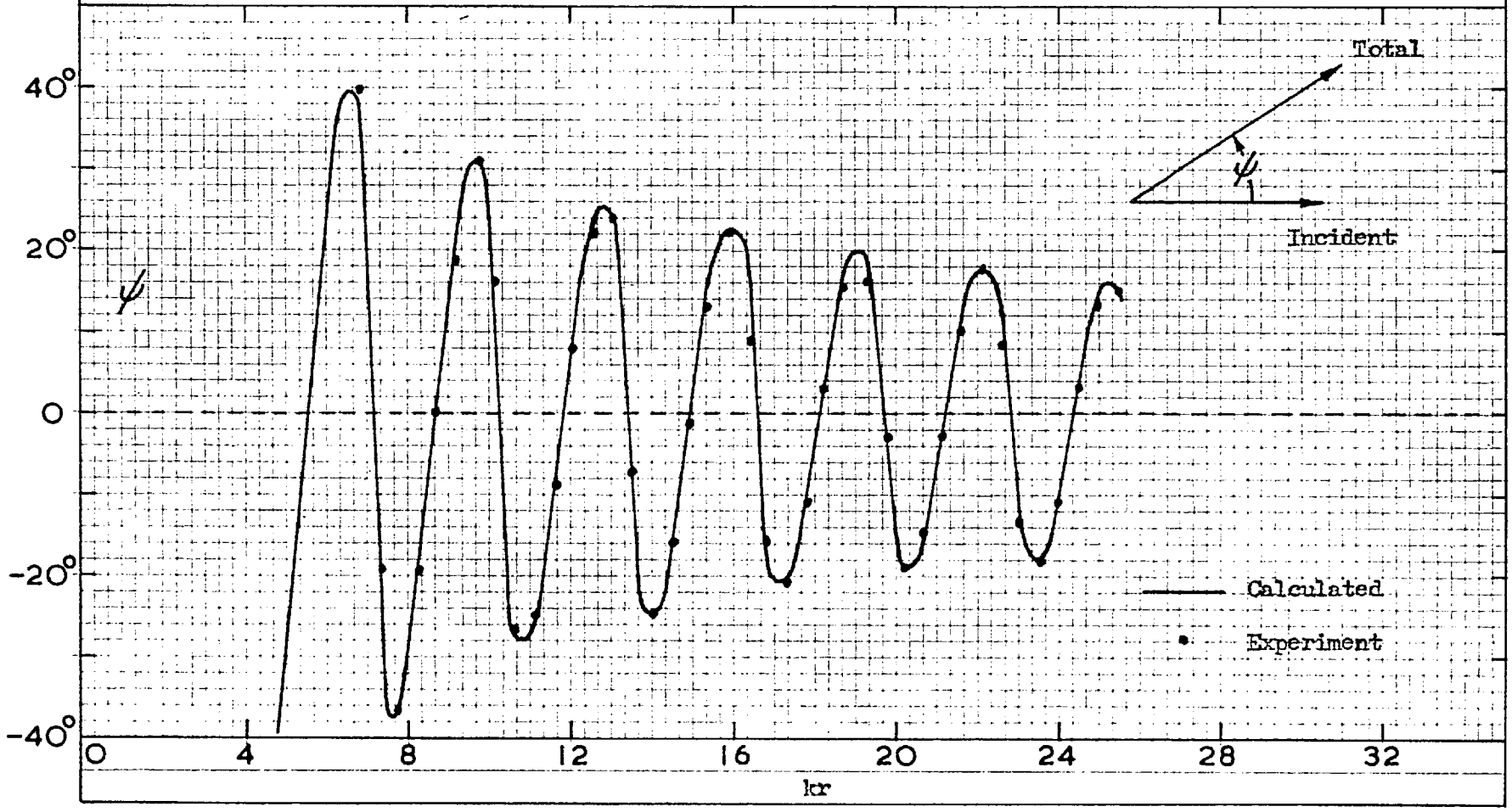

monotonically with distance from the cylinder.

The shadow data presented by these curves is perhaps best interpreted by reference to the vector diagrams of Fig. 3.12 which illustrate the shadow-field conditions for ka=2 and ka=8. The vector E_{inc} represents the incident field. The other vectors represent the total field at the points corresponding to the kr values indicated. The scattered field at each point is then represented by the third side of the vector triangle. To avoid overloading the diagram the scattered-field vectors are not shown.

At the metal surface(point A) the total field is zero and the incident and scattered field vectors coincide but are reversed with respect to each other. At a large distance from the cylinder the scattered field tends to zero and the incident and scattered field vectors tend to coincide, as at point B. A curve joining A and B and passing through the ends of the total-field vectors then constitutes the scattering curve of the cylinder.

As the cylinder radius increases the curves tend to curl around the origin(point A), as may be seen from the diagram for ka=8. As the field point moves in toward the cylinder surface, the scattered field amplitude tends to oscillate about the incident field value and the phase about an angle of 180 degrees with the incident field, in a Cornu-spiral manner.

The angle at which the curves approach point B is governed by the discussion relating to Fig. 3.19. In Fig. 3.12, for ka=2, it appears that the scattered field has an almost-constant phase for kr values greater than about 50. As the cylinder radius increases, the field point must be moved further from the cylinder to reach this constant-phase region, as the ka=8 diagram shows.

The field conditions on the illuminated side of the cylinder are illustrated by Fig. 3.13. The numbers at the vector terminals again refer to the kr values of the field points. Here the incident and scattered waves are travelling in opposite directions, resulting in the "crank" or standing-wave type of diagram. The points A and B have the same significance as before. In this case, however, the total-field vector terminal traces a spiral type of curve with increasing kr, and oscillates about the direction of the incident-field vector. The field fluctuation is identical with that which obtains in the case of the Sommerfeld diffraction problem, as one emerges from behind the half-plane into the interference region. The resultant maxima and minima of the total field will not be separated by a half wavelength, however, as long as the scattered field is changing in velocity. The scattered wave velocity is less than that of the incident field, so the separation will exceed a half wavelength.

3.2. The scattered field.

The curves of Fig. 3.14 and 3.15 illustrate the behaviour of the near forward and back scattered field for several values of ka. It is apparent that this is more complex in the shadow than on the incident side of the cylinder. In the latter case the amplitude does not exceed that of the incident field and, for a fixed value of kr, increases with the cylinder radius. It equals that of the incident field at the surface and decreases with distance from the cylinder. In the shadow, however, because of the spiralling discussed previously, the

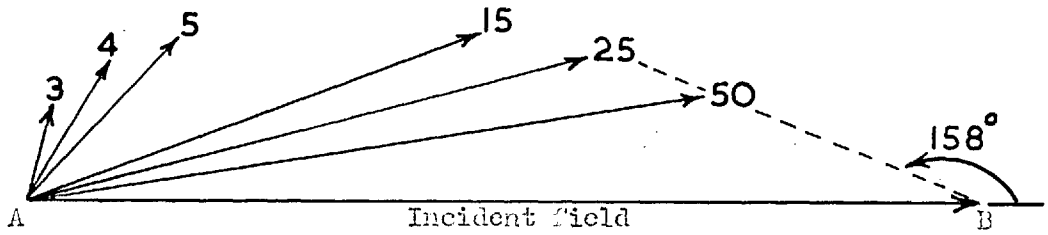

(a) ka = 2

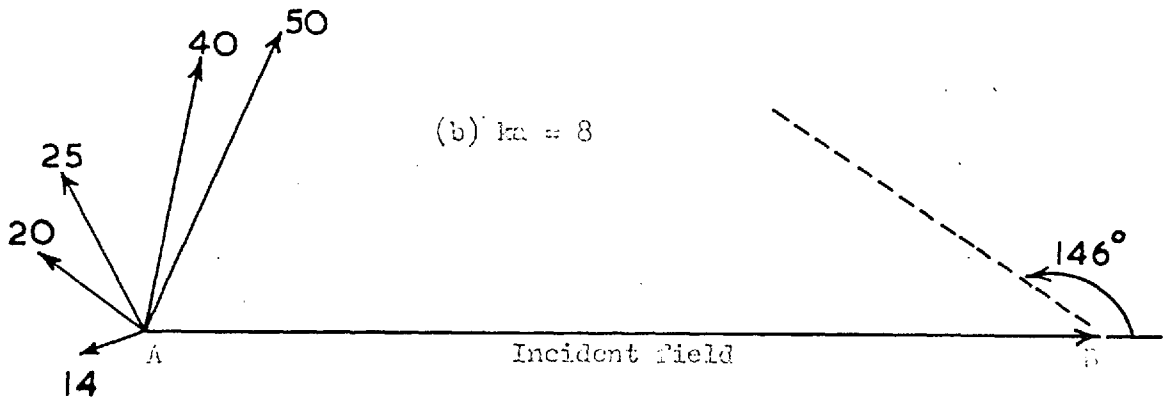

(b) ka = 8

Fig. 3.12. Vector diagrams for scattering in the forward direction by a conducting cylinder. The vectors indicate the magnitude of the total field (relative to that of the incident field) at the points corresponding to the ka values indicated.

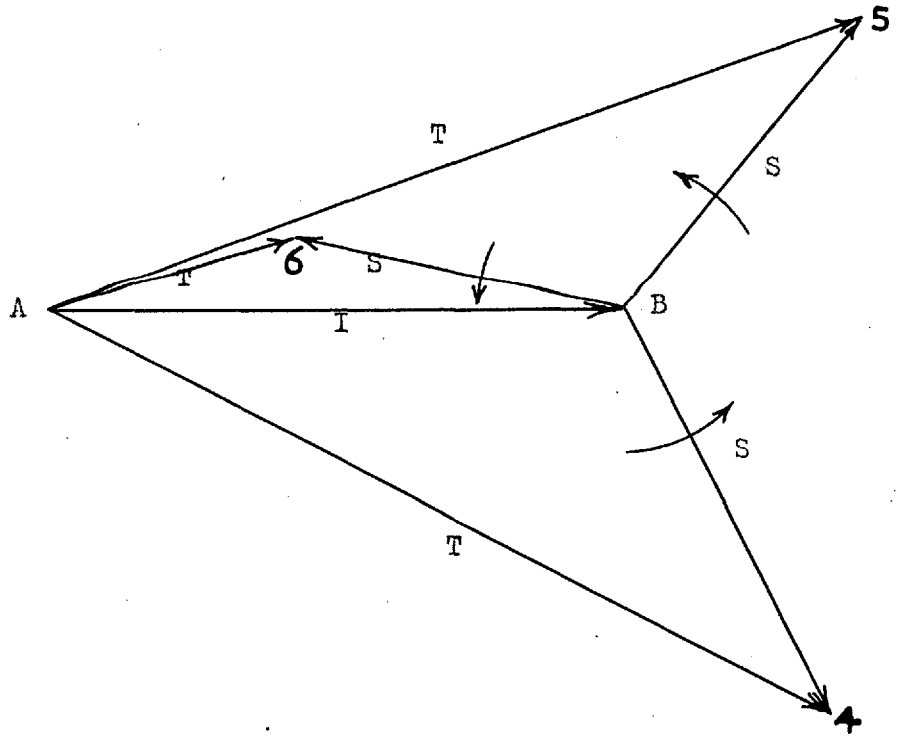

Fig. 3.13. Back-scattering vector diagram for a ka = 3 conducting cylinder at the points corresponding to the kr values indicated.

I = Incident field.
S = Scattered field.
T = Total field.

scattered field sometimes exceeds the incident amplitude and oscillates about that value. These calculations would seem to indicate that, contrary to what is often assumed, the scattered field in the shadow does not always have the property of a divergent wave in the near region and that the departure from this property extends further from the cylinder as the radius increases, i.e., as the total field vector spirals more often around the origin. As the distance from the cylinder increases, however, the

scattered field settles down to a pattern similar to that obtaining on the illuminated side. The amplitude decreases monotonically with distance and, except for small cylinders, is linear with respect to ka, for a fixed kr. Moullin(p. 247) shows a plot of the far-field amplitude vs ka, with a slope of 1.03.

Further calculations of the angular distribution of the scattered field would reveal how far around the cylinder this excess of the scattered field over the incident field prevails, and how it varies in distance with angle and cylinder radius.

Alternatively, the problem can be stated as follows, with reference to Fig. 3.12 and 3.13-

On the illuminated side of the sylinder the total-field vector spirals around point B. On the shadow side the spiralling is around point A. It would be of academic interest, if of no other, to trace the transition from the one condition to the other, by calculating the field as a function of kr for various values of ϕ between 0 and 180 degrees.

This transition can be regarded from another point of view. On the illuminated side of the sylinder the standing wave repeats itself at intervals of approximately half the incident wavelength and the total-field curve crosses the incident value for the first time close to the cylinder surface. As one moves down along the face of the cylinder, the rate of phase shift of the incident field, along a radial direction, decreases, while that of the scattered field remains practically const-

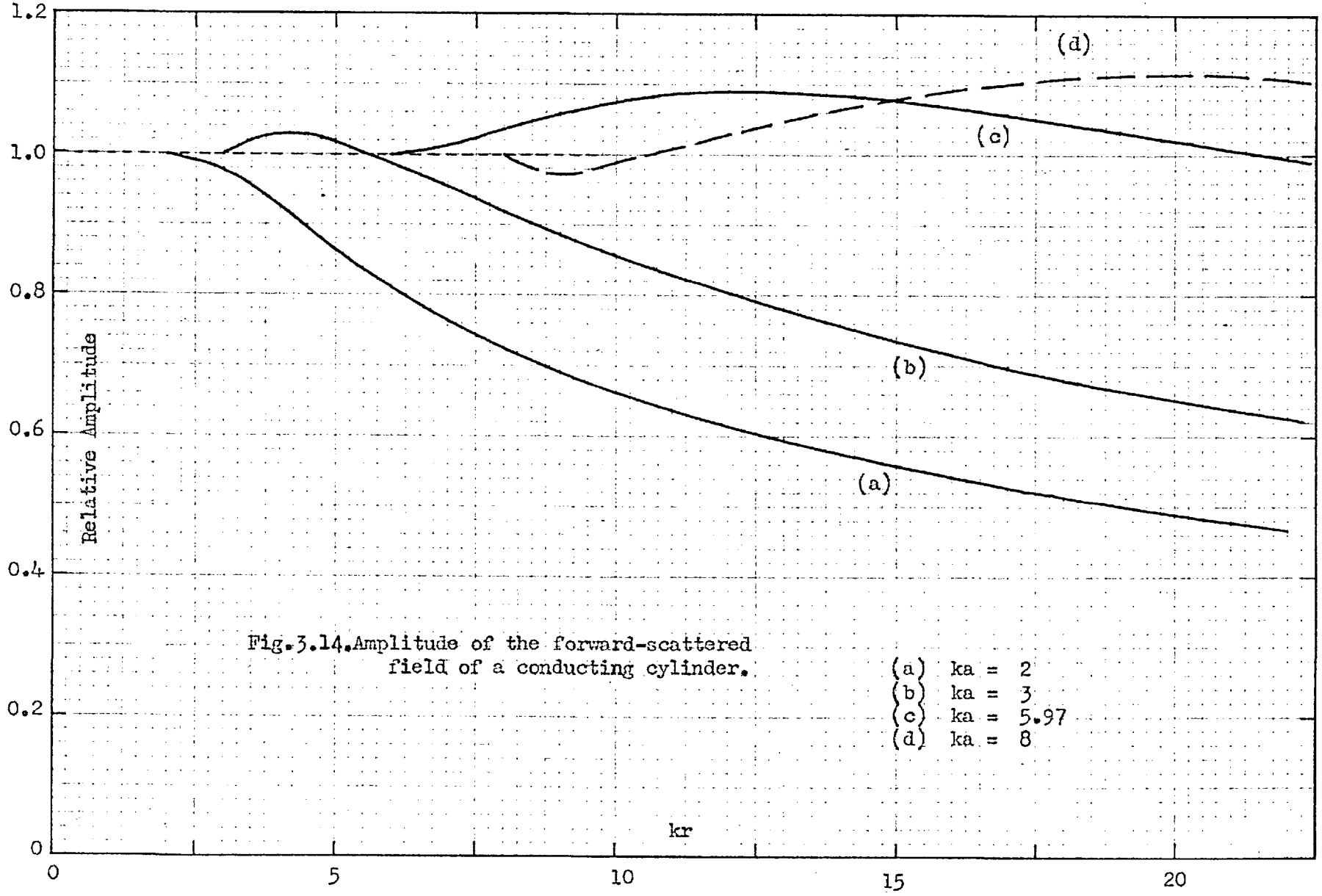

Fig.3.14. Amplitude of the forward-scattered field of a conducting cylinder.

(a) ka = 2
(b) ka = 3
(c) ka = 5.97
(d) ka = 8

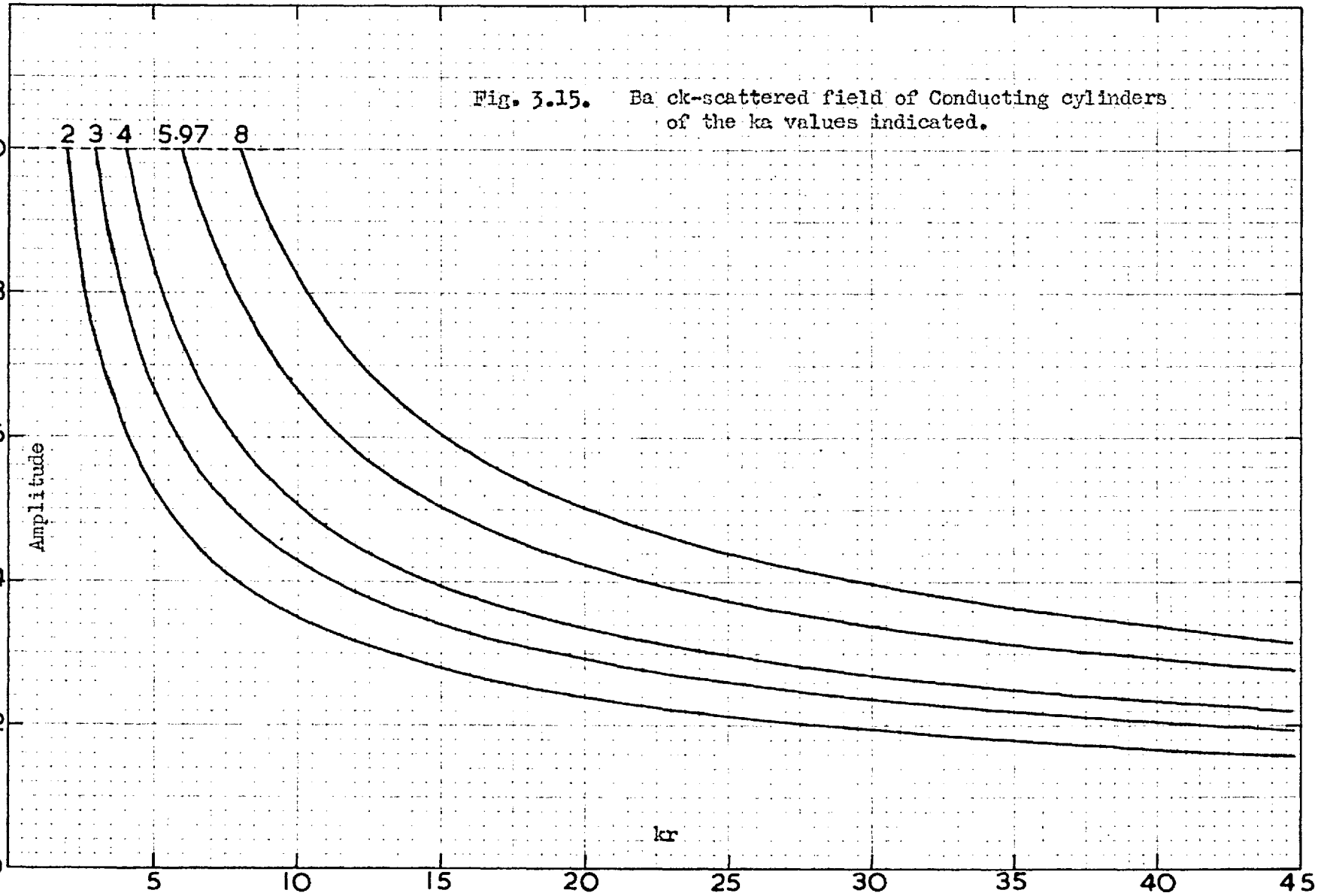

Fig. 3.15. Back-scattered field of Conducting cylinders of the ka values indicated.

WIGHTMAN MOUNTAIN LTD.
ARTILLERY HOUSE, ARTILLERY ROW, WESTMINSTER, S.W.1

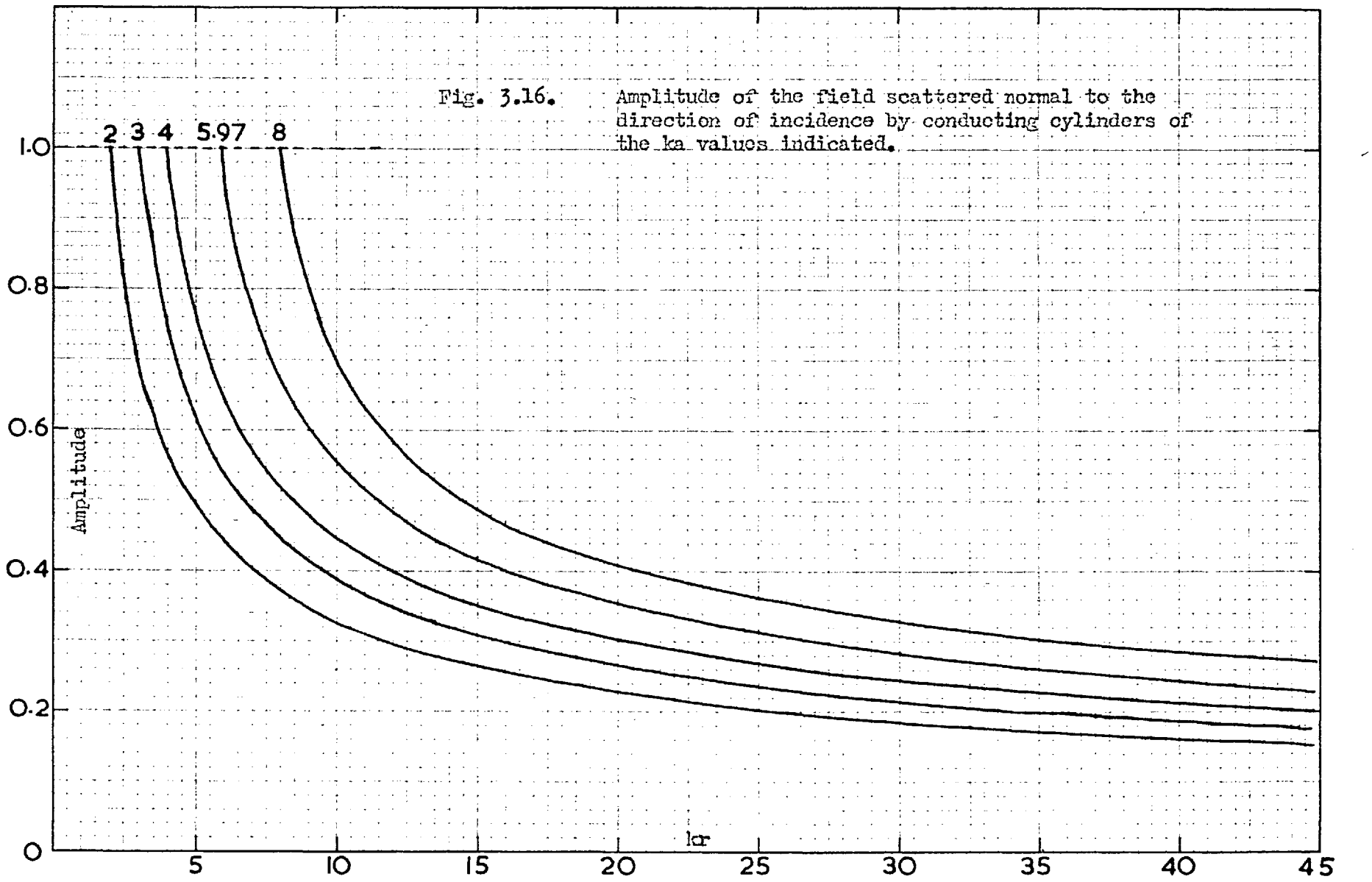

Fig. 3.16. Amplitude of the field scattered normal to the direction of incidence by conducting cylinders of the ka values indicated.

ant. Thus the rate of rotation of the scattered field vector about point B decreases and, as a result, the period of the standing wave of total field increases, as does the distance out to the first cross-over point. Thus, in the side direction, there is no variation of incident field phase and the period is close to that of the incident field. Finally, in the shadow direction, one can say that the periodicity of the total field has disappeared and the first cross-over point receded to infinity. Calculations would show the manner in which the period and the distance to the first cross-over point change with angle and radius of cylinder.

Curves of the side-scattered field are given in Fig. 3.16. They show that, as ϕ increases to $\pi/2$, the scattered-field pattern has already changed to the relatively-simple form seen previously for the illuminated side.

As the cylinder radius decreases the angular fluctuation of the scattered field gradually disappears, corresponding to the excitation of only the first scattering mode, i.e., only the first term of the series (3.7) contributes. The second mode, involving $\cos\phi$, is but weakly excited compared with the first, for $ka = 0.1$. For $ka = 0.3$ the first three modes are excited, giving the scattering pattern shown in Fig. 3.17. The scattered field is greatest in the shadow direction, a usual feature of scattering by a cylinder.

3.3. Auxiliary angles.

The concept of auxiliary angles, or phase-shift analysis, was

introduced from the field of particle scattering, into the problem of scattering of light waves by a sphere, by Van de Hulst, and by Lax and Feshbach into the problem of scattering by cylinders and spheres.

The method, as stated by Van de Hulst, and when applied to cylinders, is as follows-

From (3.7) the scattering amplitudes are of the form-

$$a_n = -B_n/(i)^n = J_n(ka)/H_n^{(1)}(ka) = \frac{1}{1 + i\, Y_n(ka)/J_n(ka)} \qquad (3.9)$$

from the form of the Hankel function.

Now make the transformation-

$$\tan \theta_n/2 = J_n(ka)/Y_n(ka) \qquad (3.10)$$

and (3.9) becomes-

$$a_n = \tfrac{1}{2}(1 - \exp i\theta_n) \qquad (3.11)$$

i.e., all the vectors a_n terminate on a circle, in the complex plane, of radius $\frac{1}{2}$ and center at the point $(\frac{1}{2},0)$. That assumes, of course, that ka is real. This circle property, and the fairly regular behaviour of the angles as compared with the irregular behaviour of the Bessel coefficients, were utilized by Van de Hulst, and also in the present calculations, as a help in detecting errors.

In the notation of Lax and Feshbach the angles can be represented by the following relation-

$$a_n = \tfrac{1}{2}(1 - \exp -i2\eta_n) \qquad (3.12)$$

Fig. 3.17. Comparison of the amplitudes of the fields scattered in several directions by a ka=.3 conducting cylinder.

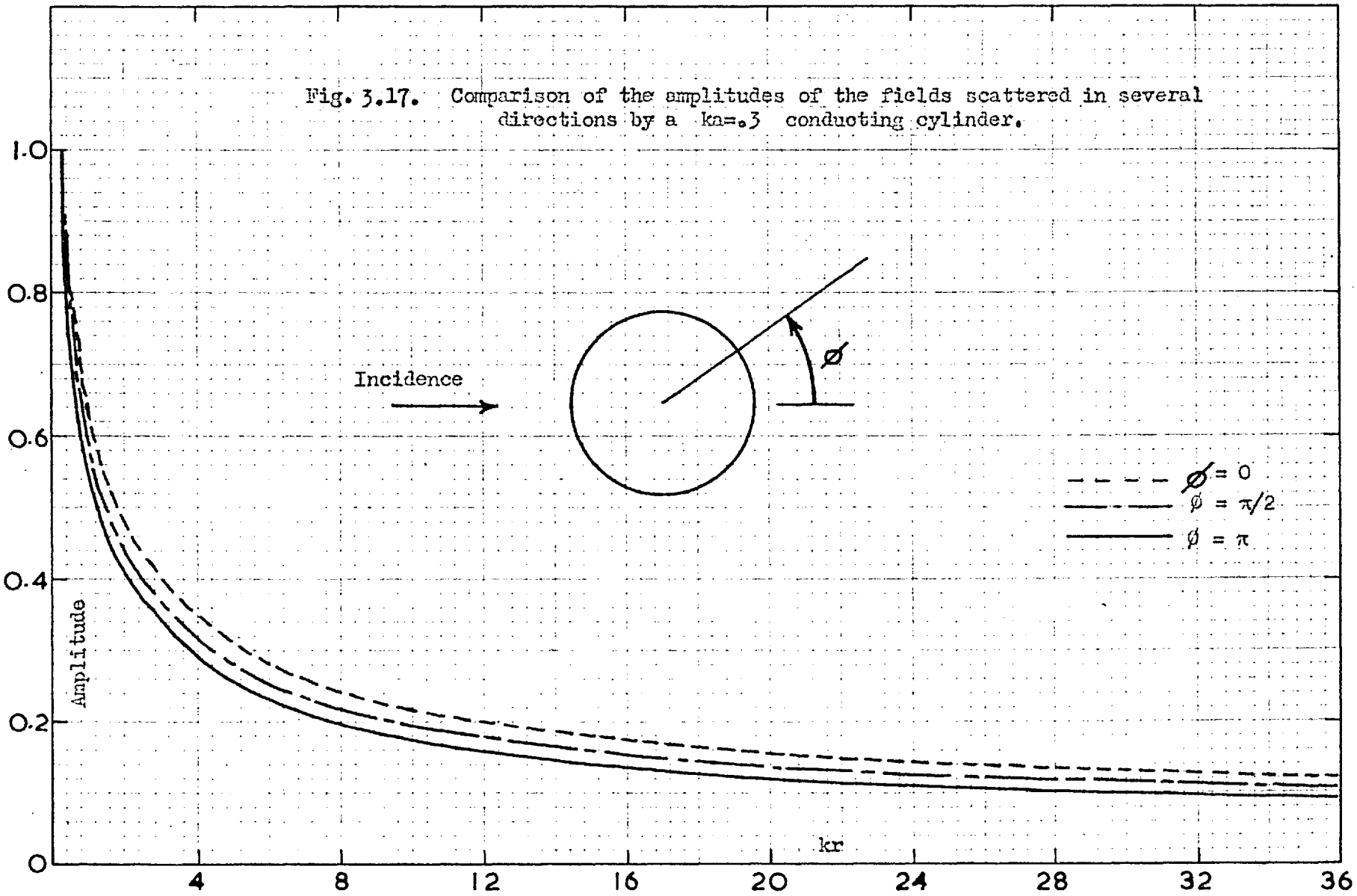

from their Eq. 12. That is, θ_n and η_n are related by $\theta_n = -2\eta_n$.

The behaviour of the θ_n, as a function of ka, is shown in Fig. 3.18 for n = 0-4. As ka increases the curves tend to become linear with a slope of -2(for the angle in radians). This can be seen from (3.9). For large ka > n,

$$a_n \sim \cos \zeta_n / \exp(i \zeta_n) = 1/(1 + i \operatorname{Tan} \zeta_n) \tag{3.13}$$

where

$$\zeta_n = ka - (2n + 1)\pi/4 \tag{3.14}$$

But $a_n = 1/(1 + i \cot \theta_n/2)$, from (3.9) and (3.10). Thus

$$\cot \theta_n/2 = \tan \zeta_n, \text{ or } \zeta_n + m\pi = \pi/2 - \theta_n/2$$

Then, from (3.14),

$$\theta_n = (n - 2m + 3/2)\pi - 2ka \tag{3.15}$$

or $d\theta_n/d\,ka = -2$.

The application of this useful "circle" concept to the equations of scattering by any lossless cylinder(circular, at least), whether metal, dielectric or coaxial, arises from the fact that, in all these cases, just as for the metal and dielectric spheres, the scattering amplitudes are of such a form that the numerator is identical with the real part of the denominator. However, while the curves for the auxiliary angles for the metal cylinders are smooth, those for the dielectrics tend to be more irregular, especially for the higher orders, because of the resonances that occur in the scattering amplitudes of the dielectric scatterers.

3.4. The distant shadow phase.

Now turn to the behaviour of the distant, shadow phase. This can

be determined from (3.7). When kr is large-

$$E_{sc}(r,\phi) = -(2/\pi kr)^{\frac{1}{2}} \exp(ikr - i\pi/4) \sum_{0}^{\infty} \varepsilon_m \frac{J_n(ka)}{H_n^{(1)}(ka)} \cos n\phi \qquad (3.16)$$

In the shadow, where $\phi = 0$, the phase difference θ, between the scattered field and the incident, is therefore given by-

$$\theta = \mathrm{Arg}\left[-\sum_{0}^{\infty} \varepsilon_n J_n(ka) / H_n^{(1)}(ka) \right] - \pi/4 \qquad (3.17)$$

Fig. 19 has been calculated from (3.17), for ka = 0.1-8.0. For very small ka only the n=0 term in the series of (3.17) need be used. Since Y_0 is negative and J_0 positive, while $|Y_0| >> J_0$, (3.17) becomes-

$$\theta = \mathrm{Arg}\left[-i\, J_0 / |Y_0| \right] - \pi/4 = -3\pi/4.$$

The limiting value of θ for large ka can be found from the paper of Papas. It can be shown from his results for large ka that the scattered field leads the incident by $3\pi/4$ radians.

Thus θ traverses the range 225-135 degrees as ka increases from a very small value. The antiphase, or 180 degrees, value, occurs at approximately ka= 0.3. Calculations show a departure from antiphase of less than 1 degree for kr in the range 0.3-50, the departure being zero at kr = 0.3.

In the near region, however, as for the amplitude one finds departures in the phase from the smooth behaviour shown in Fig. 3.19. This is illustrated by the calculated curves of Fig. 3.20. At kr=15, for example, the order of the curves has been reversed, the phase in this

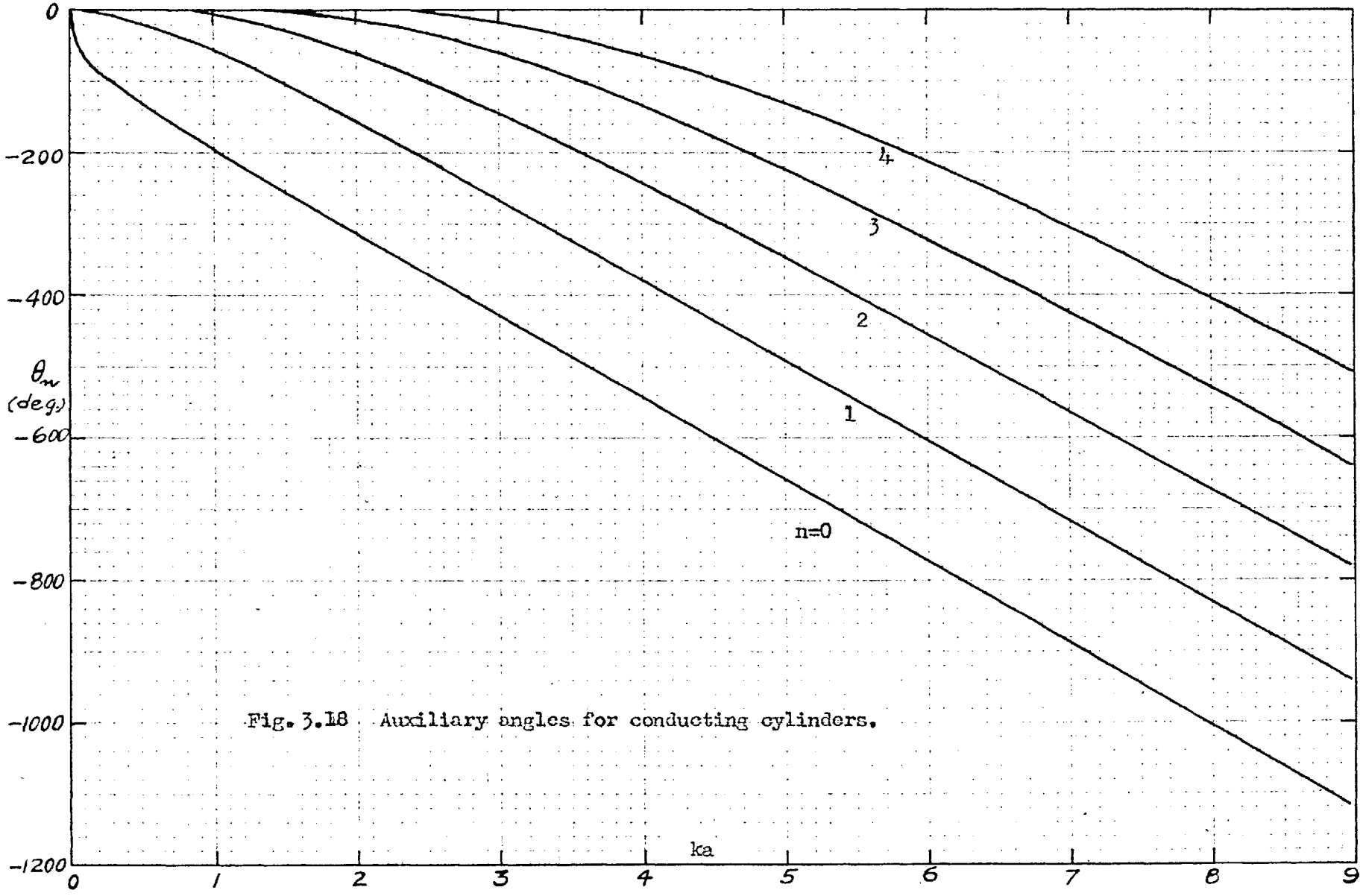

Fig. 3.18 Auxiliary angles for conducting cylinders.

Fig. 3.19 Phase difference between the incident and forward-scattered fields for a conducting cylinder.

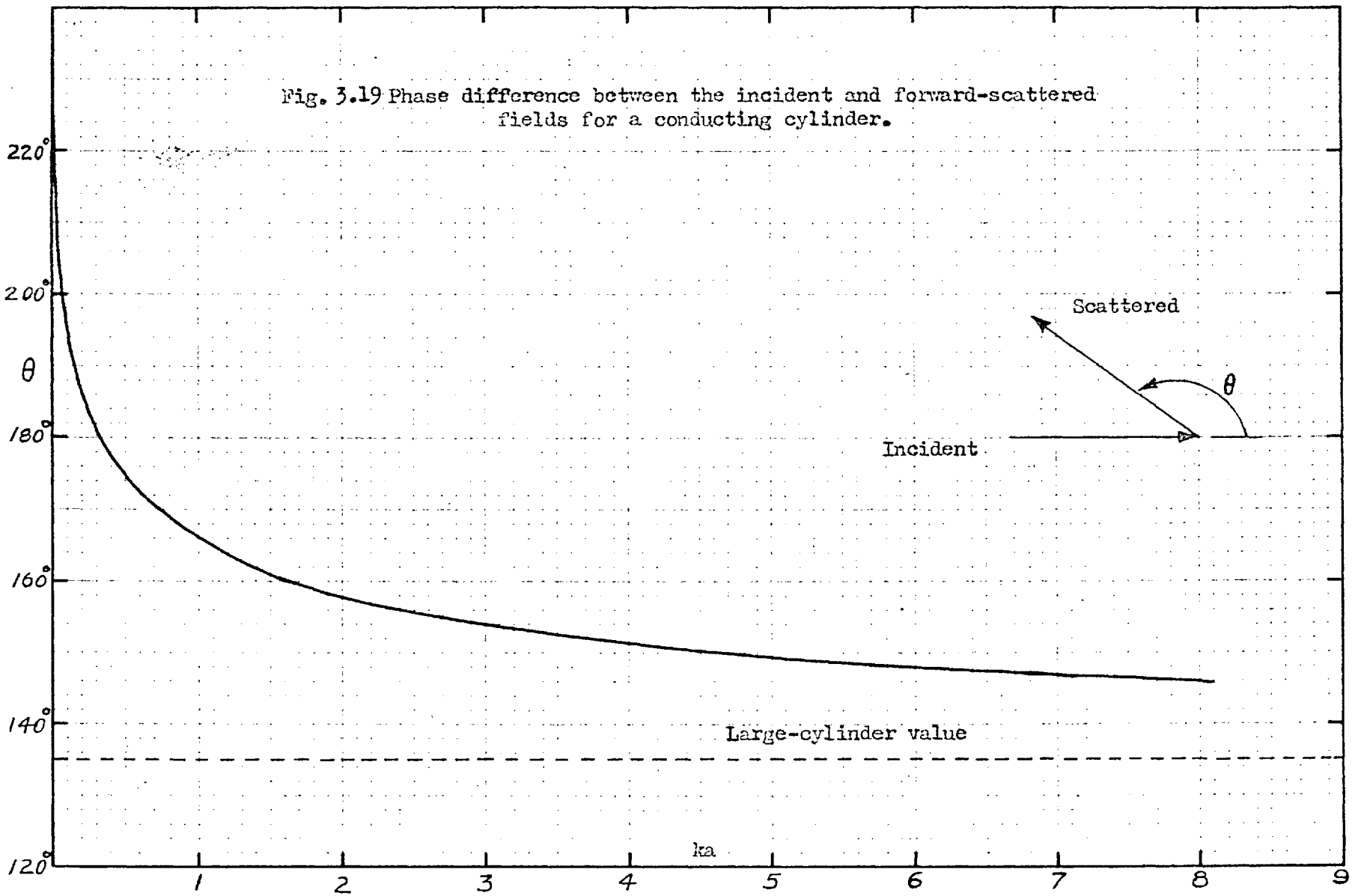

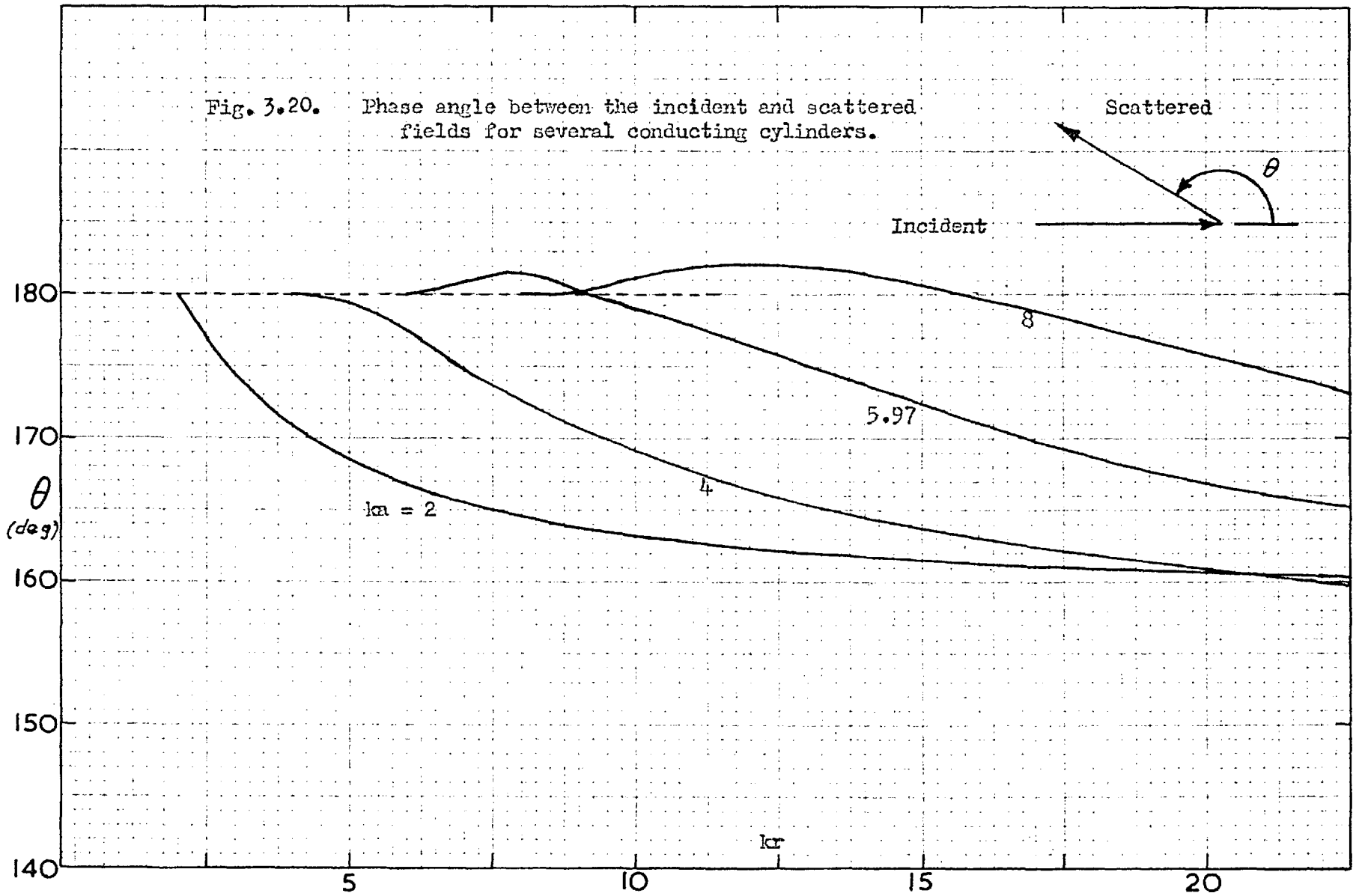

Fig. 3.20. Phase angle between the incident and scattered fields for several conducting cylinders.

region increasing with radius. For the ka values shown, the cross-over begins at about kr=20. For the larger values of ka, the spiralling effect is again in evidence by the excess of the phase over 180 degrees.

The main interest in the metal cylinder scattering was in the information that the total-field measurements would provide about the accuracy to be expected from the equipment. However, the digression to discuss the scattered fields was made to observe some of the coupling effects that might be expected for closely-spaced cylinders and to indicate one or two points in the calculation procedure.

3.5. The experimental results.

Only the shadow results were available for the initial assessment of the usefulness of the line, the others having been obtained toward the end of the measuring programme.

The former seemed to indicate, as later did the latter, that the equipment could be expected to provide results within 3 percent in amplitude and 3 degrees in phase.

It was considered justifiable, therefore, to proceed to the measurements on cylinders of other materials and cross-sections, for some of which calculations of the scattering would be available and for others of which the experimental results would have to be accepted on their own, within the limits of the accuracy of the equipment.

CHAPTER 4.

DIFFRACTION OF A PLANE WAVE BY A DIELECTRIC CYLINDER.

4.1. Theoretical solution.

In this Chapter the metal cylinder of Chapter 3 is replaced by one of permittivity ε_2, permeability μ_2, conductivity σ_2 and wave number $k_2 = 2\pi/(\text{wavelength in the cylinder material}) = \sqrt{\omega^2\mu_2\varepsilon_2 + i\omega\sigma_2\mu_2} = k_r k_1$, where $k_1^* = 2\pi/(\text{external wavelength})$ and k_r is the index of refraction of the cylinder material. The same functions as before may be employed for the incident and scattered field, but one must, in addition, seek a solution of the wave equation inside the cylinder which is finite on the cylinder axis. This is taken to be-

$$E_2(r,\phi) = \sum_0^\infty \varepsilon_n A_n J_n(k_2 r) \cos n\phi \qquad (4.1)$$

where the notation is as in Chapter 3 and Fig. 4.1.

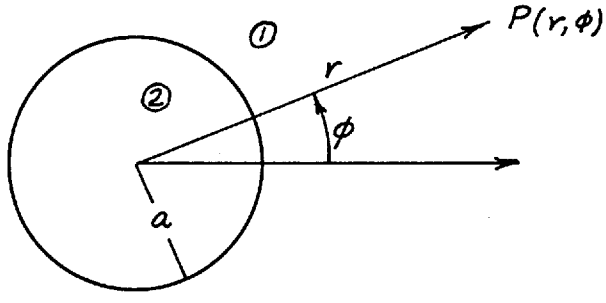

Fig. 4.1.

The A_n must be determined from the boundary conditions at the cylinder surface. The magnetic fields appropriate to each region are given by -

---

*The subscript "1" usually dropped on the graphical data.

$$H_\phi(r,\phi) = \frac{i}{\omega\mu}\frac{\partial}{\partial r}E(r,\phi)\ ;\ H_r(r,\phi) = \frac{i}{\omega\mu r}\frac{\partial}{\partial \phi}E(r,\phi) \quad (4.2)$$

Thus, by the use of (4.1), (4.2), (3.2), (3.3) and (3.4) and by equating the sum of the incident and scattered fields to the internal field, at r = a, there is obtained-

$$B_n = -(i)^n \frac{\begin{vmatrix} J_n(K_2a) & , & J_n(K_1a) \\ \frac{K_2}{\mu_2}J_n'(K_2a), & & \frac{K_1}{\mu_1}J_n'(K_1a) \end{vmatrix}}{\Delta} \quad (4.3)$$

$$A_n = (i)^n \frac{\begin{vmatrix} J_n(K_1a) & , & H_n^{(1)}(K_1a) \\ \frac{K_1}{\mu_1}J_n'(K_1a), & & \frac{K_1}{\mu_1}H_n^{(1)\prime}(K_1a) \end{vmatrix}}{\Delta} \quad (4.4)$$

where

$$\Delta = \begin{vmatrix} J_n(K_2a) & , & H_n^{(1)}(K_1a) \\ \frac{K_2}{\mu_2}J_n'(K_2a), & & \frac{K_1}{\mu_1}H_n^{(1)\prime}(K_1a) \end{vmatrix} \quad (4.5)$$

Since, in the subsequent numerical work in this Chapter on the external field, only the case where $\mu_2 = \mu_1$ will be considered, the numerator of (4.3) will not be expanded further in its present form.

With $\mu_2 = \mu_1$, (4.3) becomes-

$$B_n = -(i)^n \frac{C_n}{C_n + i\,D_n} \quad (4.6)$$

where

$$C_n = J_n(k_2a)J_{n+1}(k_1a) - k_rJ_{n+1}(k_2a)J_n(k_1a) \quad (4.7a)$$

$$D_n = J_n(k_2a)Y_{n+1}(k_1a) - k_rJ_{n+1}(k_2a)Y_n(k_1a) \quad (4.7b)$$

By expanding (4.4) the amplitude of the internal field is obtained as-

$$A_n = (i)^n \frac{\kappa_1}{\mu_1} \frac{X_n}{Z_n} \tag{4.8}$$

where-

$$X_n = J_n(\kappa_1 a) H_{n+1}^{(1)}(\kappa_1 a) - J_{n+1}(\kappa_1 a) H_n^{(1)}(\kappa_1 a) \tag{4.9a}$$

$$Z_n = \frac{n}{a}\left\{\frac{1}{\mu_2} J_n(\kappa_2 a) H_n^{(1)}(\kappa_1 a) - \frac{1}{\mu_1} J_n(\kappa_2 a) H_n^{(1)}(\kappa_1 a)\right\} + \left\{\frac{\kappa_1}{\mu_1} J_n(\kappa_2 a) H_{n+1}^{(1)}(\kappa_1 a) - \frac{\kappa_2}{\mu_2} J_{n+1}(\kappa_2 a) H_n^{(1)}(\kappa_1 a)\right\} \tag{4.9b}$$

(4.8) can be transformed by the Bessel function Wronskian relation (McLachlan, p. 156) to-

$$A_n = (i)^{n-1}\left(2/\pi\mu_1 a\right) \Big/ \left[\frac{n}{a}\left(1 - \frac{\mu_r}{\mu_2}\right) J_n(\kappa_2 a) H_n^{(1)}(\kappa_1 a) + \frac{\kappa_1}{\mu_1}\left\{J_n(\kappa_2 a) H_{n+1}^{(1)}(\kappa_1 a) - \frac{\kappa_r}{\mu_r} J_{n+1}(\kappa_2 a) \times H_n^{(1)}(\kappa_1 a)\right\}\right] \tag{4.10}$$

where $\mu_r = \mu_2/\mu_1$. If $\mu_r = 1$, the internal field associated with (4.6) is-

$$A_n = (i)^{n-1}\left(2/\pi\kappa_1 a\right) \Big/ (C_n + i D_n) \tag{4.11}$$

4.2. Near fields.

Based on (3.1), (3.3) and (4.6) calculations have been made for the case of a polystyrene cylinder of $k_r = 1.60$, for values of $k_1 a$ up to 10.0 for the far fields and for a smaller range for the near fields.

(a) The calculated total field in the cylinder shadow- This is shown by Figs. 4.2 - 4.12, with the corresponding measured values. The amplitude and phase references are as for the metal cylinder.

The results indicate that, just as for the metal case, a deep shadow can be produced behind a polystyrene cylinder. But whereas, in the

metal case, the shadow deepened with the increased cylinder radius, the polystyrene cylinder shadow increases with k_1a up to approximately 4.55, when it again decreases. At the same time the phase curves show a change of form at the same k_1a value. With the initial increase of k_1a the phase increases until approximately $k_1a = 3.75$. Beyond that value the phase increases for the nearer fields, but decreases for the more remote. Finally, an apparent discontinuity of 360 degrees occurs at the latter field points.

The trends indicated by these curves can best be illustrated by combining, for each cylinder, the amplitude and phase into a vector diagram. This has been done for several values of k_1a and is shown in Fig. 4.13. The family of curves tends to spiral about the point B, with the $k_1a = 6$ cylinder practically completing the first turn. The shadow deepens until that value of k_1a is reached for which the curve passes through the origin, after which the shadow decreases. For that value of k_1a and k_1r the phase is indeterminate. The zero-field region is very localized with respect to both k_1a and k_1r, the field rising sharply for k_1r values on either side of approximately 23. For k_1a values less than the critical, the phase decreases monotonically on moving the field point away from the cylinder. For greater values the phase first decreases and then increases, tending toward 360 degrees rather than 0. This behaviour was predicted by Kodis in his experiments on polystyrene cylinders,* as was that of the scattered amplitude's sometimes exceeding the incident value. This latter is illustrated in the calculated curves. In the case of the scattered

* although he did not expect the shadows to be present directly behind the cylinder.

DATA SHEET NO. 21 S10THS SECTIONAL. SCALE 9 INCHES × 6 INCHES

WIGHTMAN MOUNTAIN LTD.
ARTILLERY HOUSE, ARTILLERY ROW, WESTMINSTER, S.W.1

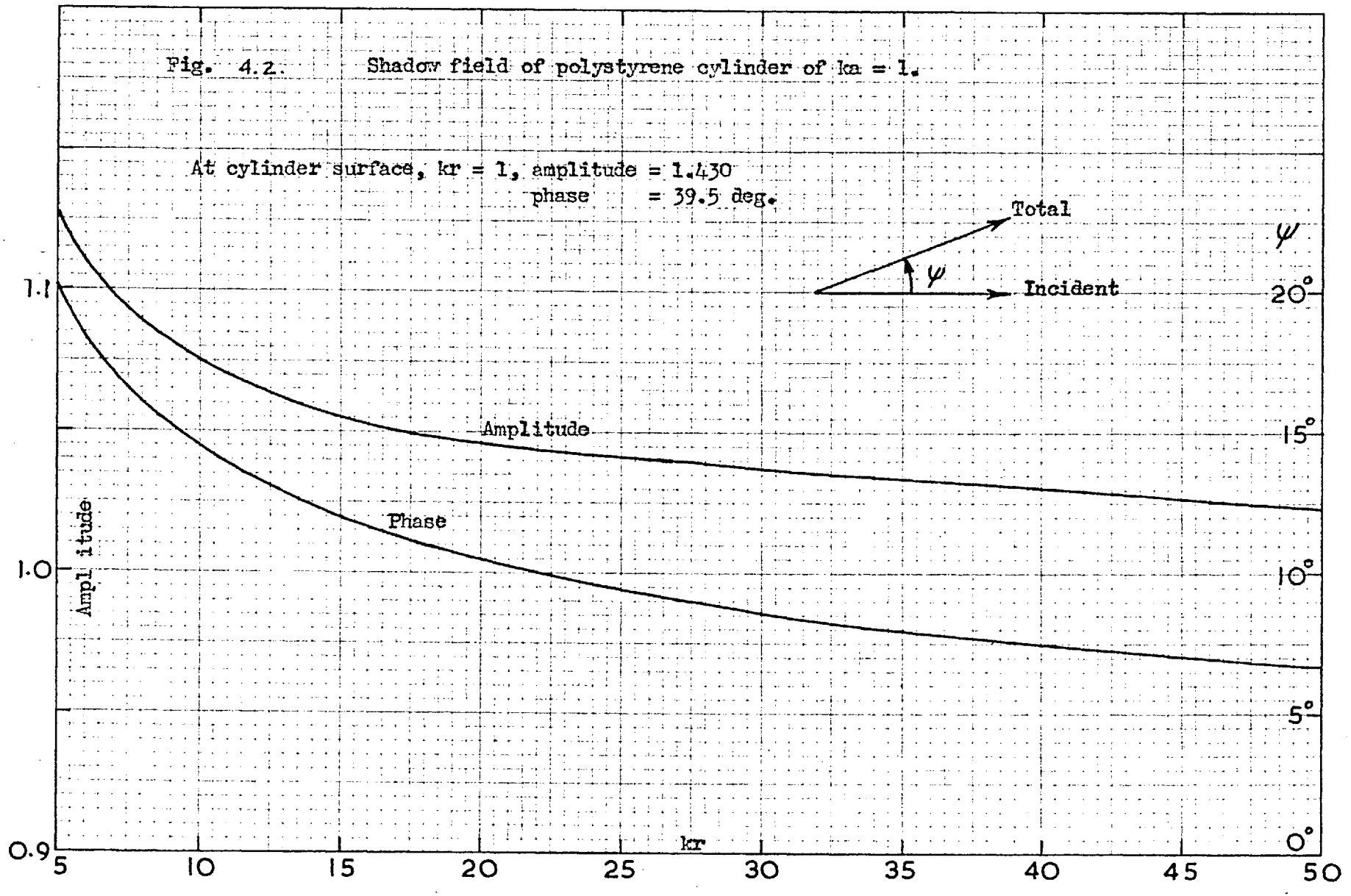

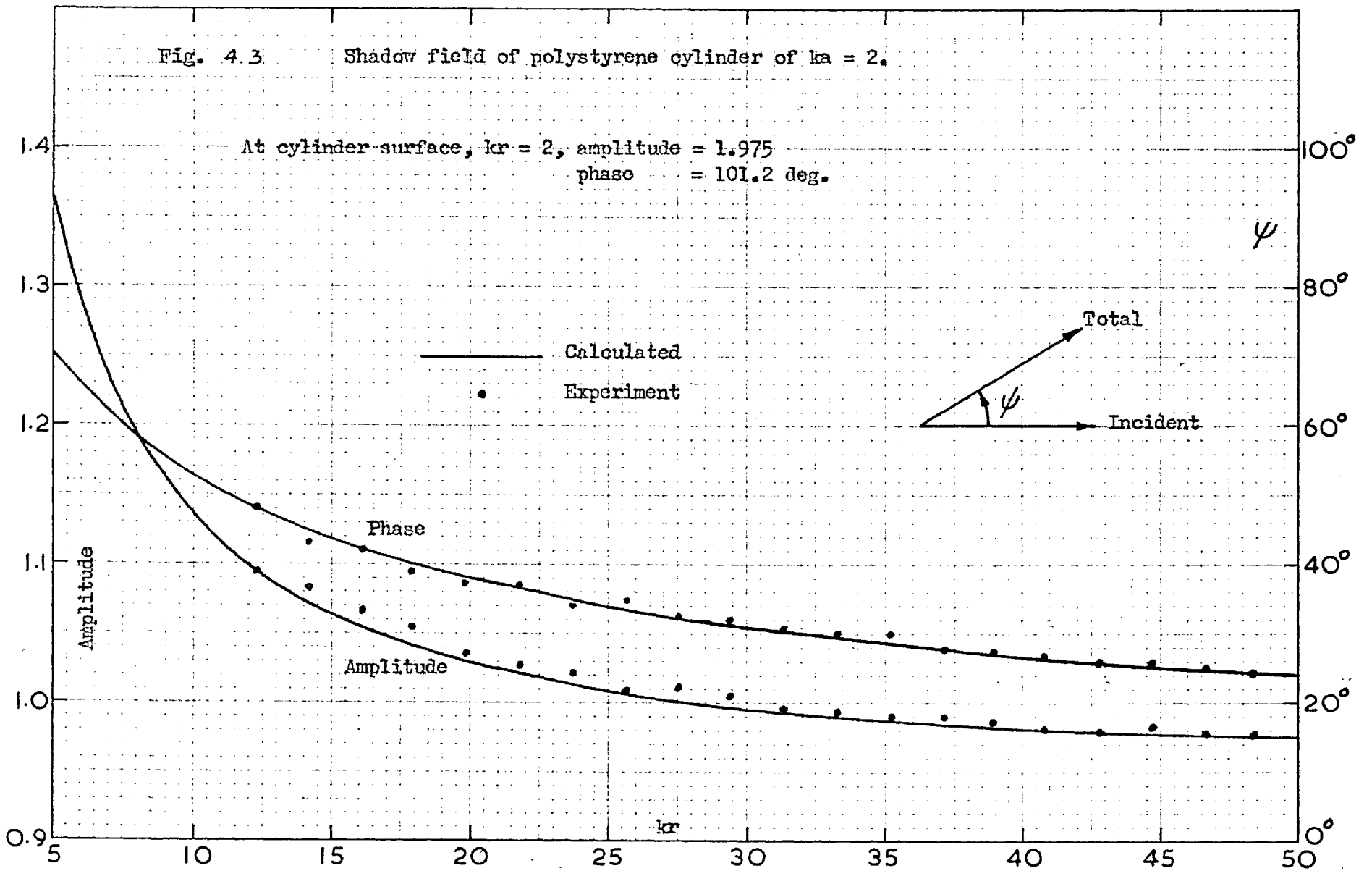

Data Sheet No. 215 Metric Sectional. Scale 9 Inches = 6 Inches

Wightman Mountain Ltd.
Artillery House, Artillery Row, Westminster, S.W.1

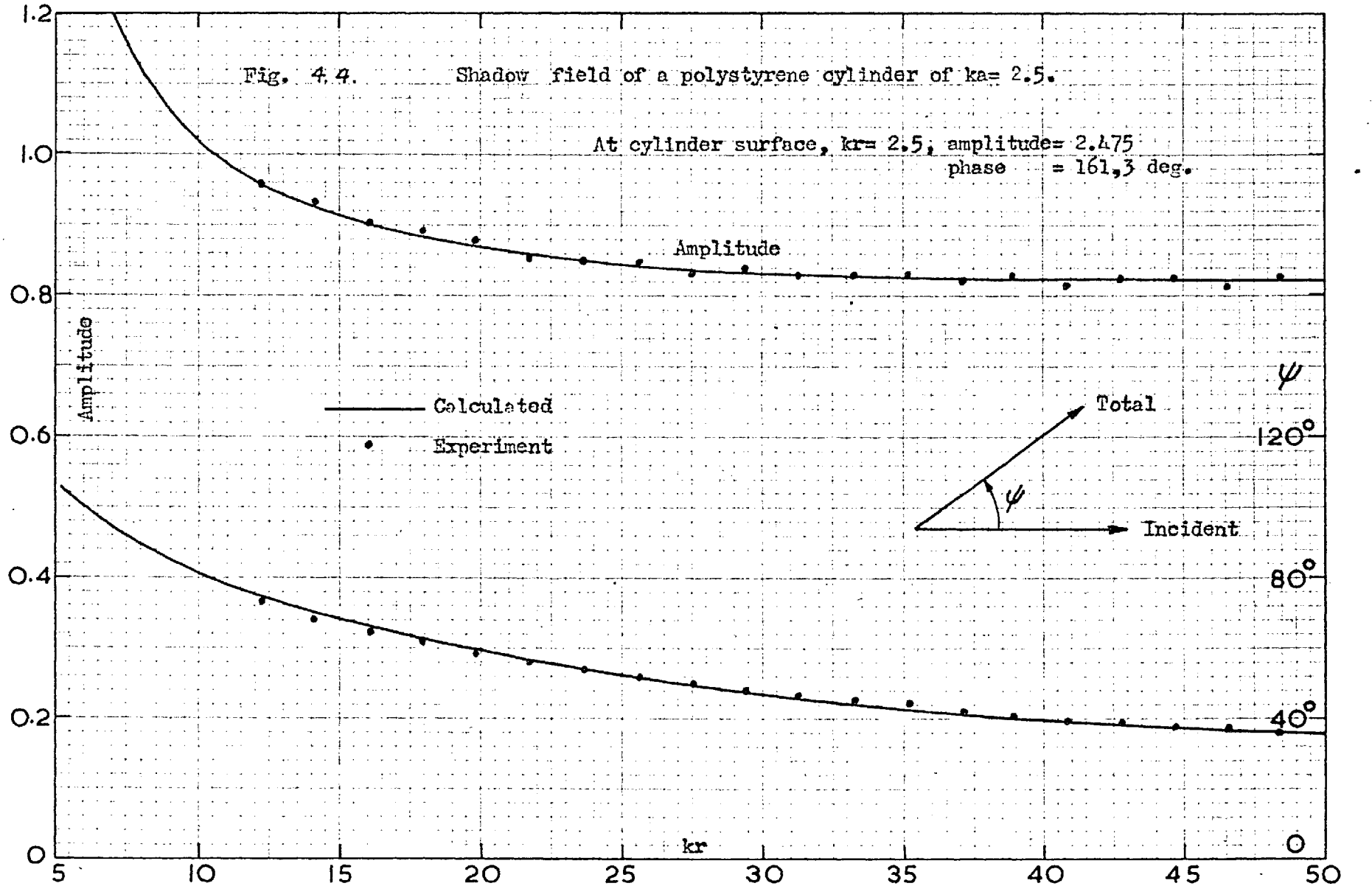

Wightman Mountain Ltd.
Artillery House, Artillery Row, Westminster, S.W.1

Fig. 4.5. Shadow field of polystyrene cylinder of ka = 3.

At cylinder surface, kr = 3, amplitude = 2.370
phase = 173.2 deg.

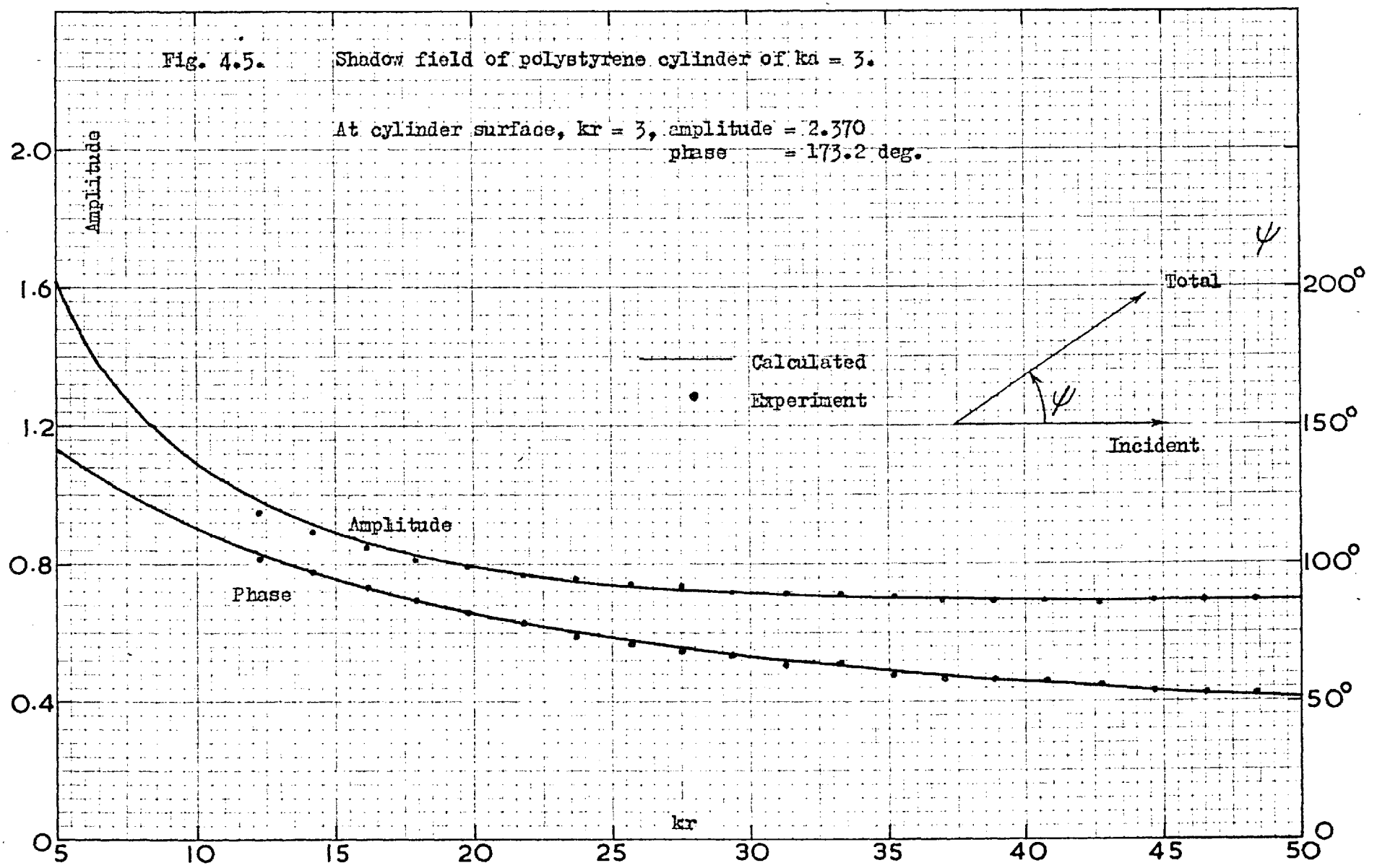

DATA SHEET No. 3 - S 10TH SECTIONAL. SCALE 9 INCHES = 8 INCHES

WIGHTMAN MOUNTAIN LTD.
ARTILLERY HOUSE, ARTILLERY ROW, WESTMINSTER, S.W.1

Fig. 4.6. Shadow field of polystyrene cylinder of ka = 3.5.

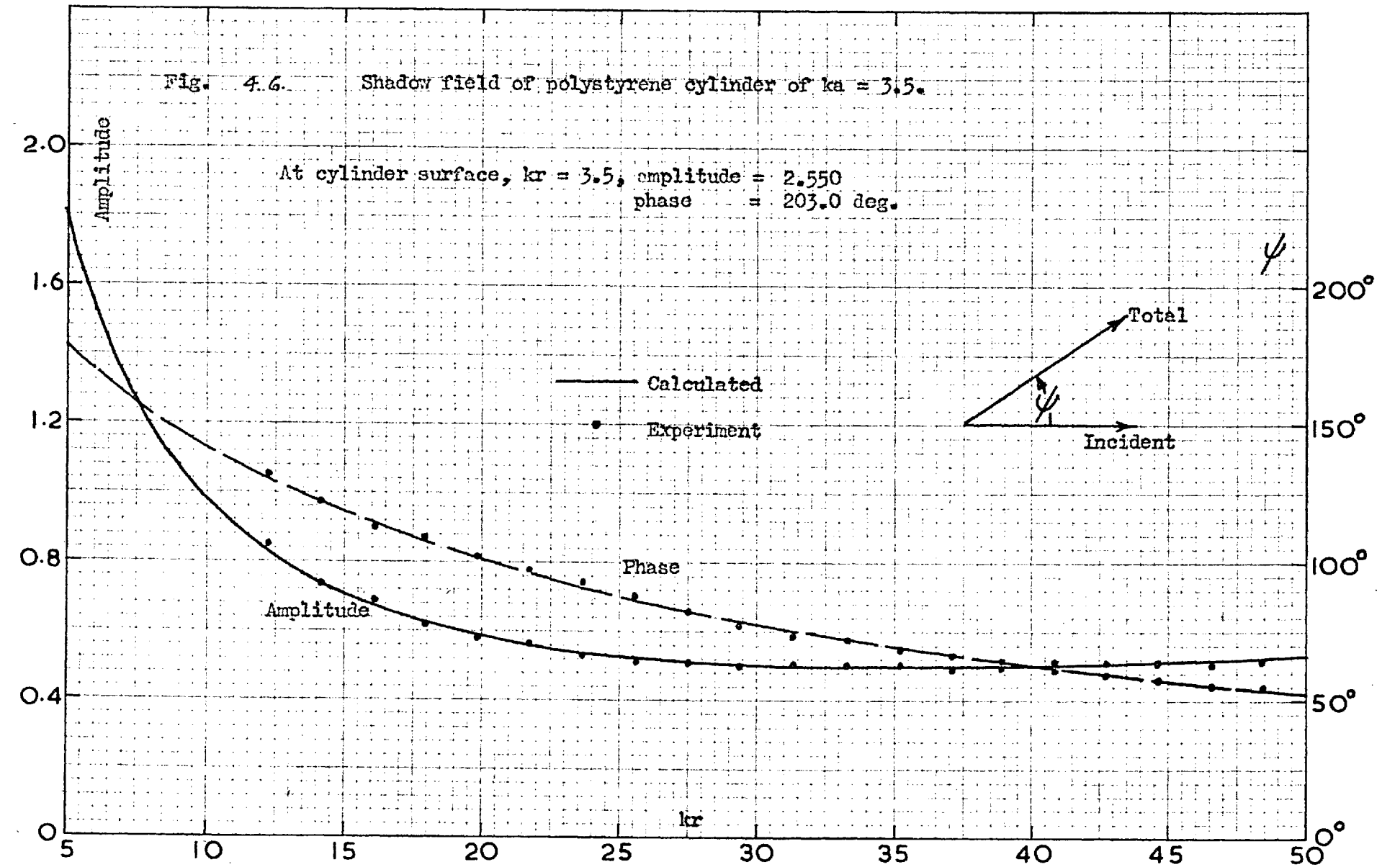

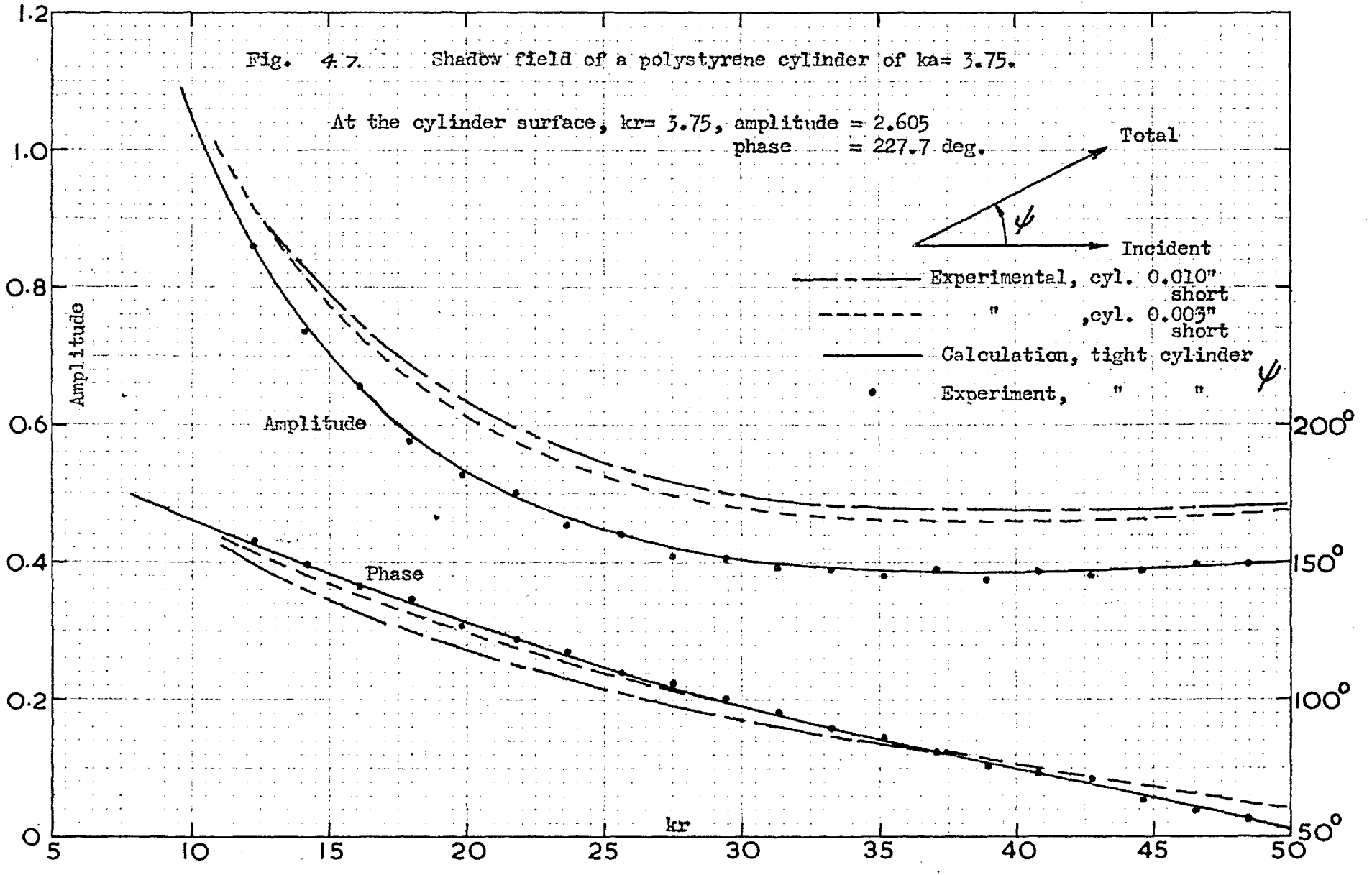

Data Sheet No. 21.S 10ths Sectional. Scale 9 Inches = 6 Inches

Wightman Mountain Ltd.
Artillery House, Artillery Row, Westminster, S.W.1

Fig. 4.8. Shadow field of polystyrene cylinder of ka = 4.

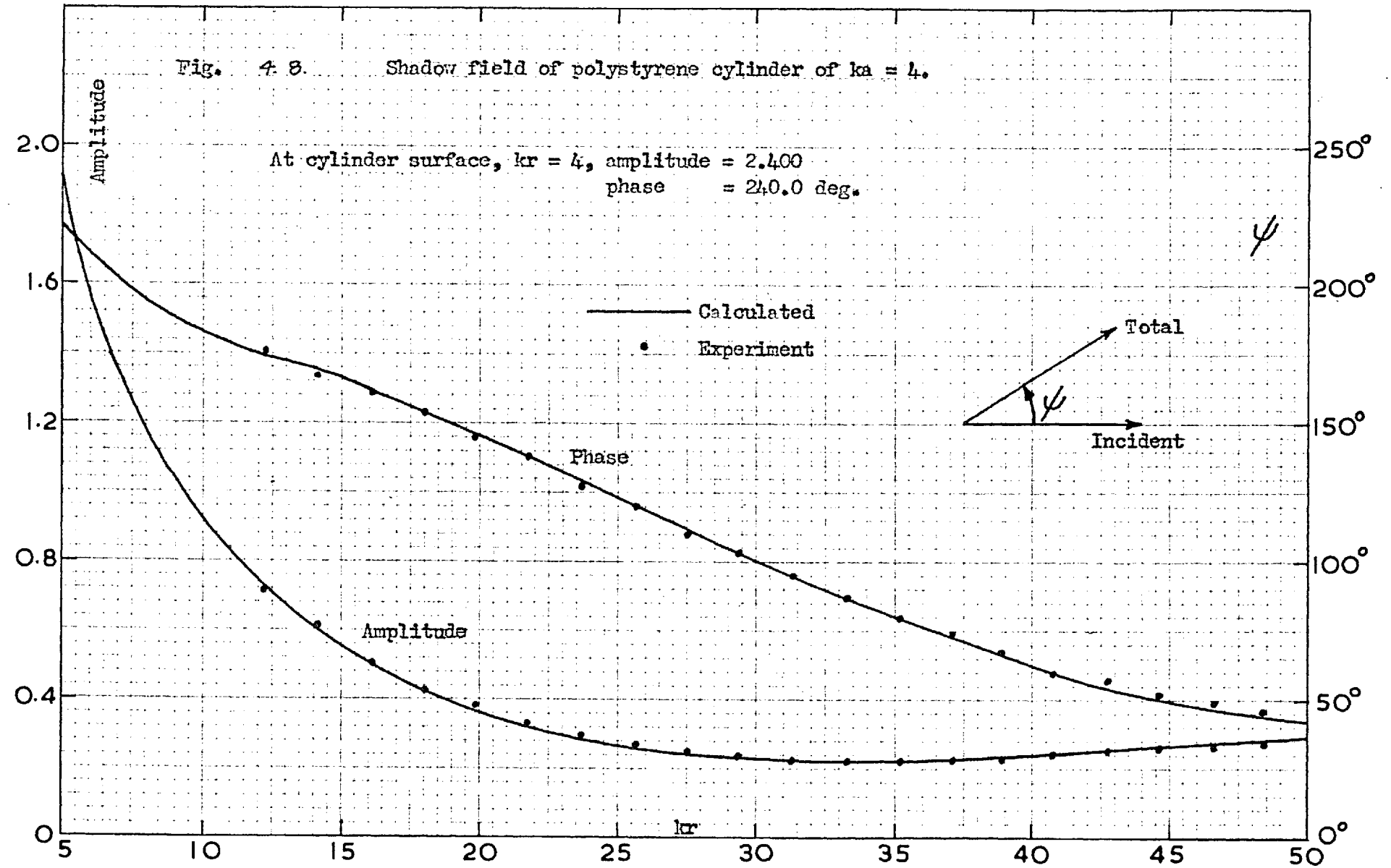

Data Sheet No. 318 Bilog Sectional. Scale 9 Inches x 6 Inches

Wightman Mountain Ltd.
Artillery House, Artillery Row, Westminster, S.W.1

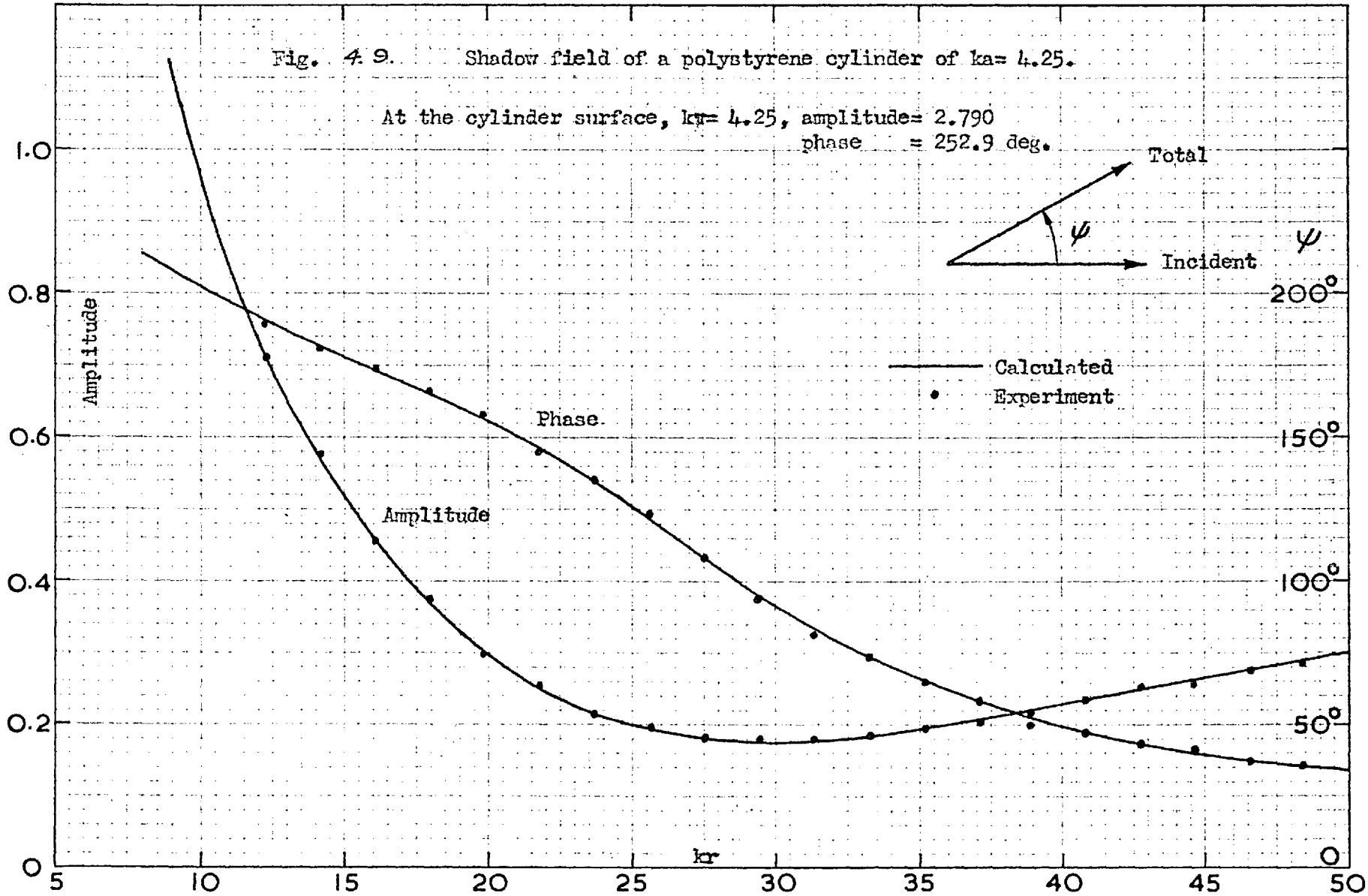

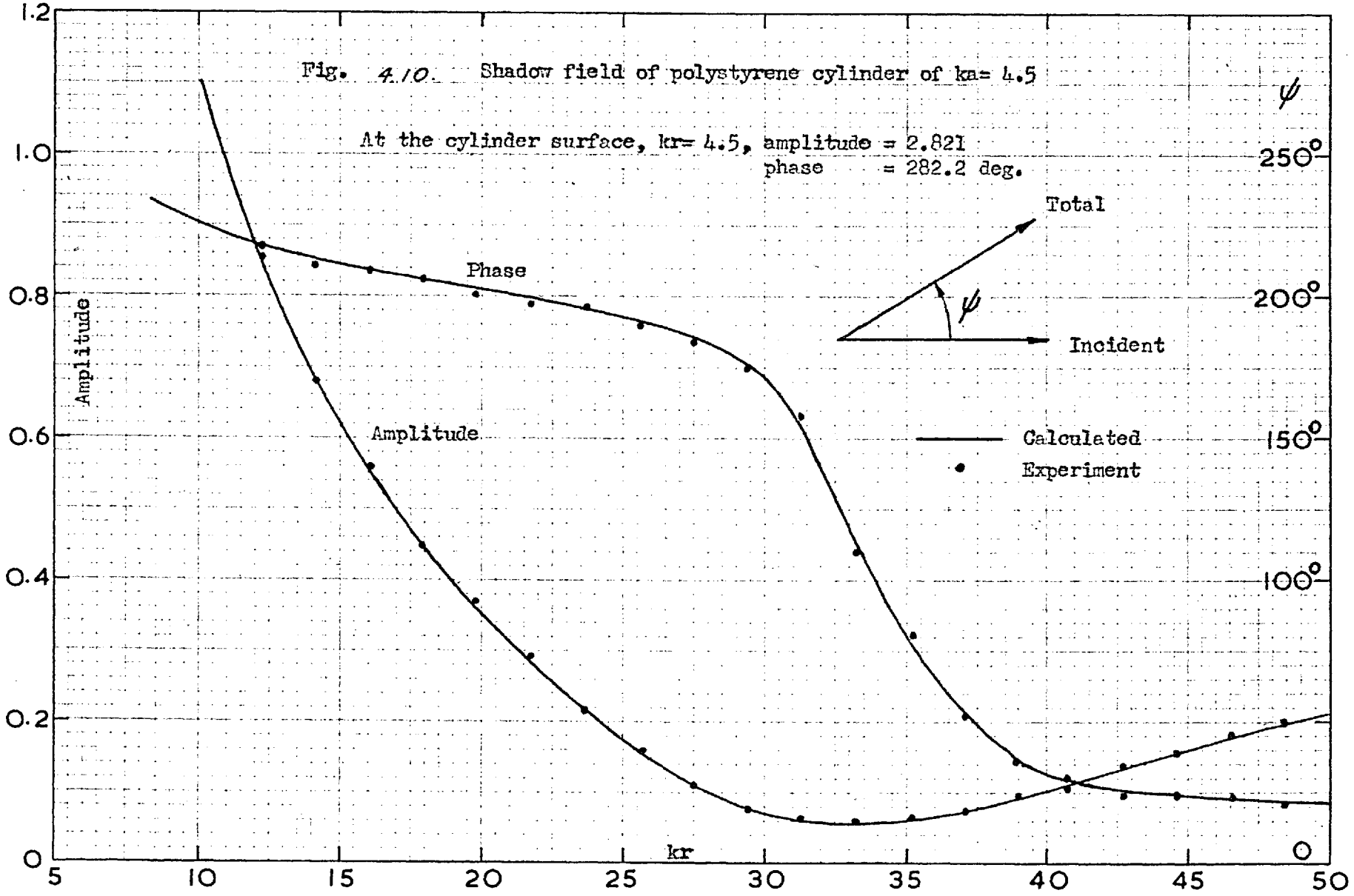

Data Sheet No. 71.S 10ths Sectional. Scale 9 Inches = 6 Inches

Wightman Mountain Ltd.
Artillery House, Artillery Row, Westminster, S.W.1

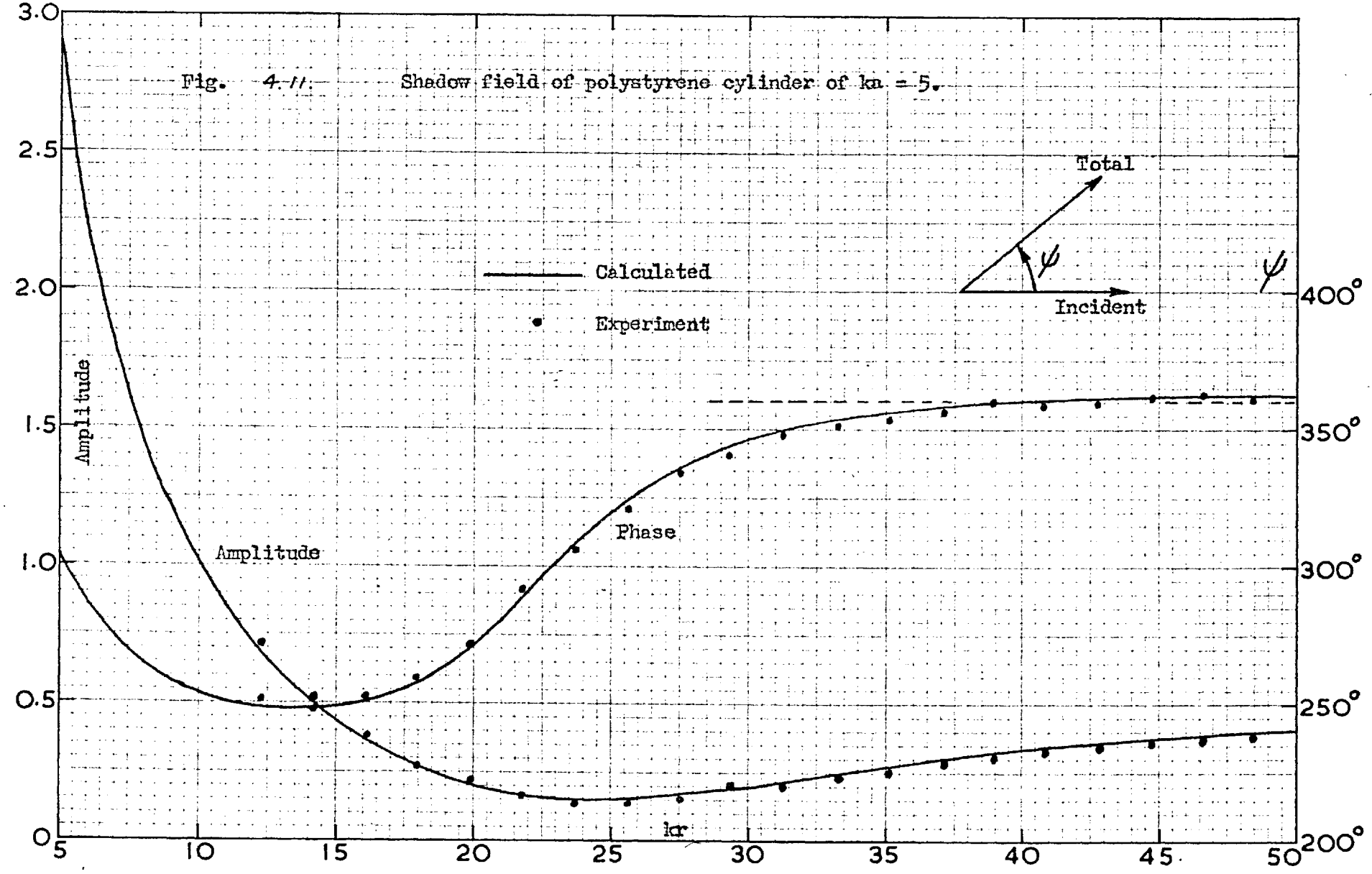

Data Sheet No. 31.S 10ths Sectional. Scale 9 Inches = 6 Inches

Wightman Mountain Ltd
Artillery House, Artillery Row, Westminster, S.W.1

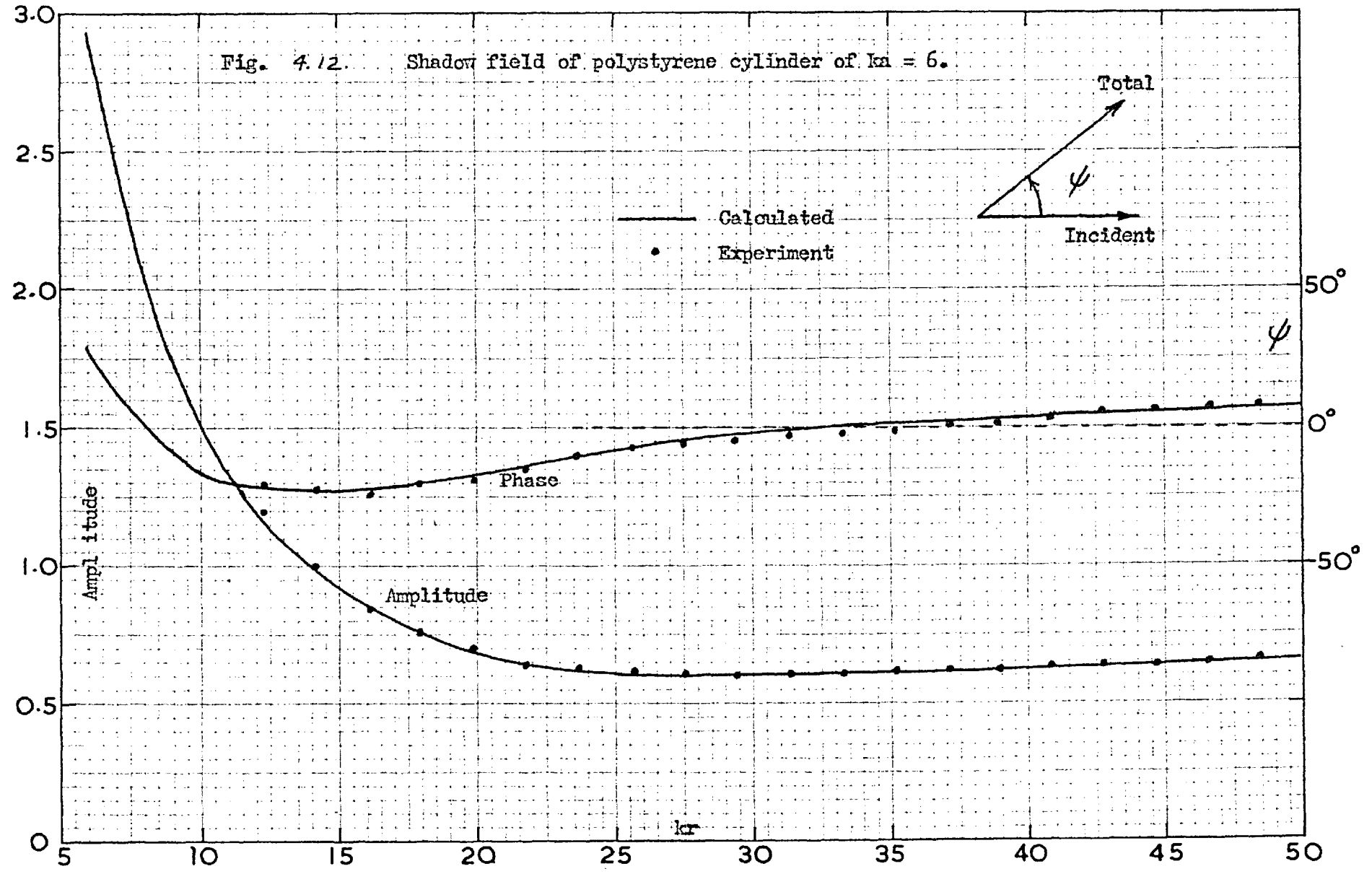

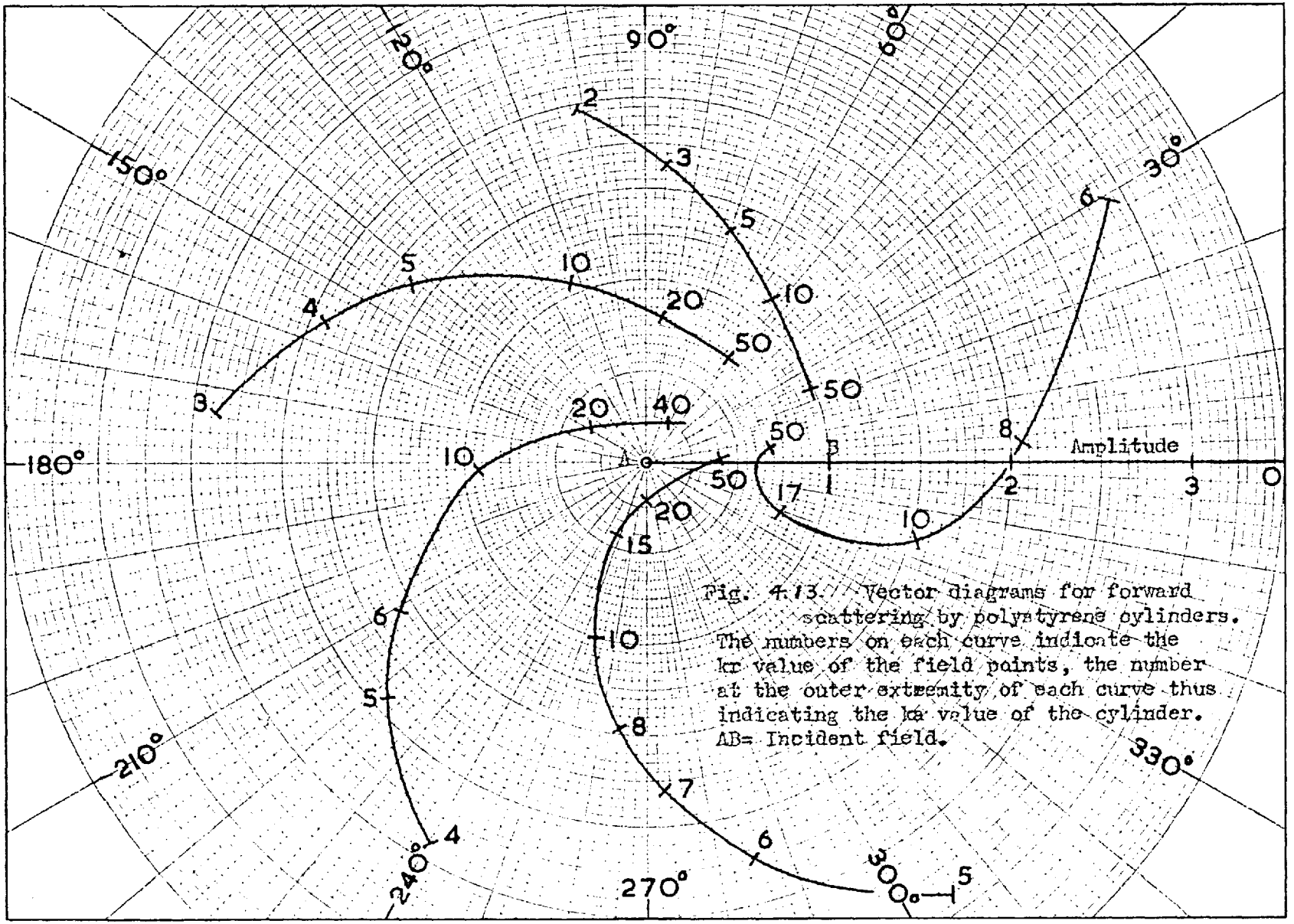

Fig. 4.13. Vector diagrams for forward scattering by polystyrene cylinders. The numbers on each curve indicate the kr value of the field points, the number at the outer extremity of each curve thus indicating the ka value of the cylinder. AB= Incident field.

field, $k_1a = 6$ differs from the others shown in that the field does not decrease monotonically with increasing k_1r but has a rise for k_1r between 17 and 50. The angles at which the curves approach point B are discussed later in treating the far fields.

The curves all show a rapid rise above the incident amplitude near the cylinder, with the surface value tending to increase with k_1a in an oscillating manner.

Just as there is a combination of k_1a and k_1r on the first spiral turn giving a zero total field, there well might be another for k_1a values just above 6 giving zero scattered field, for which the curve would pass through point B.

(b) Field on the illuminated side. The calculated and experimental results for the total field on the incidence side of several polystyrene cylinders are given in Figs. (4.14)-(4.19). They have not been carried out to as large distances from the cylinder as was done for the shadow fields, since the calculations require more field points and also because no special features appear to be introduced at the larger distances. In the main the curves follow the pattern already seen for the metal cylinders, with the interference between the incident and scattered fields producing a standing-wave distribution of field. As will be seen shortly, however, the scattered field in this region for a dielectric cylinder does not always drop off monotonically with distance from the cylinder. The amplitude of the standing wave does not therefore always decrease with increasing k_1r. This can be seen from Fig. 4.15 for $k_1a = 3$, and Fig. 4.16 for $k_1a = 4$, where the amplitude actually rises for some distance, before finally decreasing. The

phase curves Figs. 4.18 and 4.19 show the same feature. In the case of ka = 4 there is a tendency for the curves to flatten for small values of $k_1 r$ - Figs. 4.16 and 4.19. This flattening of the field is continued for some distance inside the cylinder(Fig. 6.6b).

(c) Scattered fields- Some of the scattered fields calculated from (4.6) have been plotted in Figs. 4.20 and 4.21. and 4.22. While, in the case of the metal cylinder, it was found that the complexities of the near scattered field occurred in the shadow, here they appear on the illuminated side of the dielectric cylinder. Starting out smoothly for $k_1 a = 1$, they develop a depression that moves out from the cylinder with increasing $k_1 a$. The field first drops sharply with increasing kr, then rises sharply to a maximum before finally falling off with distance. The depression becomes broader with increasing $k_1 a$. Finally, after about $k_1 r = 32$ has been passed, the curves seem to have settled down to a definite, relative position.

In the shadow the scattered fields are more orderly. An increase takes place up to $k_1 a = 4$, for the curves drawn, then a decrease. The slight maximum in the $k_1 a = 6$ curve, previously referred to, is seen at approximately $k_1 r = 28$. A definite order has been reached for $k_1 r = 9$. The general trend of Fig. 4.20 can be read from Fig. 4.13 where the increase in the scattered field occurs as the curves move to the left from the scattered-field origin, B, then the decrease as the curves move around the turn toward the right.

One observes the large values of the scattered field amplitude near the cylinder surface in Fig. 4.20, as well as the large back-to-

Fig. 4.14.

Amplitude of the field on the illuminated side of a polystyrene cylinder of ka= 2.

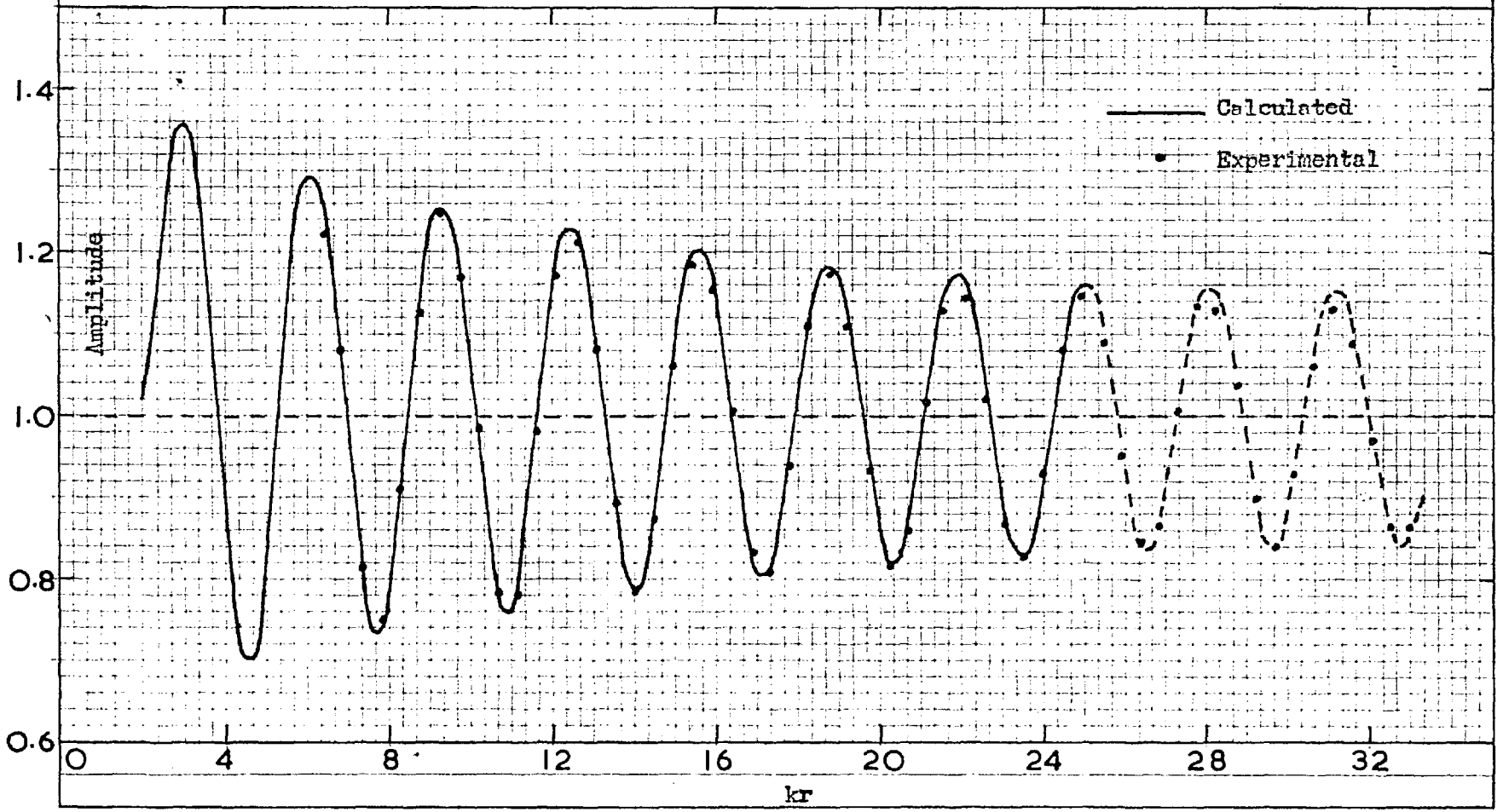

Data Sheet No. 2. 105 Divisions x 45 Divisions

Wightman Mountain Ltd.,
Artillery House, Artillery Row, Westminster, S.W.1

Fig. 4.15.

Amplitude of the field on the illuminated side of a polystyrene cylinder of ka= 3.

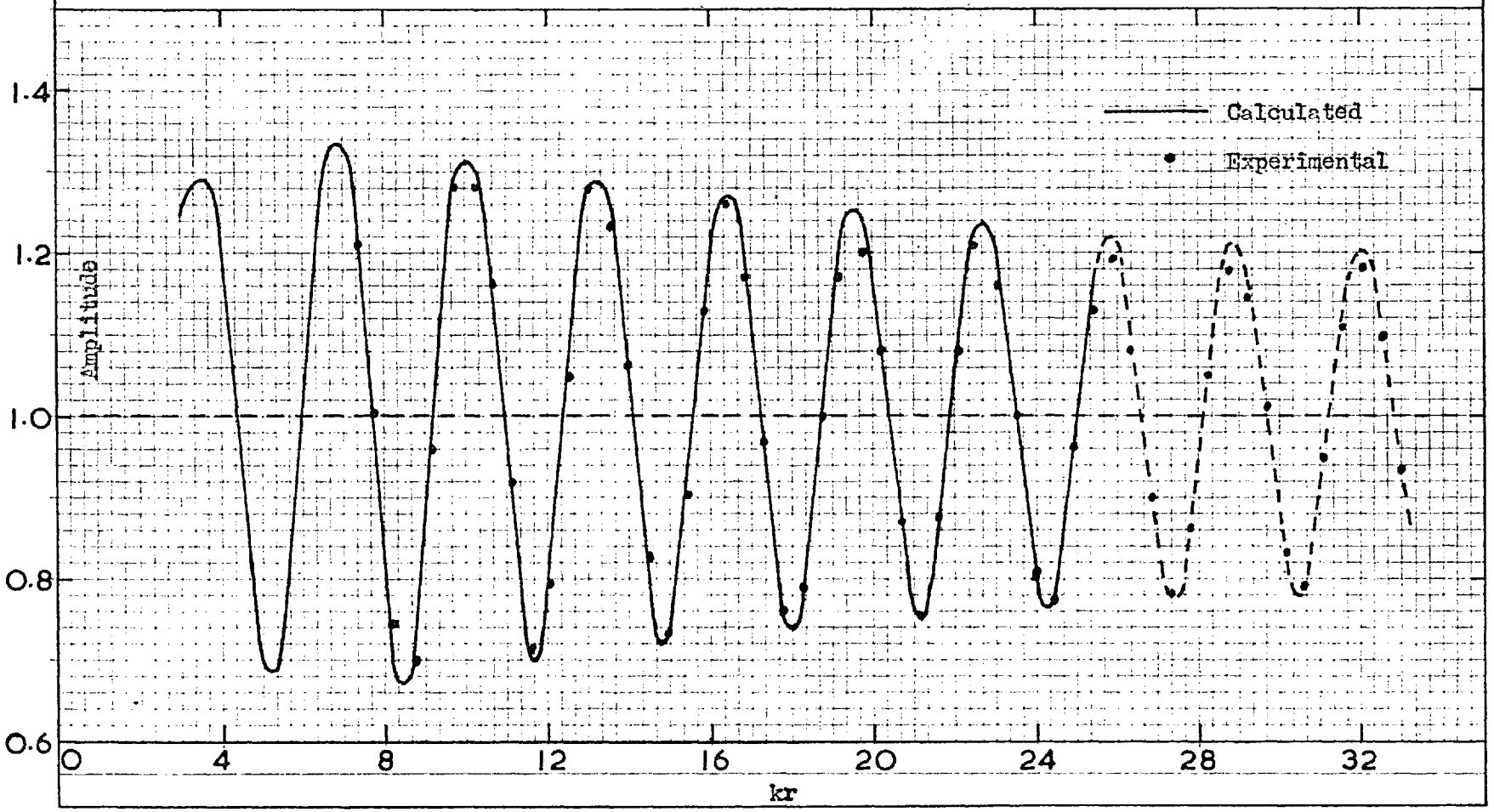

DATA SHEET No. 2. 105 DIVISIONS × 45 DIVISIONS

ADLARD & SON LTD.,
ARTILLERY HOUSE, ARTILLERY ROW, WESTMINSTER, S.W.1

Fig. 4.16.

Amplitude of the field on the illuminated side of a polystyrene cylinder of ka= 4.

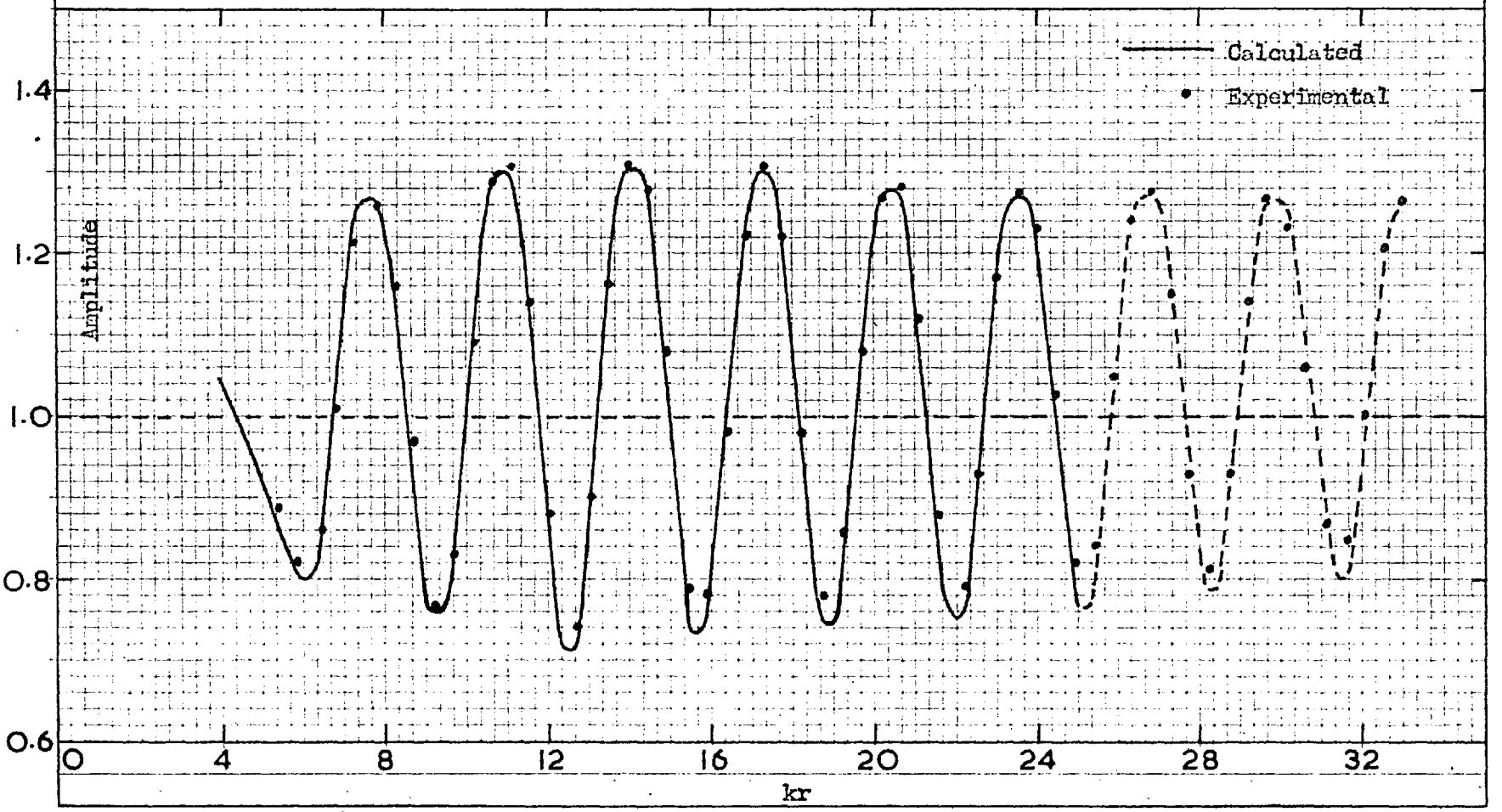

DATA SHEET No. 2. 105 DIVISIONS x 45 DIVISIONS

WIGHTMAN MOUNTAIN LTD.,
ARTILLERY HOUSE, ARTILLERY ROW, WESTMINSTER, S.W.1

Fig. 4.17.

Phase of the field on the illuminated side of a polystyrene cylinder of ka= 2.

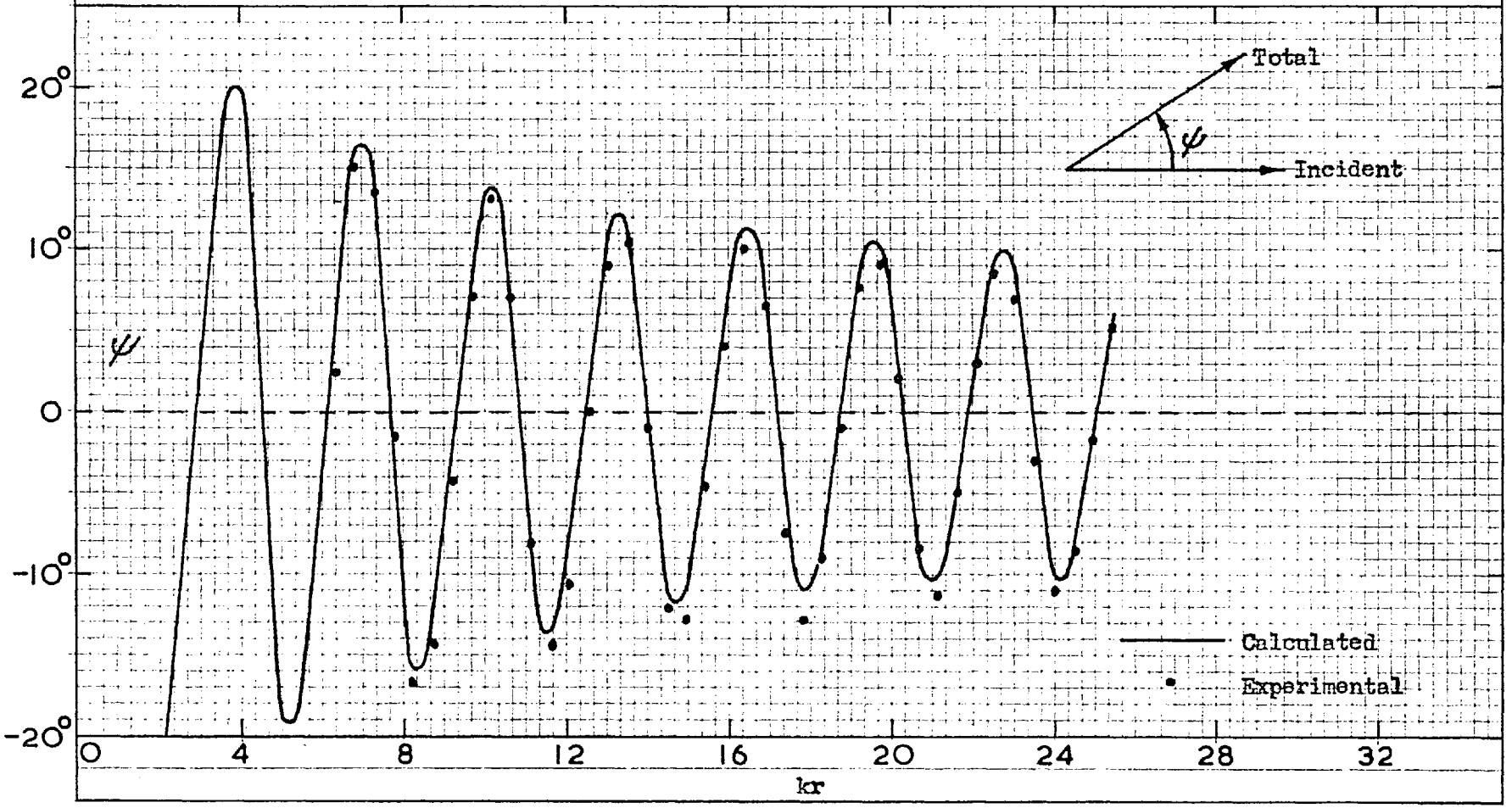

DATA SHEET No. 2. 105 DIVISIONS x 45 DIVISIONS

WHITTMAN MOUNTAIN LTD.,
ARTILLERY HOUSE, ARTILLERY ROW, WESTMINSTER, S.W.1

Fig. 4.18

Phase of the field on the illuminated side of a polystyrene cylinder of ka= 3.

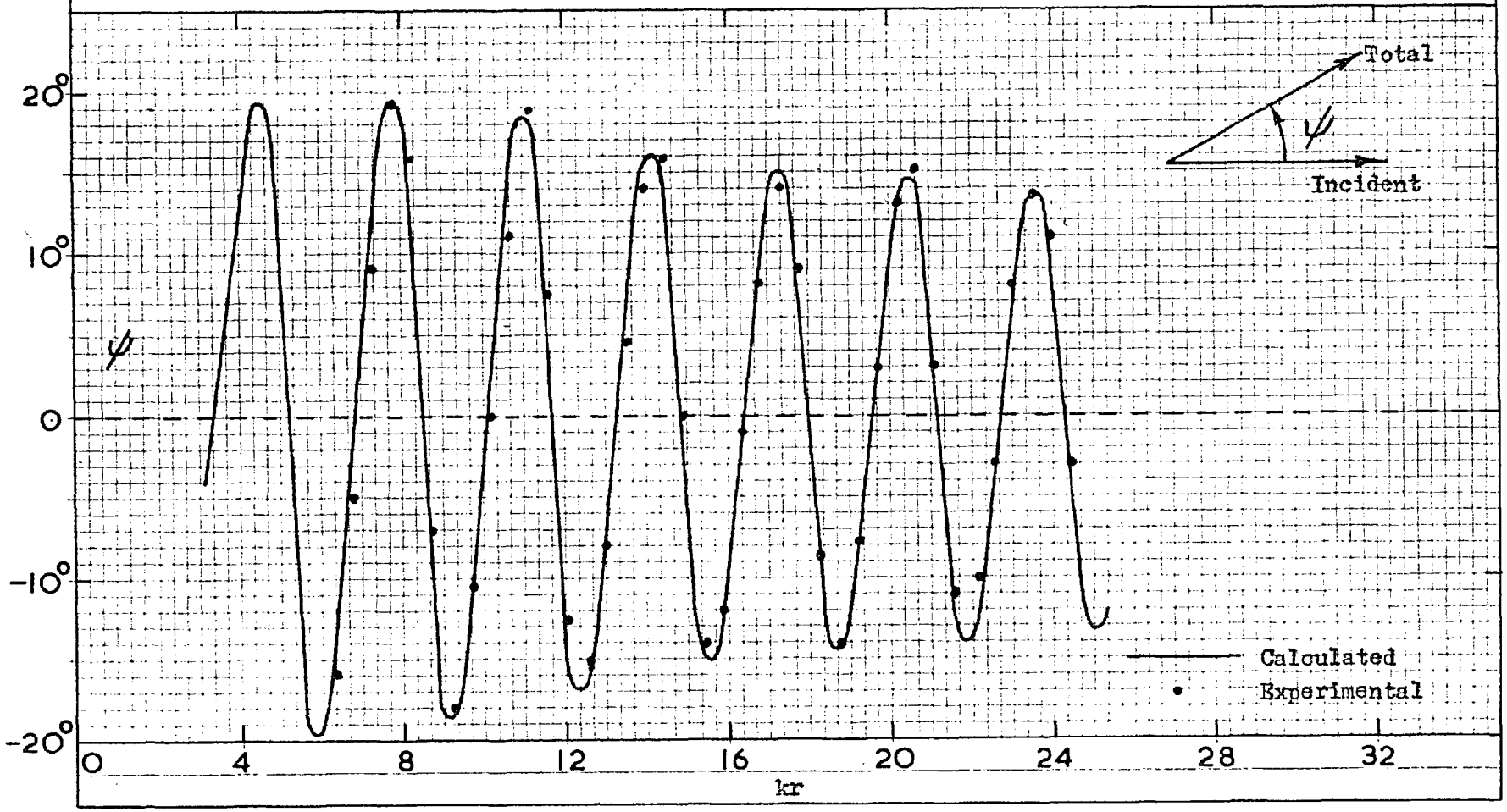

DATA SHEET No. 2. 105 DIVISIONS × 45 DIVISIONS

WIGHTMAN MOUNTAIN LTD.,
ARTILLERY HOUSE, ARTILLERY ROW, WESTMINSTER, S.W.1

Fig. 4.19.

Phase of the field on the illuminated side of a polystyrene cylinder of ka= 4.

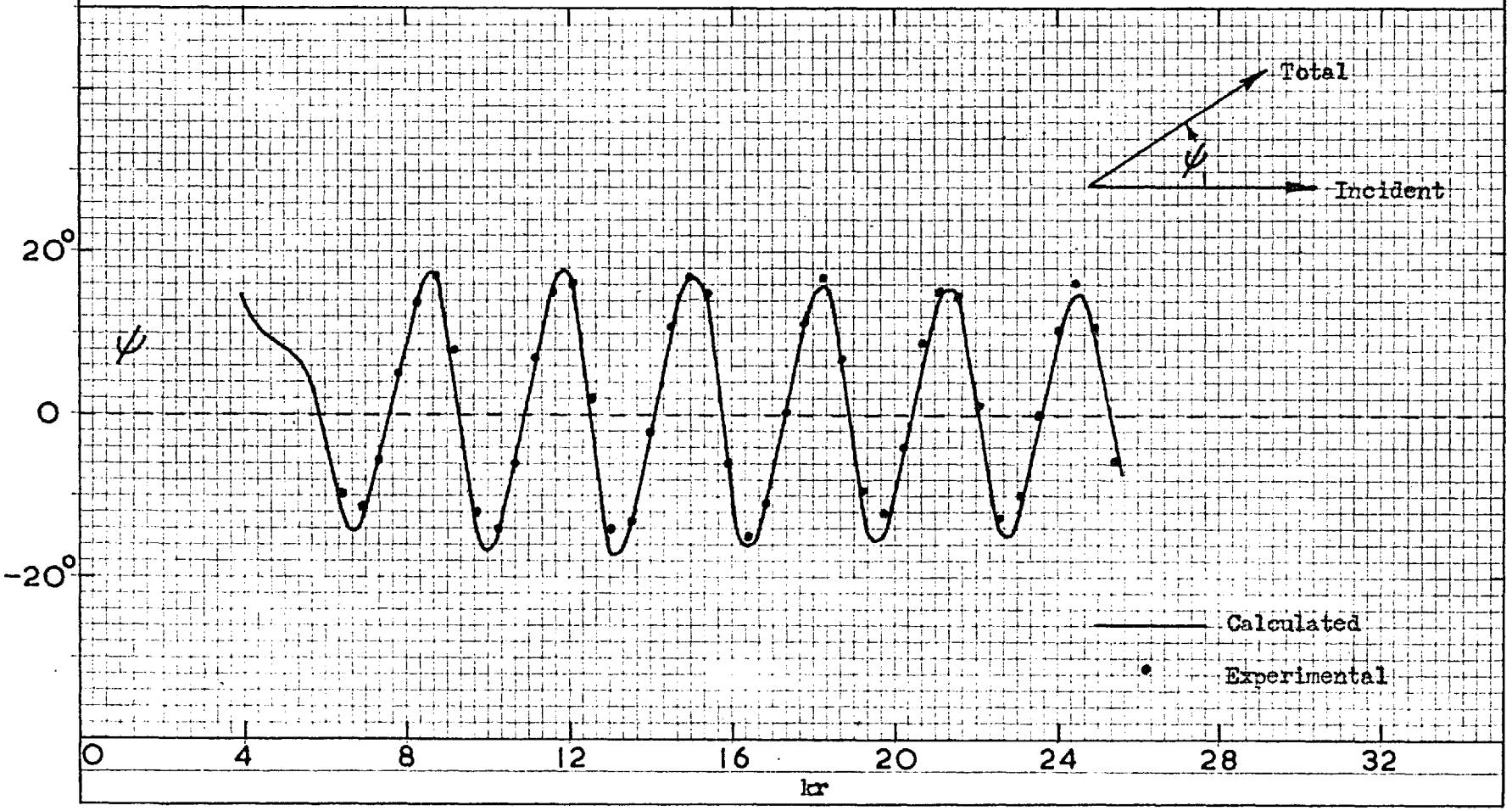

WIGHTMAN MOUNTAIN LTD.,
ARTILLERY HOUSE, ARTILLERY ROW, WESTMINSTER, S.W.1

Fig. 4.20.

Forward-scattered field of polystyrene cylinders of the ka values indicated.
The short, vertical lines represent the cylinder surface.

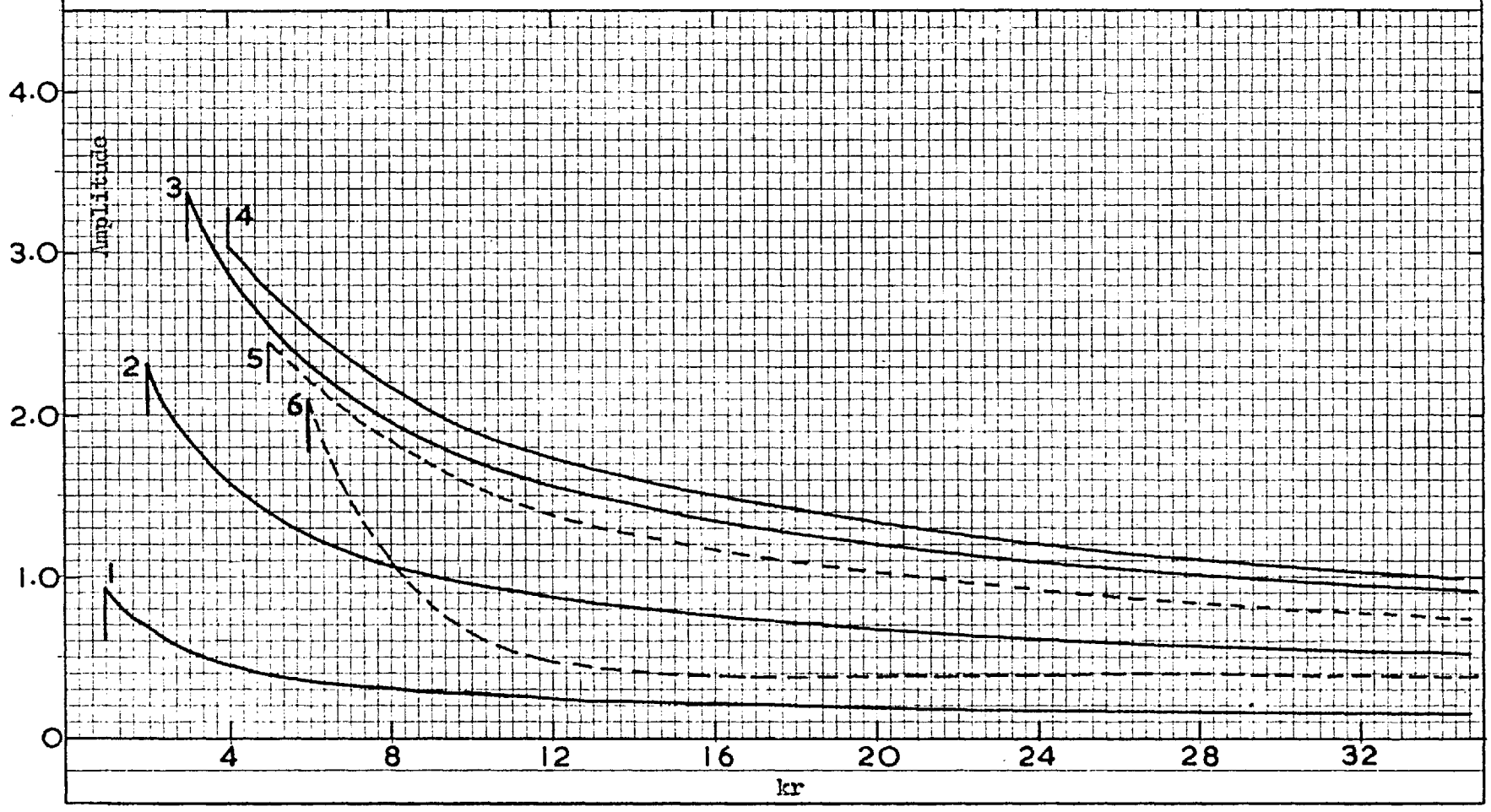

DATA SHEET No. 2. 105 DIVISIONS × 45 DIVISIONS

WIGHTMAN MOUNTAIN LTD.,
ARTILLERY HOUSE, ARTILLERY ROW, WESTMINSTER, S.W.1

Fig. 4.21.

Back-scattered field of polystyrene cylinders of the ka values indicated.

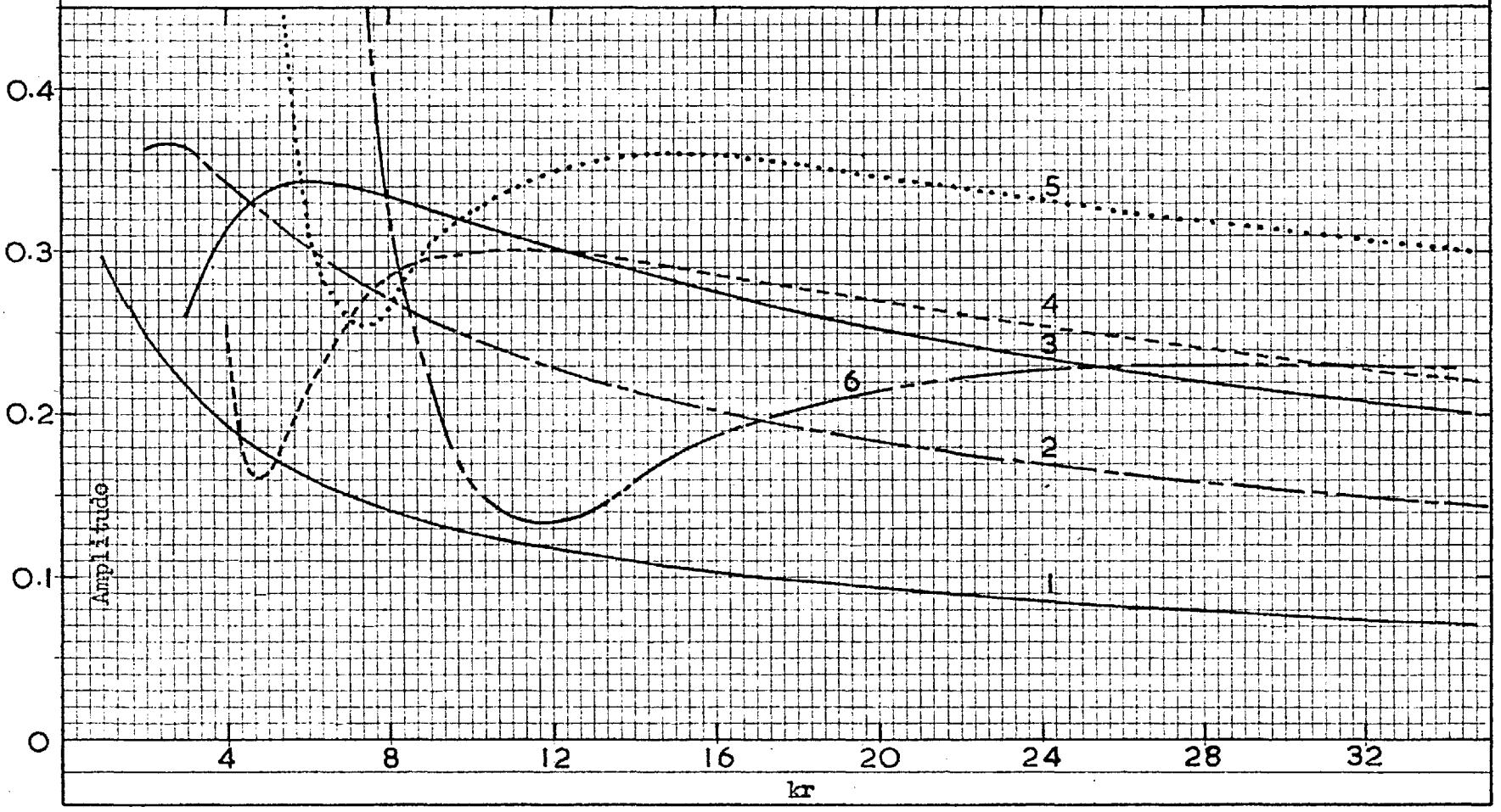

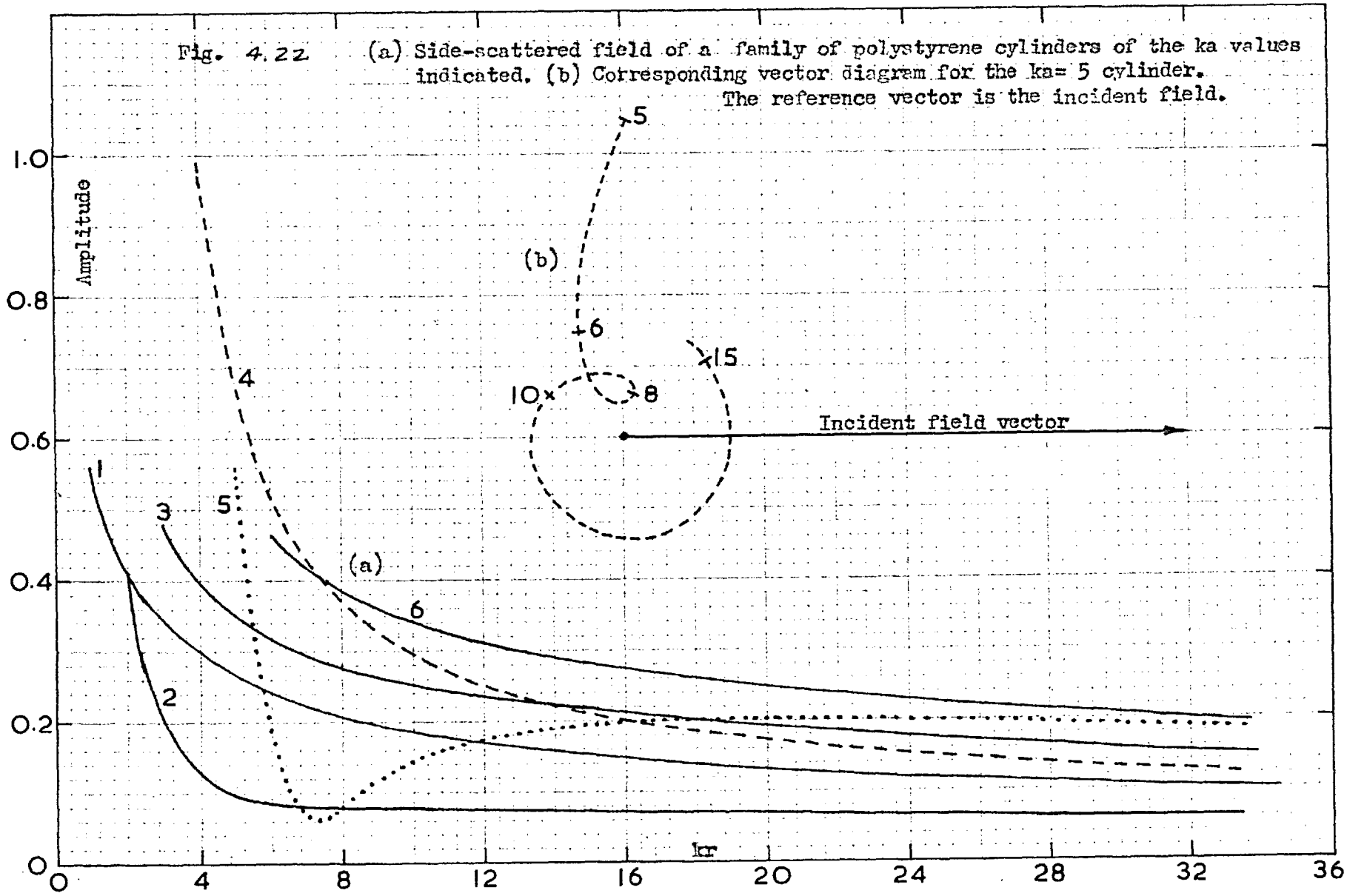

Fig. 4.22 (a) Side-scattered field of a family of polystyrene cylinders of the ka values indicated. (b) Corresponding vector diagram for the ka= 5 cylinder. The reference vector is the incident field.

front ratio on comparison of a pair of curves of Fig. 4.20 and 4.21. The latter feature has been noted by several workers in the case of scattering by a dielectric sphere, and is attributed to the constructive interference in the forward direction, and vice versa, of the fields due to the elementary polarization currents produced in the dielectric material.

4.3. Auxiliary angles.

From the form of (4.3) for the scattered amplitude it is seen that the auxiliary angle concept, discussed in Sec. 3.3 for the case of a metal cylinder, is applicable here also. Thus-

$$- B_n/(i)^n = C_n / (C_n + i D_n)$$

and

$$\tan \theta_n/2 = C_n/D_n \qquad (4.12)$$

where C_n and D_n are given by (4.7) when $\mu_2 = \mu_1$.

While the curves of the auxiliary angles are here not as simple as for the metal cylinder, they are sufficiently regular to permit their use as an aid in detecting errors in computation. Fig. 4.23 illustrates their general behaviour. They have been drawn for only $n = 0$ and $n = 1$, since the higher orders would overlay these and make difficult an observation of their properties. They occur in pairs, interleaving with each other, because of the relation connecting a Bessel function of one order with the corresponding function of the next higher order. The locations of the rapid rises and the flat parts of the curves are associated with the behaviour of the functions C_n and D_n of (4.7).

These functions have been plotted in Figs. 4.24-4.27 for the first four orders. They, too, have been plotted in pairs, for the same reason as before. Two pairs have been plotted for each function, instead of one, for a reason to be discussed later in connection with the resonance conditions for scattering by a dielectric cylinder. The C_n begin at the origin, the D_n at a large negative value, and both then oscillate about the k_1a axis. Because of the availability of polystyrene as a scattering material and because a large proportion of the computation time is spent in evaluating these functions, it was considered justifiable to tabulate their values in Appendices I and II. They were evaluated on a desk machine with the use of 5-place Tables.

If, for checking purposes, one attempts to predict the positions, along the k_1a axis, of the steep and flat parts of the curves, he is merely led back to conditions that involve the curves of Fig. 4.24-4.27. However, it is more profitable to attempt to predict the cross-over points of a pair of curves such as those of Fig. 4.23. For this condition,

$$C_o / D_o = C_1 / D_1 \qquad (4.13)$$

from the definition of θ_n. From (4.7) it can be seen that -

$$C_o / D_o = C_1 / D_1 = J_1(k_1a)/Y_1(k_1a) \quad , \text{ if } J_1(k_2a) = 0$$

$$= 2\, k_r / k_1a \quad , \text{ if } J_o(k_2a) = 0.$$

The roots of these two functions and the corresponding cross-over values of k_1a are listed below($k_2a = 1.60k_1a$)-

WIGHTMAN MOUNTAIN LTD.,
ARTILLERY HOUSE, ARTILLERY ROW, WESTMINSTER, S.W.1

Fig. 4.23.

Auxiliary angles for polystyrene cylinders.

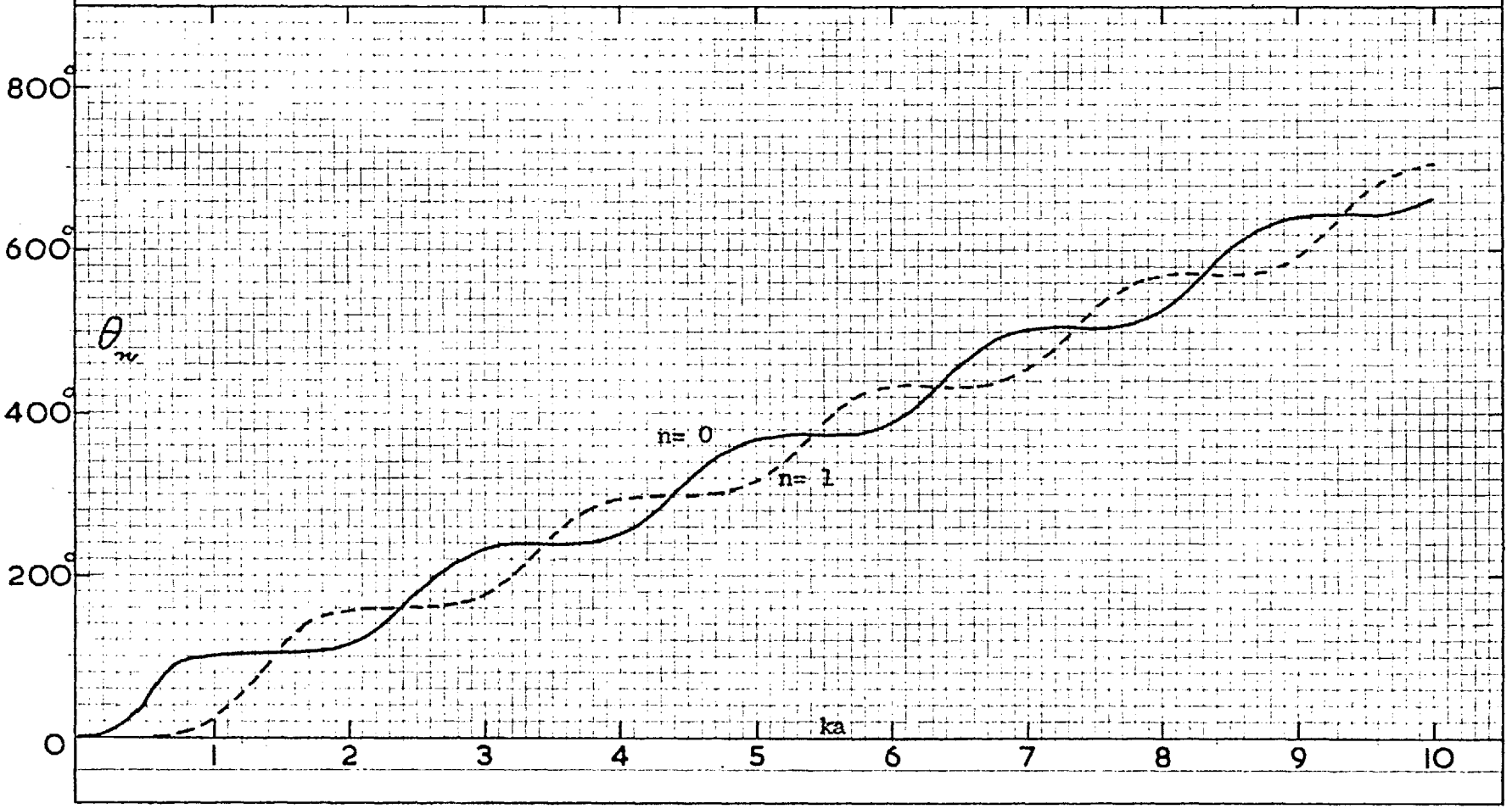

DATA SHEET NO. 2. 105 DIVISIONS × 45 DIVISIONS

WIGHTMAN MOUNTAIN LTD.,
ARTILLERY HOUSE, ARTILLERY ROW, WESTMINSTER, S.W.1

Fig. 4.24.

Plot of the function $C_n = J_n(k_2a)J_{n+1}(k_1a) - 1.60J_{n+1}(k_2a)J_n(k_1a)$ for n=0 and n=1.

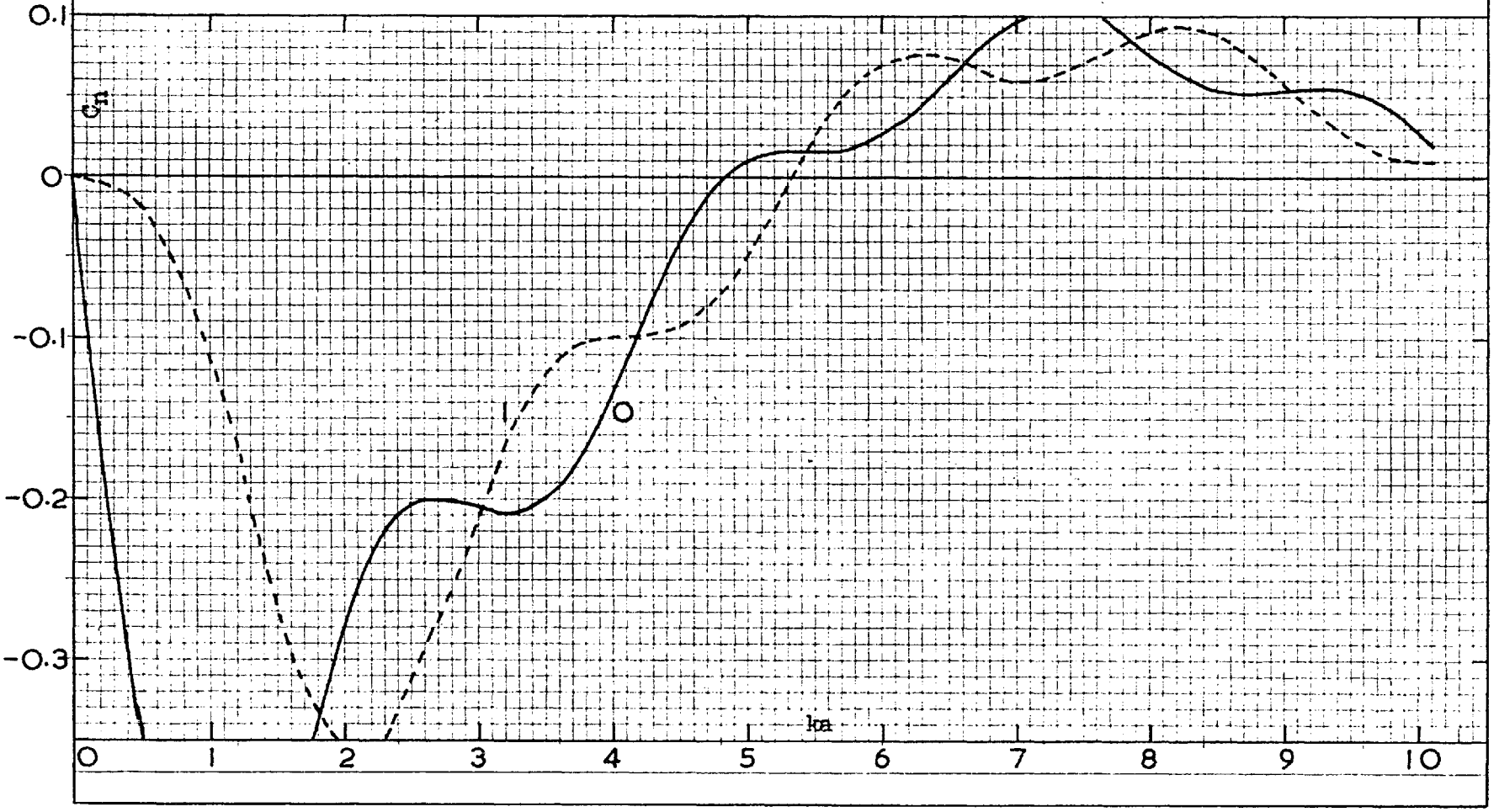

DATA SHEET No. 2. 105 DIVISIONS × 45 DIVISIONS

TIGHTMAN MOUNTAIN LTD.,
ARTILLERY HOUSE, ARTILLERY ROW, WESTMINSTER, S.W.1

Fig. 4.25.

Plot of the function $C_n = J_n(k_2a)J_{n+1}(k_1a) - 1.60\, J_{n+1}(k_2a)J_n(k_1a)$ for n= 2 and n= 3.

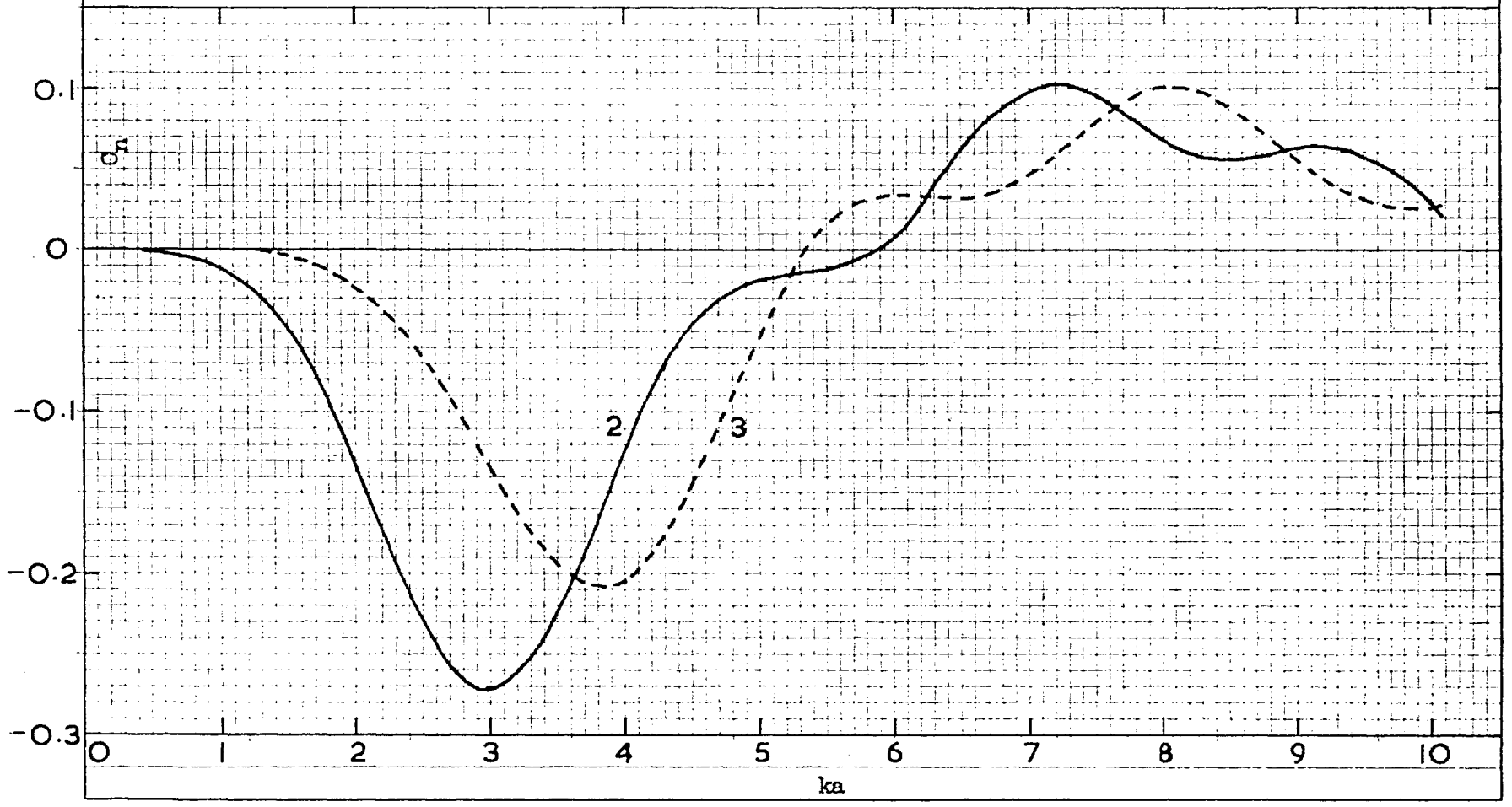

DATA SHEET No. 2. 105 DIVISIONS × 45 DIVISIONS

WIGHTMAN MOUNTAIN LTD.,
ARTILLERY HOUSE, ARTILLERY ROW, WESTMINSTER, S.W.1

Fig. 4.26.

Plot of the function $D_n = J_n(k_2a)Y_{n+1}(k_1a) - 1.60\, J_{n+1}(k_2a)Y_n(k_1a)$ for n= 0 and n= 1.

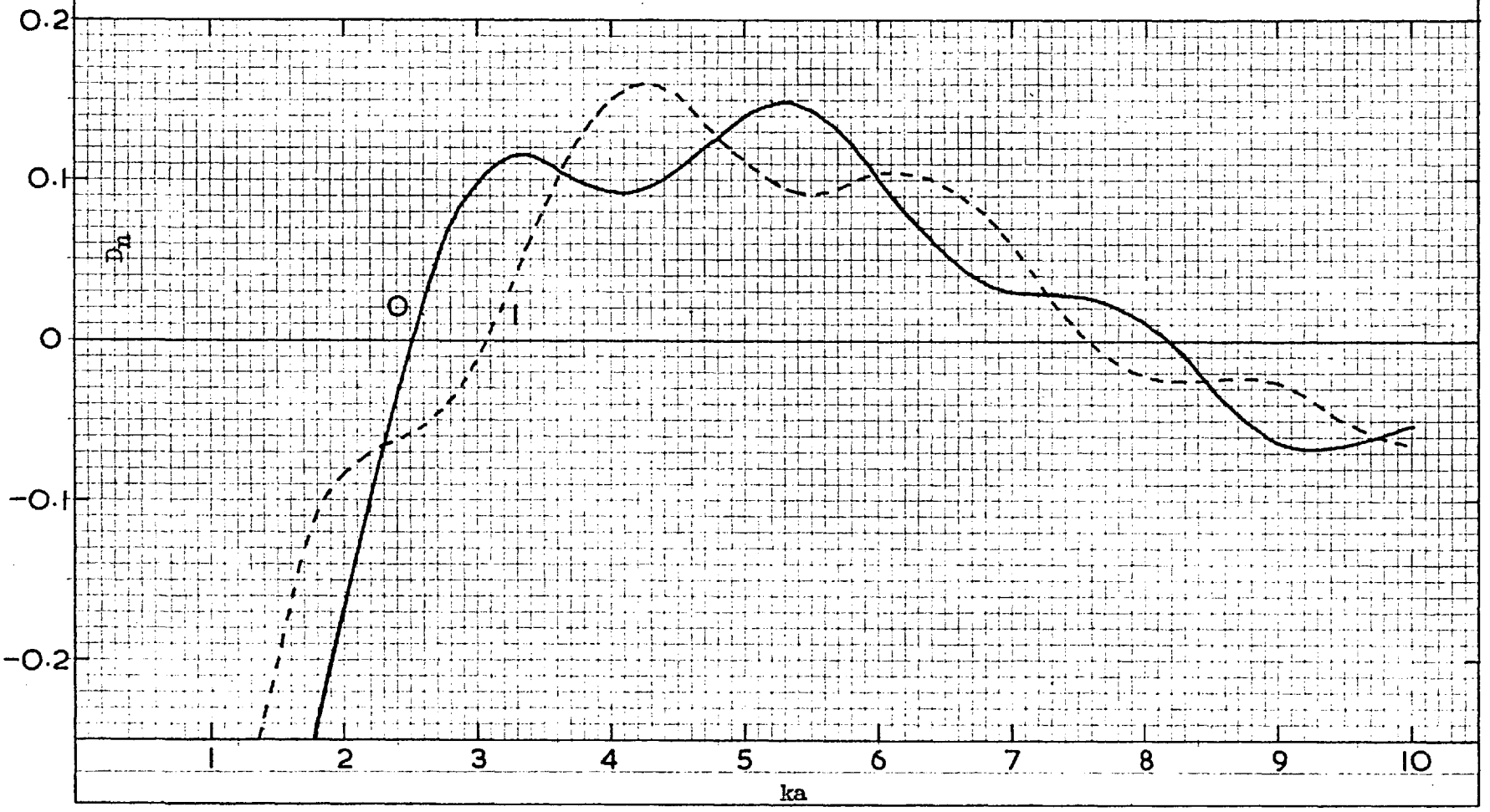

Fig. 4.27

Plot of the function $D_n = J_n(k_2a)Y_{n+1}(k_1a) - 1.60\, J_{n+1}(k_2a)Y_n(k_1a)$ for n= 2 and n= 3.

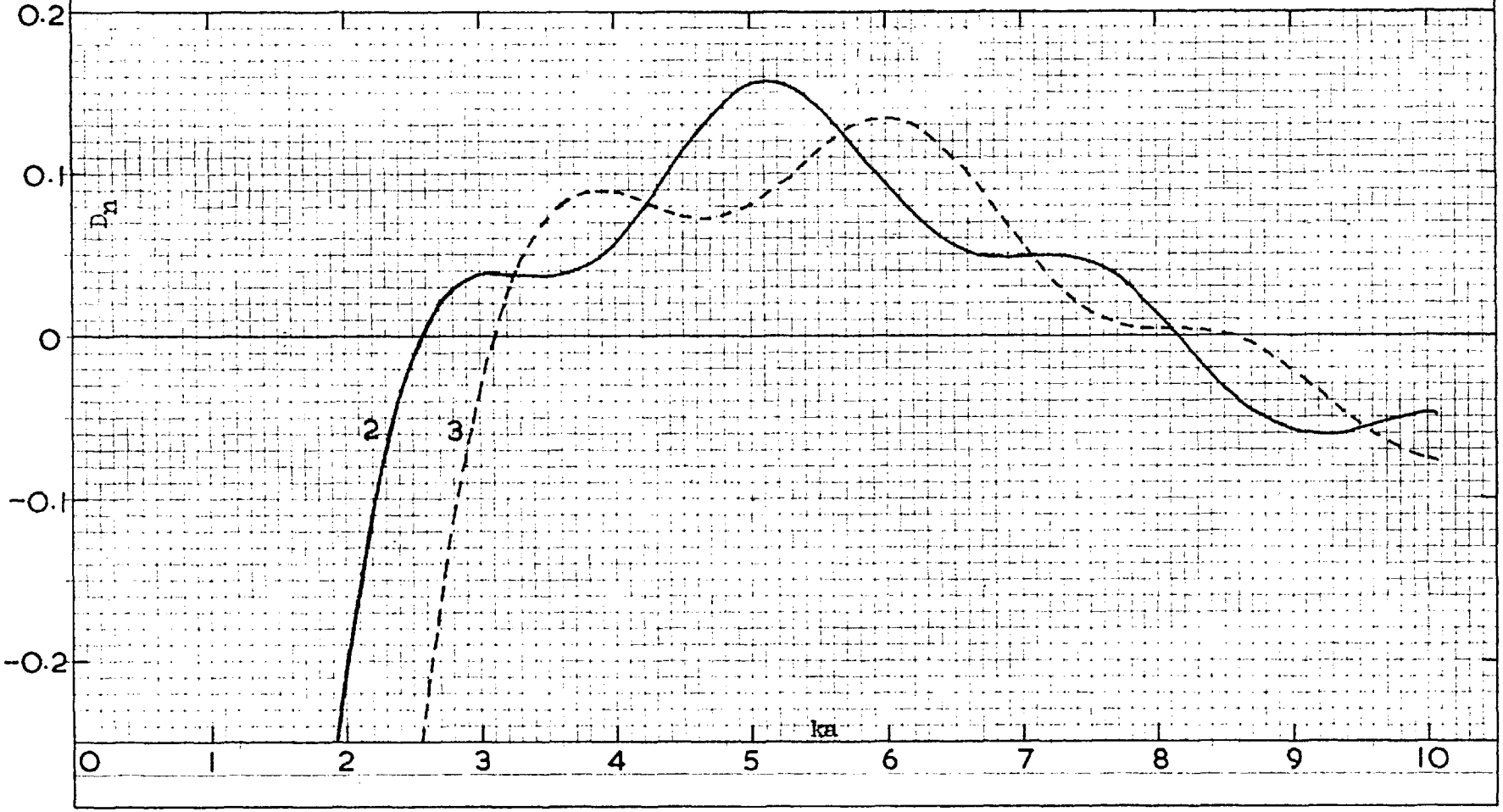

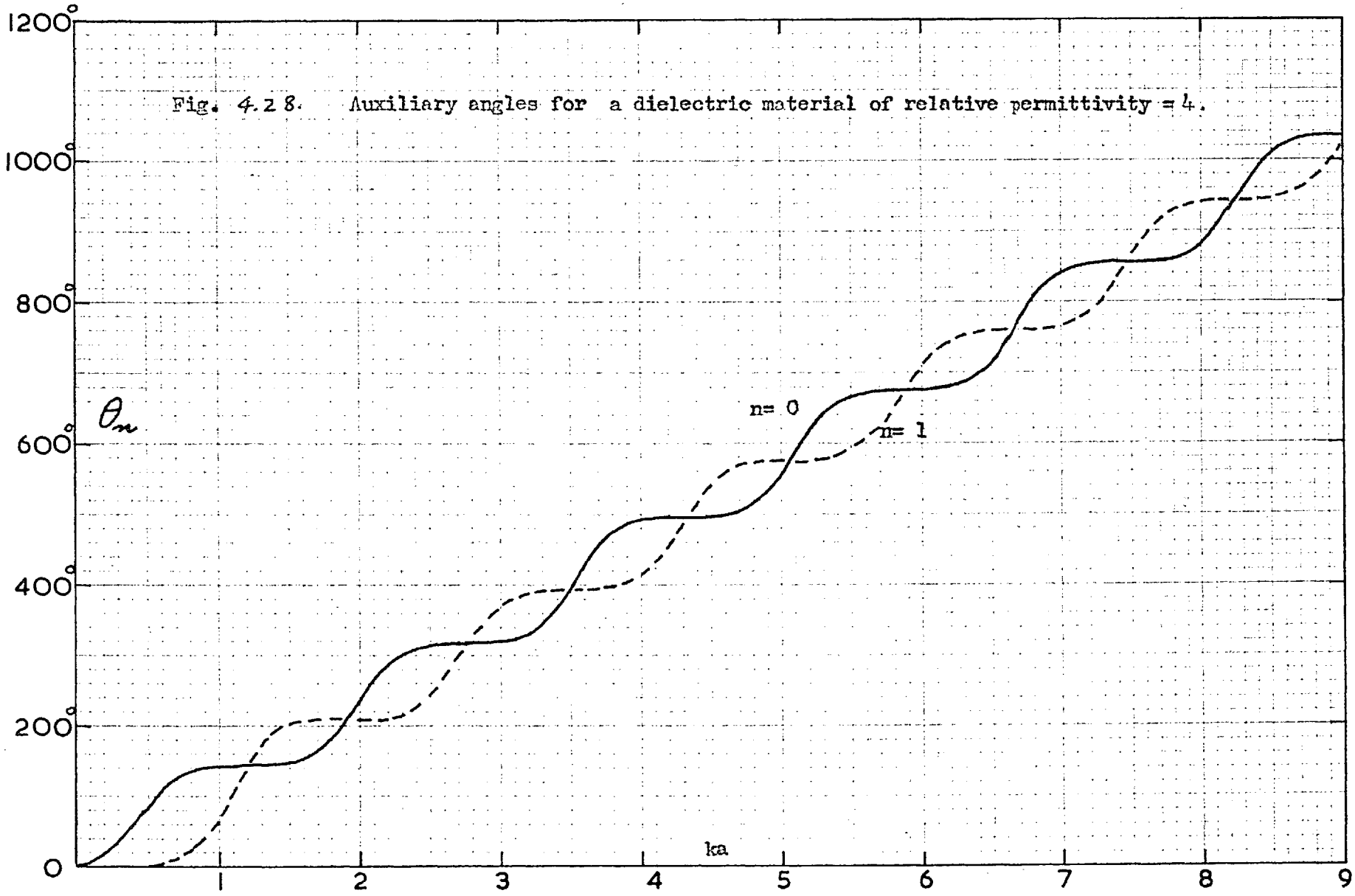

Fig. 4.2 8. Auxiliary angles for a dielectric material of relative permittivity = 4.

DATA SHEET No. 2. 105 DIVISIONS x 45 DIVISIONS

WIGHTMAN MOUNTAIN LTD.,
ARTILLERY HOUSE, ARTILLERY ROW, WESTMINSTER, S.W.1

Fig. 4.29.

Plot of the function $C_n = J_n(k_2a)J_{n+1}(k_1a) - 2.0\, J_{n+1}(k_2a)J_n(k_1a)$ for the first three orders.

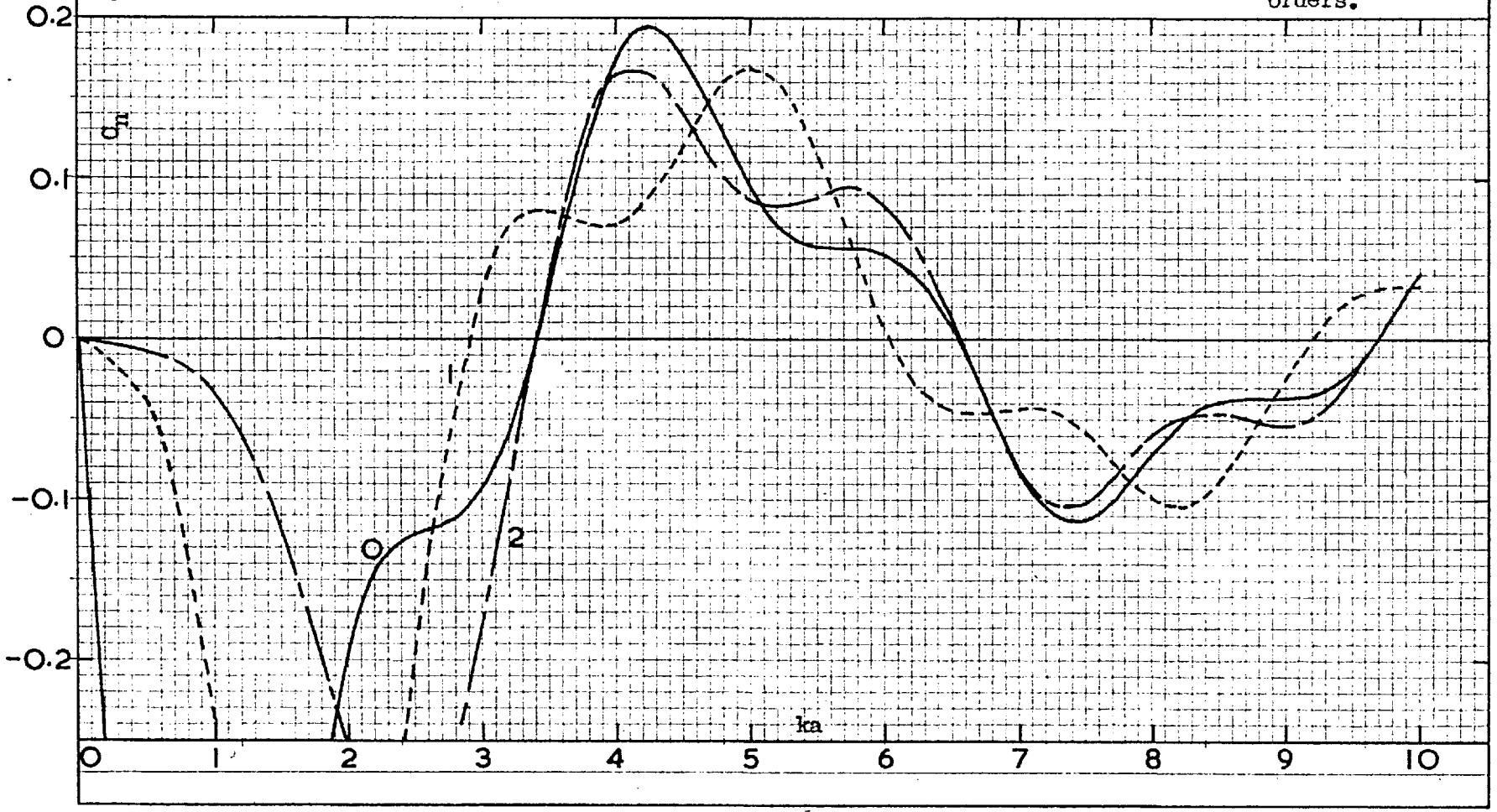

DATA SHEET No. 2. 105 DIVISIONS × 45 DIVISIONS

WIGHTMAN MOUNTAIN LTD.,
ARTILLERY HOUSE, ARTILLERY ROW, WESTMINSTER, S.W.1

Fig. 4.30.

Plot of the function $D_n = J_n(k_2a)Y_{n+1}(k_1a) - 2.0\, J_{n+1}(k_2a)Y_n(k_1a)$ for the first three orders.

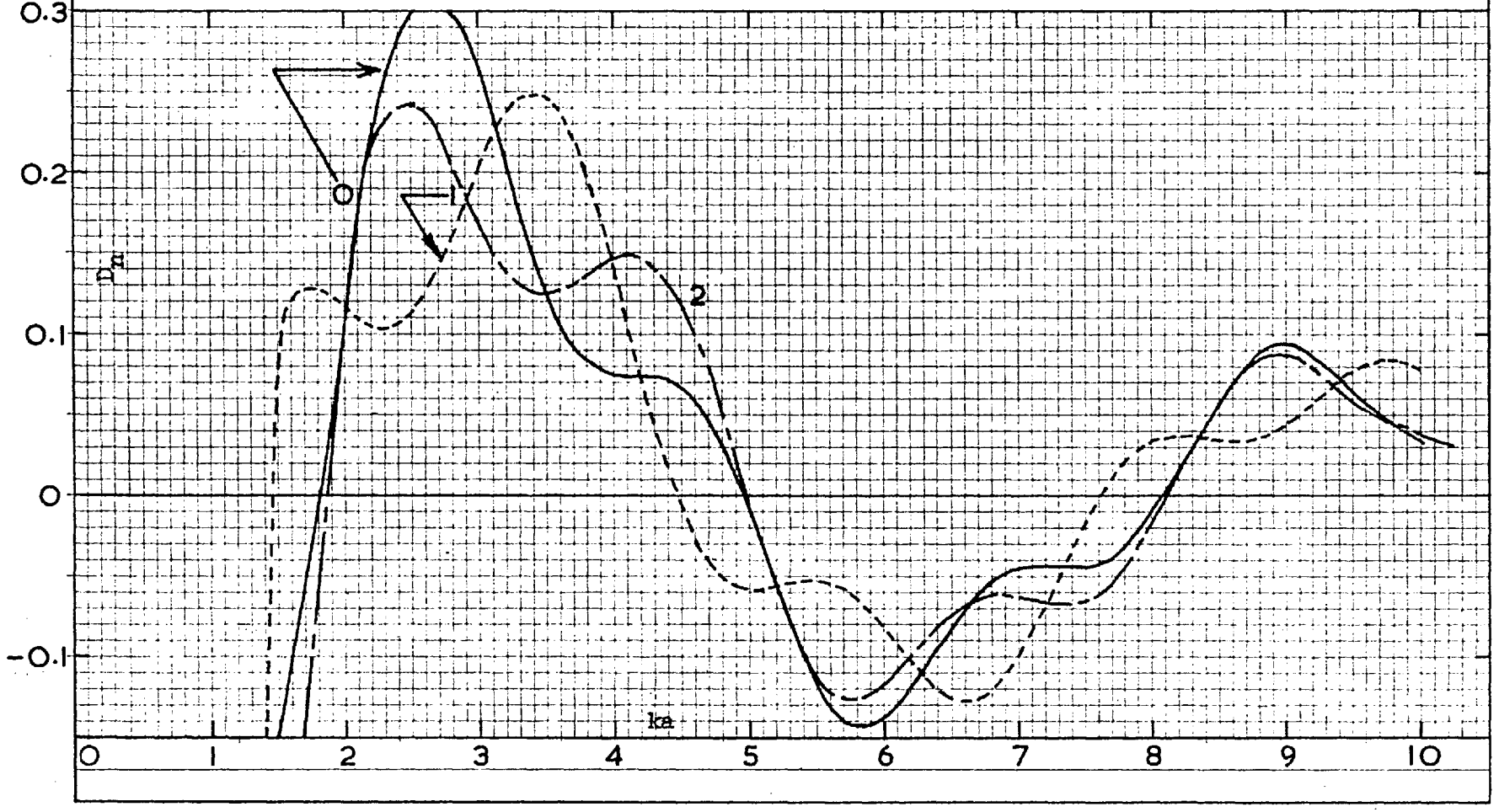

TABLE I Roots of $J_0(k_2a) = 0$

k_2a	k_1a
2.40	1.50
5.52	3.45
8.65	5.41
11.79	7.36
14.93	9.33

TABLE II Roots of $J_1(k_2a) = 0$

k_2a	k_1a
3.83	2.40
7.02	4.39
10.17	6.35
13.32	8.32

The k_1a values agree with those taken from Fig. 4.23. In general, for a pair of curves of θ_n and θ_{n+1}, the cross-over values of k_1a are given by the roots of $J_n(k_2a) = 0$ and $J_{n+1}(k_2a) = 0$. Thus the k_1a interval between cross-over points tends toward the value $\pi/2K_r$ for the higher roots.

The above curves of auxiliary angles and the functions C_n and D_n have been repeated for the case of a material of $k_r = 2$ and are shown in Figs. 4.28-4.30. The k_1a intervals between the cross-over points are seen to be smaller than for Fig. 4.23, in accordance with the observation in the previous paragraph.

4.4. Scattering resonances for the dielectric cylinder.

From the form of (4.6) it is apparent that the amplitude of the scattering by a dielectric cylinder is governed by the relative values of the functions C_n and D_n. Thus $-B_n/(i)^n$ can fluctuate between a maximum amplitude of unity, when $D_n = 0$, and zero, when $C_n = 0$. The condition $C_n = D_n = 0$ simultaneously will not occur, because of the Bessel function Wronskian condition.

The scattering resonance condition can be derived by considering the fields inside and outside the cylinder under the condition that the incident field has been removed, from the continuity relations across the cylinder boundary. Postulating the same series as before for the scattered and internal fields, the boundary conditions yield at the cylinder surface-

$$A_n J_n(k_2 a) = B_n H_n^{(1)}(k_1 a) \tag{4.14}$$

$$k_2 /\mu_2 \; A_n J_n'(k_2 a) = k_1 /\mu_1 \, B_n H_n^{(1)\prime}(k_1 a) \tag{4.15}$$

The resonance condition is obtained by dividing (4.15) by (4.14)-

$$(k_2 /\mu_2) J_n'(k_2 a)/J_n(k_2 a) = (k_1/\mu_1) H_n^{(1)\prime}(k_1 a)/H_n^{(1)}(k_1 a) \tag{4.16}$$

This is identical with the vanishing of the expression for Δ in (4.5), which has been shown to be impossible, at least for real values of the arguments. There can thus be no undamped oscillations of the cylinder for, even if the external and internal media were lossless, there would still be radiation damping.

The resonance problem has been discussed by Schaefer and by Thilo. The latter arrives at a resonance condition corresponding to the observation previously made- that the resonances(or peaks in the amplitude of scattering) are related to the vanishing of the D_n - by supposing that the lossless cylinder is surrounded by a metal sleeve at a large distance from the axis to eliminate the radiation damping. The functions for the scattered field are then the standing-wave Y_n instead of the travelling-wave $H_n^{(1)}$ and (4.16) becomes equivalent to $D_n = 0$.

Return is now made to Figs. 4.24-4.27. All four orders show a tendency for D_n to be large numerically for small k_1a, then decreasing to zero for k_1a near 3, then increasing again to a peak in the region 4-6. The C_n show the opposite variation, with high values in the neighbourhood of $k_1a = 3$ and falling to zero for $k_1a = 5$-6. These variations are in agreement with the observations made before with regard to the calculations of scattered fields in the shadow. The process is not simply additive, however, for the different orders, because of the presence of the $(i)^n$ in (4.6) for the scattered amplitude, but the trend is apparent. When the far fields are discussed, the $(i)^n$ will disappear and the situation become a little more straightforward.

An estimation of the behaviour of the scattered field with k_1a for the $k_r = 2$ material can be read from Figs. 4.29 and 4.30. Because of the higher refractive index the k_1a distance between zeros on any one curve is smaller than for polystyrene. One would expect the first peak in the scattering to occur near $k_1a = 1.7$, where the C_n are large and the D_n small. The first minimum would occur near $k_1a = 3$, followed by another peak near $k_1a = 5$, and so on.

4.5. Far fields.

If the field point in question is considered far enough from the cylinder that the Hankel functions can be replaced by the first term of their asymptotic expansions, the scattered field becomes-

$$E_{sc}(r,\phi) = \left(\frac{2}{\pi K_1 r}\right)^{1/2} e^{i(K_1 r - \pi/4)} \sum_{0}^{\infty} \varepsilon_n B_n \cos n\phi \qquad (4.17)$$

where the B_n are given by (4.3) or (4.6) with the omission of the $(i)^n$. It may be noted that the far-field scattering amplitudes have been obtained in an alternative way using the variational method of Levine and Schwinger and integral transformations given by Schwinger. By this method the solution of the wave equation is obtained in the form of an integral equation by either (a) an application of Green's 2nd Theorem or (b) by a consideration of the polarization currents which produce the scattered field, and their relation to the internal field. The integral equation is of the form-

$$E(r,\phi) = E_{inc}(r,\phi) + k_1^2 (\varepsilon_r - 1) \int_S E(r')\, G(r, r')\, ds' \qquad (4.18)$$

where ε_r is the relative permittivity of the cylinder, S is its cross section and $G(r, r') = (i/4)\, H_o^{(1)}(k_1 |\overline{r - r'}|)$ is the Green's function for a line current in Schwinger's notation. The subsequent procedure, which is not given, follows the pattern given by Papas in his treatment of the metal cylinder.

In what follows when the "amplitude" of the far, scattered field is referred to, it will be considered to be of the form-

$$\text{Amplitude} = (\pi k_1 r/2)^{\frac{1}{2}} \; E = \exp i(k_1 r - \pi/4) \sum_o^\infty \varepsilon_n B_n \cos n\phi \qquad (4.19)$$

Thus the far field results will differ in interpretation from the near fields in the respect that the amplitude will depend on the frequency. Thus, when the abscissa of a curve is given as $k_1 a$(or ka), the variable

will be considered to be "a". On the other hand, in the case of the near fields the variable could be either the wavelength or the radius.

Calculations have been made from (4.19) of the amplitude of the field scattered forward, back and to the side by a polystyrene cylinder. These are given in Fig. 4-3/. One significant feature of these curves- as well as of the other far-field curves plotted as a function of $k_1 a$- is the presence of well-defined ripples. Curves of the scattering cross-section for spheres- and those of Montroll and Hart for cylinders- have usually been drawn as smooth curves. Since, as will be shown later, there is a simple relation between the cross-section for scattering and the amplitude of the forward-scattered field, it is assumed that the latter would appear in the same form. Some departures from the smooth curve are given by Van de Hulst(1949, p.21), but only for the initial rising part of the curves. These he attributes to resonance effects in the sphere. An attempt will be made to examine this point in a little more detail later on.

The forward-scattered field has a large amplitude of fluctuation, while that scattered back is more nearly constant in mean value. The front-to-back ratio thus has correspondingly large fluctuations. The first peak in the forward scattering occurs in the region of $k_1 a = 3$-4 and the first minimum for the region 5-6, as for the near fields.

The side-scattered field, while fluctuating widely, does not appear to have a regular ripple frequency, as do the other two curves. It may well be that its ripple pattern would be changed somewhat if the $k_1 a$ interval in the computations were taken smaller.

The curves of Fig. 4.33 of the corresponding scattered fields for

the $k_r = 2$ cylinder show similar characteristics, with the addition that the main fluctuations in the forward scattering are more frequent, as was found for the C_n and D_n for this case.

The phase of the far, forward scattered field relative to that of the incident field has been plotted in Fig. 4.32. For low values of $k_1 a$, θ tends to 45 deg. and then appears to oscillate about a value of approximately 135 deg. It, too, shows the tendency to rippling. The value for small $k_1 a$ can be shown as follows–

For small $k_1 a$ only the first term of the series 4.19 will be needed. The amplitude is then given by–

$$\text{Amplitude} = - \exp i(k_1 r - \pi/4)\ C_o /(C_o + i\ D_o)$$

$$\simeq - \exp i(k_1 r - \pi/4)\ C_o /i\ D_o \qquad (4.20)$$

since $|D_o| >> |C_o|$. Both C_o and D_o are negative, so that the phase is $\exp i(k_1 r + \pi/4)$, i.e., differs from the incident field $\exp i\ k_1 r$ by 45 deg.

The phase curve for the $k_r = 2$ material, given in Fig. 4.34, is similar to that of polystyrene in its limit for low $k_1 a$, its rippling and its oscillation about a mean value of approximately 135 deg. The last has the typical higher frequency.

From Fig. 4.32 one can determine the angle at which the curves of Fig. 4.13 approach point B. Since, for the $k_1 a$ values shown, θ does not appear to exceed 180 degrees, the curves for $k_1 a$ exceeding 6 would be expected to travel over the same general route as that for 6, crossing the horizontal axis downward to the right of B and upward to the left.

DATA SHEET NO. 2. 105 DIVISIONS × 45 DIVISIONS

IGHTMAN & OUNTAIN LTD.,
ARTILLERY HOUSE, ARTILLERY ROW, WESTMINSTER, S.W.1

Fig. 4.31.

Far-field scattered by polystyrene cylinders.

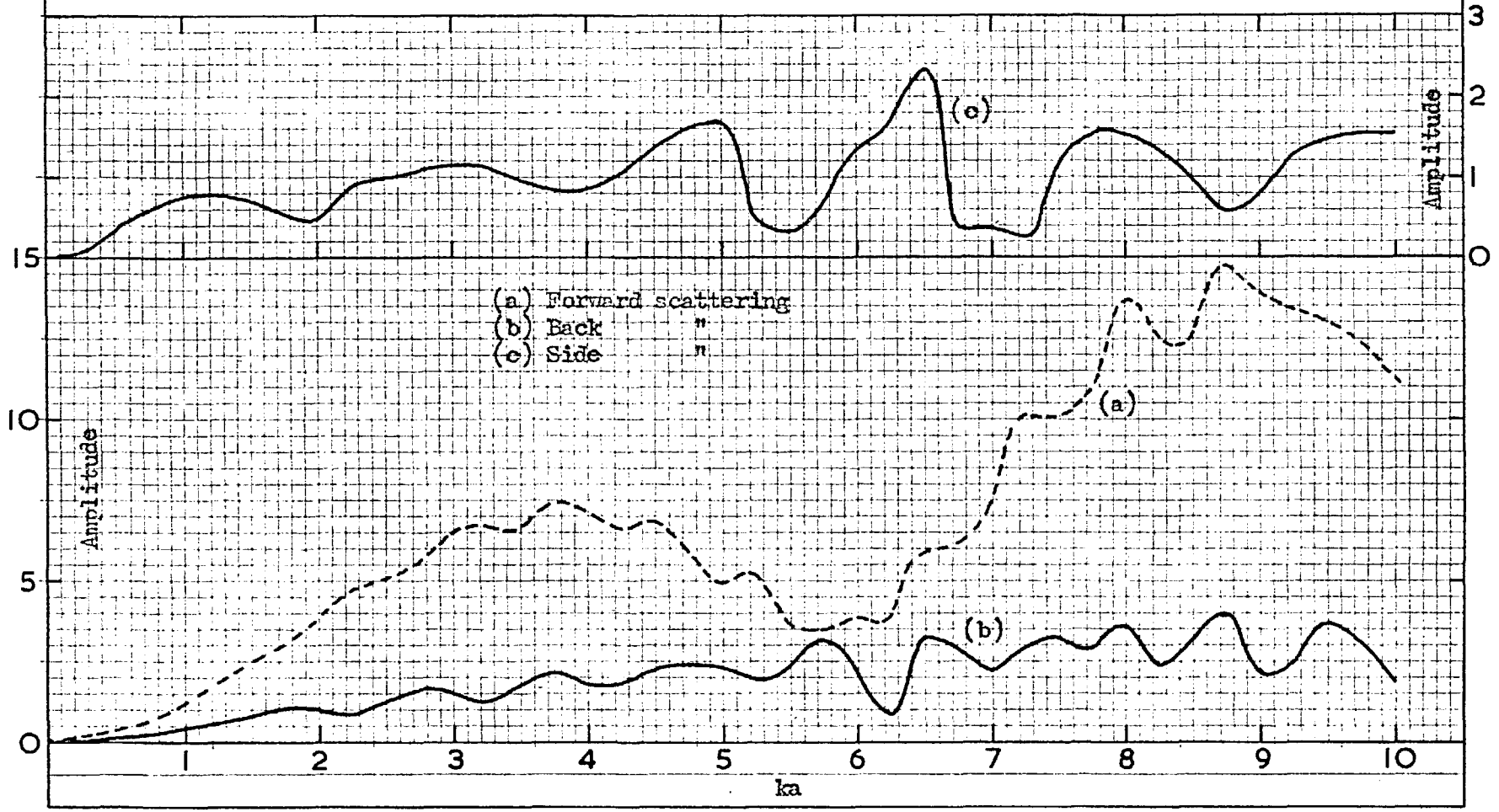

DATA SHEET No. 2. 105 DIVISIONS × 45 DIVISIONS
WIGHTMAN MOUNTAIN LTD.,
ARTILLERY HOUSE, ARTILLERY ROW, WESTMINSTER, S.W.1

Fig. 4.32.

Phase of the far, forward-scattered field of polystyrene cylinders relative to the incident field.

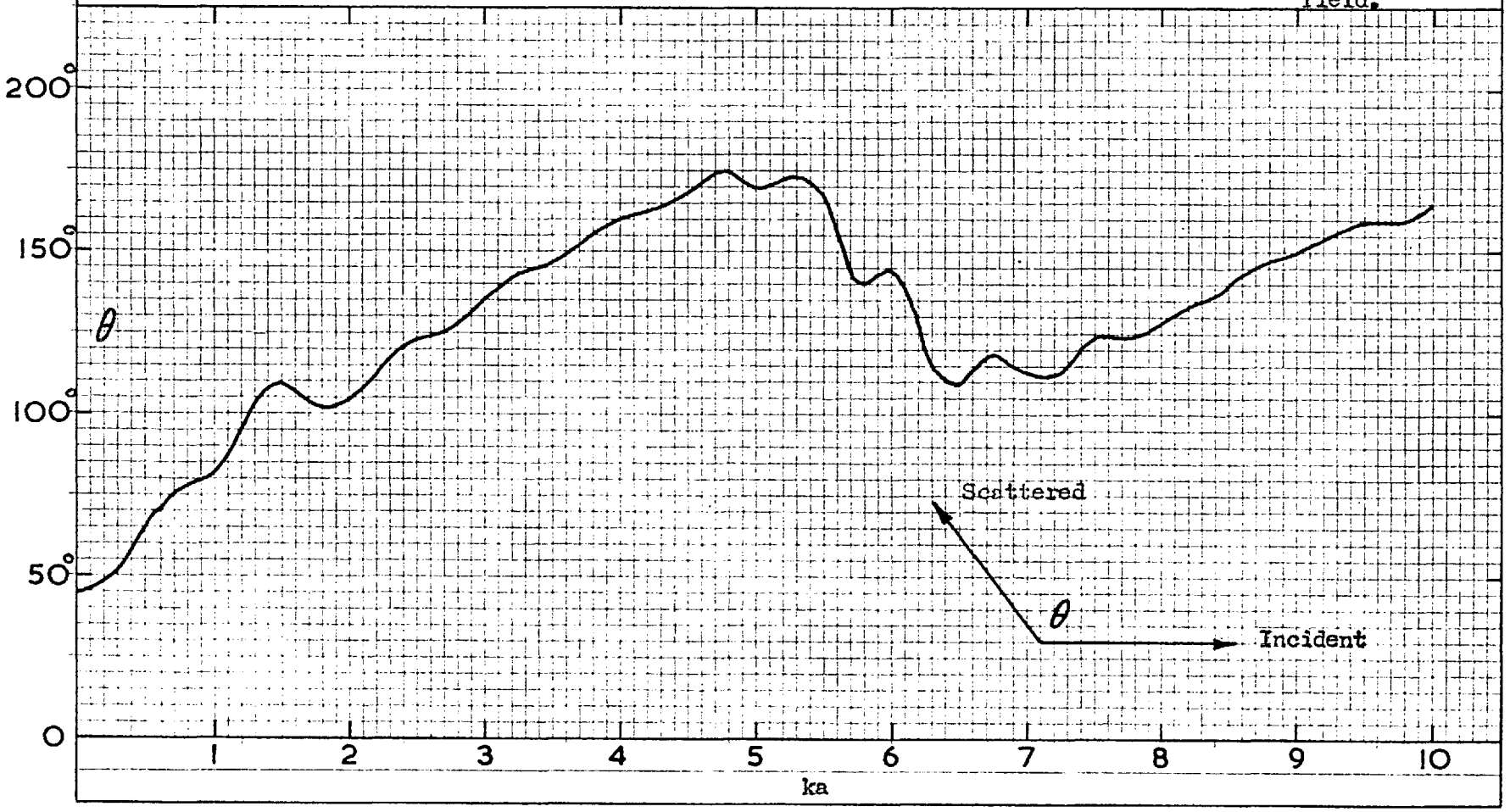

DATA SHEET NO. 2. 105 DIVISIONS × 45 DIVISIONS

HEFFER & SONS LTD.,
ARTILLERY HOUSE, ARTILLERY ROW, WESTMINSTER, S.W.1

Fig. 4.33.

Far-scattered field by cylinders of relative permittivity = 4.

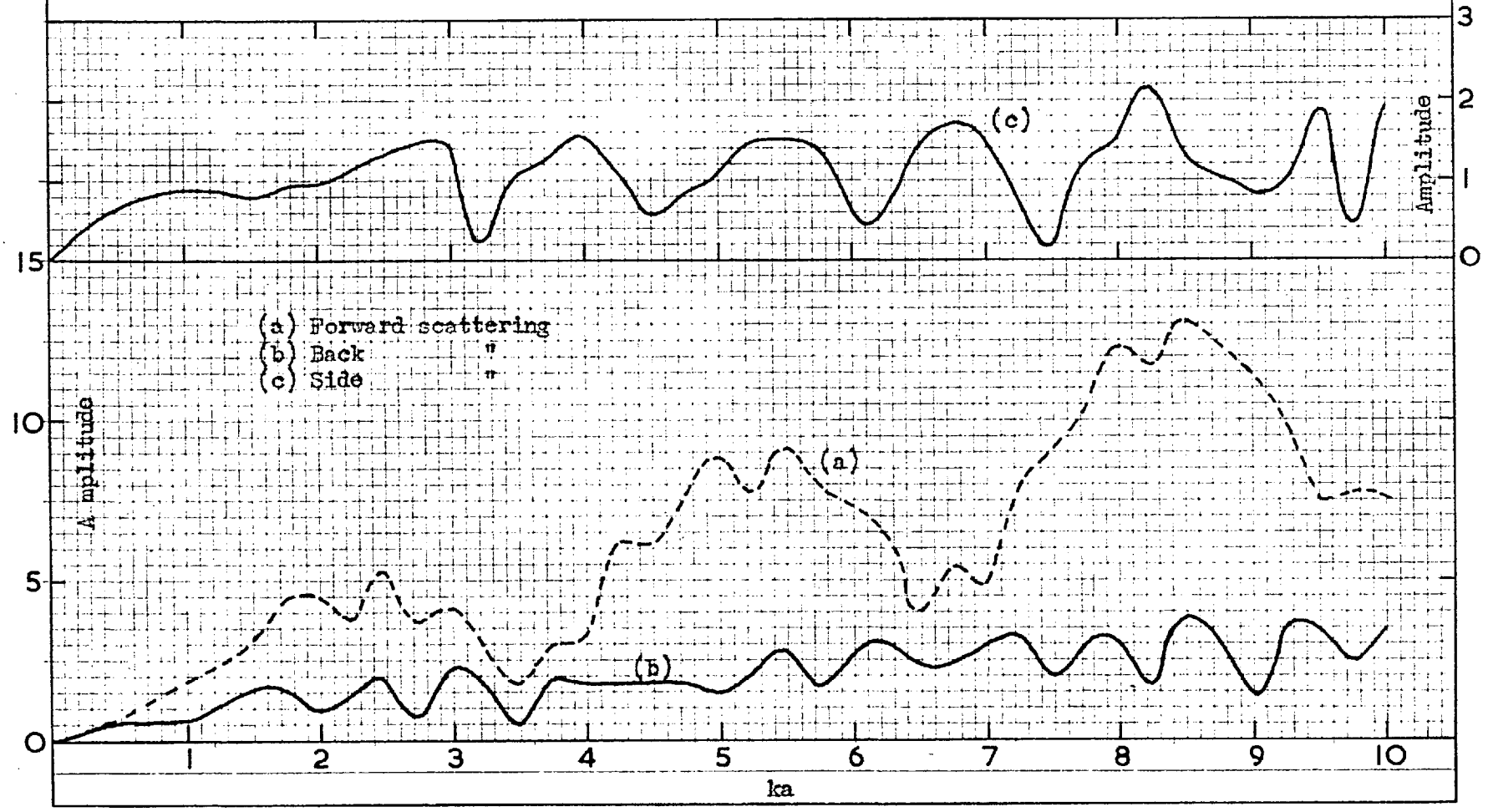

DATA SHEET NO. 2. 105 DIVISIONS x 45 DIVISIONS

WHITEMAN MOUNTAIN LTD.,
ARTILLERY HOUSE, ARTILLERY ROW, WESTMINSTER, S.W.1

Fig. 4.34.

Phase of the far, forward-scattered field of cylinders of relative permittivity = 4, relative to the phase of the incident field.

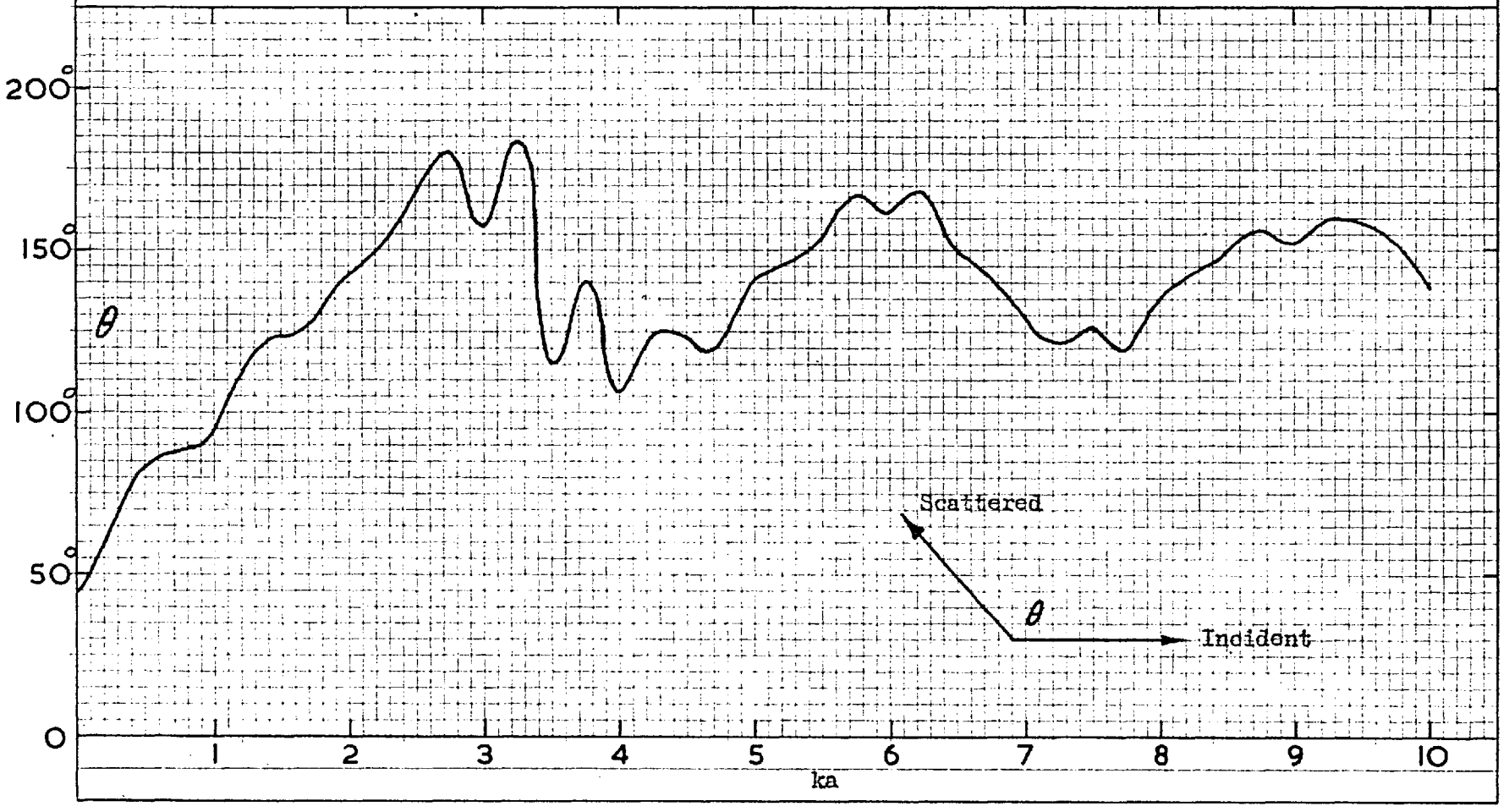

4.6. Scattering cross-section.

The scattering cross-section of an obstacle is defined as the ratio of the power scattered by it to the incident power density. For a cylinder it is taken as the ratio of the power scattered per unit length of cylinder to the incident power density.

The scattered power density is given by -

$$T = \tfrac{1}{2} \mathrm{Re} \left(E_{sc} \times H_{sc}^{*} \right) \tag{4.21}$$

where $H_{sc} = \frac{i}{\omega \mu_1} \frac{\partial}{\partial r} E_{sc}$ and * refers to the complex conjugate.

Substituting in (4.21) from (4.17) there results-

$$T = \frac{1}{\pi \omega \mu_1 r} \sum \sum^{*} \tag{4.22}$$

where $\sum$ refers to the series of (4.17). Because of the orthogonality property of the cos $n\phi$ of (4.17), ~~(4.22) becomes-~~

~~$$T = \frac{1}{\pi \omega \mu_1 r} \sum_{0}^{\infty} \varepsilon_n^2 B_n B_n^{*} \cos^2 n\phi \tag{4.23}$$~~

The total scattered power is obtained as -

$$P_{sc} = \frac{1}{\pi \omega \mu_1 r} \int_0^{2\pi} \sum_0^{\infty} \varepsilon_n^2 B_n B_n^{*} \cos^2 n\phi \; r \, d\phi$$

$$= \frac{2}{\omega \mu_1} \sum_0^{\infty} \varepsilon_n B_n B_n^{*} \tag{4.24}$$

The incident power density is given by-

$$S_{inc} = k_1 / 2 \omega \mu_1 \tag{4.25}$$

Thus the scattering cross-section is, by definition-

$$\sigma = P_{sc} / S_{inc} = (4/k_1) \sum_{o}^{\infty} \varepsilon_n B_n B_n^*$$

$$= (4/k_1) \sum_{o}^{\infty} \varepsilon_n |B_n|^2 \qquad (4.26)$$

which may be written more conveniently as-

$$\frac{\sigma}{2a} = (2/k_1 a) \sum_{o}^{\infty} \varepsilon_n |B_n|^2 \qquad (4.27)$$

This may also be expressed in terms of the auxiliary angles as-

$$\frac{\sigma}{2a} = (1/k_1 a) \sum_{o}^{\infty} \varepsilon_n (1 - \cos \theta_n) \qquad (4.28)$$

by use of the circle relation $B_n = -\frac{1}{2}(1 - \exp i\theta_n)$, as has been done by Van de Hulst for the sphere(1946, p.10).

Using as a basis the zero power flow across a lossless cylinder surface, one can obtain another expression for the scattering cross-section(Appendix III)-

$$\frac{\sigma}{2a} = -(2/k_1 a) \operatorname{Re} \sum_{o}^{\infty} \varepsilon_n B_n \qquad (4.29)$$

which can easily be shown to be equivalent to (4.27), and which gives a simple relation between the scattering cross-section and the amplitude scattered forward. As is shown in the Appendix, if the cylinder is lossy $\frac{\sigma}{2a}$ in (4.29) represents the sum of the scattering and absorption cross-sections.

Computations, based on (4.29), have been made for cylinders of polystyrene and for others of $k_r = 2$. The former curve is given in Fig. 4.35 and the latter in Fig. 4.36. They are similar in that each oscillates about a value of 2, and has the characteristic ripples found on

ARTILLERY HOUSE, ARTILLERY ROW, WESTMINSTER, S.W.1

Fig. 4.35.

Scattering cross-section of polystyrene cylinders.

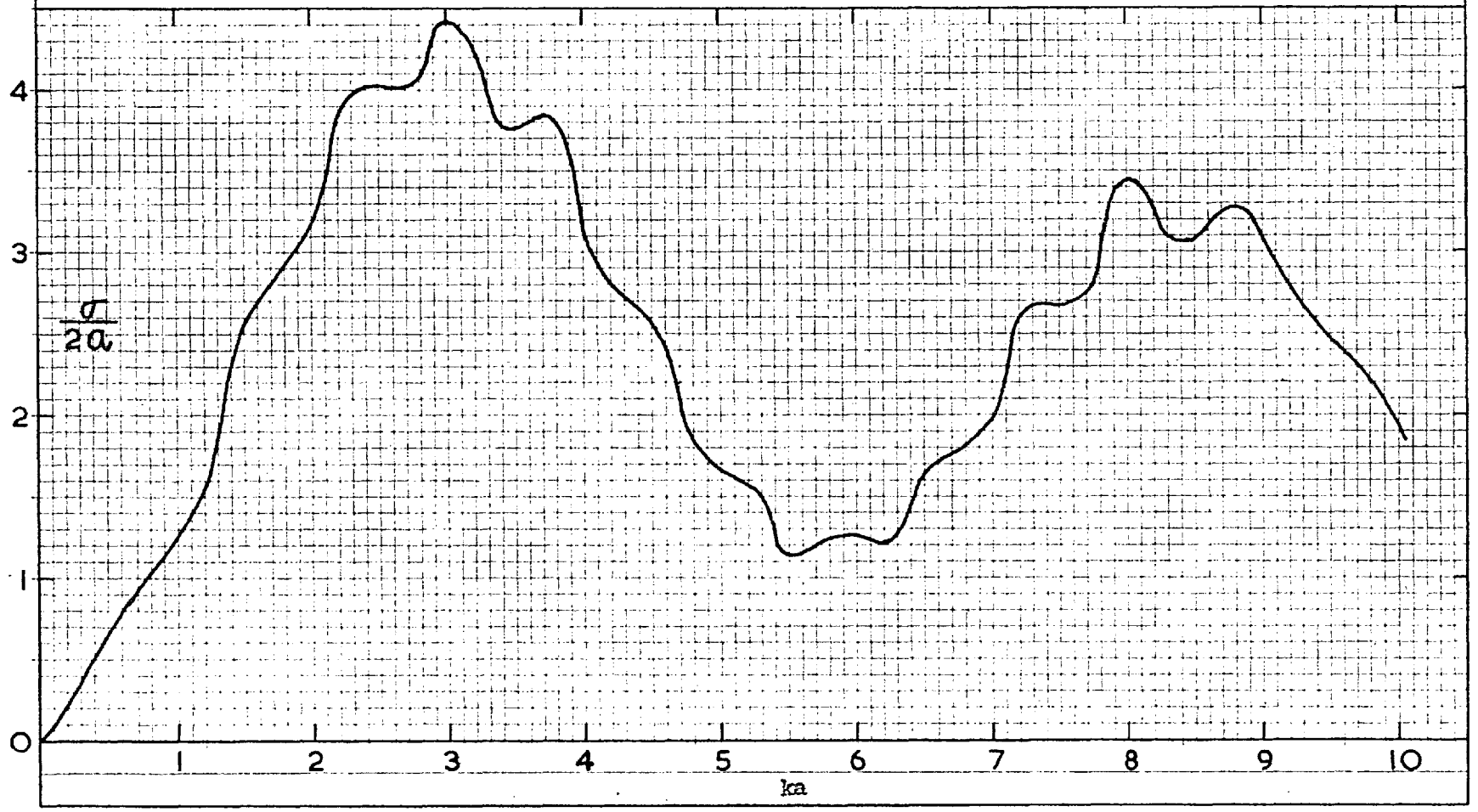

DATA SHEET No. 2. 105 DIVISIONS × 45 DIVISIONS
ARTILLERY HOUSE, ARTILLERY ROW, WESTMINSTER, S.W.1

Fig. 4.36.

Scattering cross-section of cylinders of relative permittivity = 4.

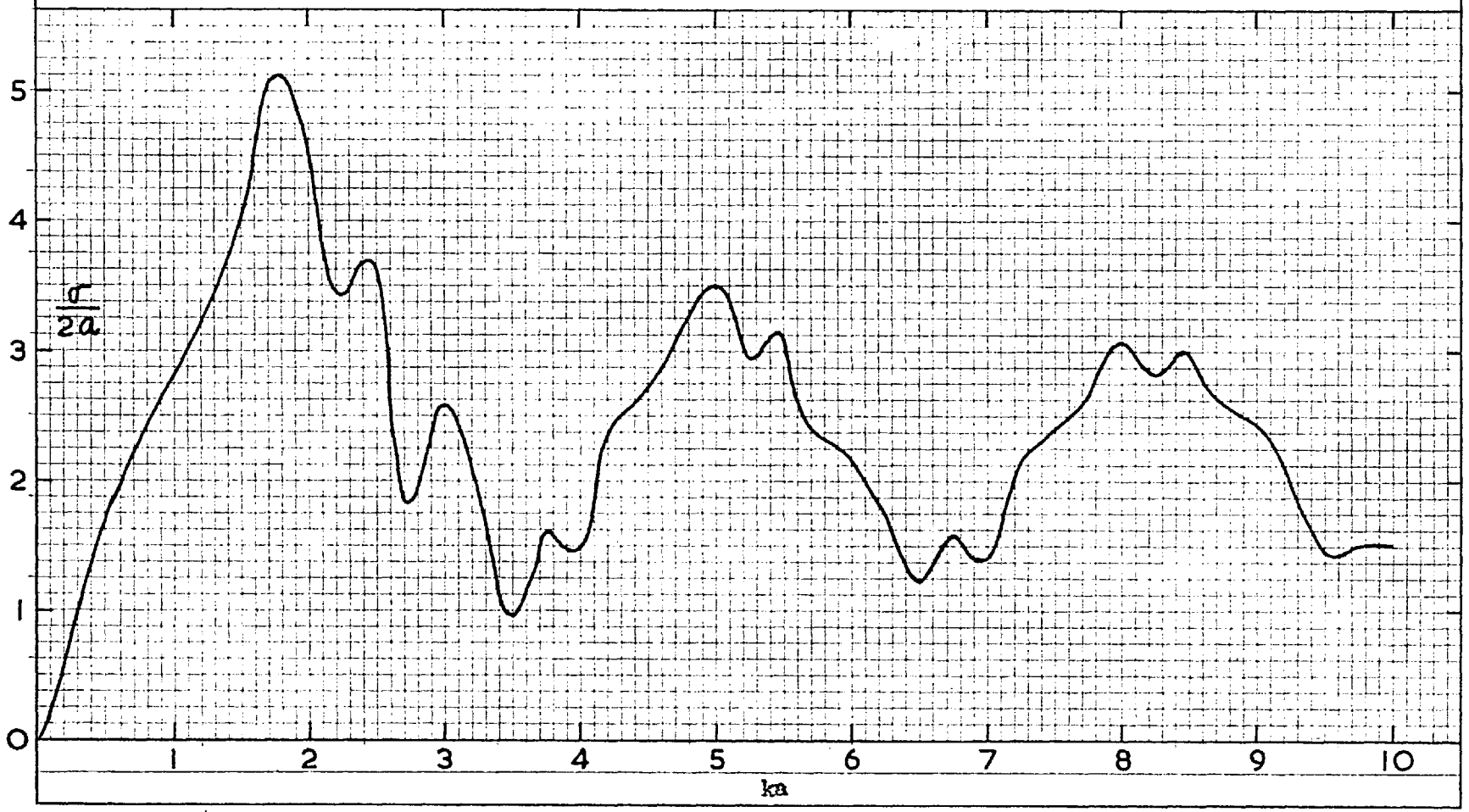

all the previous far-field curves. The positions of the maxima and the minima correspond closely to those of the far, forward-scattered field of Figs. 4.37 and 4.33 respectively, indicating the close relation between the real part of the scattered field and the total. From the form of the B_n all the real parts add while the imaginary parts tend to change sign with n. The maxima and minima obviously correspond to the maxima of C_n and D_n respectively.

The ripples on the curves still require explanation. Recently the results of a programme of computation of the scattering cross-section for dielectric spheres was published by Goldberg. These showed the appearance of a systematic ripple on the curves. They had been computed at k_1a intervals of 0.1 and the ripple was attributed to this small interval. Another way of stating it would be that the ripple is due to the manner in which the various orders of the function B_n make their contribution to the total scattering cross-section. This is equivalent to the resonance explanation of Van de Hulst(p.54) since, in addition to the main fluctuations in the cross-section curve, there can be minor resonances corresponding to the individual behaviour of the various terms of the series.

From the definition of B_n -

$$- \text{Re } B_n = \text{Re } C_n /(C_n + i D_n) = C_n^2 /(C_n^2 + D_n^2) \qquad (4.30)$$

This function has been drawn in Fig. 4.37 for polystyrene for the first four terms of the series and in Fig. 4.38 for $k_r = 2$, for the values of k_1a which involve the first main peak in Figs. 4.35 and 4.36 respectively.

One notes from the definition of the scattering cross-section (4.29) that an increase in the contribution of a series term with increasing $k_1 a$ is partly neutralized by the $1/k_1 a$ factor, while a decrease is accentuated for the same reason. Also, the contributions for $n > 0$ have to be doubled because of the ε_n. Then Figs. 4.35 and 4.37 are compared and the following points seen to obtain-

	Fig. 4.35.	Fig. 4.37.
1.	Flat between $\frac{2}{4}.3$ and $\frac{2}{4}.7$.	Small increase in n=2 and n=3 compensated for by an increase in $k_1 a$.
2.	Rise between 2.7 and 3.0.	Large increase in n=3 and a small decrease in n=0.
3.	Fall between 3.0 and 3.5.	Slight increase in n=4(which begins at $k_1 a = 3.0$) not compensating for the decrease in n=1 and n=3.
4.	Flat between 3.5 and 3.75.	Rise in n=4(max. at $k_1 a = 3.75$) compensated for by fall in n=1.
5.	Fall between 3.75 and 4.0.	n=3 flat. All the others falling.

On making the corresponding comparison between Figs. 4.36 and 4.38 one obtains-

	Fig. 4.36.	Fig. 4.38.
1.	Fall between 1.8 and 2.25.	Fall in n=0 and n=2 not neutralized by increase in n=3.
2.	Recovery between 2.25 and 2.5.	Large increase in n=3 and small decrease in n=0 and n=1.

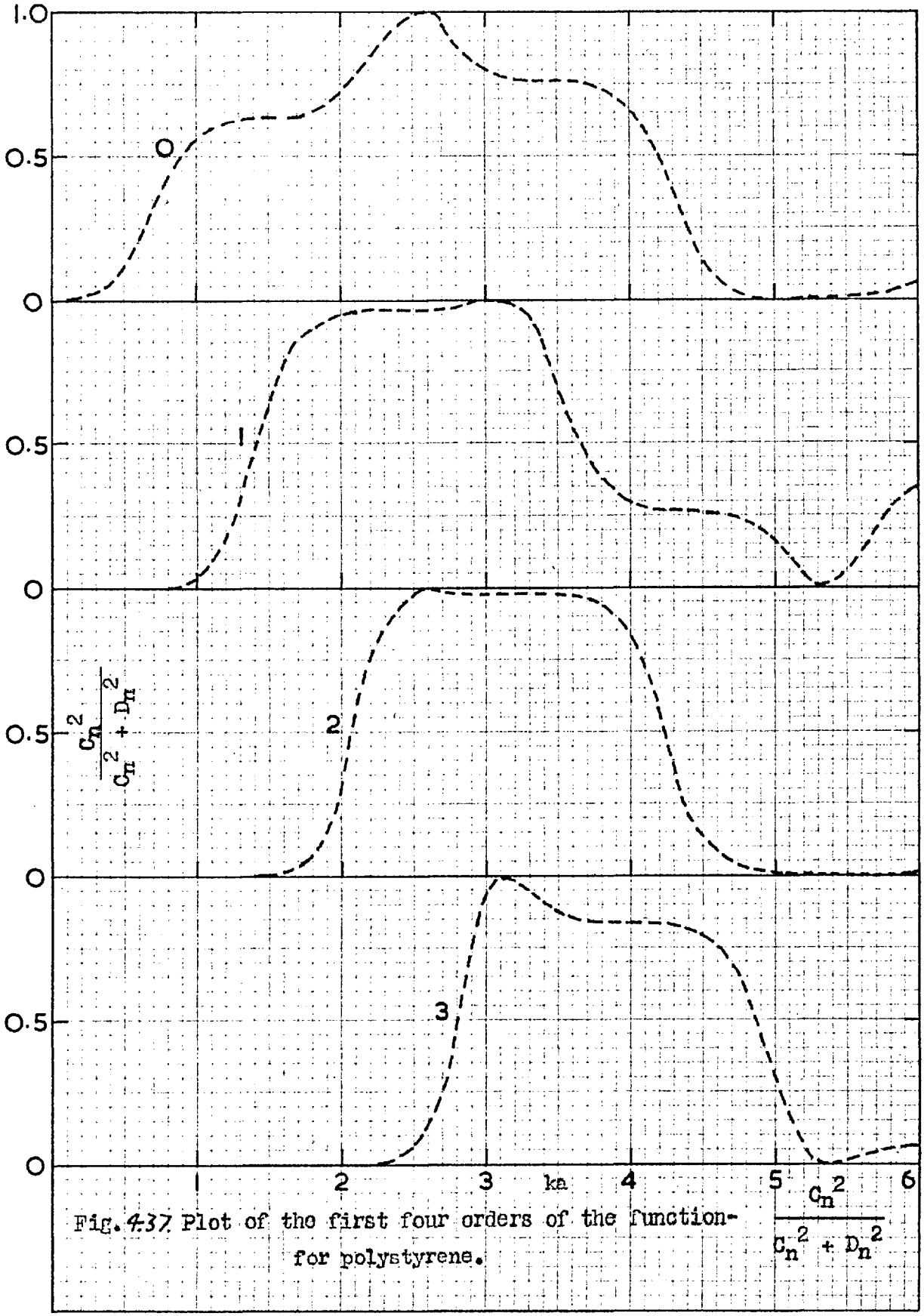

Fig. 4.37 Plot of the first four orders of the function- for polystyrene.

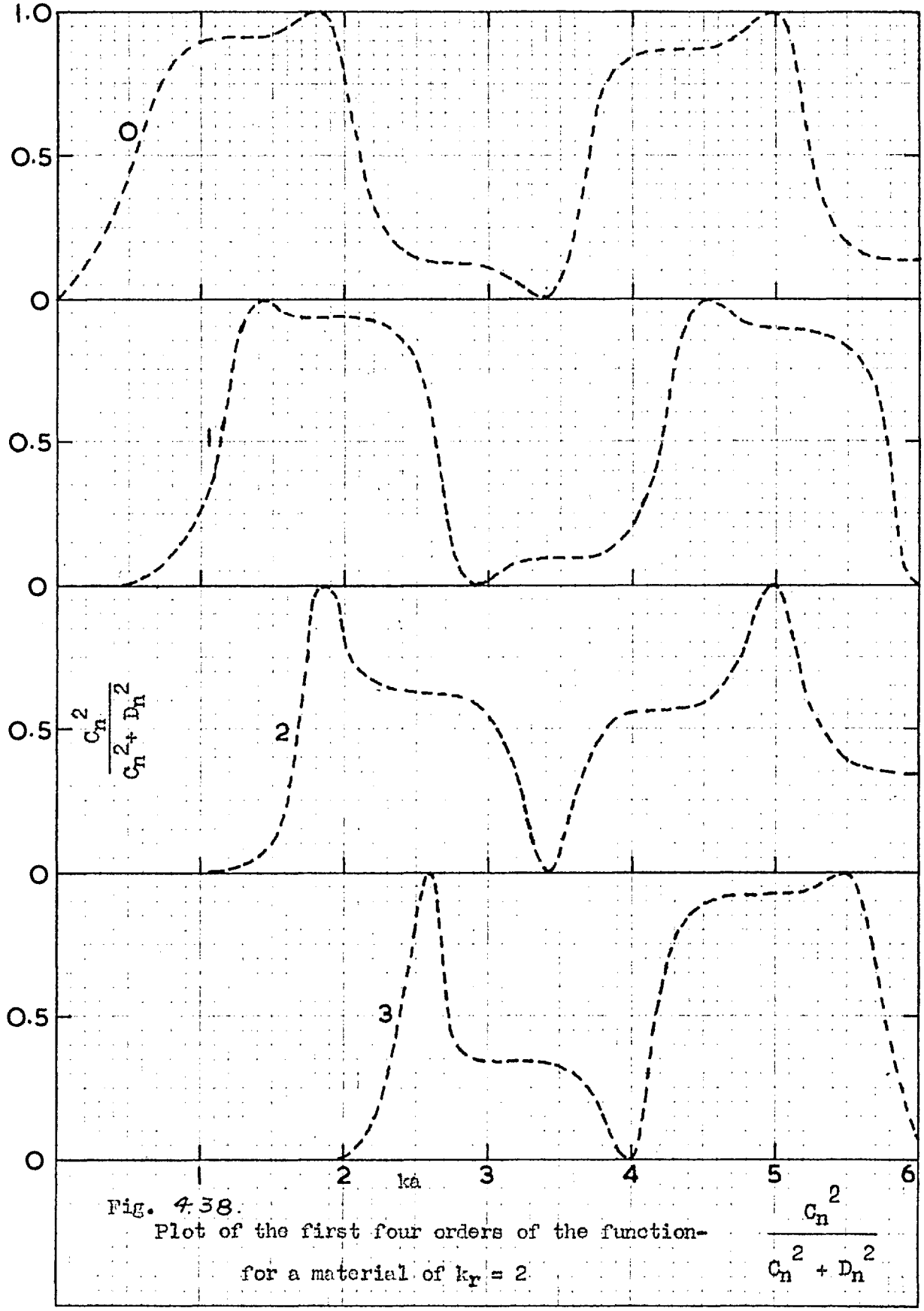

Fig. 4.38.
Plot of the first four orders of the function- $\frac{C_n^2}{C_n^2 + D_n^2}$ for a material of $k_r = 2$

	Fig. 4.36.	Fig. 4.38.
3.	Fall between 2.5 and 2.75.	Fall in n=1 and n=3.
4.	Rise between 2.75 and 3.0.	Rise in n=4, which has a maximum at 3.1.

For the two cases considered, therefore, there would seem to be some justification for the explanation offered.

4.7. Angular distribution of the far scattered field.

From (4.17) computations have made of the angular distribution of the far scattered field of several polystyrene cylinders. The amplitudes are shown in Figs. 4.39-4.42, drawn to the same scale. The complex lobe structure for the larger cylinders is understandable from the presence of the factor cos $n\phi$ in the solution, each term being able to give rise to a pair of lobes. The number of lobes on each half of the pattern thus tends to equal the k_1a value of the cylinder. The high concentration of the scattered field in the forward direction is apparent for all the cylinders. Even the smallest, $k_1a = 1$, shows some dissymmetry. Very weak scattering is seen for some angles for the larger cylinders, mainly near the $\phi = 90$ deg. direction.

The phase distributions are given in Fig. 4.43, with reference to exp $i(k_1 r - \pi/4)$ of (4.17). The rapid changes of phase associated with the amplitude depressions are apparent, being greatest near 90 deg. for the largest cylinders, as observed before. The curves for $k_1a = 4$ and $k_1a = 5$ tend to develop a new phase pattern for angles in the region of 120-170 and 130-170 degrees respectively. This pattern can be explained by reference to Figs. 4.44 and 4.45, where the scattering distributions for $k_1a = 3$ and

$k_1 a = 4$ respectively have been drawn in the complex plane. The former, in which the curve encircles the origin, is associated with the fairly-smooth curve for $k_1 a = 3$ of Fig. 4.43. The latter shows that the phase depression for $k_1 a = 4$ in Fig. 4.43 is associated with the loop of the curve which does not encircle the origin.

No experimental check of these angular results could be made on the present equipment, but the general lobe structure, in the case of $k_1 a = 3$ and 5, was established in the course of some preliminary development work on a parallel-plate spectrometer operating at a wavelength of 1.25 cms. The incident beam was broad enough for the cylinder to be considered illuminated by a plane wave, but narrow enough to permit traversing all the side lobes without the receiving horn's picking up the directly-transmitted wave. The cylinder-receiver separation, of approximately 50 wavelengths, was sufficient to validate the far-field assumption.

The corresponding near-field calculations were not attempted, because of computational difficulties. It would not be sufficient to do them for only one value of $k_1 r$, since it has been seen that the scattered field can vary rapidly with distance from the cylinder. But the information would be valuable in enabling one to predict the interaction between polystyrene cylinders closely-spaced in an array- at least with respect to their first-order or primary scattering.

4.8. Experiments on miscellaneous materials.

The shadow measurements were repeated for families of cylinders of

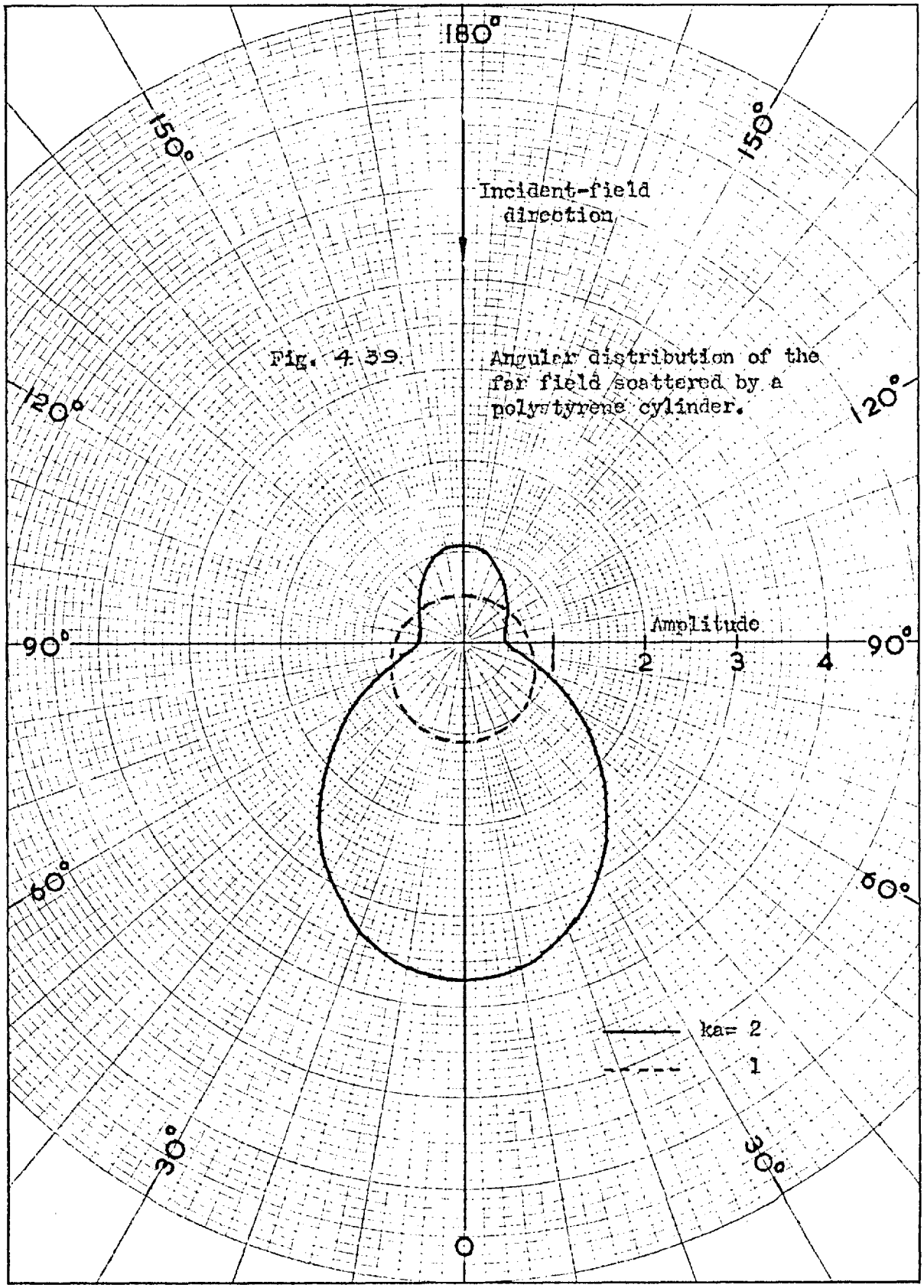

Fig. 4.39. Angular distribution of the far field scattered by a polystyrene cylinder.

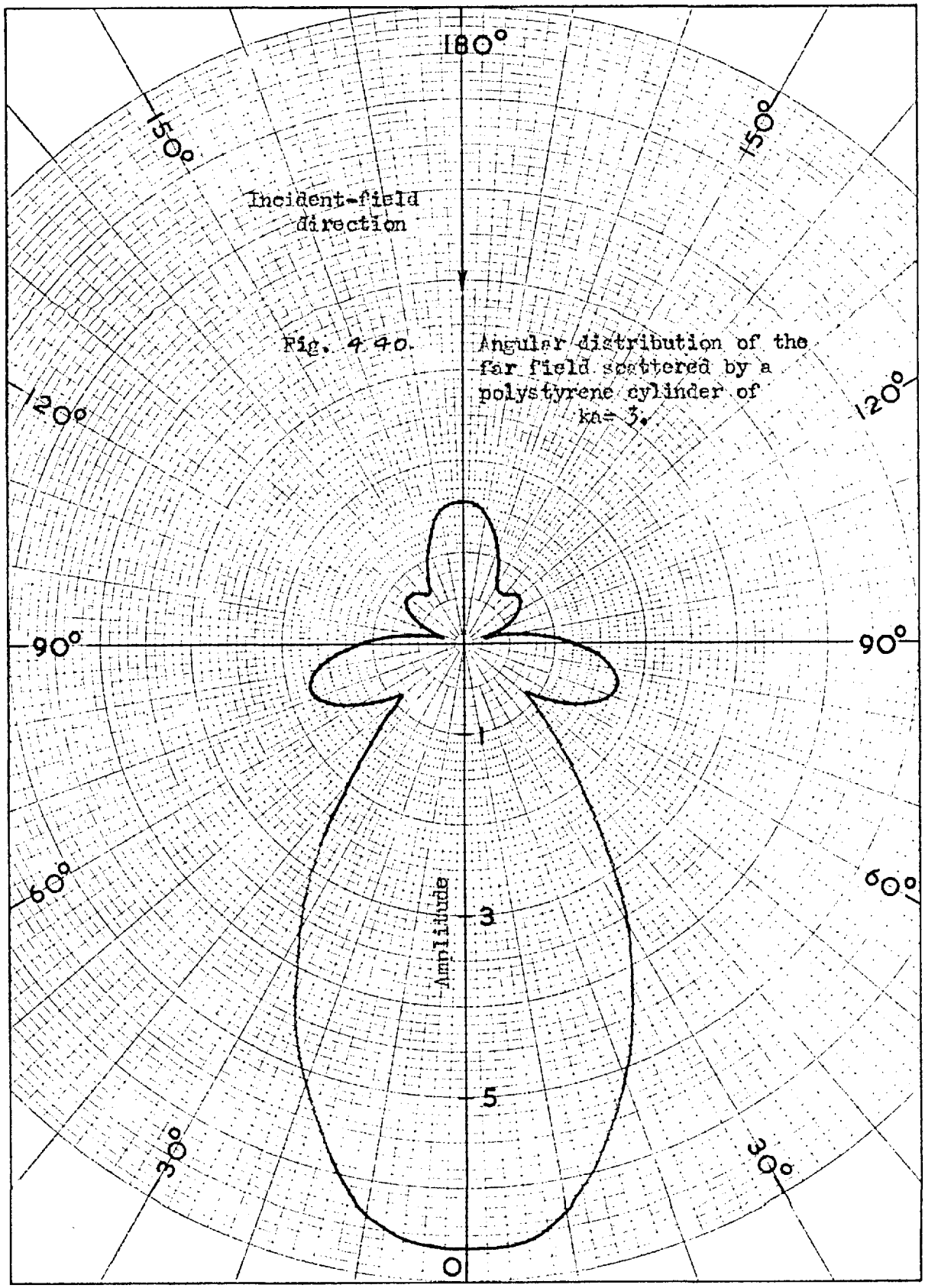

Fig. 4.40. Angular distribution of the far field scattered by a polystyrene cylinder of ka= 3.

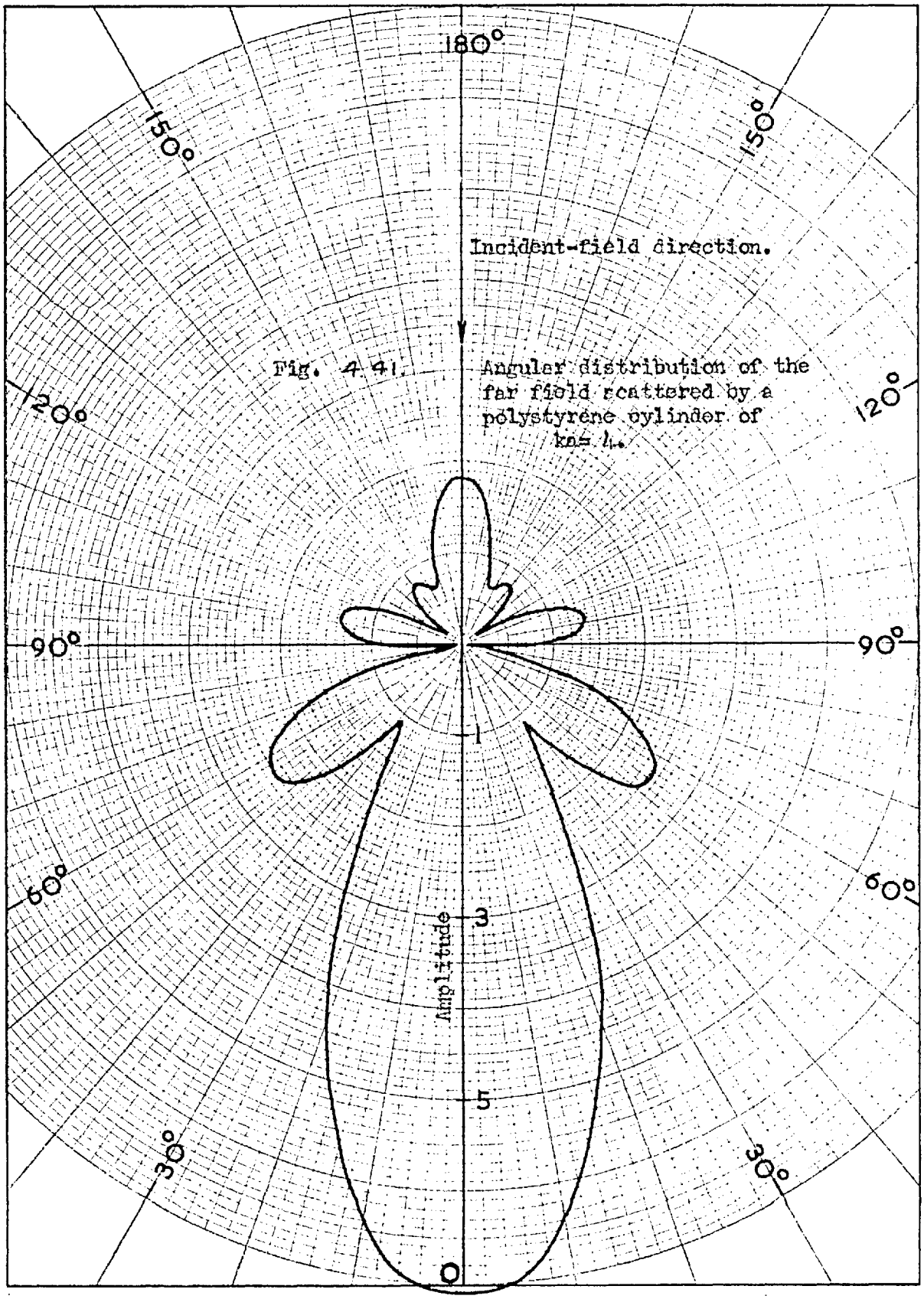

Fig. 4.41. Angular distribution of the far field scattered by a polystyrene cylinder of $ka = 4$.

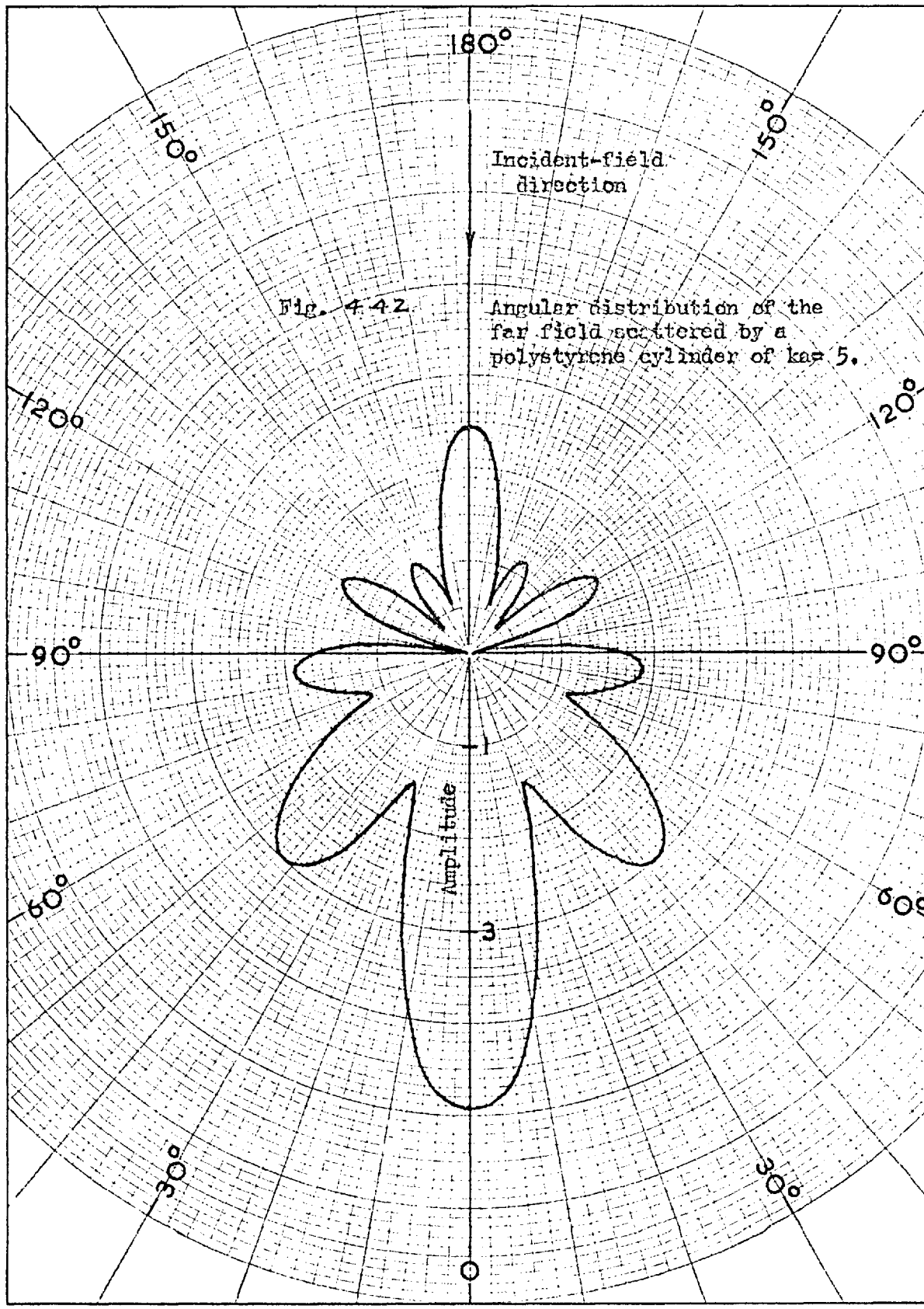

Fig. 4.42 Angular distribution of the far field scattered by a polystyrene cylinder of ka= 5.

Fig. 4.43. Phase of the far field scattered by polystyrene cylinders of the ka values indicated.

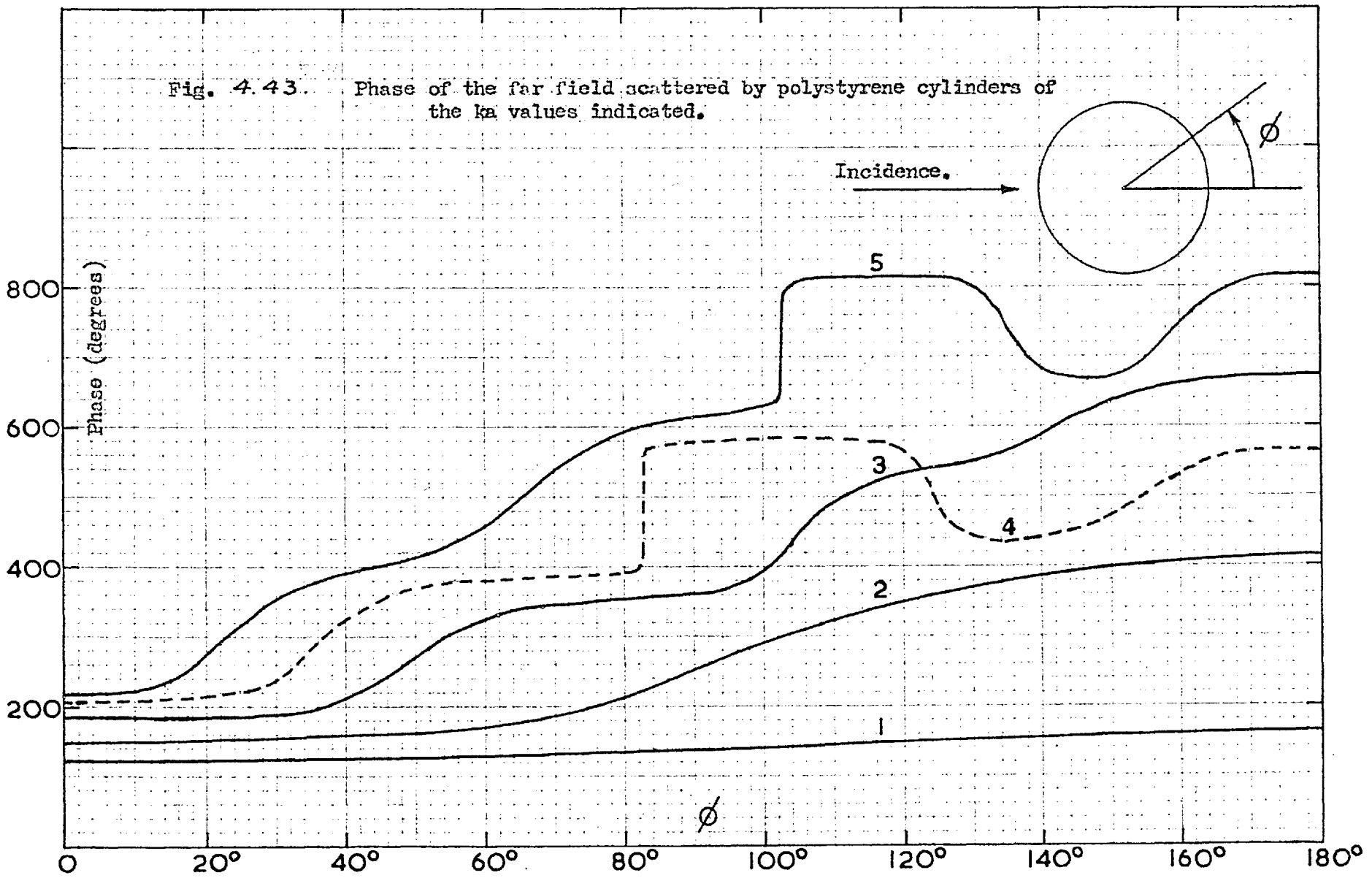

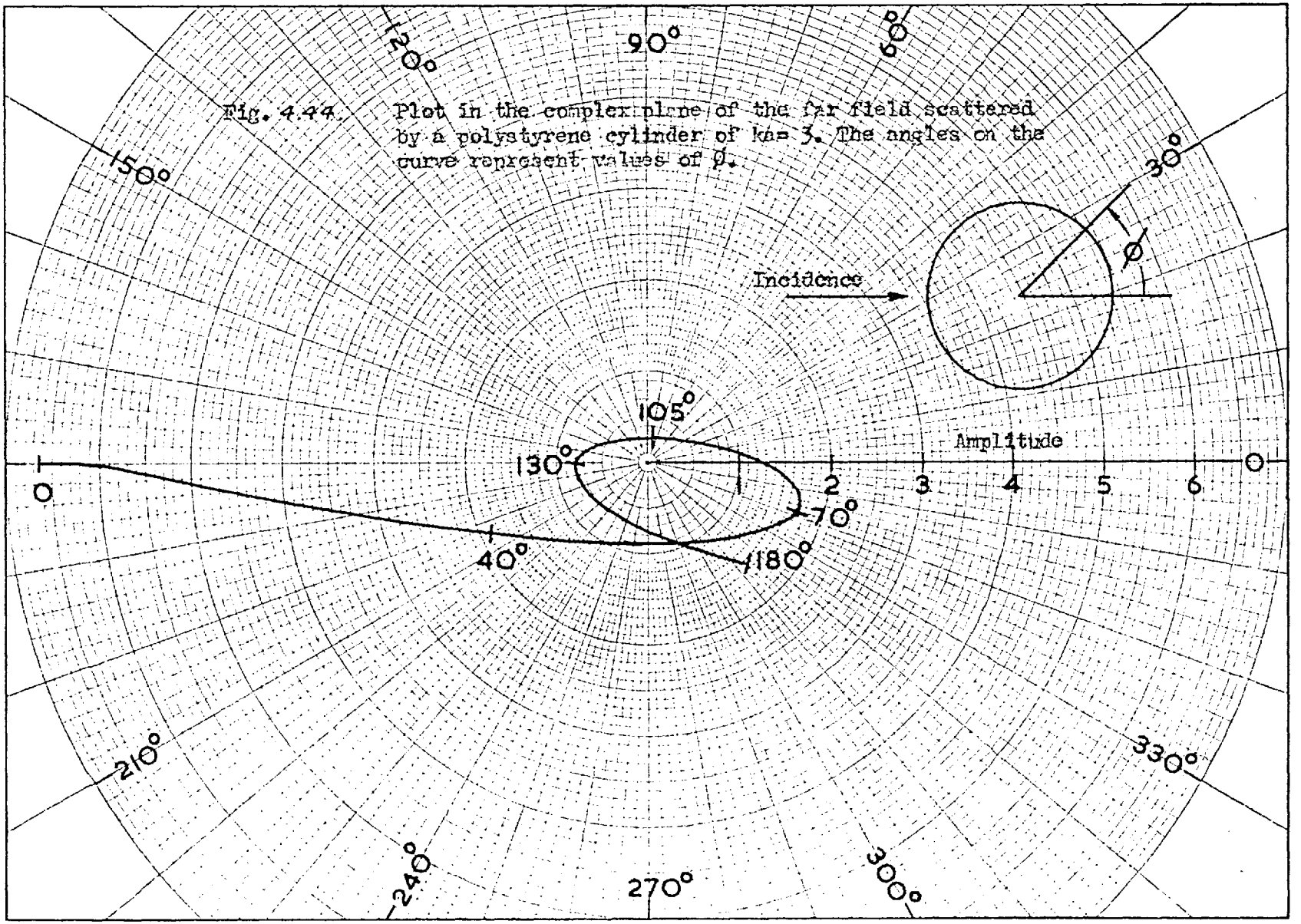

Fig. 4.44. Plot in the complex plane of the far field scattered by a polystyrene cylinder of ka= 3. The angles on the curve represent values of Ø.

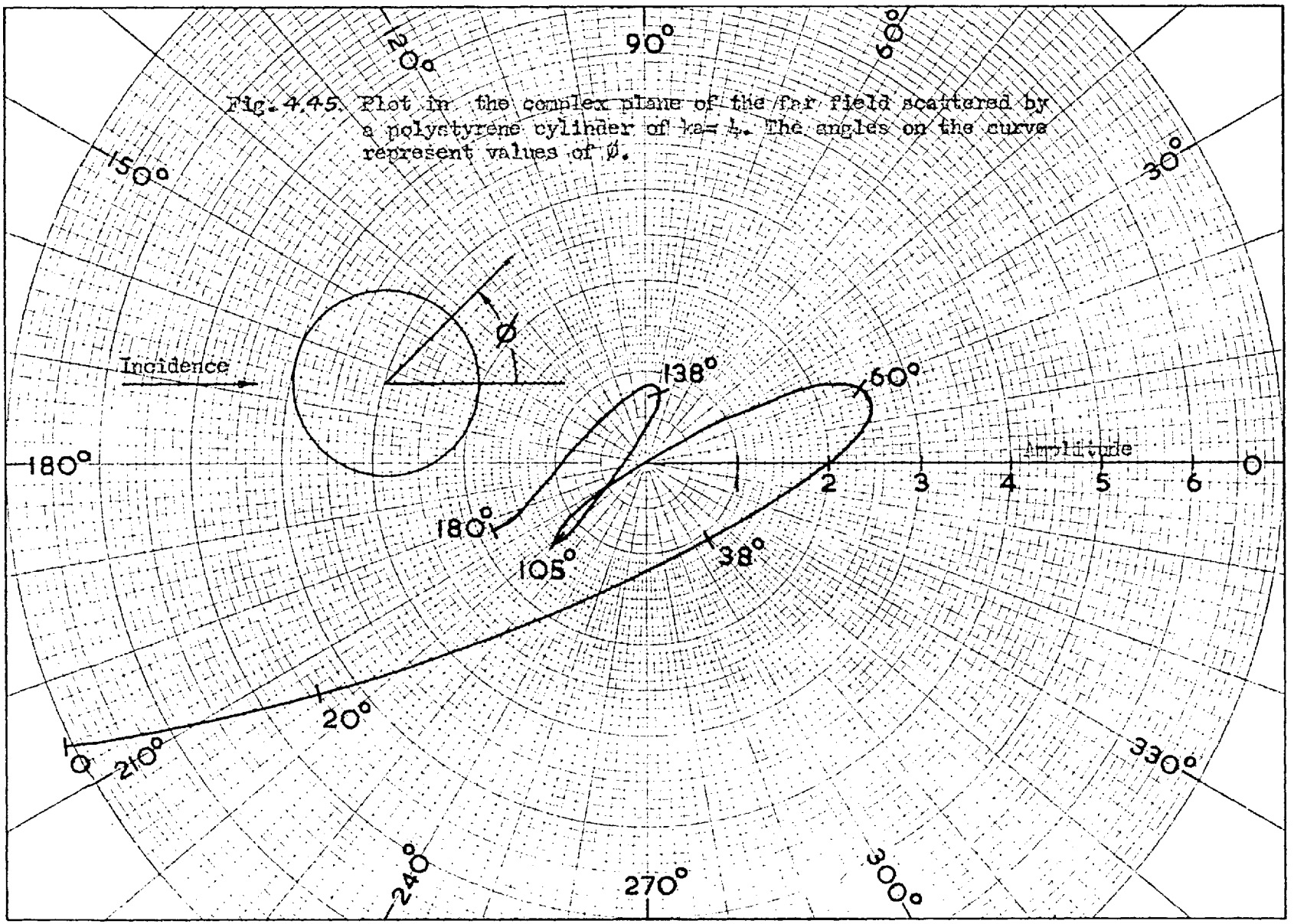

Fig. 4.45. Plot in the complex plane of the far field scattered by a polystyrene cylinder of $ka = 4$. The angles on the curve represent values of ϕ.

several other readily-available materials, to determine the effect on the scattering of the change of permittivity and the presence of appreciable loss. The corresponding calculations were not done, however, because of the lack of tables of Bessel functions with complex argument. The results have been presented in polar form, rather than in field-point detail, in Figs. 4.46-4.49, for the following materials respectively- polythene, graphite, and two resin-base plastics.

Fig. 4.46 gives the results for polythene. It has been observed previously, in discussing Fig. 4.13, the corresponding diagram for polystyrene, that the minima in the scattered field, as a function of $k_1 a$, correspond to the curves which lie toward point B in the spiral group. In comparing the results for polystyrene with those for the material of $k_r = 2$, it was also found that the spiral turns were completed for smaller $k_1 a$, in the latter case. Thus, since the relative permittivity of polythene is smaller than that of polystyrene, one would expect the curves for polythene to lie at smaller angles in the complex plane than the corresponding curves for polystyrene. This is seen to be the case. It is more difficult to compare the amplitudes, on the basis of permittivity. One would expect the scattered amplitude to approach zero in the limit of vanishing difference between the permittivities of the scatterer and the surrounding medium. This could also be inferred from Fig. 4.32, on the basis of the first peak's moving to the right for smaller permittivities. Fig. 4.46 does show a lower scattered amplitude for polythene than is indicated by Fig. 4.13 for polystyrene. On the other hand a previous comparison of Figs. 4.32 and 4.34 has shown a higher level of forward-scattered

field for polystyrene than for the $k_r = 2$ material.

The results for the graphite cylinders are given in Fig. 4.47. This shows the similarity between the graphite and metal cylinders for scattering. The scattered field increases with cylinder radius and the left-hand terminal of the curve tends toward the origin. One is led to speculate on the probable type of transition between the arrangement of the curves in Fig. 4.47 and, for example, those of Fig. 4.13 for a dielectric of relatively-low permittivity. For some complex value of permittivity there would be a transition from the case of Fig. 4.13, in which one crosses curves of decreasing $k_1 a$ on following upward a normal to the reference axis, to the latter, where the opposite obtains. For that permittivity there would perhaps be but a very small change in the scattering over a considerable range of $k_1 a$. One might also infer that condition from the observation previously made- that the curves tend to move more closely together for an increase in permittivity.

The effect on the scattering of increasing both the permittivity and the loss is indicated by Fig. 4.48. The curve passing through the origin corresponds to a lower value of $k_1 a$ than for polystyrene, because of the former. The latter, since it decreases the scattered field, has had the result of moving the pattern to the right- toward point B.

The effect of still-higher material constants is given in Fig. 4.49. Some of the curves are not shown, to avoid overcrowding the diagram. But sufficient are given to show the general features and the start of the second turn in the pattern, the curve for $k_1 a = 5.5$ lying below and to the left of that for $k_1 a = 5$. There was speculation, previously,

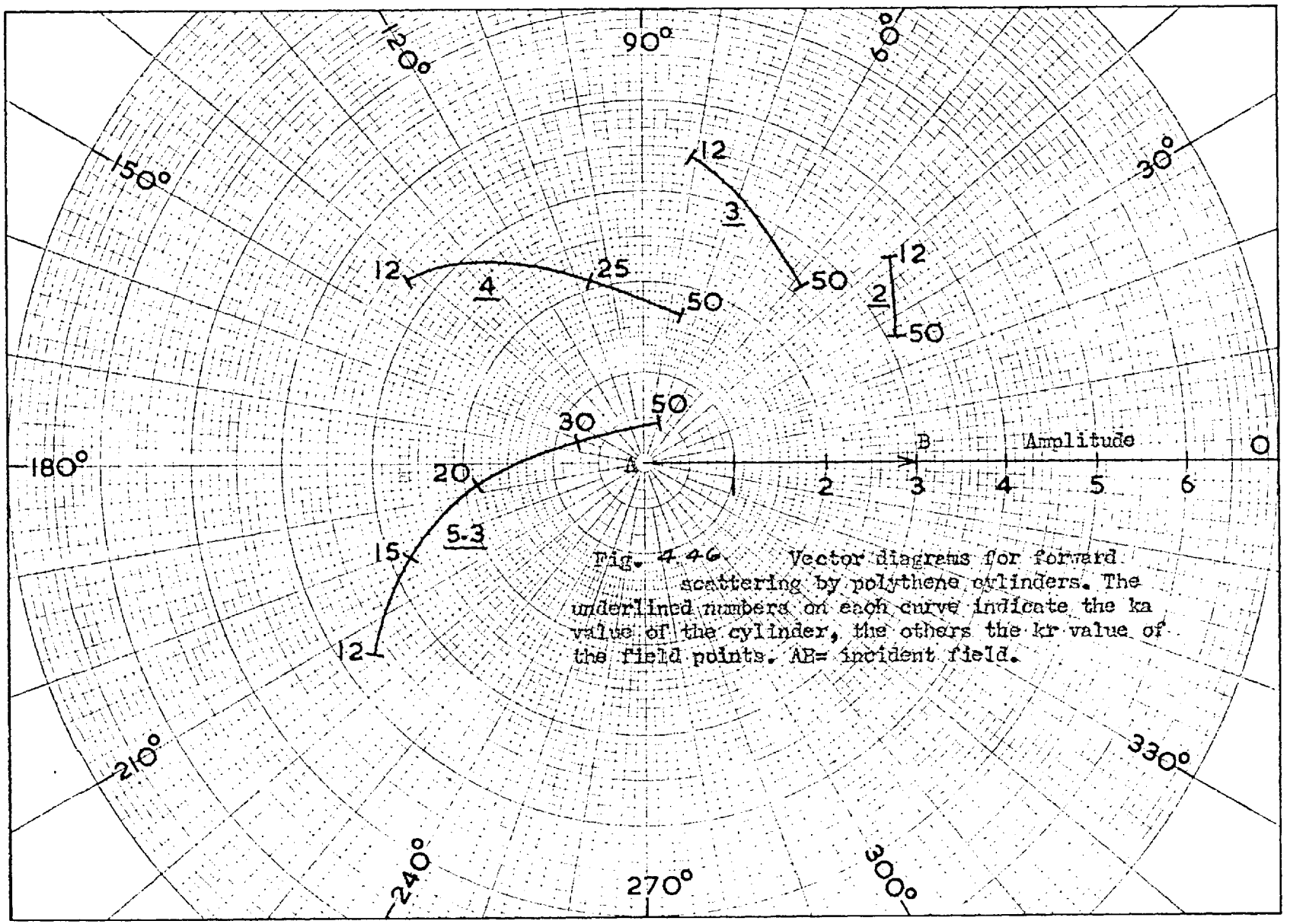

Fig. 4.46. Vector diagrams for forward scattering by polythene cylinders. The underlined numbers on each curve indicate the ka value of the cylinder, the others the kr value of the field points. AB= incident field.

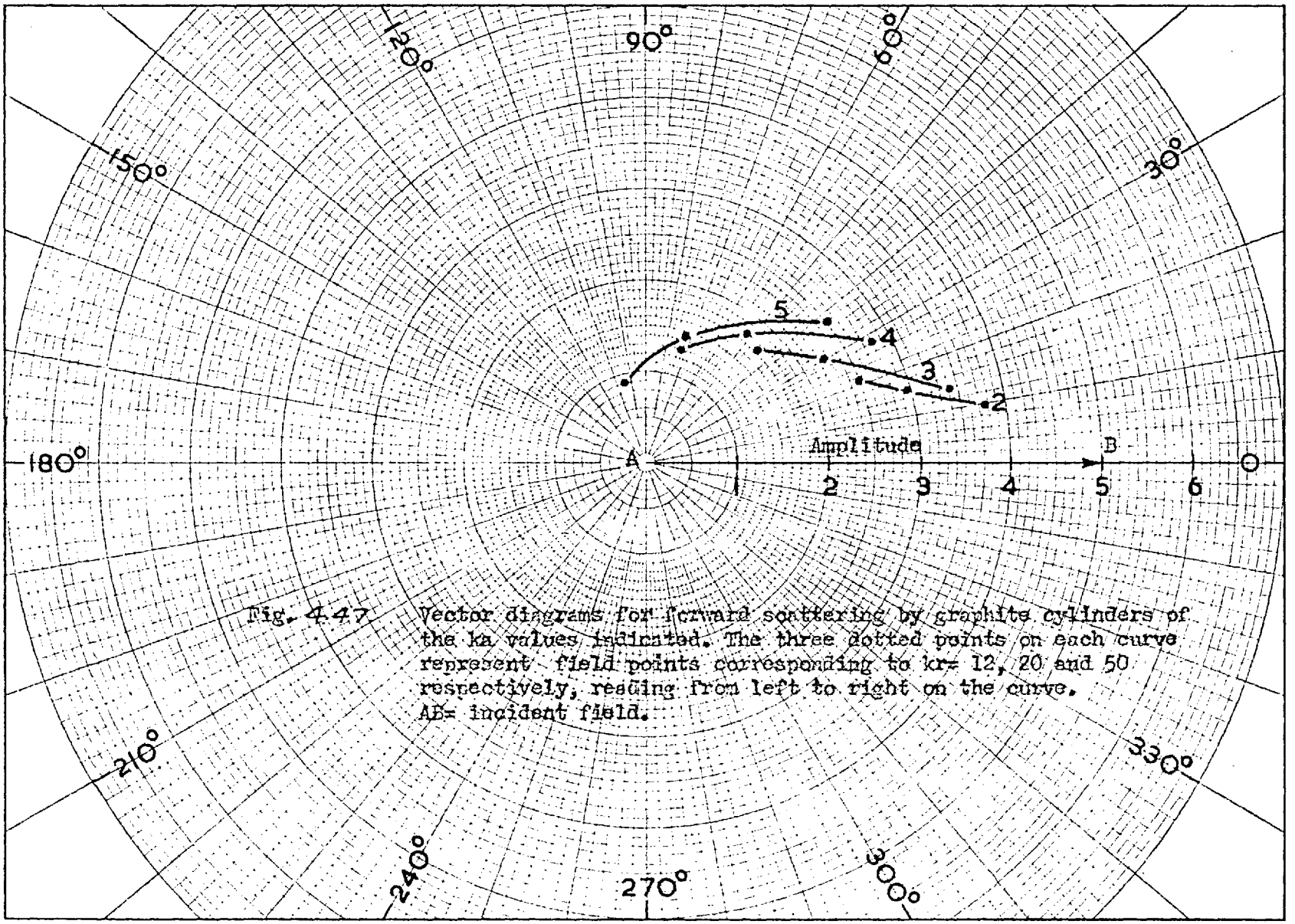

Fig. 447 Vector diagrams for forward scattering by graphite cylinders of the ka values indicated. The three dotted points on each curve represent field points corresponding to kr= 12, 20 and 50 respectively, reading from left to right on the curve. AB= incident field.

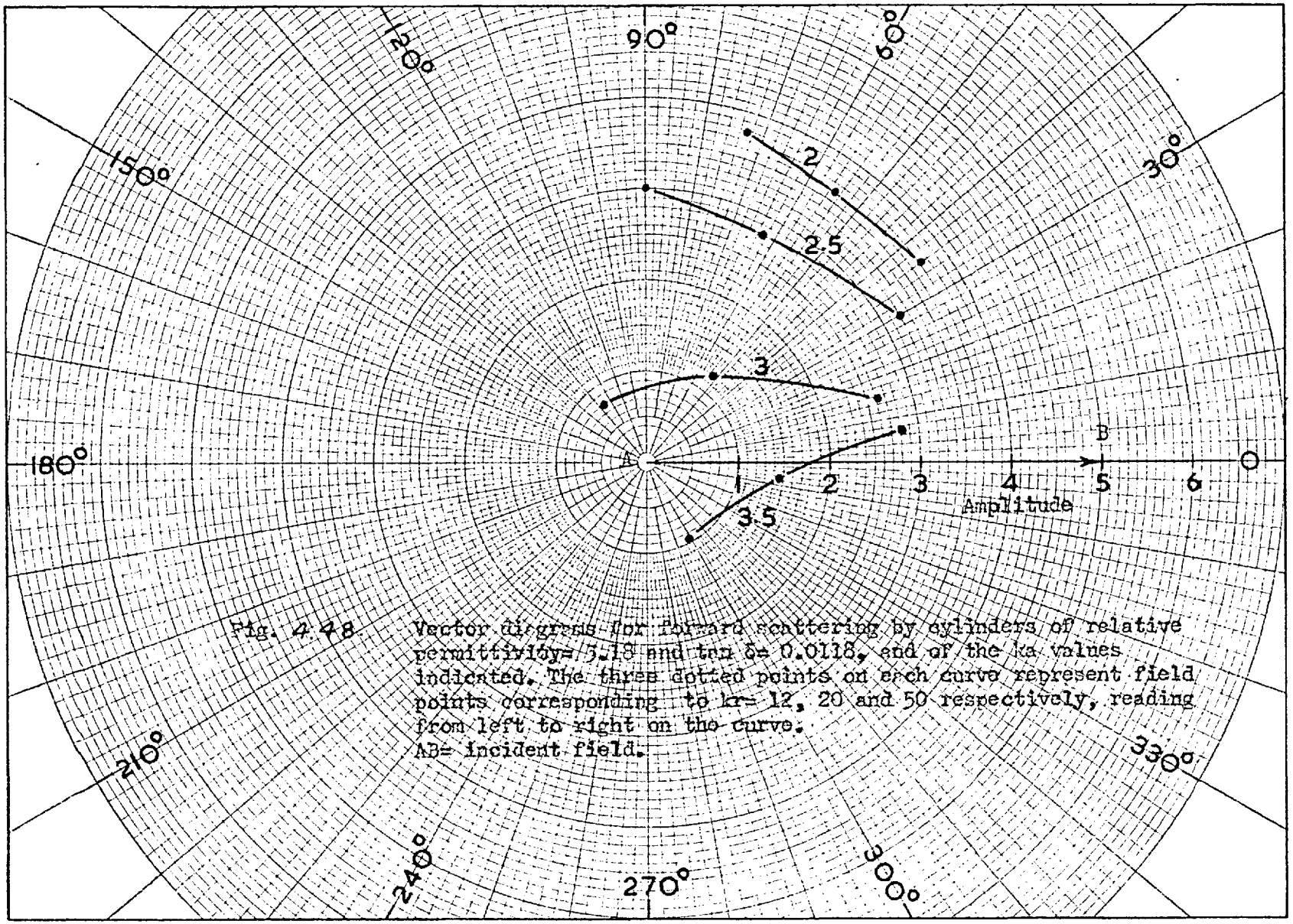

Fig. 4.48. Vector diagrams for forward scattering by cylinders of relative permittivity= 3.18 and tan δ= 0.0118, and of the ka values indicated. The three dotted points on each curve represent field points corresponding to kr= 12, 20 and 50 respectively, reading from left to right on the curve.
AB= incident field.

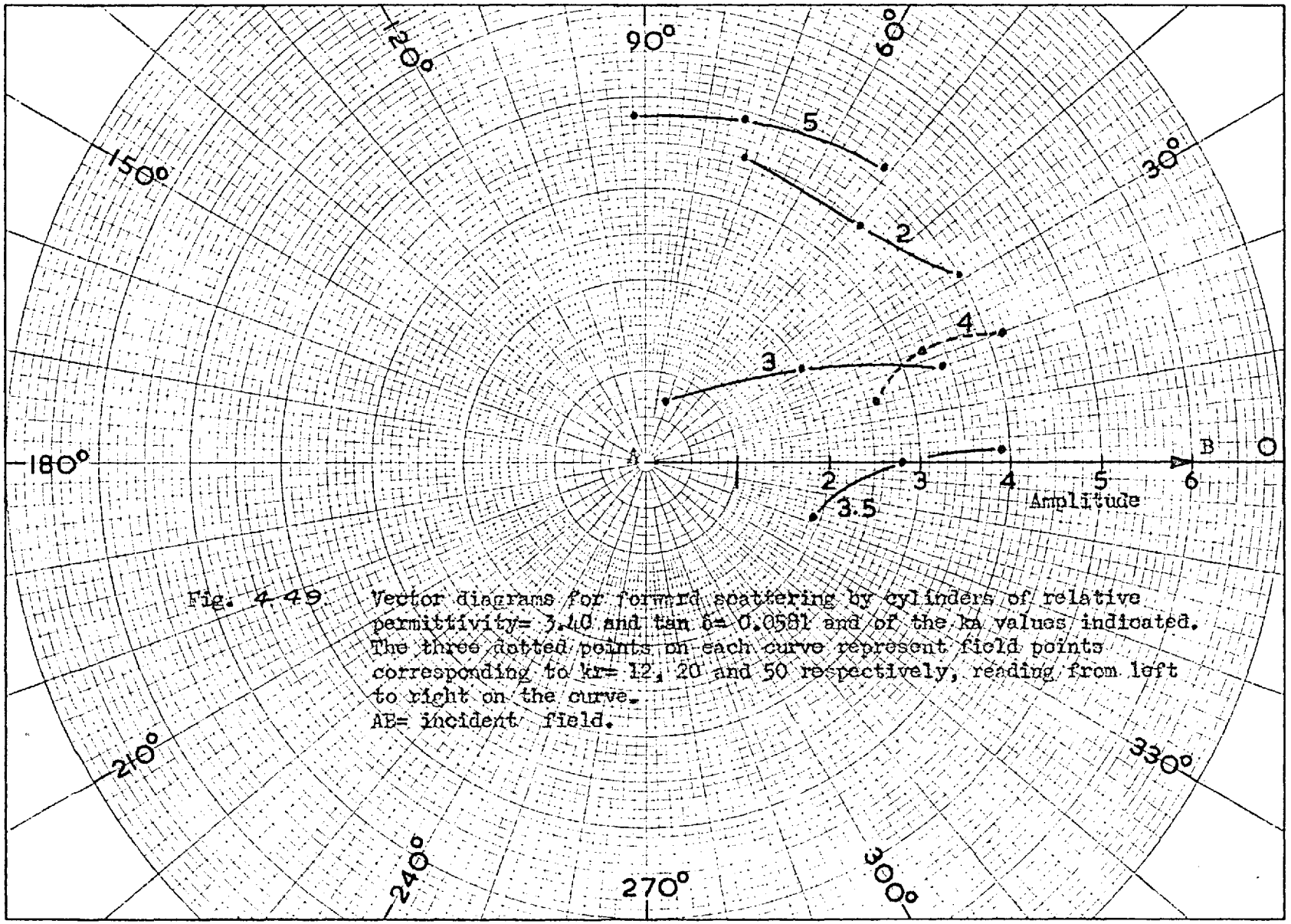

Fig. 4.49. Vector diagrams for forward scattering by cylinders of relative permittivity= 3.10 and tan δ= 0.0581 and of the ka values indicated. The three dotted points on each curve represent field points corresponding to kr= 12, 20 and 50 respectively, reading from left to right on the curve.
AE= incident field.

in discussing Fig. 4.13, as to the probable manner in which the second-turn curves would approach point B, i.e., the far-field phase shifts for the larger cylinders. It would appear that the curves for $k_1a = 4$ and 5 in the present figure approach in the same manner as on the first turn.

NOTE

The additional data for $k_1a = 3.75$, in Fig. 4.7, were taken in an attempt to determine the effect on the scattering of the cylinder's not fitting tightly between the two parallel plates. It appears that the initial small gap exerts a greater influence than the subsequent larger one, as far as the amplitude is concerned. The near field phase seems to be affected by the gap more than does the far. One might have suspected that the nature of the contact between the bottom plate and the cylinder would be inconsistent once the initial gap had been made, because then only the weight of the cylinder would be tending to force it into contact with the plate. However the results were found to be reproducible within the normal experimental error, as they were when the bottom cylinder surface was coated with a 0.001" layer of tinfoil. But in the latter case the results were always about 3 percent lower than before(in amplitude).

CHAPTER 5.

DIFFRACTION OF A CYLINDRICAL WAVE BY A DIELECTRIC CYLINDER.

5.1. The problem of the effect of the curvature of the incident wave front on the scattering properties of an obstacle arises whenever one employs an equipment involving a restriction on the maximum separation possible between source and obstacle. It also arises in the study of scattering by arrays of obstacles, since each obstacle is excited by waves originating at its neighbours.

One is interested not only in the conditions under which plane-wave excitation of the obstacle can be assumed, but also the extent to which the curvature of the wave front adds to the complexity of the scattering calculations.

5.2. Theoretical solution.

A line source, of as yet unspecified strength, is situated parallel to the axis of a dielectric cylinder and at a distance b from it. As before the external wave number is k_1, the internal one k_2, where $k_2 = \sqrt{\mu_r \varepsilon_r}\, k_1$, μ_r is the relative permeability of the cylinder and ε_r is its relative permittivity. Many of the details will be omitted, since the method is identical with that used in the plane-wave case.

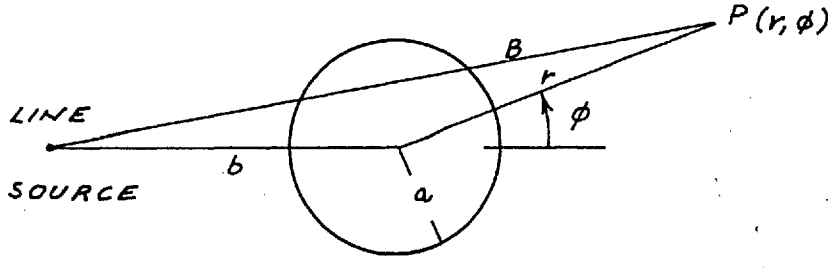

Fig. 5.1.

The fields can be written as-

$$E_{inc}(r,\phi) = A\, H_o^{(1)}(k_1 B) = A \sum_{o}^{\infty} \varepsilon_n (-i)^n H_n^{(1)}(k_1 b) J_n(k_1 r) \cos n\phi \quad (r < b) \qquad (5.1a)$$

$$= A \sum_{o}^{\infty} \varepsilon_n (-i)^n H_n^{(1)}(k_1 r) J_n(k_1 b) \cos n\phi \quad (r > b) \qquad (5.1b)$$

from Stratton, p.374.

$$E_{sc}(r,\phi) = \sum_{o}^{\infty} \varepsilon_n B_n H_n^{(1)} k_1 r) \cos n\phi \qquad (5.2)$$

$$E_{int}(r,\phi) = \sum_{o}^{\infty} \varepsilon_n A_n J_n(k_2 r) \cos n\phi \qquad (5.3)$$

The constants A_n and B_n are determined from the usual boundary conditions at r=a. The scattering amplitudes are then given by-

$$B_n = A(i)^n H_n^{(1)}(K_1 b) \begin{vmatrix} J_n(K_2 a) & , & (i)^n J_n(K_1 a) \\ \frac{n}{\mu_2 a} J_n(K_2 a) - \frac{K_2}{\mu_2} J_{n+1}(K_2 a), & (i)^n \left[\frac{n}{\mu_1 a} J_n(K_1 a) - \frac{K_1}{\mu_1} J_{n+1}(K_1 a)\right] \end{vmatrix} \Big/ \begin{vmatrix} J_n(K_2 a) & , & -H_n^{(1)}(K_1 a) \\ \frac{n}{\mu_2 a} J_n(K_2 a) - \frac{K_2}{\mu_2} J_{n+1}(K_2 a), & -\left[\frac{n}{\mu_1 a} H_n^{(1)}(K_1 a) - \frac{K_1}{\mu_1} H_{n+1}^{(1)}(K_1 a)\right] \end{vmatrix} \qquad (5.4)$$

This expression differs from the corresponding (4.3) for the plane-wave case only through the factor-

$$R = A\,(i)^n H_n^{(1)}(k_1 b) \qquad (5.5)$$

which will be called the "curvature" factor.

Since the effect of wave-front curvature, rather than amplitude, is being studied, it is now specified in (5.1a) that, in the absence of the cylinder, the incident amplitude always be unity at the position of

the cylinder axis. The factor A then becomes $1/H_o^{(1)}(k_1 b)$ and the "curvature" factor in (5.5)-

$$R = (i)^n H_n^{(1)}(k_1 b)/H_o^{(1)}(k_1 b) \qquad (5.6)$$

If b becomes very large in (5.4), one obtains (4.3) of the plane-wave case.

From (5.4) and (5.6) one sees that, if the plane wave calculations have been made, the scattering of a cylindrical wave can be determined by applying the "curvature" factor (5.6).

If one is interested in only the scattered field, (5.4) holds for all values of r. If the total field is required, the appropriate expression in (5.1) must be added.

5.3. Curvature effects.

The factor (5.6) has been applied to the case of the far-field scattering by a polystyrene cylinder of ka= 3, already computed for plane-wave incidence, for kb= 6 and 15. The resulting angular scattering distributions are compared with the plane-wave pattern to observe the curvature effect. The amplitudes are given in Fig. 5.2 and the phases in Fig. 5.3.

One can note the following effects-

(a) for certain angles the curvature seems to have little effect.

(b) the direction of convergence to the plane-wave case, in the case of the amplitude, is not always monotonic.

(c) rapid rates of change in amplitude are accompanied by

corresponding rapid phase changes, as in the plane-wave case.

(d) the forward-scattered field increases with the curvature, while the opposite holds for the back-scattered field.

(e) there is some shift in the positions of the side lobes, but it is not always in the same direction.

Calculations have also been made of the effect on the near fields. Figs. 5.4, 5.5, 5.6 show the results for forward, back and side-scattering, respectively. The curvature effect seems to be most marked in the case of back scattering- Fig. 5.5- where the form of the field, within a half wavelength of the cylinder surface, is changed for the highest curvatures. The forward scattered field is least affected. The phase conditions corresponding to Fig. 5.5 are given in Fig. 5.7. As for the amplitude, there is a marked curvature effect near the cylinder. Further away the phase curves tend to be parallel, with a phase constant of approximately 56.4 degrees per unit kr- slightly slower than for a plane wave in free space.

5.4. Analysis of the "curvature" factor.

An analysis of the "curvature" factor R in (5.6) is necessary for a prediction of the effect of the curvature on the scattering. The effect disappears when the factor converges to 1 + i 0, for all the n used, and for increasing b. The following Table lists the value of the factor for some of the terms considered in the above case. The values of kb are 6, 15, 25, 18π.

From this particular case, therefore, it would appear that, to reduce the curvature effect to a negligible value, a b/a ratio of the order of 25 would be required. The maximum value of n required is not

Fig. 5.2. Effect of the curvature of the incident wave front on the angular distribution of the far field scattered by a polystyrene cylinder of ka = 3.

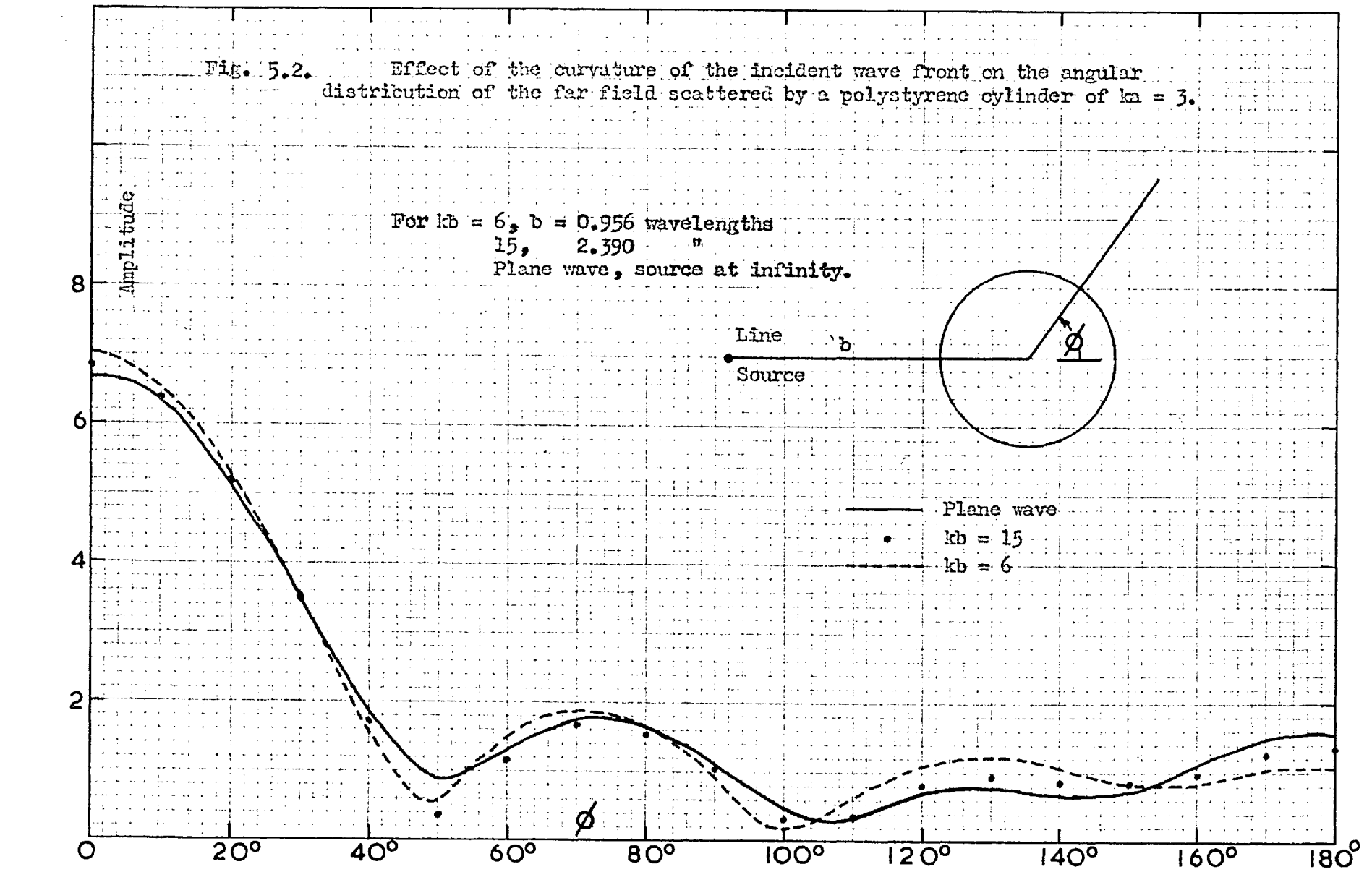

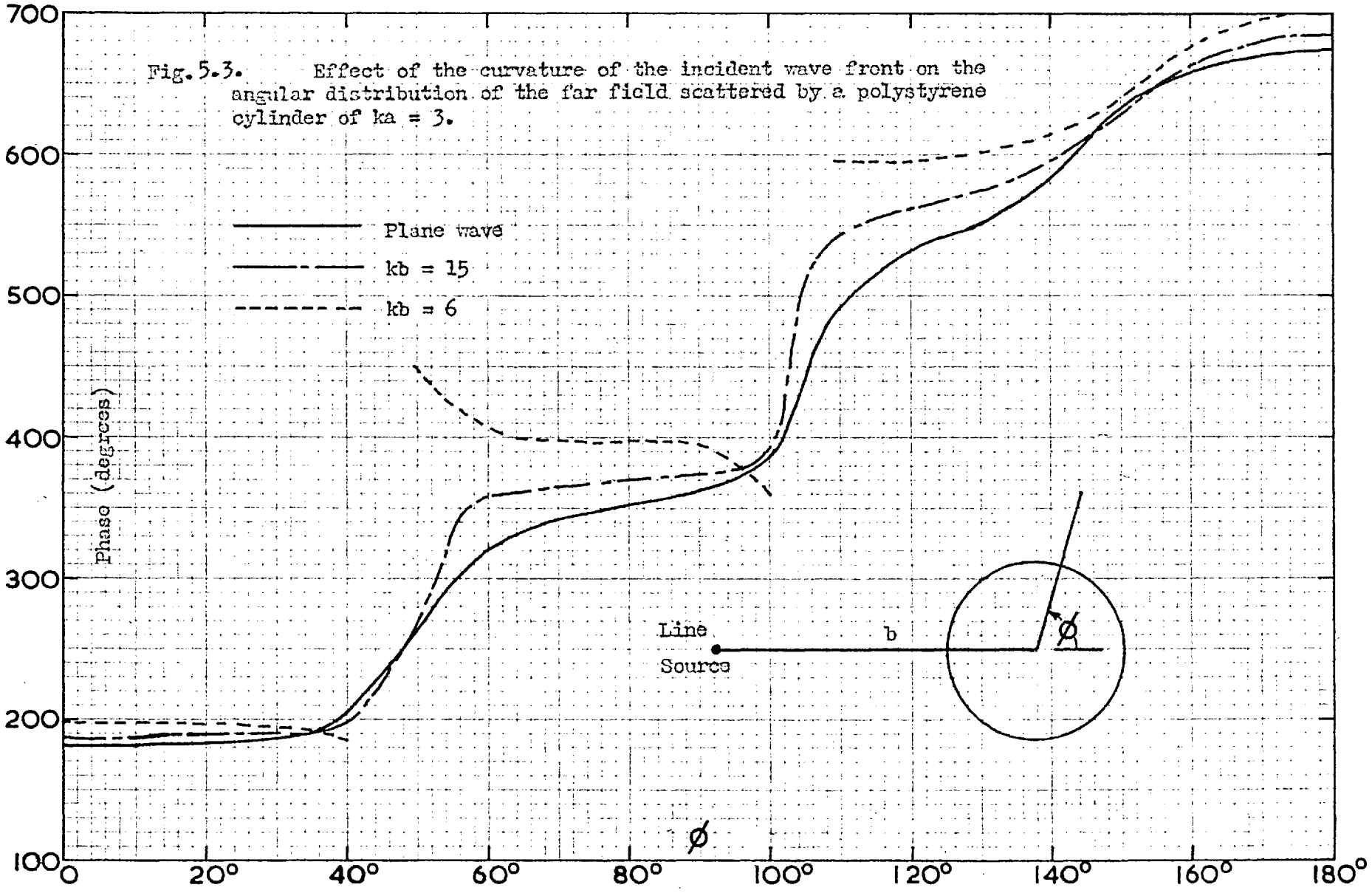

Fig. 5.3. Effect of the curvature of the incident wave front on the angular distribution of the far field scattered by a polystyrene cylinder of ka = 3.

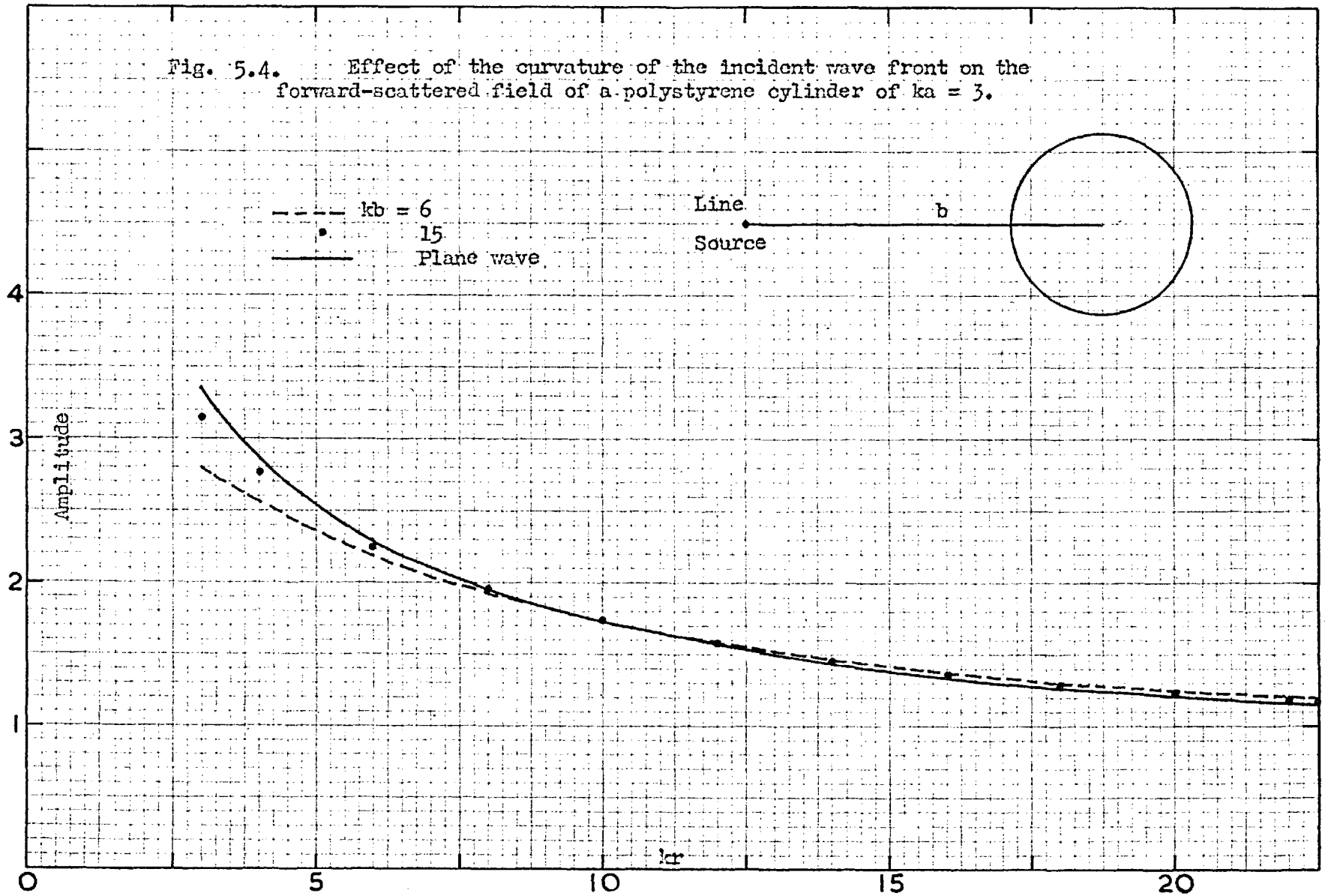

Fig. 5.4. Effect of the curvature of the incident wave front on the forward-scattered field of a polystyrene cylinder of ka = 3.

Fig. 5.5. Effect of the curvature of the incident wave front on the back-scattered field of a polystyrene cylinder of ka = 3.

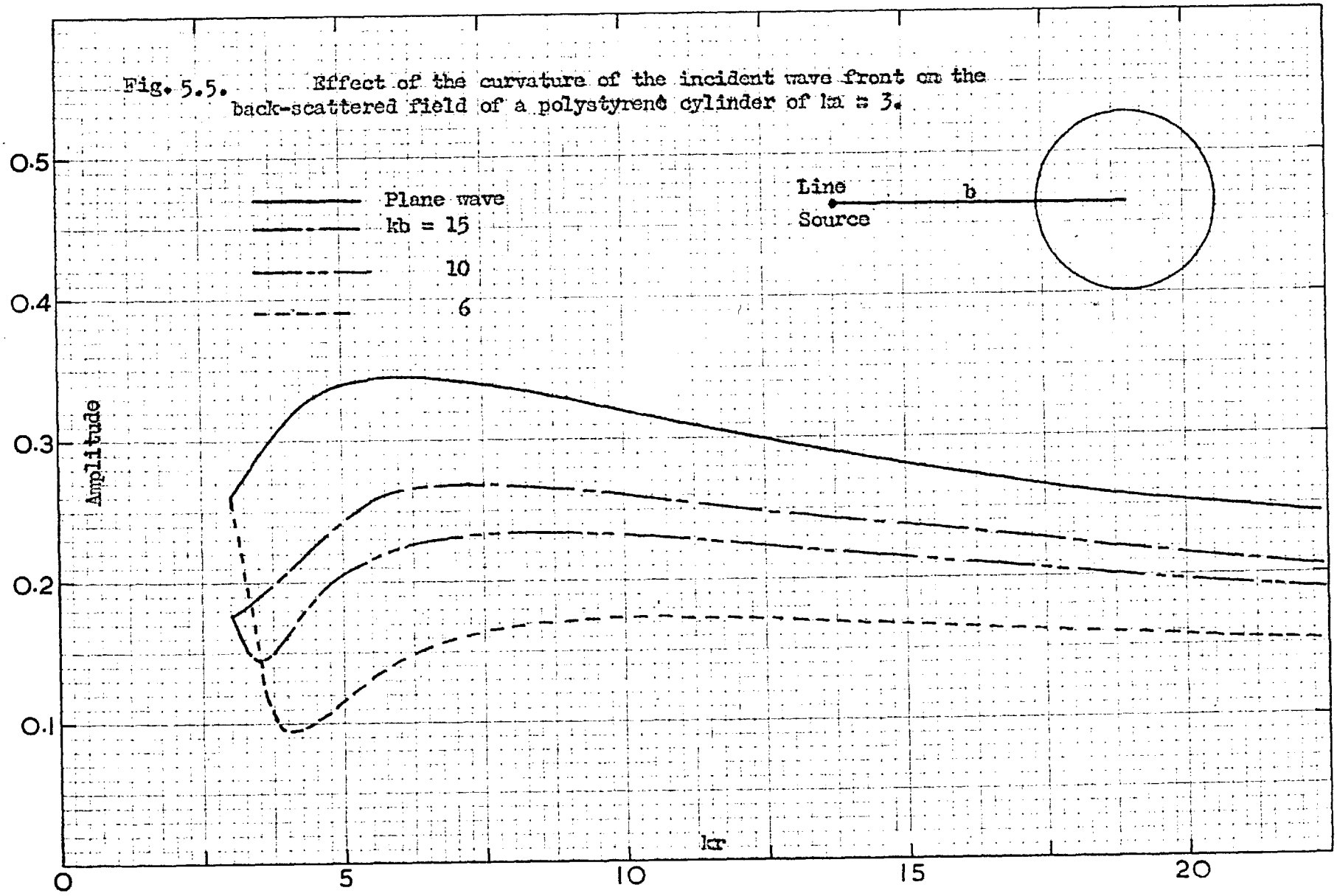

Fig. 5.6. Effect of the curvature of the incident wave front on the side-scattered field of a polystyrene cylinder of ka = 3.

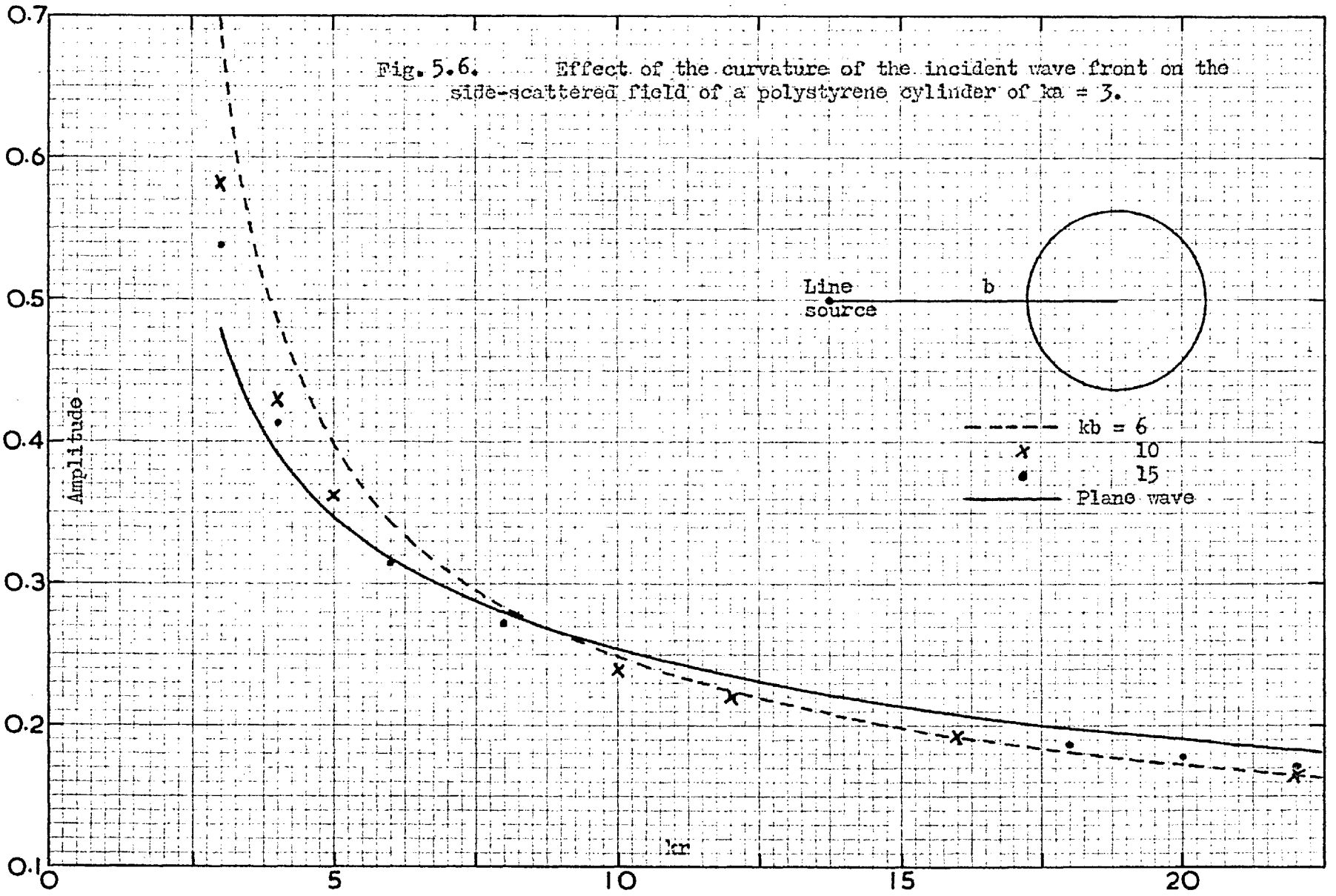

Data Sheet No. 71 Supplement to Scale & Radius Factors

Wightman Mountain Ltd
Artillery House, Artillery Row, Westminster, S.W.1

Fig. 5.7 Effect of the curvature of the incident wave front on the phase of the back-scattered field of a polystyrene cylinder of ka = 3.

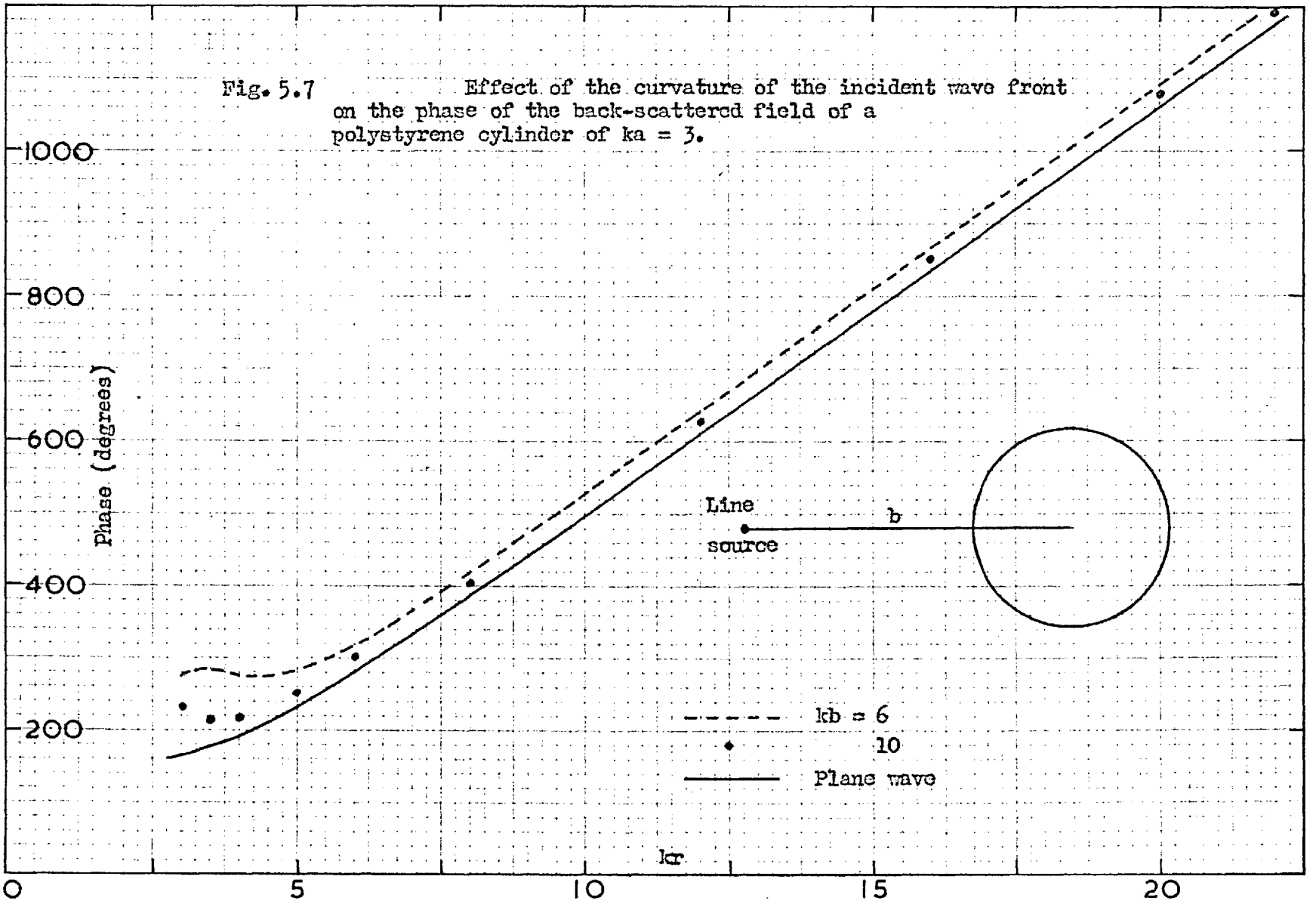

TABLE- The effect of the value of kb on the curvature factor R.

	R			
n	kb = 6	15	25	18π
0	1.000 + i0.000	1.000 + i0.000	1.000 + i0.000	1.000 + i0.000
1	1.006 + i0.081	1.001 + i0.033	1.000 + i0.020	1.000 + i0.013
2	0.972 + i0.334	0.996 + i0.133	0.998 + i0.080	1.000 + i0.040
3	0.780 + i0.731	0.965 + i0.299	0.987 + i0.180	0.997 + i0.084
4	0.241 + i1.115	0.876 + i0.520	0.955 + i0.317	0.991 + i0.146

highly-sensitive to the value of the constants of the cylinder material, since the convergence of the determinant in (5.4) depends mainly on the Hankel functions, whose argument is independent of those constants.

As an example of the incident phase lag across the ka=3 cylinder due to the wave front curvature, the incident field at the extremity of a diameter normal to a line through the source and the cylinder axis lags that at the axis by approximately 20 degrees for kb=15 and 40 degrees for kb=6.

Two observations on the R factor can be made on the basis of the Reciprocity Theorem-

(a) if one has calculated the field at the point (b,π) for plane wave incidence in the direction $\phi = 0$, then there has also been calculated the far field in the direction $\phi=\pi$ for excitation from a line source at (b,π).

Since the former shows fluctuations about the unobstructed

value as b is changed- the amplitude of the fluctuations decreasing with increasing b- then the far field of a line source in front of the cylinder will show the same characteristics.

(b) if one has calculated the field at the point (b,0) for a plane wave incident in the direction $\phi=0$, then there has also been calculated the far field in the direction $\phi=\pi$ for a line source at (b,0).

The former has been shown to reveal a zero field for certain combinations of b and k_2a, and thus the far field is zero for that cylinder and the line source at that value of b. This zero condition does not seem to occur for metal cylinders(except for the obvious case b=a).

NOTE

After this work had been completed, a letter by Faran(1953), who treated the far fields of the acoustic case with boundary conditions corresponding to a metal cylinder in electromagnetics, indicated that the normalizing procedure given above in 5.2 had been discussed by Morse, Lowan, Feshbach and Lax(see Morse). Faran's numerical results indicated the same trends as given here.

CHAPTER 6.

INTERNAL FIELD OF A DIELECTRIC CYLINDER.

6.1. If one knew the field distribution over the cross-section of a diffracting cylinder, he could write an expression for the external field, even though he might not be able to evaluate the resulting expression. The field inside a scattering, dielectric cylinder is often not even discussed in papers on that subject, since it cannot be measured. However, it has been seen that Rayleigh's(1918) method of treating scattering by large cylinders is based on an assumption about the form of the internal field. That assumption- that the internal field is the same as existed there with the cylinder absent- would not be valid in the cases being considered in this study, and one might be led to inquire as to the complexity, in amplitude and phase, of the internal field in some typical cases.

6.2. The form of the field.

From Eqs. 4.8 and 4.9 the internal field of a cylinder of radius a, permeability μ_2, permittivity ε_2 and wave number $k_2 = \sqrt{\mu_r \varepsilon_r}\, k_1$, where $\mu_r = \frac{\mu_2}{\mu_1}$, $\varepsilon_r = \frac{\varepsilon_2}{\varepsilon_1}$ and the subscripts 1 and 2 refer to the external and internal regions, respectively, is given by-

$$E(r,\phi) = \sum_{0}^{\infty} \varepsilon_n A_n J_n(k_2 r) \cos n\phi \qquad (6.1)$$

where

$$A_n = (i)^n \frac{k_1}{\mu_1} B_n \Big/ \left[\frac{n_1}{a} P_n + Q_n\right] \qquad (6.2a)$$

$$B_n = J_n(k_1 a) H_{n+1}^{(1)}(k_1 a) - J_{n+1}(k_1 a) H_n^{(1)}(k_1 a) \qquad (6.2b)$$

$$P_n = \frac{1}{\mu_2} J_n(k_2 a) H_n^{(1)}(k_1 a) - \frac{1}{\mu_1} J_n(k_2 a) H_n^{(1)}(k_1 a) \qquad (6.2c)$$

$$Q_n = \frac{\kappa_1}{\mu_1} J_n(k_2 a) H_{n+1}^{(1)}(k_1 a) - \frac{\kappa_2}{\mu_2} J_{n+1}(k_2 a) H_n^{(1)}(k_1 a) \qquad (6.2d)$$

By expanding the B_n and applying the Bessel function Wronskian relationship (Mc.Lachlan, p.156) one obtains for the internal field-

$$A_n = (i)^n \frac{\kappa_1}{\mu_1} (2/i\pi k_1 a) / \left[\frac{n}{a} P_n + Q_n \right] \qquad (6.3)$$

If $\mu_r = 1$, the expression (6.3) simplifies to-

$$A_n = (i)^n (2/i\pi k_1 a) / \left[J_n(k_2 a) H_{n+1}^{(1)}(k_1 a) - k_r J_{n+1}(k_2 a) H_n^{(1)}(k_1 a) \right] \qquad (6.4)$$

where $k_r = k_2/k_1 = \sqrt{\varepsilon_r}$.

If only the field on the cylinder axis is being considered, then only the first term of (6.3) is needed, because of the presence of the expression $J_n(k_2 r)$ in (6.1). Then-

$$E(0) = A_o = (2/i\pi k_1 a) / \left[J_o(k_2 a) H_1^1(k_1 a) - \frac{\kappa_r}{\mu_r} J_1(k_2 a) H_o^1(k_1 a) \right] \qquad (6.5)$$

For small cylinders one can use the small-argument approximations for the Bessel functions to obtain from (6.5)-

$$E(0)\Big|_{k_2 a \text{ small}} = \frac{4}{i} \frac{1}{\pi \kappa_2^2 a^2 \left(1 - \frac{\kappa_r^2}{\mu_r}\right) - i2\left(2 - \frac{\kappa_2^2 a^2}{\mu_r} \ln \frac{2}{\gamma \kappa_1 a}\right)} \qquad (6.6)$$

where γ is Euler's constant. For vanishingly-small $k_2 a$ this becomes unity, the incident amplitude.

For large cylinders the large-argument approximations can be applied to obtain, after using the exponential form of the cosine functions-

$$E(0)\Big|_{k_2 a \text{ large}} = \frac{2\mu_r\sqrt{\kappa_r}}{e^{i\alpha}} \frac{1}{\omega_1 e^{-i\beta} - \omega_2 e^{i\beta}}$$

$$= \frac{2\mu_r\sqrt{\kappa_r}}{e^{i\alpha}} \frac{\omega_1 e^{-i\beta} + \omega_2 e^{i\beta}}{\omega_1^2 e^{-i2\beta} - \omega_2^2 e^{i2\beta}} \qquad (6.7)$$

where- $$\alpha = \kappa_1 a - \pi/4 \; ; \quad \omega_1 = \kappa_r + \mu_r$$

$$\beta = \kappa_2 a - \pi/4 \; ; \quad \omega_2 = \kappa_r - \mu_r \qquad (6.8)$$

Now make the transformation- $$\delta = \frac{1}{\kappa_r}\left(\kappa_2 a - \pi/4\right) = \kappa_1 a - \pi/4\kappa_r \qquad (6.9)$$

and (6.7) becomes-

$$E(0)\Big|_{k_2 a \text{ large}} = \sqrt{\kappa_r}\, e^{i\tau\pi/4}\left[\frac{2\mu_r\omega_1 e^{i(\delta-\beta)} + 2\mu_r\omega_2 e^{i(\delta+\beta)}}{\omega_1^2 e^{i2(\delta-\beta)} - \omega_2^2 e^{i2(\delta+\beta)}}\right] \qquad (6.10)$$

where $\tau = (k_r - 1)/k_r$.

But the bracketed expression in (6.10) is identical with that for the center field of a parallel-sided slab of the same material as the cylinder, centered on the origin and of half-thickness, d, given by-

$$d = a - \pi/4k_2 \quad , \text{ i.e., } k_2 d = k_2 a - \pi/4$$

from (6.8) and (6.9) (Stratton, p.511), and on which a plane wave of unit amplitude is incident normally from medium k_1. The amplitude of E (0) has, however, been increased by a factor of $\sqrt{\kappa_r} = (\mu_r \varepsilon_r)^{1/4}$ and there is an increase of phase given by exp $i\pi(k_r - 1)/4k_r$.

Fig. 6.1 has been plotted from (6.5) for polystyrene $\mu_r = 1$, $\kappa_r = 1.6$. Included are the corresponding calculations for a polystyrene slab of half-thickness, a. The amplitude has been normalized to an incident amplitude of

unity and the phase refers to the incident phase at the cylinder axis or the slab center.

From (6.10) the ratio of the amplitudes should be $\sqrt{k_r} = \sqrt{1.6}$ = 1.264, and the lead in phase of the cylinder curve should be $\frac{\pi(k_r - 1)}{4k_r}$ = 16.9 degrees. The displacement of the cylinder pattern along the k_1a axis should be, from (6.9)-

$$\Delta\, k_1a = \pi/4k_r = 0.491.$$

The peaks in each pattern should repeat at intervals of $\pi/1.6 = 1.96$.

All these characteristics appear in the curves, even for the small values of k_1a used. One notices also, that, whereas the slab-field amplitude never exceeds the free-space value, the cylinder field oscillates about it between the limits k_r and $1/k_r$.

One might anticipate that this relationship between the fields in the cylinder and slab would hold even when the field point was not on the axis. It holds as long as the distance from the axis is small enough that only the low-order $J_n(k_2r)$ in (6.1) have appreciable value. Then the denominator of (6.3) and (6.4) can be approximated as before. In this case, however, the solution appears in two parts, for n odd and for n even. But by use of the two Bessel function relationships (McLachlan, p. 160)-

$$\sum (i)^n \varepsilon_n J_n(k_2r) \cos n\phi = \cos(k_2r\cos\phi) \quad (\text{n even})$$
$$= i \sin(k_2r\cos\phi) \quad (\text{n odd})$$

the same result as before can be obtained.

Some additional calculations for a polystyrene cylinder, for several values of k_1a, are shown in Figs. (6.2)-(6.9). The fields are

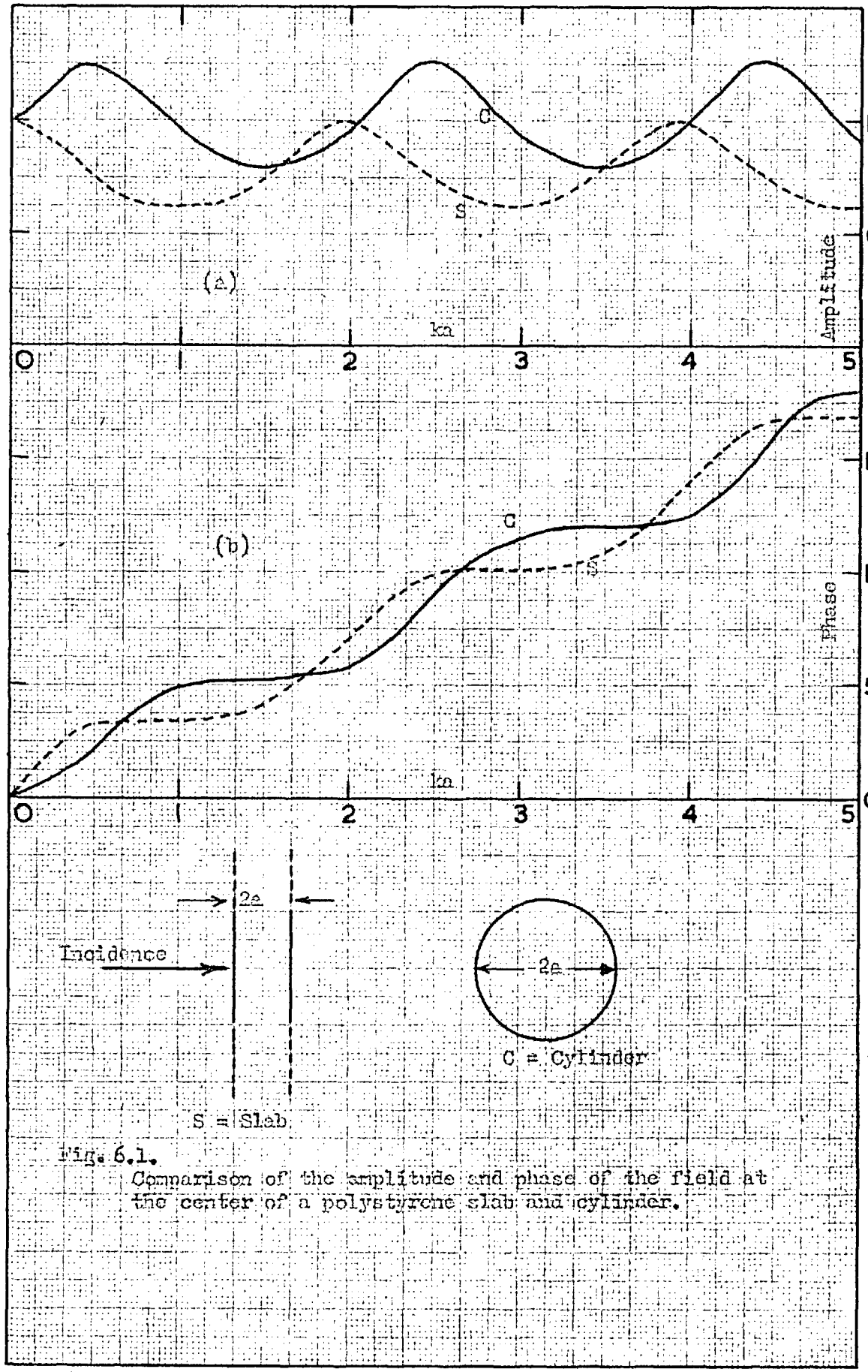

Fig. 6.1.
Comparison of the amplitude and phase of the field at the center of a polystyrene slab and cylinder.

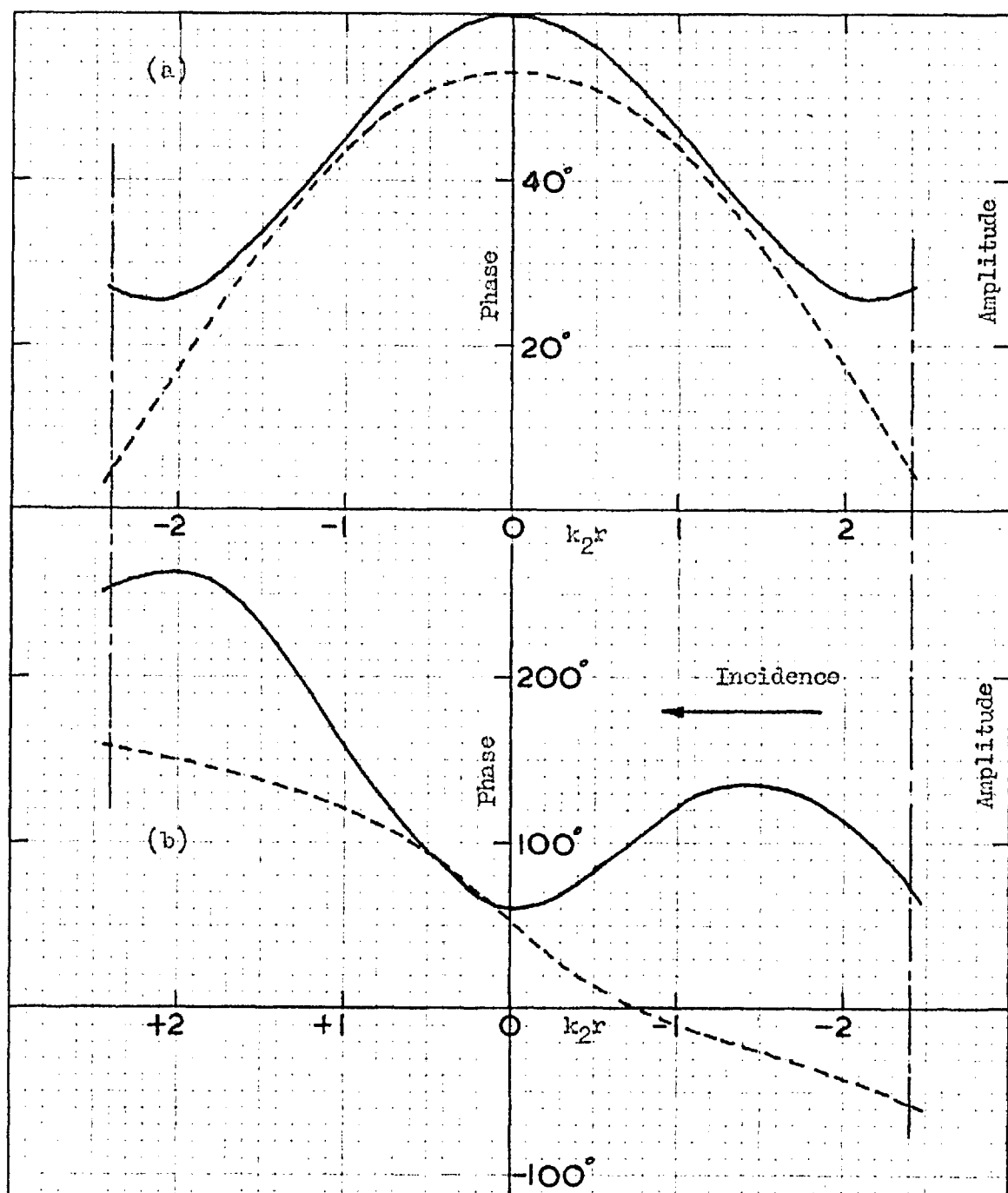

Fig. 6.2. Internal field of a polystyrene cylinder of ka = 1.5 along a diameter-

(a) Normal to the direction of incidence
(b) In the direction of incidence

——— Amplitude
- - - Phase

$k_2 = 2\pi /$ Internal wavelength

The vertical dot-dash lines indicate the cylinder surface.

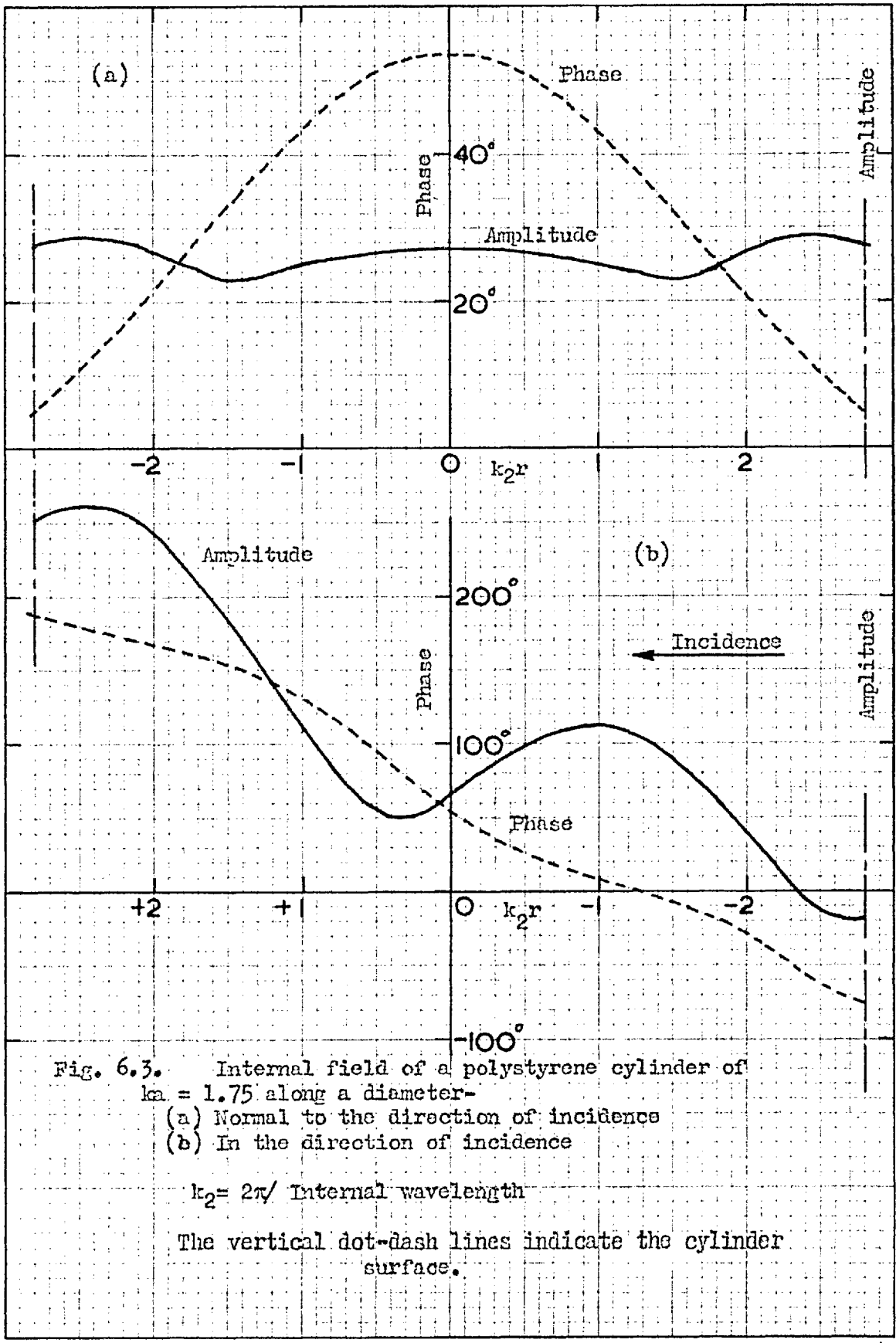

Fig. 6.3. Internal field of a polystyrene cylinder of $ka = 1.75$ along a diameter-
(a) Normal to the direction of incidence
(b) In the direction of incidence

$k_2 = 2\pi /$ Internal wavelength

The vertical dot-dash lines indicate the cylinder surface.

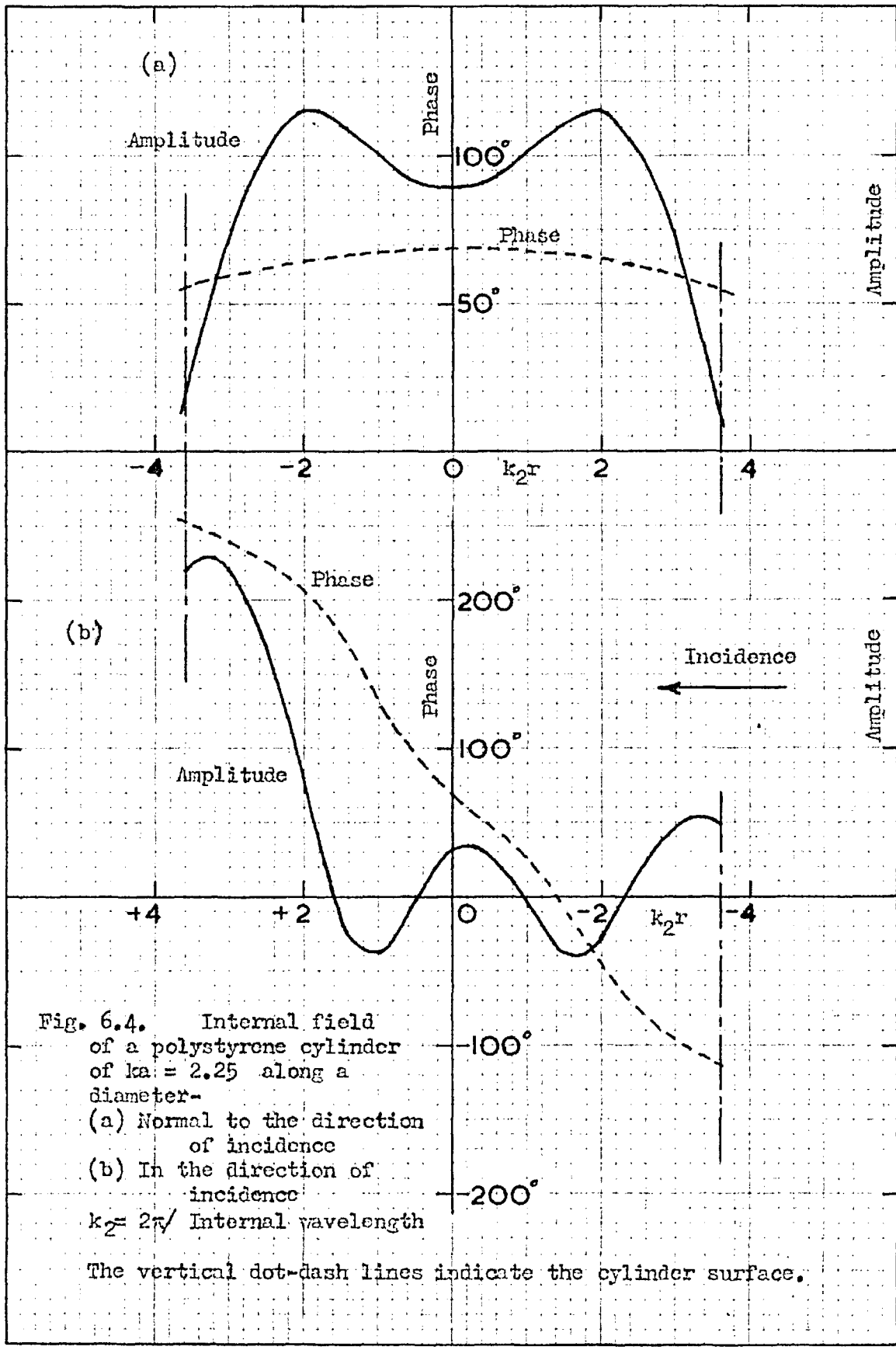

Fig. 6.4. Internal field of a polystyrene cylinder of ka = 2.25 along a diameter-
(a) Normal to the direction of incidence
(b) In the direction of incidence
$k_2 = 2\pi/$ Internal wavelength

The vertical dot-dash lines indicate the cylinder surface.

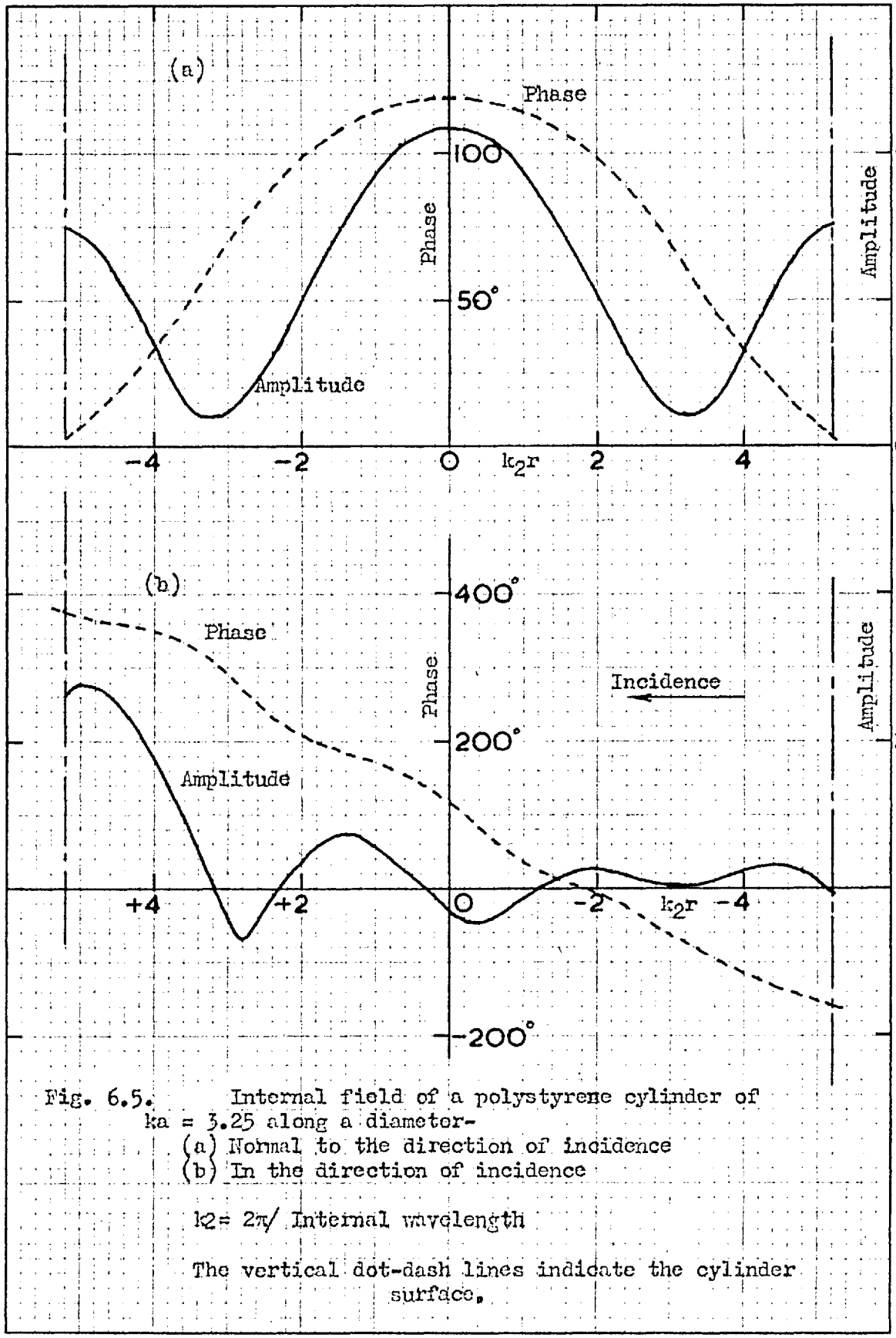

Fig. 6.5. Internal field of a polystyrene cylinder of ka = 3.25 along a diameter-
(a) Normal to the direction of incidence
(b) In the direction of incidence

$k_2 = 2\pi/$ Internal wavelength

The vertical dot-dash lines indicate the cylinder surface.

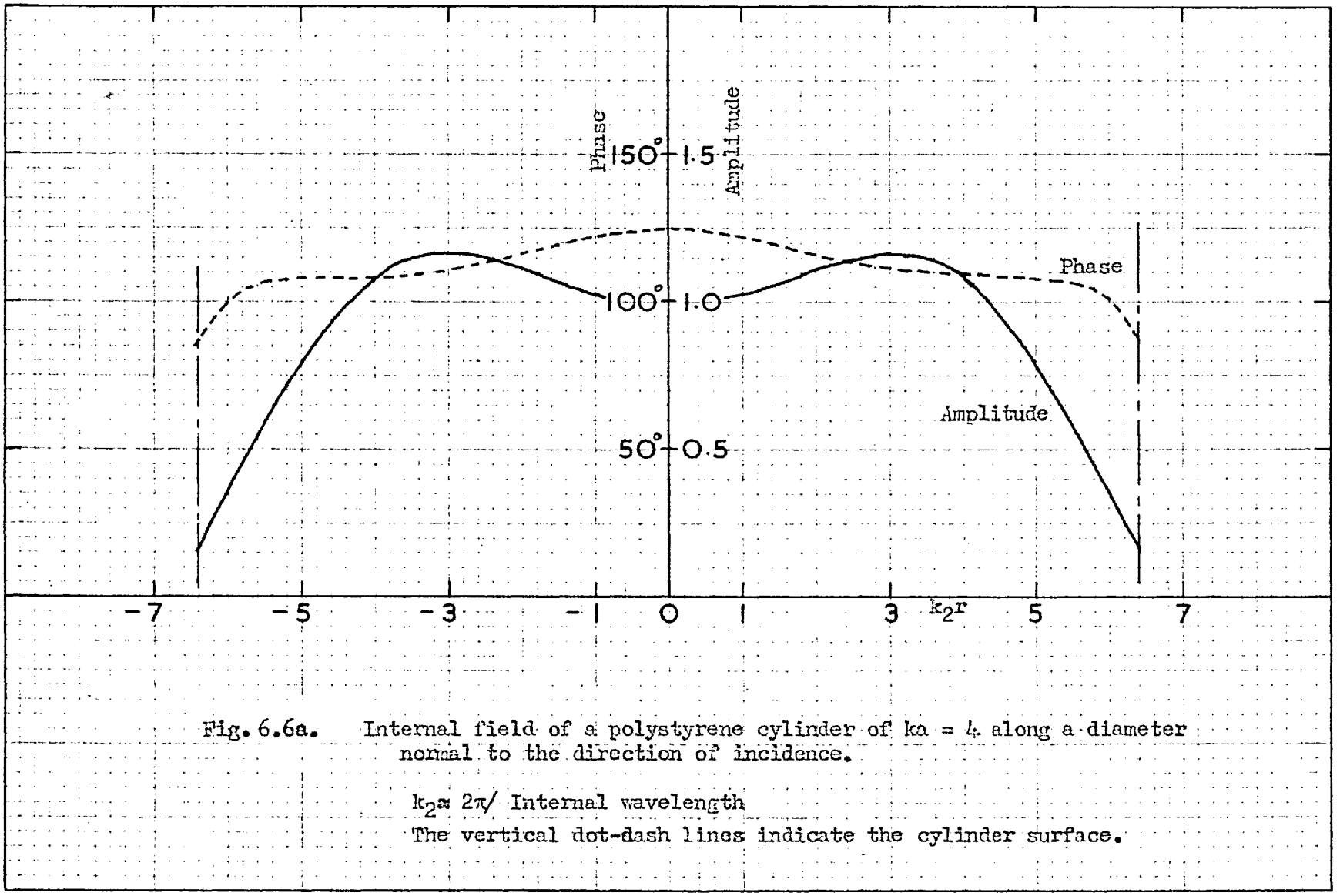

Fig. 6.6a. Internal field of a polystyrene cylinder of ka = 4 along a diameter normal to the direction of incidence.

$k_2 = 2\pi/$ Internal wavelength

The vertical dot-dash lines indicate the cylinder surface.

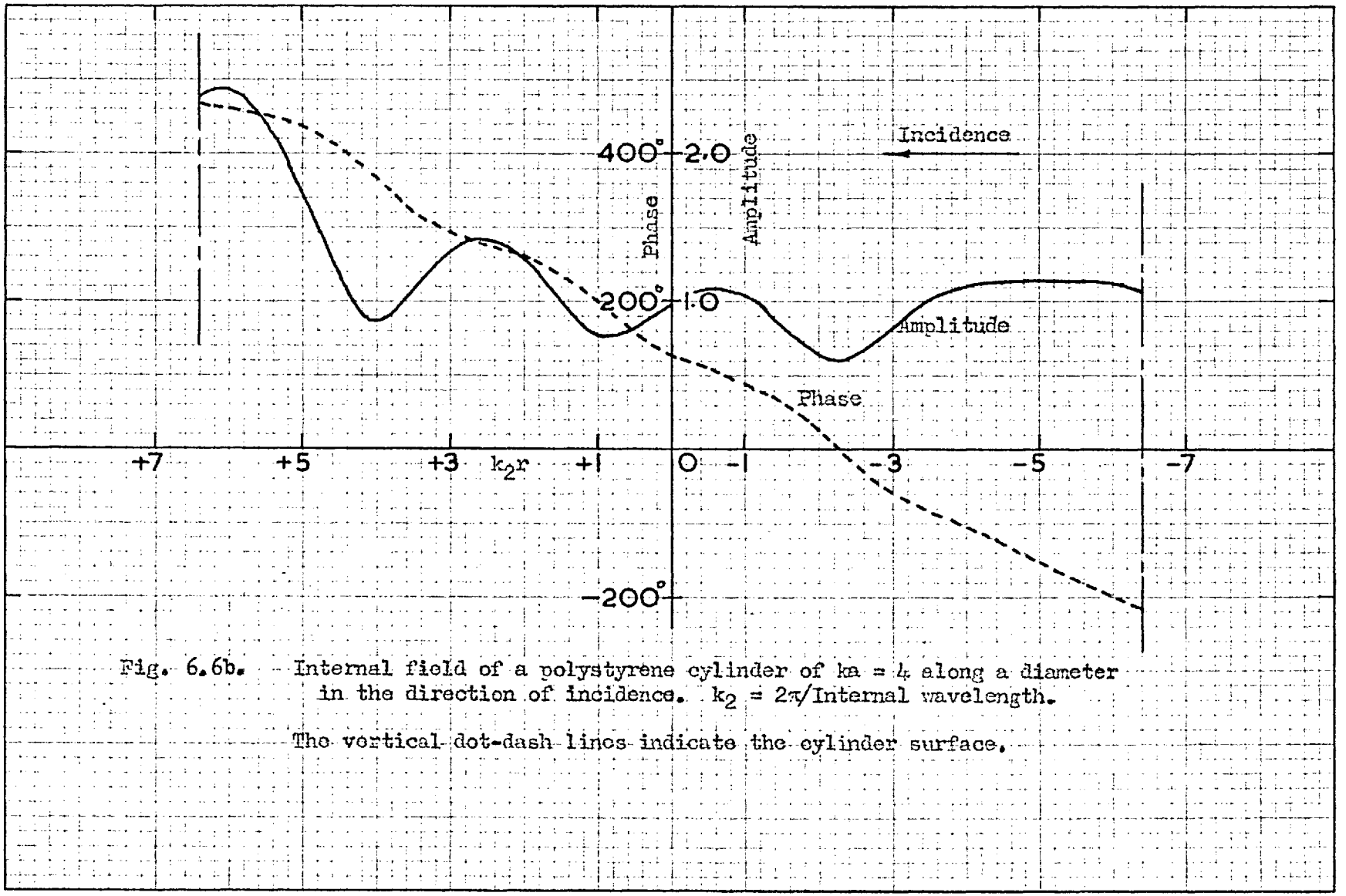

Fig. 6.6b. Internal field of a polystyrene cylinder of ka = 4 along a diameter in the direction of incidence. $k_2 = 2\pi/\text{Internal wavelength}$.

The vertical dot-dash lines indicate the cylinder surface.

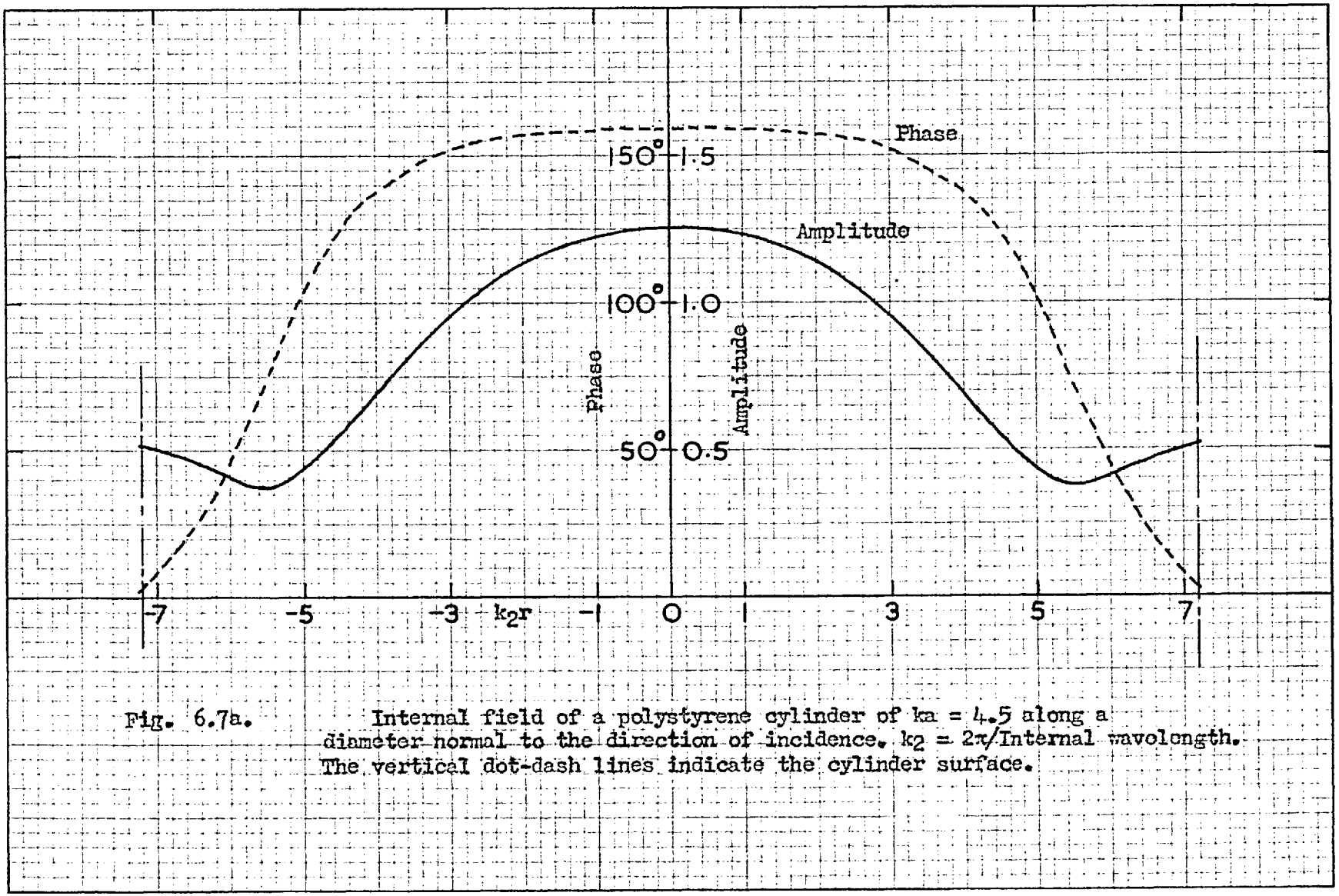

Fig. 6.7a. Internal field of a polystyrene cylinder of ka = 4.5 along a diameter normal to the direction of incidence. $k_2 = 2\pi/$Internal wavelength. The vertical dot-dash lines indicate the cylinder surface.

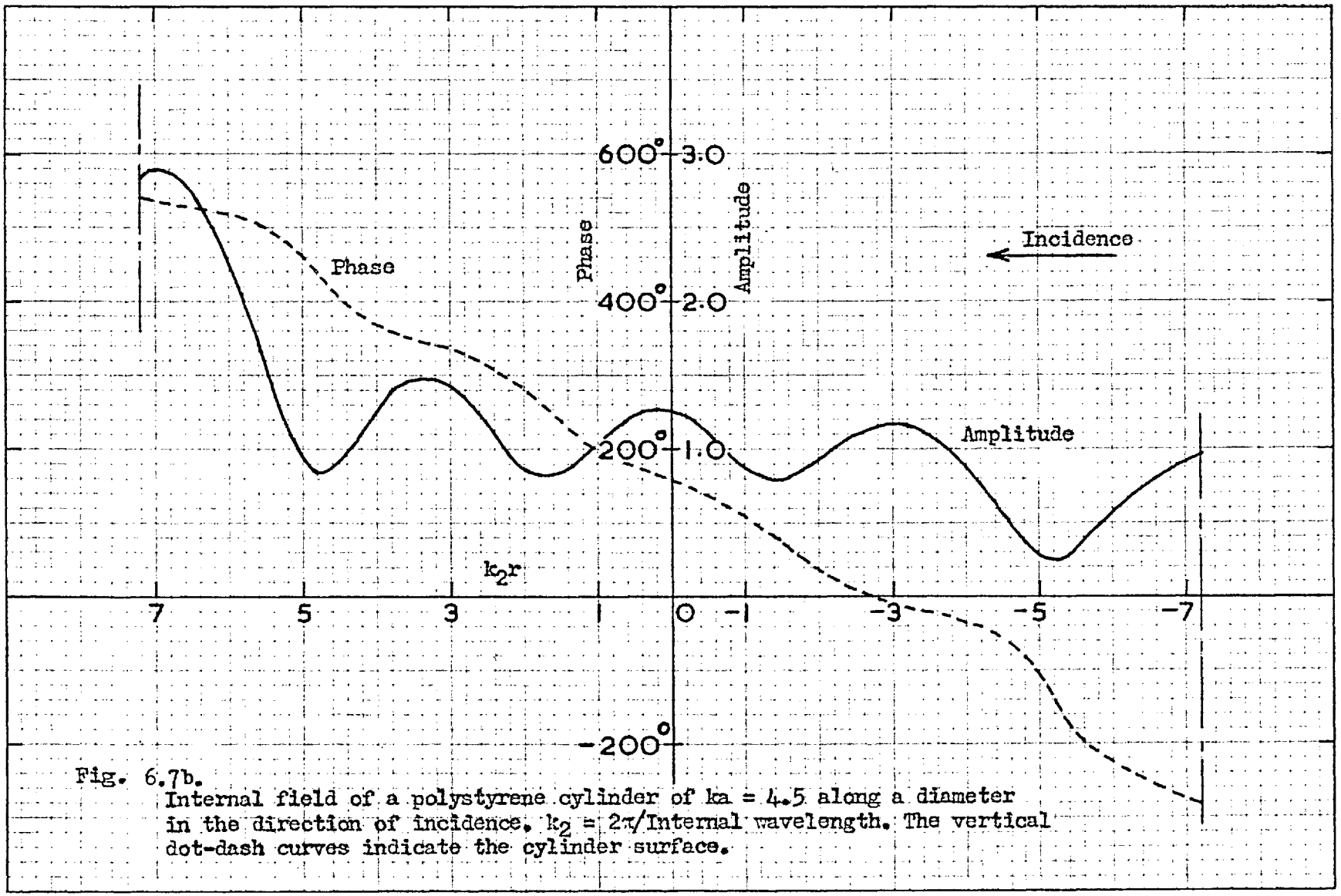

Fig. 6.7b.
Internal field of a polystyrene cylinder of ka = 4.5 along a diameter in the direction of incidence. $k_2 = 2\pi/\text{Internal wavelength}$. The vertical dot-dash curves indicate the cylinder surface.

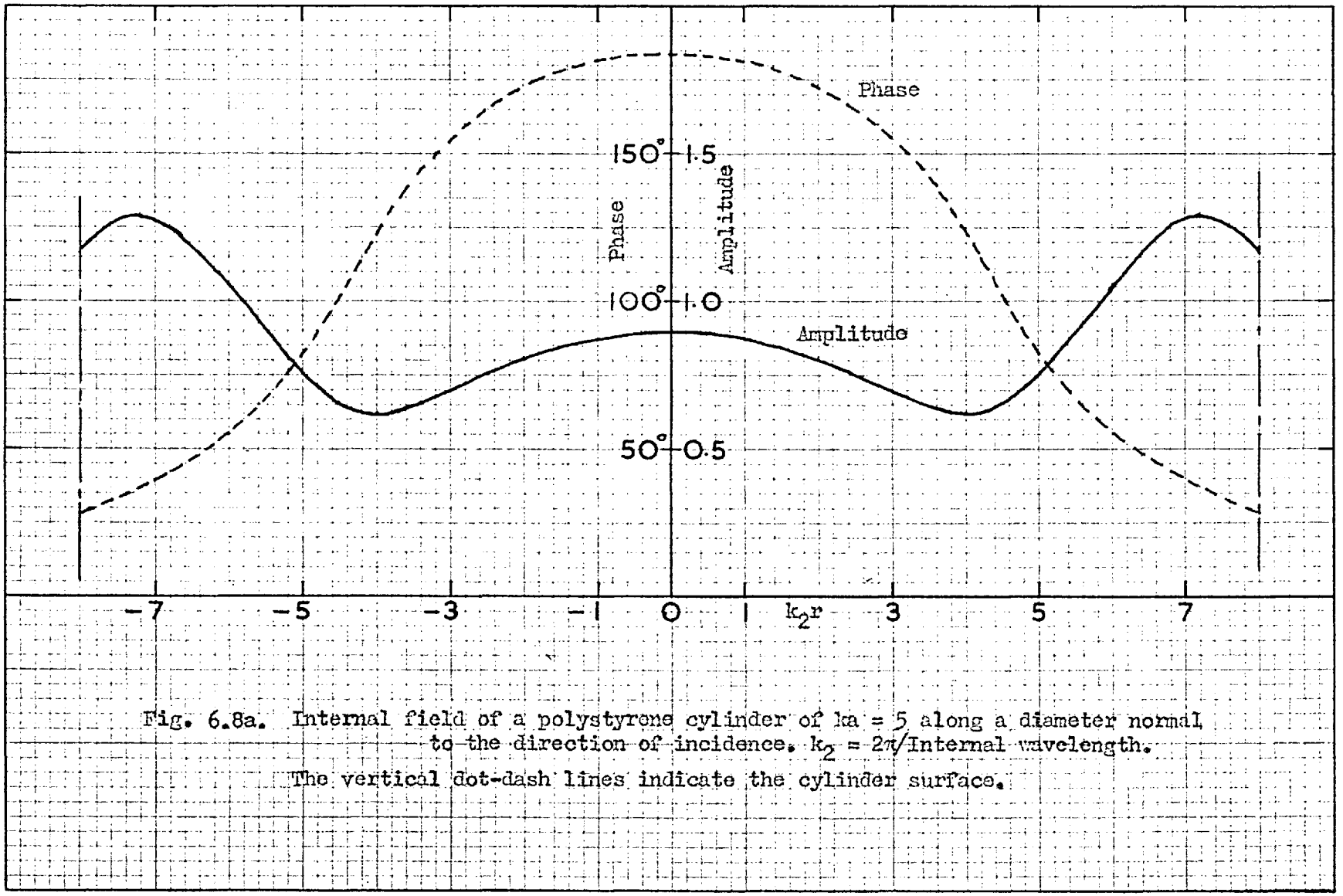

Fig. 6.8a. Internal field of a polystyrene cylinder of ka = 5 along a diameter normal to the direction of incidence. $k_2 = 2\pi/\text{Internal wavelength}$.

The vertical dot-dash lines indicate the cylinder surface.

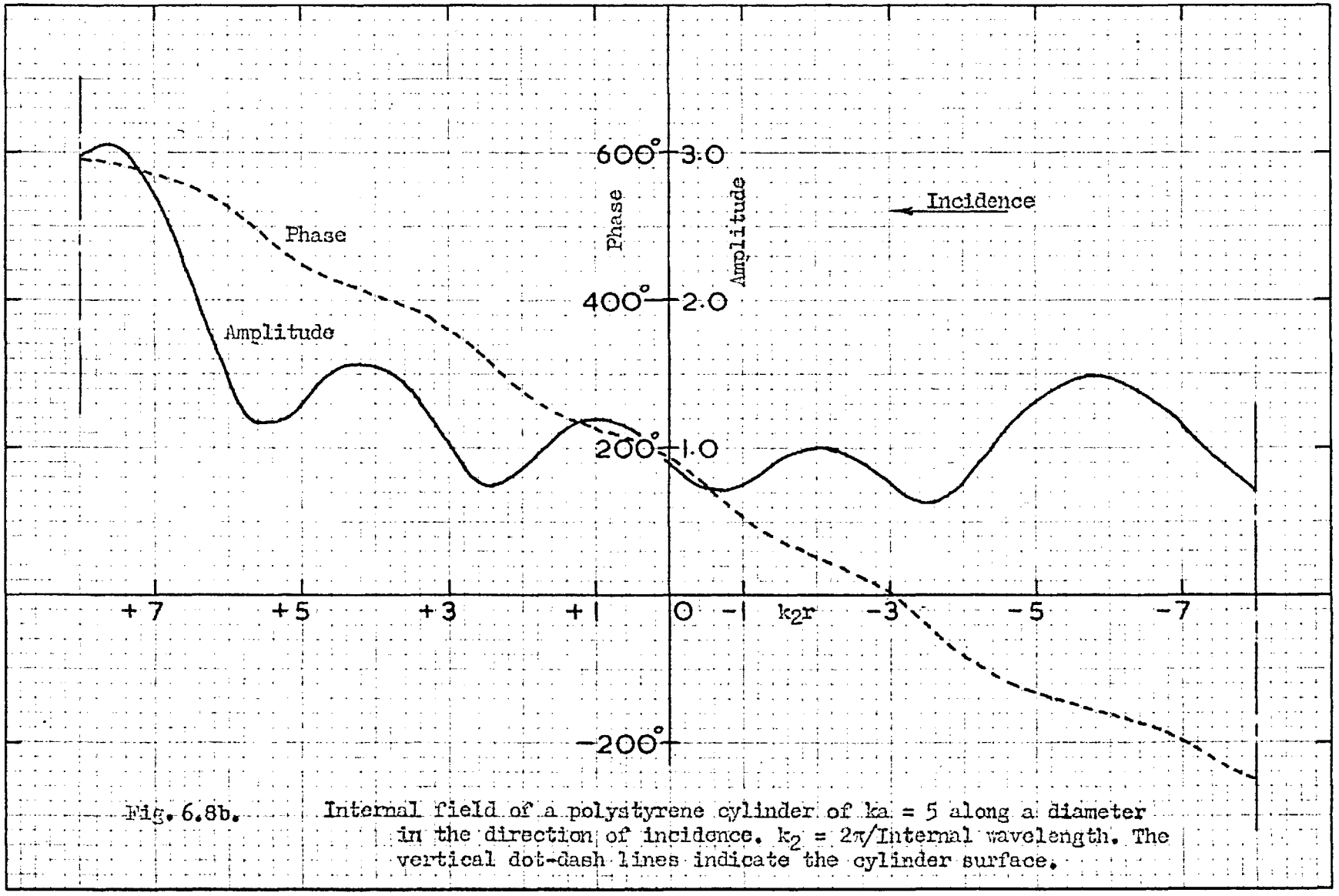

Fig. 6.8b. Internal field of a polystyrene cylinder of ka = 5 along a diameter in the direction of incidence. $k_2 = 2\pi/\text{Internal wavelength}$. The vertical dot-dash lines indicate the cylinder surface.

Artillery House, Artillery Row, Westminster, S.W.1

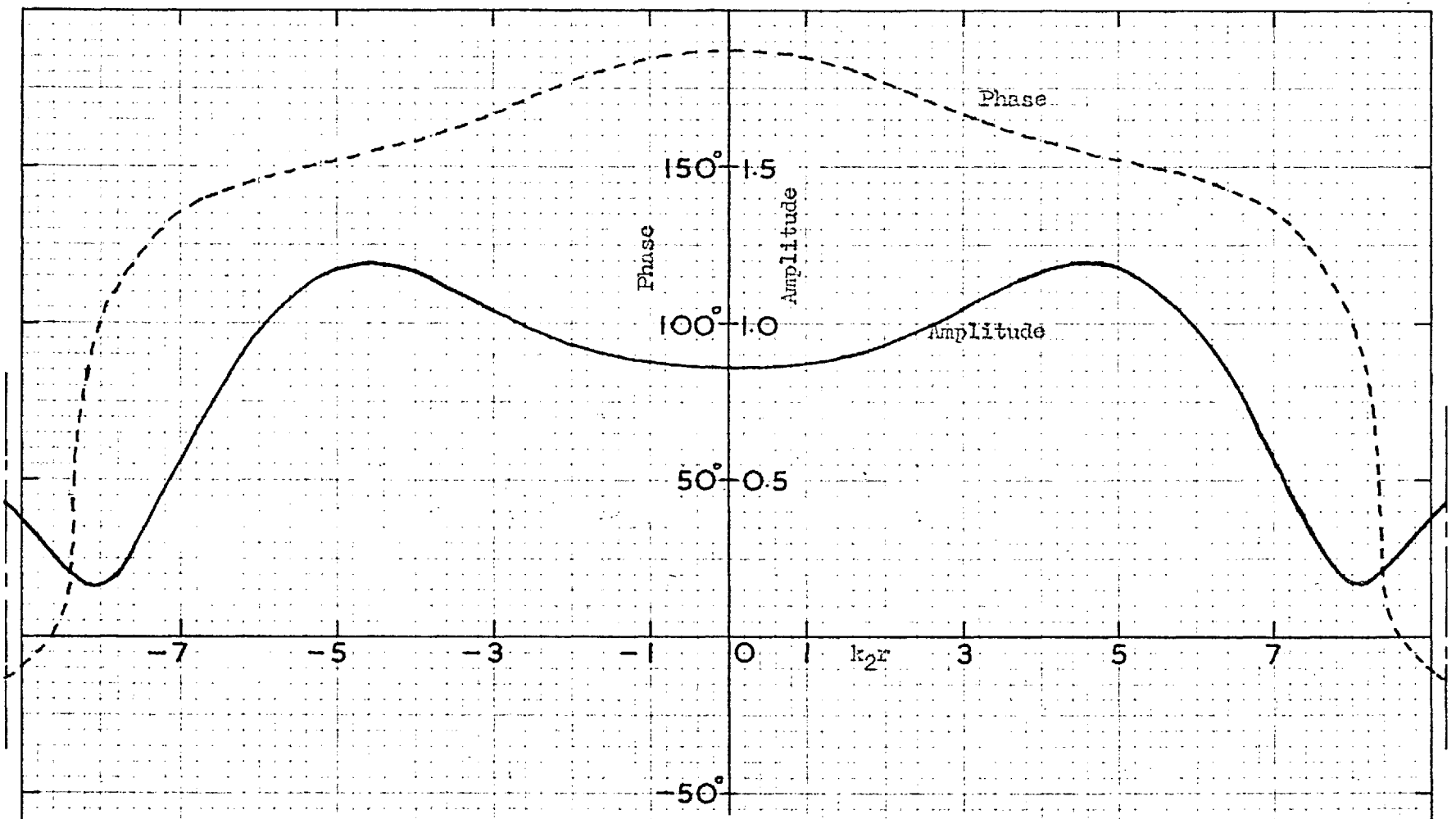

Fig. 6.9a. Internal field of a polystyrene cylinder of ka = 5.75 along a diameter normal to the direction of incidence. $k_2 = 2\pi/\text{Internal wavelength}$. The vertical dot-dash lines indicate the cylinder surface.

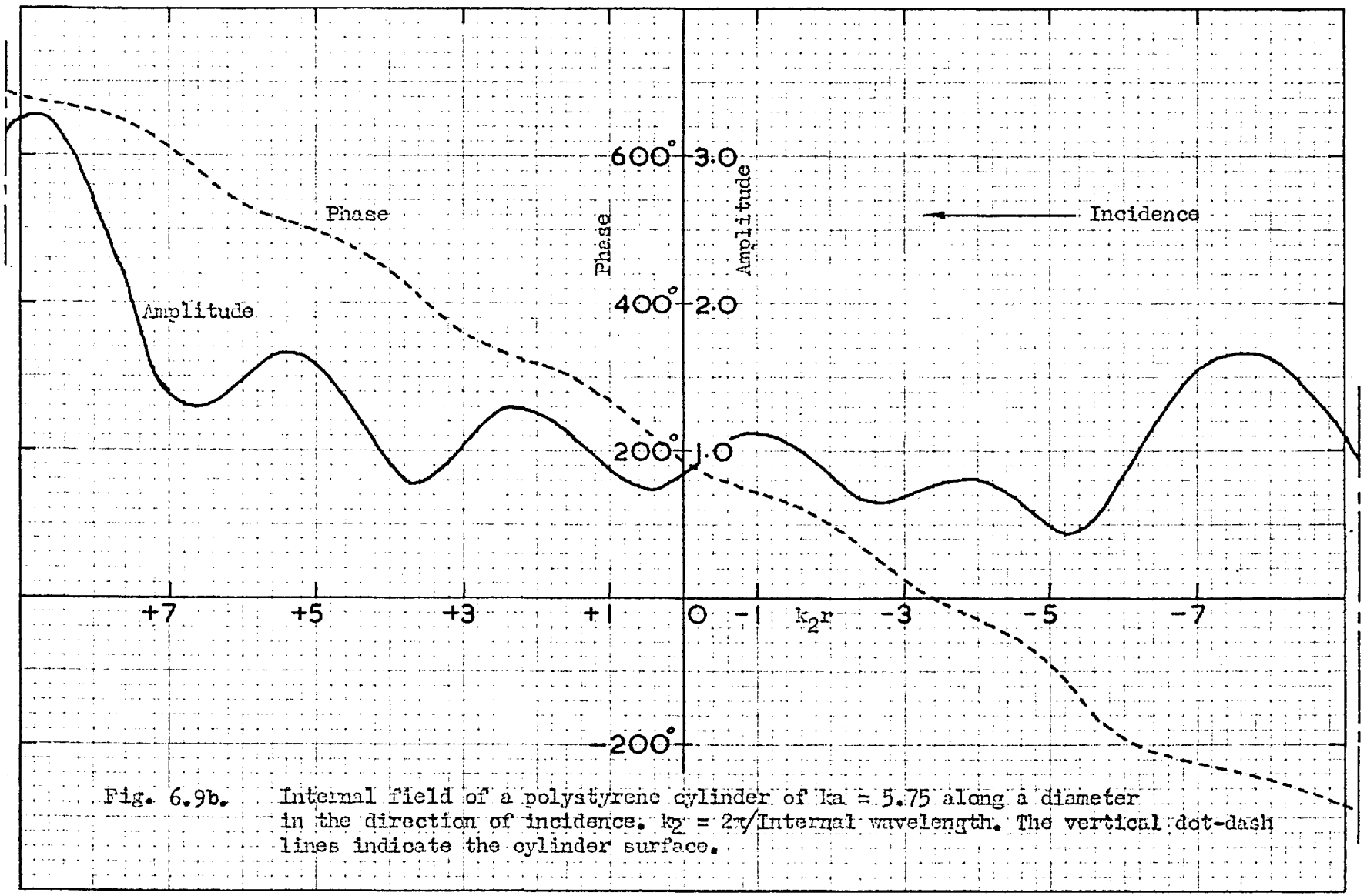

Fig. 6.9b. Internal field of a polystyrene cylinder of ka = 5.75 along a diameter in the direction of incidence. k_2 = 2π/Internal wavelength. The vertical dot-dash lines indicate the cylinder surface.

taken along two mutually-perpendicular diameters-(a) normal to the direction of incidence and (b) along the direction of incidence. The amplitude and phase references are as before.

The reason for calculating this series of curves was twofold-

(1) to trace the variation in the internal field pattern through the equivalent of a period in the thickness of the parallel-sided slab.

(2) to see if any correlation could be observed between the variation of the form of the internal field and those found externally, particularly for the radii giving the deep shadow effect.

In the first respect one can see the tendency for the field pattern along the normal diameter to be repeated for the cylinder pairs having the k_1a values (a) 1.75 and 5.0 and (b) 1.5 and 4.5, which pairs correspond roughly to increments of 1.5 wavelengths in polystyrene.

In the second respect, in the k_1a range 4-5 there does not seem to be any marked change in the field pattern, at least along the two diameters selected. But the correlation with the external field variation must obviously be there, when the complete cross-section is considered. There is a tendency for the field to flatten off just inside the illuminated surface of $k_1a=4$ (fig. 6.6b), matching that already found for the external field (fig. 4.16). A sharp dip in amplitude occurs just inside the illuminated surface of $k_1a= 4.5$(Fig. 6.7b). There are no marked phase variations corresponding to those found for the external field.

The curves show, in addition, (a) the standing-wave of amplitude

along the incidence diameter- the repetitions increasing in number with the radius- and (b) the tendency for the field to be concentrated on the shadow side of the cross-section, with a large peak just inside the shadow surface. The field distribution is, in general, complex, and not obviously amenable to the use of simple trial functions for the internal field in approximate methods for the solution of the scattering problem.

6.3. Resonances of the internal field.

It has been shown in Sec. 4.4 that the scattering from a dielectric cylinder is governed by the resonance equation-

$$\frac{J_n'(k_2a)}{J_n(k_2a)} = \sqrt{\frac{\mu_r}{\varepsilon_r}}\frac{Y_n'(k_1a)}{Y_n(k_1a)} \tag{6.11}$$

For small cylinders, for which only the lowest, or zero-order mode is excited, this relation becomes-

$$\frac{J_1(k_2a)}{J_0(k_2a)} = \sqrt{\frac{\mu_r}{\varepsilon_r}}\frac{Y_1(k_1a)}{Y_0(k_1a)} \tag{6.12}$$

For small cylinders and $\mu_r >> \varepsilon_r$, this condition corresponds to the zeros of $J_0(k_2a)$, since the right-hand side is large because of (a) $\frac{\mu_r}{\varepsilon_r} >> 1$, (b) $Y_1(k_1a) > Y_0(k_1a)$. In Table I are given the first few roots of $J_0(k_2a) = 0$ -

TABLE I

Root No.	k_2a	Root No.	k_2a
1	2.40	5	14.93
2	5.52	6	18.07
3	8.65	7	21.21
4	11.79	8	24.35

For the second case, $\frac{\mu_r}{\varepsilon_r} << 1$, the identification of the resonances is not as simple, because now $\frac{\mu_r}{\varepsilon_r}$ and $Y_1(k_1a)/Y_0(k_1a)$ can tend to balance each other. However, for very small values of the former and values of k_1a such that the latter is not large, i.e., $0.1 < k_1a < 0.7$, the resonance condition corresponds to the zeros of $J_1(k_2a)$. The first few roots of $J_1(k_2a) = 0$ are given in Table II-

TABLE II

Root No.	k_2a	Root No.	k_2a
1	3.83	5	16.47
2	7.02	6	19.62
3	10.17	7	22.76
4	13.32	8	25.90

To illustrate the first case, $\frac{\mu_r}{\varepsilon_r} >> 1$, Fig. 6.10 has been drawn from calculations made from (6.5), for the axial field of a small cylinder for several values of the ratio $\frac{\mu_r}{\varepsilon_r}$. If the relation $k_2a = \sqrt{\mu_r \varepsilon_r}\, k_1a$ is applied to Table I, the k_1a values obtained are found to agree with those corresponding to the field peaks of Fig. 6.10, particularly for the higher permeability material.

Fig. 6.11 illustrates the second case, $\frac{\mu_r}{\varepsilon_r} < 1$, with the resonance values of k_1a being closely predicted by the roots of Table II, especially for the higher permittivity material.

One would expect a certain agreement between the resonance conditions in the cylinder and those in the scattered field. Not only does the same resonance equation apply but also the scattered field is produced by the

internal polarization currents which are themselves proportional to the internal field.

In both Figs. 6.10 and 6.11 the spacing between peaks tends towards $\pi/k_r = \pi/\sqrt{\mu_r\varepsilon_r}$, as for the slab case. The corresponding phase curves of Figs. 6.12 and 6.13 show the typical rapid increases corresponding to the amplitude peaks.

An interpretation of the mean slope of the phase curves(and that of Fig. 6.1b) cannot be made easily from (6.5), but some estimation of it can be made from (6.10). Rewriting the bracketed part as -

$$e^{-i(\delta-\beta)} \quad \frac{A + Be^{i2\beta}}{C + De^{i4\beta}} \qquad (6.13)$$

one sees that the repetition interval for amplitude is, as before, $\Delta 2\beta = 2\pi$, which gives, from (6.8), $\Delta K_1 a = \frac{\pi}{\sqrt{\mu_r\varepsilon_r}}$. The phase change, $\Delta\theta$, in a period of the curves, is thus, from (6.13)-

$$\Delta\theta = \Delta\beta - \Delta\delta = \pi - \Delta K_1 a \quad \text{from (6.9)}$$

$$= \pi\left[1 - 1/\sqrt{\mu_r\varepsilon_r}\right] \qquad (6.14)$$

and $$\Delta\theta/\Delta K_1 a = \sqrt{\mu_r\varepsilon_r} - 1 \,. \qquad (6.15)$$

The following slopes are then found-

TABLE III

$\sqrt{\mu_r\varepsilon_r}$	$\Delta\theta/\Delta K_1 a$
20	1090 deg.
10	516 "
1.6	34.4 "

Fig. 6.10. Variation with radius of the amplitude of the field at the center of a cylinder of relative permittivity = 5.

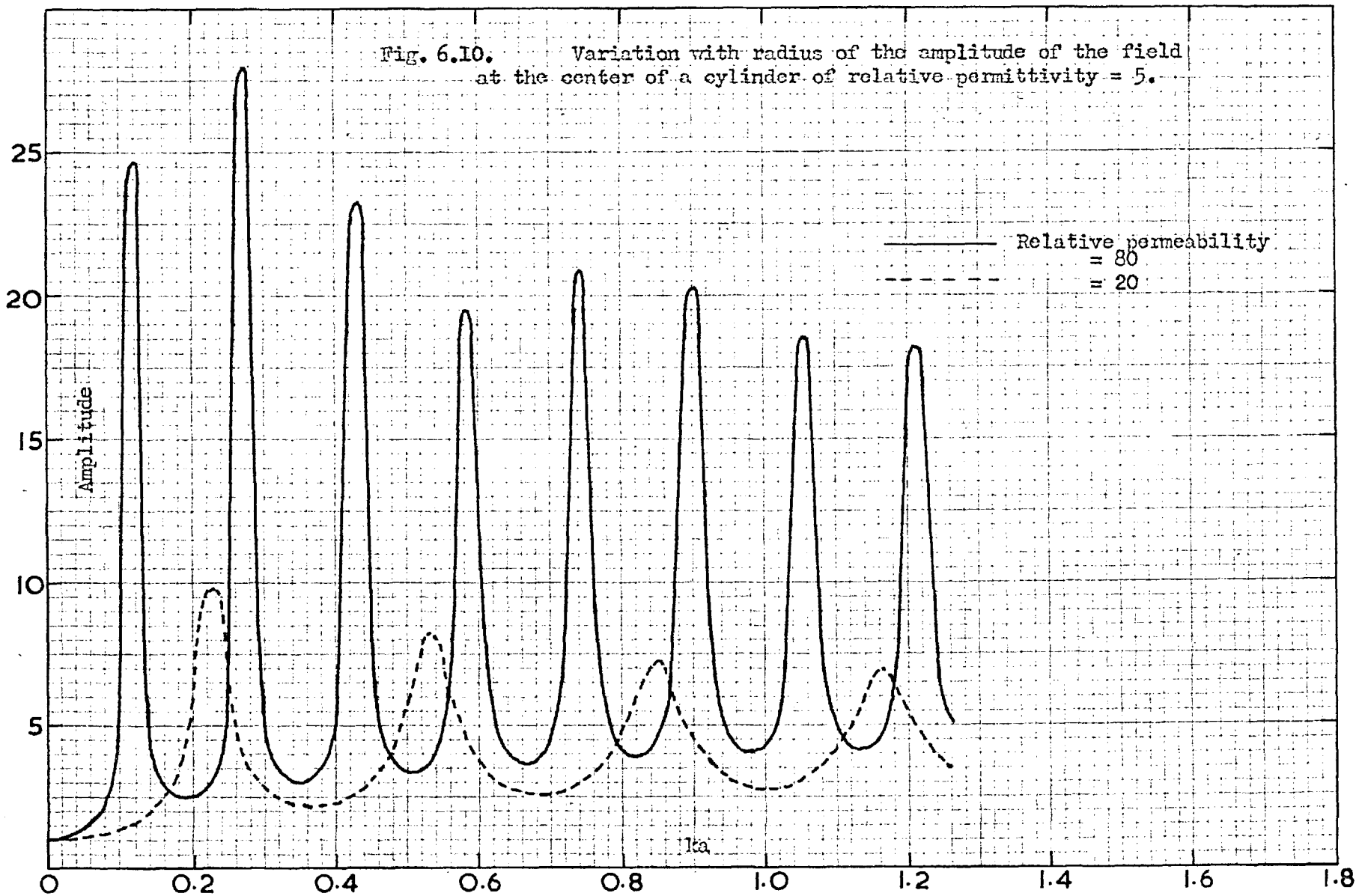

Fig. 6.11.
Variation with radius of the amplitude at the center of a cylinder of relative permeability = 5.

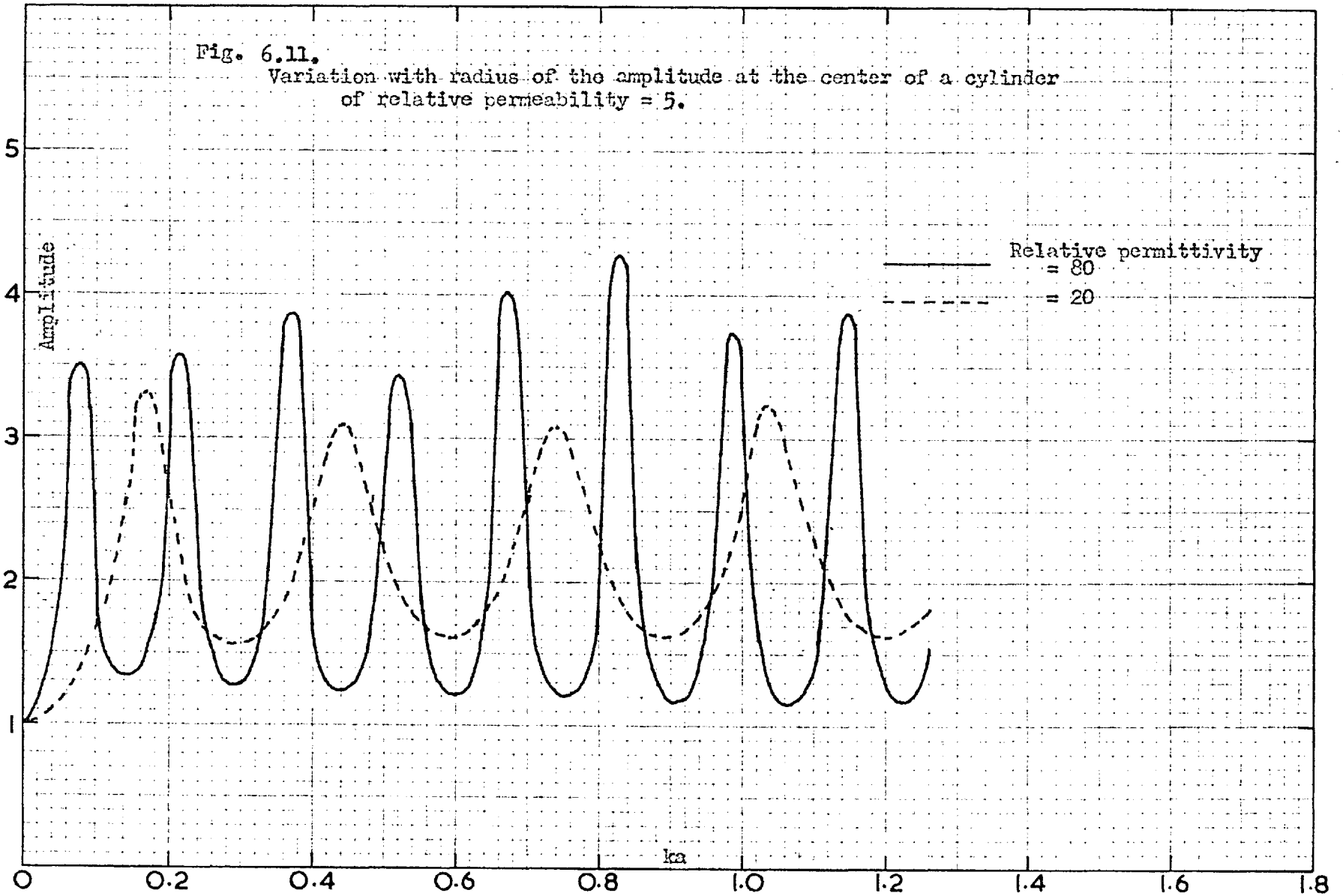

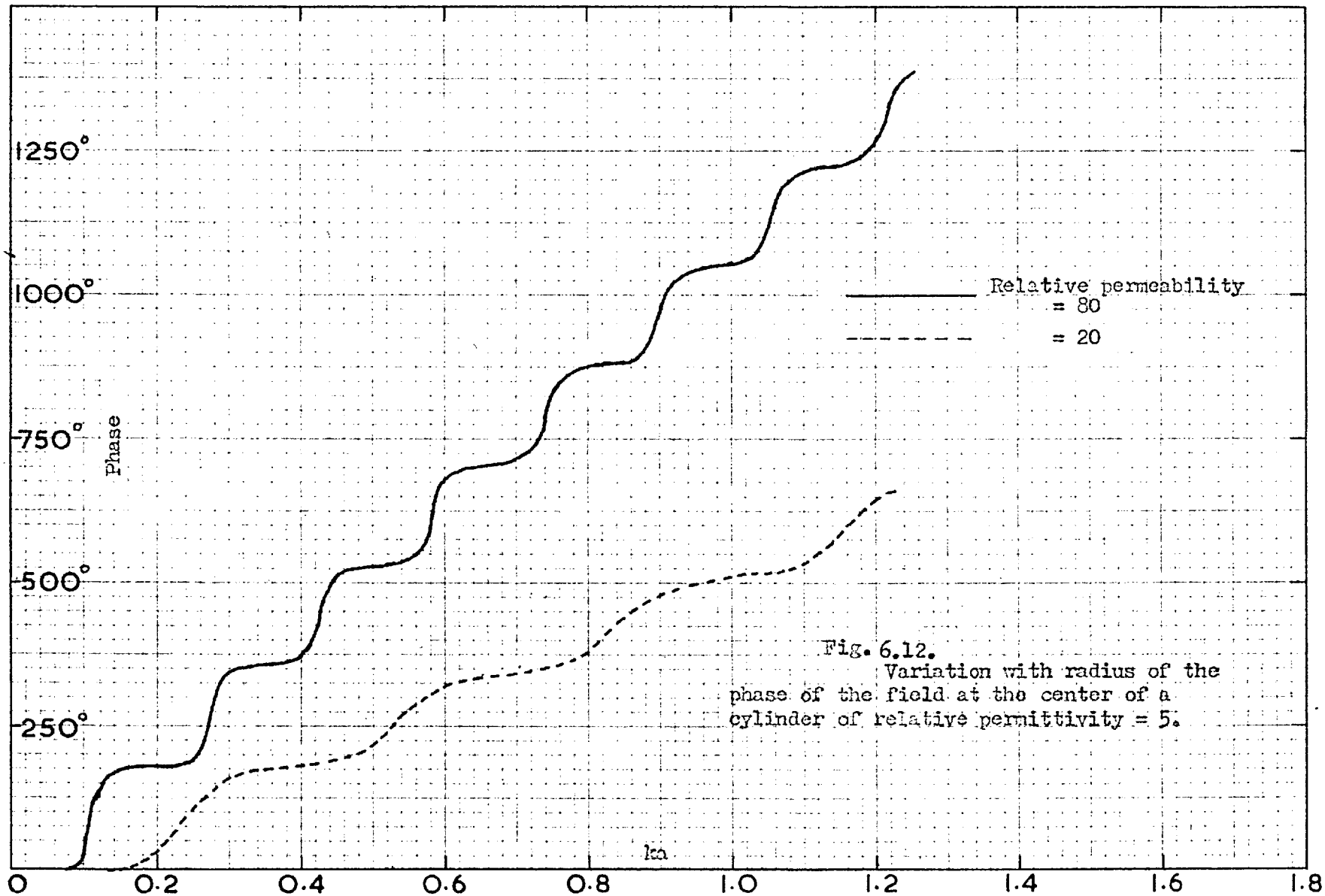

Fig. 6.12.
Variation with radius of the phase of the field at the center of a cylinder of relative permittivity = 5.

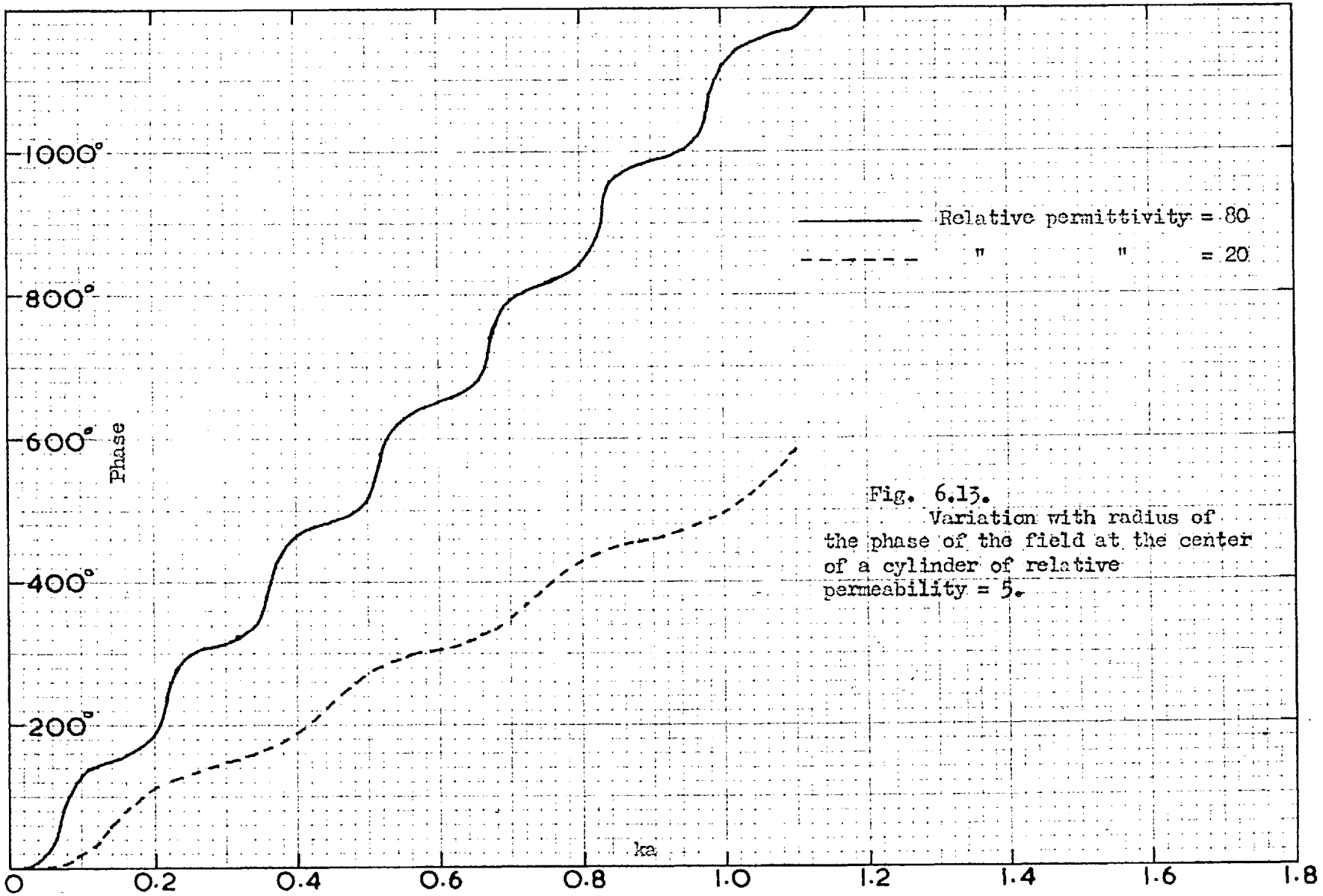

Fig. 6.13.
Variation with radius of the phase of the field at the center of a cylinder of relative permeability = 5.

which agree substantially with those of the phase curves of Figs. 6.1, 6.12 and 6.13.

From Figs. 6.10 and 6.11 one sees that the amplitude fluctuates about the value $\sqrt{\mu_r}$. Thus in Fig. 6.10 there is a different level for each curve, while in Fig. 6.11 there is the same level for both curves.

For each curve in Fig. 6.11 there is seen to be a resonance that is not included in Table II- the lowest one. This is due to the circumstance noted previously in discussing this case, that both sides of (6.12) could tend to equality at a finite value. That value, with the corresponding values of ε_r and $k_1 a$, are shown in the following Table IV-

TABLE IV

ε_r	$\sqrt{\mu_r/\varepsilon_r}\, Y_1(k_1 a)/Y_0(k_1 a)$	$k_1 a$
80	approx. 1	approx. 0.08
20	" 3/2	" 0.17

the values of $k_1 a$ agreeing favourably with those read from Fig. 6.11.

One must not assume that, because the field amplitude is large on the axis of these small, "resonant" cylinders, it is large over the whole cross-section. Although $k_1 a$ may be small, $k_2 a$ is not. In fact, for the first resonance for $\mu_r = 80$ in Fig. 6.10, $k_2 a$ is 2.4 or the diameter is approximately 2/3 wavelength in the cylinder material.

The results of Figs. 6.10 and 6.11 can be compared with those for the other polarization, studied by Page, of the magnetic field parallel to the cylinder axis. There it was found that a plot of the total flux through a cross-section showed a peak for <u>one</u> value of the variable, $k_1 a$, (except

in the case of μ_r of the order of 100, when some small, secondary ripples appeared). The curves were for $\varepsilon_r = 9$, μ_r in the range 9-100 and $k_1 a$ up to approximately 1.0. Page was interested in the efficiency of the rods as cores for loop receiving antennas. The analogous application here would be that of a very thin, receiving wire antenna, coated with a layer of high-μ_r material of such a thickness as to produce a resonance on the axis, i.e., at the wire. The highest possible permeability would be desirable, since a thin coating would then provide the resonant diameter. Whether the losses in such materials would nullify the resonant effect would be another matter. Of course, because of the periodicity of the Bessel functions it is not obvious how the resonant amplitudes would vary with increase in the permeability.

CHAPTER 7.

DIFFRACTION BY A COAXIAL CYLINDER.

7.1. Theoretical solution.

If the cylinder obstructing the incident wave comprises several structures arranged coaxially with respect to each other, the analysis becomes more complicated, because of the increase in the number of regions to be considered. Thilo gave the solution in terms of Bessel functions for a cylinder formed of two structures- a central core and an enclosing sleeve. The present discussion will be confined to that case.

The notation and the arrangement of the cylinder are given in Fig. 7.1.

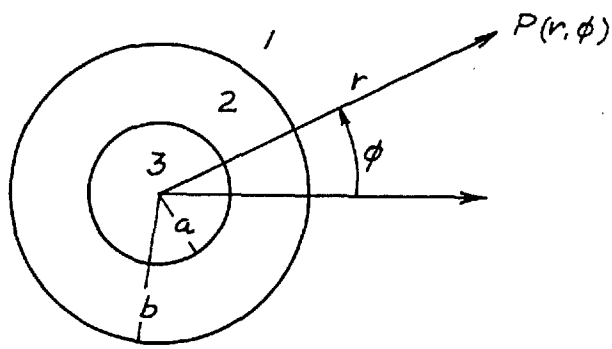

Fig. 7.1.

The j th region is characterized by the properties- ~~relative~~ permittivity ε_j, ~~relative~~ permeability μ_j and wave number k_j, each of which may be complex. As before the cylinder axis and the incident electric vector are parallel and the incident field has an amplitude of unity and propagates in the $\phi = 0$ direction. With the same field notation as for the previous

cylinder forms, the field in the three regions are given by-

Region 1

$$E_{inc}(r,\phi) = \exp(i\, k_1 r \cos\phi) = \sum_{0}^{\infty} \varepsilon_n (i)^n J_n(k_1 r)\cos n\phi \tag{7.1}$$

$$E_{sc}(r,\phi) = \sum_{0}^{\infty} \varepsilon_n B_n H_n^{(1)}(k_1 r)\cos n\phi \tag{7.2}$$

Region 2

$$E_2(r,\phi) = \sum_{0}^{\infty} \varepsilon_n \left[D_n J_n(k_2 r) + C_n Y_n(k_2 r) \right] \cos n\phi \tag{7.3}$$

Region 3

$$E_3(r,\phi) = \sum_{0}^{\infty} \varepsilon_n A_n J_n(k_3 r) \cos n\phi \tag{7.4}$$

Application of the usual boundary conditions at the interfaces between the several regions gives the following expression for the scattered amplitudes in (7.2)-

$$B = \frac{\begin{vmatrix} -(i)^n J_n(p) & -J_n(s) & -Y_n(s) & 0 \\ -\frac{\kappa_1}{\mu_1}(i)^n J_n'(p) & -\frac{\kappa_2}{\mu_2} J_n'(s) & -\frac{\kappa_2}{\mu_2} Y_n'(s) & 0 \\ 0 & J_n(m) & Y_n(m) & -J_n(l) \\ 0 & \frac{\kappa_2}{\mu_2} J_n'(m) & \frac{\kappa_2}{\mu_2} Y_n'(m) & -\frac{\kappa_3}{\mu_3} J_n'(l) \end{vmatrix}}{\Delta} \tag{7.5}$$

where $l = k_3 a$, $m = k_2 a$, $s = k_2 b$, $p = k_1 b$. Δ is obtained from the numerator of (7.5) by the following changes in the first column-

$$\begin{aligned} -(i)^n J_n(p) &\longrightarrow H_n^{(1)}(p) \\ -(i)^n J_n'(p) &\longrightarrow H_n^{(1)\prime}(p) \end{aligned} \tag{7.6}$$

The corresponding expressions for the amplitudes in the other regions are obtained in the same way.

The total external field is then obtained by substituting from (7.5) and (7.6) in (7.2) and adding to (7.1).

If a=b, $k_3 = k_2$, $\mu_3 = \mu_2$ in (7.5) and (7.6), one obtains the expressions previously given for the solid dielectric cylinder.

The general case given by (7.5) and (7.6) is rather complicated to treat numerically, so it was decided instead to consider the slightly simpler case in which the central core is a conducting cylinder. From (7.1), (7.2) and (7.3) and the boundary conditions of tangential field continuity at the interface 1,2 and zero field at r=a, there is obtained-

$$B_n = \frac{\begin{vmatrix} -(i)^n J_n(\beta) & , -J_n(s) & , -Y_n(s) \\ 0 & , J_n(m) & , Y_n(m) \\ -\frac{K_1\mu_2}{K_2\mu_1}(i)^n J_n'(\beta) & , -J_n'(s) & , -Y_n'(s) \end{vmatrix}}{T} \qquad (7.7)$$

where

$$T = \begin{vmatrix} H_n^{(1)}(\beta) & , -J_n(s) & , -Y_n(s) \\ 0 & , J_n(m) & , Y_n(m) \\ \frac{K_1\mu_2}{K_2\mu_1} H_n^{(1)\prime}(\beta) & , -J_n'(s) & , -Y_n'(s) \end{vmatrix} \qquad (7.8)$$

$$D_n = P\, Y_n(m)/T \qquad (7.9) \qquad C_n = -P\, J_n(m)/T \qquad (7.10)$$

$$P = (i)^n \frac{K_1\mu_2}{K_2\mu_1} \begin{vmatrix} H_n^{(1)}(\beta) & , J_n(\beta) \\ H_n^{(1)\prime}(\beta) & , J_n'(\beta) \end{vmatrix} = (i)^{n-1} \cdot \frac{2}{\pi\beta} \cdot \frac{K_1\mu_2}{K_2\mu_1} \qquad (7.11)$$

from the Bessel function Wronskian relation(McLachlan, p.156). Substituting

from (7.7) and (7.8) in (7.2) and adding to (7.1) gives the total external field, and from (7.9)-(7.11) in (7.3) gives the field in the dielectric sleeve.

A further expansion of the determinant of (7.7) and (7.8) gives-

$$B_n = -(i)^n \frac{J_n(p).F + k\, J_n'(p).G}{H_n^{(1)}(p).F + k\, H_n^{(1)\prime}(p).G} \tag{7.12}$$

where $$F = \begin{vmatrix} J_n(m) & Y_n(m) \\ -J_n'(s) & -Y_n'(s) \end{vmatrix} \tag{7.13}$$ $$G = \begin{vmatrix} -J_n(s) & -Y_n(s) \\ J_n(m) & Y_n(m) \end{vmatrix} \tag{7.14}$$

$$k = \mu_1 K_2 / K_1 \mu_2 \tag{7.15}$$

Thus (7.12) is of the form $B_n = -(i)^n a_n/(a_n + i\, b_n)$ as was found for the conducting and dielectric cylinders. The discussion given there regarding auxiliary angles therefore applies to this case also, as it does to (7.5).

7.2. Thin-sleeve approximation.

(a) Conducting core- If the sleeve is thin, i.e., $t = b-a < a$, one can simplify (7.12) further. From the Taylor expansion for the Bessel function expressions-

$$J_n(k_2 b) = J_n(k_2 a) + k_2 t\, J_n'(k_2 a) \tag{7.16a}$$

$$Y_n(k_2 b) = Y_n(k_2 a) + k_2 t\, Y_n'(k_2 a) \tag{7.16b}$$

and the Wronskian formula, one can write (7.13) and (7.14) as -

$$F = 2\,\frac{b(b-2a)(n+1)+a^2n}{\pi mab} \tag{7.17}$$

$$G = 2t/\pi a \tag{7.18}$$

(b) Dielectric core- By the same method as for (a) it is found, from (7.5) and (7.6), that-

$$B_n = A/B \tag{7.19}$$

where
$$A = -(i)^n J_n(p)\left[\left(\frac{K_2}{\mu_2}\right)^2\left\{2t\left[\frac{b(m^2-n^2)-nt}{\pi m^2 a b}\right]\right\}J_n(\ell) + Z\left\{2\left[\frac{b(b-2a)(n+1)+a^2n}{\pi m a b}\right]\right\}J_n'(\ell)\right] - \frac{K_1}{\mu_1}(i)^n J_n'(p)\left[\frac{K_2}{\mu_2}\left(\frac{2}{\pi m}\right)J_n(\ell) + \frac{K_3}{\mu_3}\left(\frac{2t}{\pi a}\right)J_n'(\ell)\right] \tag{7.20}$$

$$Z = K_2K_3/\mu_2\mu_3 \tag{7.21}$$

and B can be obtained from A by making the changes indicated in (7.6).

7.3. Calculations and experimental results.

Calculations were made of the internal and external fields for $\phi = 0$ for the case of a metal core and a polystyrene sleeve. For the internal field (7.3), (7.9), (7.10) and (7.11) were used. For the external field (7.1), (7.2), (7.12)-(7.15) were used. The parameters were-

$$m = k_2a = 2.0 \quad ; \quad p = k_1b = 2.5,\ 3.0 \text{ and } 4.0.$$

$$s = k_2p/k_1 = 1.6p = 4.0,\ 4.8,\ 6.4.$$

where $k_2/k_1 = k_r = 1.6$ is the index of refraction of polystyrene. The experiments were limited in scope by the difficulty of machining the cylinders so that uniform contact with the line plates was made by both

the metal and polystyrene areas.

The external field calculations are given in Figs. (7.2) and (7.3), with the experimental points. The internal field calculations are given in Fig. (7.4). Three points in particular are to be noted from the results-

(a) for the smallest cylinder there is an almost-complete matching of the shadow-field amplitude. Reference to Fig. 4.4 for $k_1a=2.5$ shows that, if the metal core were replaced by polystyrene, the field would rise sharply on approaching the cylinder. If the polystyrene sleeve were removed, or replaced by metal, the shadow would extend to a considerable distance from the cylinder.

The phase conditions are different, however. While the phase shift is less than for the polystyrene case, it is greater than for the metal case of $k_1a = k_2a/1.6 = 1.25$, although less near the cylinder than for a $k_1b = 2.5$ metal cylinder.

(b) the change in the form of the phase curves for a polystyrene cylinder, which appears at $k_1a = 4$ (Fig. 4.8), is absent from Fig.(7.2c), which has the smooth form typical of the metal cylinder curves.

(c) the internal fields do not exhibit the rapid fluctuations characteristic of those for polystyrene(Figs. (6.2)-(6.9)), but rather resemble the external metal cylinder curves(except for the fact that they rise above the incident-field value).

7.4. Correction for a curved incident wave front.

If the incident wave is not plane, but propagates from a line

Data Sheet No. 31S 10ths Sectional. Scale 9 Inches × 6 Inches
Wightman Mountain Ltd.
Artillery House, Artillery Row, Westminster, S.W.1

Fig. 7.2. Shadow field phase of a coaxial cylinder comprising a conducting core with a polystyrene sleeve.

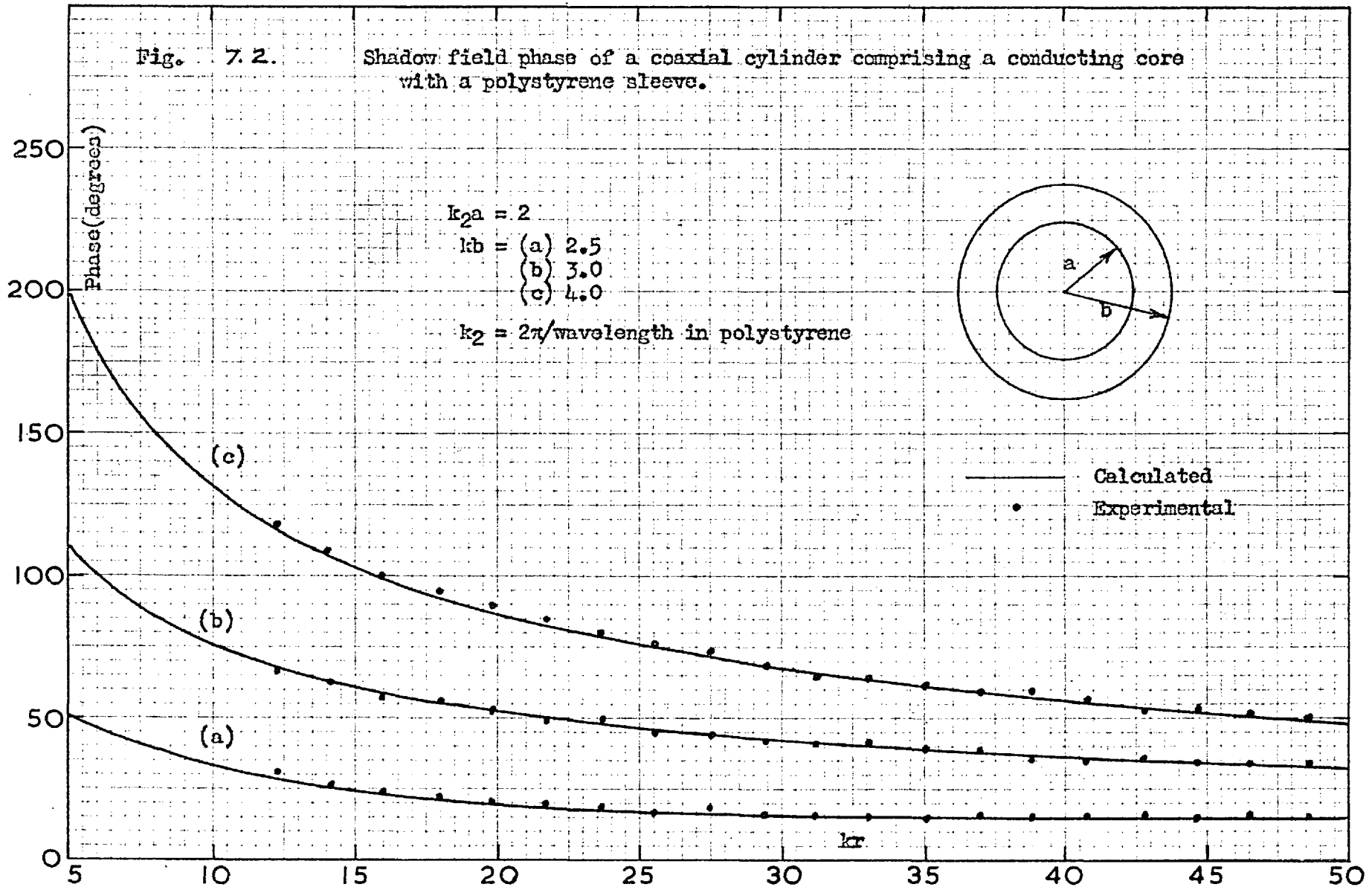

DATA SHEET NO. 31.S 10THS SECTIONAL SCALE 9 INCHES = 6 INCHES
ARTILLERY HOUSE, ARTILLERY ROW, WESTMINSTER, S.W.1

Fig. 7.3. Shadow field amplitude of a coaxial cylinder comprising a conducting core with a polystyrene sleeve.

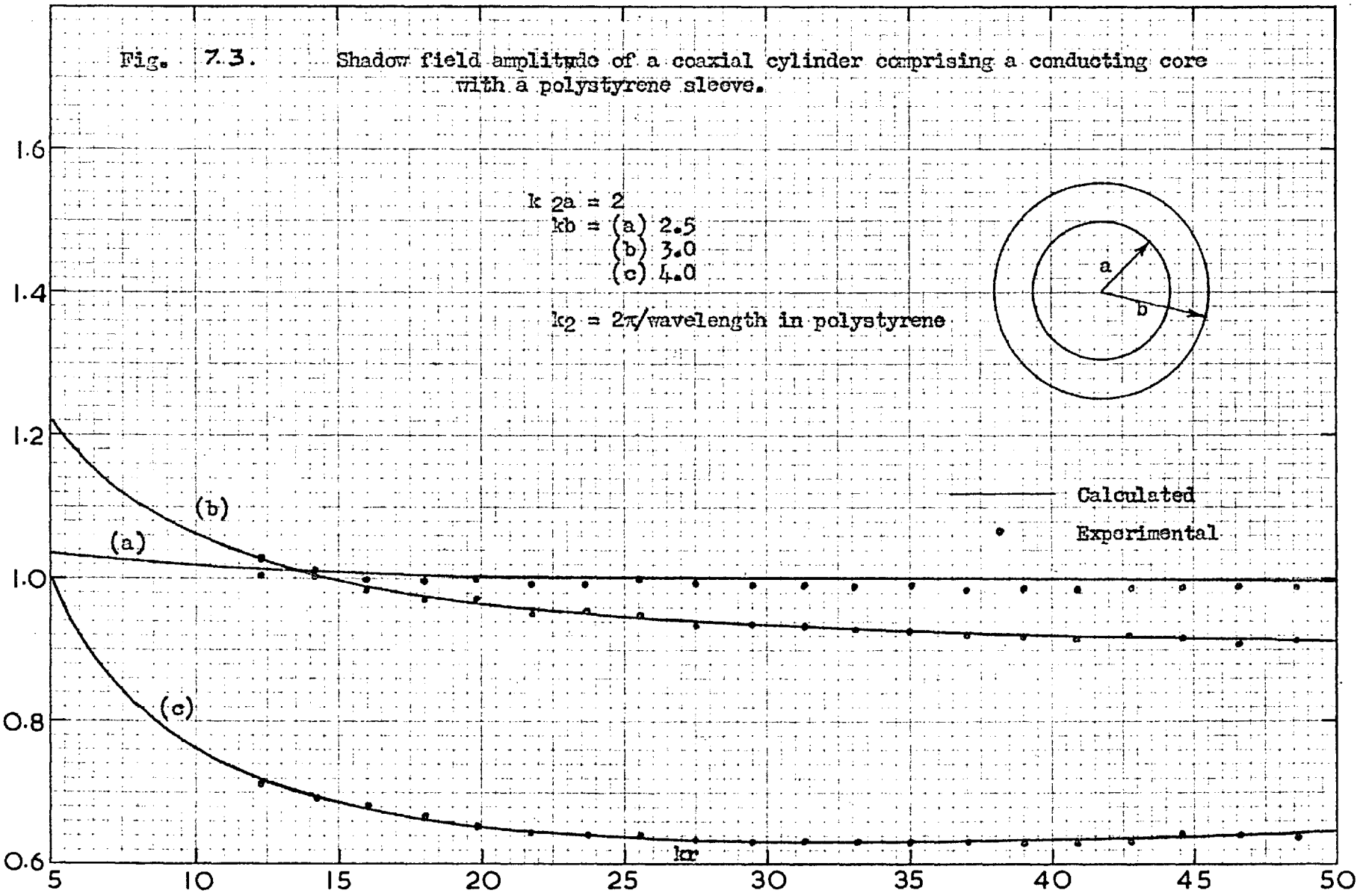

Fig. 7.4. Field amplitude in the shadow of the core of a coaxial cylinder comprising a conducting core and a polystyrene sleeve.

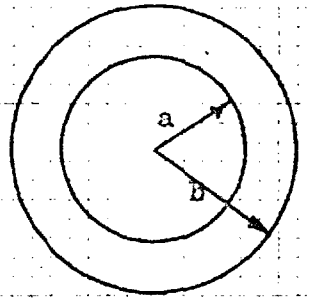

Field in polystyrene
External field
Air-polystyrene interface

(a)
(b)
(c)

$k_2a = 2$
kb = (a) 2.5
(b) 3.0
(c) 4.0

k_2 = 2π/wavelength in polystyrene

Amplitude

k_2r

0
0.4
0.8
1.2
1.6
2.0
2
3
4
5
6

source at a finite distance from the cylinder, a correction factor, identical with that discussed in the case of the homogeneous cylinder, must be applied to the plane-wave scattering results to account for the incident wave front curvature.

7.5. Line source on the cylinder axis.

If a line source is situated on the cylinder axis, the field expressions are comparatively simple, because no series are involved and there is no angular dependence. The outgoing, or transmitted waves are represented by the $H_o^{(1)}$, or first Hankel functions, and the incoming, or reflected waves by the $H_o^{(2)}$, or second Hankel functions. The problem is analogous to that of a point source at the center of a spherical shell, as discussed by Keller.

Let the source strength be I. Then the radiated field is given by $-(\omega\mu_3 I/4)\ H_o^{(1)}(k_3 r)$ (Stratton, p. 595). The fields in the three dielectric regions are then -

$$E_1(r) = A\ H_o^{(1)}(k_1 r) \tag{7.22}$$

$$E_2(r) = B\ H_o^{(1)}(k_2 r) + C\ H_o^{(2)}(k_2 r) \tag{7.23}$$

$$E_3(r) = -(\omega\mu_3 I/4)\ H_o^{(1)}(k_3 r) + D\ H_o^{(2)}(k_3 r) \tag{7.24}$$

The transmitted and reflected amplitudes A and D, respectively, are determined in the usual way and are-

$$A = \frac{\begin{vmatrix} H_0^{(2)}(\ell) & -H_0^{(1)}(m) & -H_0^{(2)}(m) & \frac{\omega\mu_3 I}{4} H_0^{(1)}(\ell) \\ \frac{\kappa_3}{\mu_3} H_0^{(2)\prime}(\ell) & -\frac{\kappa_2}{\mu_2} H_0^{(1)\prime}(m) & -\frac{\kappa_2}{\mu_2} H_0^{(2)\prime}(m) & \frac{\omega\mu_3 I}{4} \frac{\kappa_3}{\mu_3} H_0^{(1)\prime}(\ell) \\ 0 & H_0^{(1)}(s) & H_0^{(2)}(s) & 0 \\ 0 & \frac{\kappa_2}{\mu_2} H_0^{(1)\prime}(s) & \frac{\kappa_2}{\mu_2} H_0^{(2)\prime}(s) & 0 \end{vmatrix}}{V} \tag{7.25}$$

$$D = \frac{\begin{vmatrix} \frac{\omega\mu_3 I}{4} H_0^{(1)}(\ell) & -H_0^{(1)}(m) & -H_0^{(2)}(m) & 0 \\ \frac{\omega\mu_3 I}{4} \frac{\kappa_3}{\mu_3} H_0^{(1)\prime}(\ell) & -\frac{\kappa_2}{\mu_2} H_0^{(1)\prime}(m) & -\frac{\kappa_2}{\mu_2} H_0^{(2)\prime}(m) & 0 \\ 0 & H_0^{(1)}(s) & H_0^{(2)}(s) & -H_0^{(1)}(b) \\ 0 & \frac{\kappa_2}{\mu_2} H_0^{(1)\prime}(s) & \frac{\kappa_2}{\mu_2} H_0^{(2)\prime}(s) & -\frac{\kappa_1}{\mu_1} H_0^{(1)\prime}(b) \end{vmatrix}}{V} \tag{7.26}$$

and V can be obtained by making the following changes in the numerator of (7.26)-

$$\frac{\omega\mu_3 I}{4} H_0^{(1)}(\ell) \longrightarrow H_0^{(2)}(\ell) \tag{7.27a}$$

$$\frac{\omega\mu_3 I}{4} \frac{\kappa_3}{\mu_3} H_0^{(1)\prime}(\ell) \longrightarrow \frac{\kappa_3}{\mu_3} H_0^{(2)\prime}(\ell) \tag{7.27b}$$

If a = b, $k_3 = k_2$, $\mu_3 = \mu_2$, one has the case of a line source on the axis of a cylinder of radius, b, and constants k_2, ε_2, μ_2. The transmitted and reflected amplitudes of (7.25) and (7.26) then reduce to-

$$A = \frac{\omega\mu_2 I}{4} \frac{\kappa_2}{\mu_2} \frac{\begin{vmatrix} H_0^{(2)}(s) & H_0^{(1)}(s) \\ H_0^{(2)\prime}(s) & H_0^{(1)\prime}(s) \end{vmatrix}}{W} \tag{7.28}$$

$$D = \frac{\omega\mu_2 I}{4} \frac{\begin{vmatrix} H_0^{(1)}(s) & -H_0^{(1)}(b) \\ \frac{\kappa_2}{\mu_2} H_0^{(1)\prime}(s) & -\frac{\kappa_1}{\mu_1} H_0^{(1)\prime}(b) \end{vmatrix}}{W} \tag{7.29}$$

where

$$W = \begin{vmatrix} H_0^{(2)}(s) & , & -H_0^{(1)}(p) \\ \frac{\kappa_2}{\mu_2} H_0^{(2)\prime}(s), & & -\frac{\kappa_1}{\mu_1} H_0^{(1)\prime}(p) \end{vmatrix} \qquad (7.30)$$

Two limiting cases that can arise are-

(a) if b becomes very large, while r-b remains finite, the Hankel functions can be replaced by their exponential asymptotic expansions to yield, from (7.28) and (7.29) the expressions for propagation across a plane interface between two different media, with the direction of incidence normal to the interface(the incident wave approaching a limiting form of a plane wave).

(b) if a becomes very large, but b-a and r-b remain finite, the field expressions, (7.25) and (7.26) reduce to those for the transmission and reflection coefficients of a parallel slab of dielectric for a plane wave incident normally.

The procedure merely involves algebraic detail which will be omitted.

CHAPTER 8.

DIFFRACTION BY CYLINDERS OF SQUARE AND RECTANGULAR CROSS-SECTION.

8.1. The only previous results that appear to be available on diffraction by a cylindrical obstacle of square or rectangular cross-section are those theoretical ones by Jones for the diffraction of a plane wave by a thick, metal plate of finite length. They do not strictly apply, however, to the case of interest in this study, i.e., obstacles whose dimensions are comparable with the wavelength and of dielectric as well as of metal.

It was decided, therefore, to investigate experimentally the shadow field for several cases. Those considered were-

(a) metal and polystyrene squares for the two cases of incidence along a normal to the sides and along a diagonal.

(b) metal and polystyrene rectangles for incidence along a normal to each of the two dimensions.

For the case of one of the orientations of the rectangles(metal) a very rough approximation regarding the surface currents was used to make calculations for comparison with the experimental results.

8.2. Metal squares.

The measurements were made on a family of seven metal squares in the range of $k_1 a = 1.45\text{-}5.07$, where $k_1 a/2\pi$ is the half-side in wavelength units. The results were not plotted in detail for presentation for each obstacle, since the effect of the dimensions on the scattering could best be observed by plotting the field values as a function of $k_1 a$. Thus the results were

first plotted in detail and then a cross-section taken through the family of curves for several values of $k_1 r$, to indicate the manner in which the variation with $k_1 a$ changed with increasing distance from the obstacles.

Fig. 8.1 gives the results for normal incidence and Fig. 8.2 for diagonal incidence. The behaviour with respect to $k_1 a$ is similar to that for the metal, circular cylinders- a deepening of the shadow and an increase in phase as the dimension is increased and an increase in amplitude and decrease in phase as the distance from the obstacle is increased.

An additional feature of the former case, however, is the tendency for both the amplitude and phase curves to flatten for $k_1 a$ values between 3 and 4, the tendency increasing with $k_1 r$. A polar plot of the results showed that, for diagonal incidence, a sharp bend in the curves occurred for $k_1 a$ values of 1.6 and 3.3, which correspond to sides of approximately 1/2 and 1 external wavelength respectively. The bends became more pronounced with increasing $k_1 r$. Only one bend occurred in the curves for normal incidence, between $k_1 a$ values of 2.3 and 3.4, corresponding to a side of the order of an external wavelength. It, too, was more pronounced for increasing $k_1 r$.

Comparison of these results with those of the circular cylinder suggests itself, from the point of view of determining the radius of the equivalent circular cylinder. The circular cylinder curves are smooth as a function of $k_1 a$, while the curves for the squares are oscillating functions of the half-side. The following points are observed on making the comparison-

DATA SHEET NO. 2. 105 DIVISIONS × 45 DIVISIONS
WIGHTMAN MOUNTAIN LTD.,
ARTILLERY HOUSE, ARTILLERY ROW, WESTMINSTER, S.W.1

Fig. 8./. Shadow field of metal squares. Normal incidence.

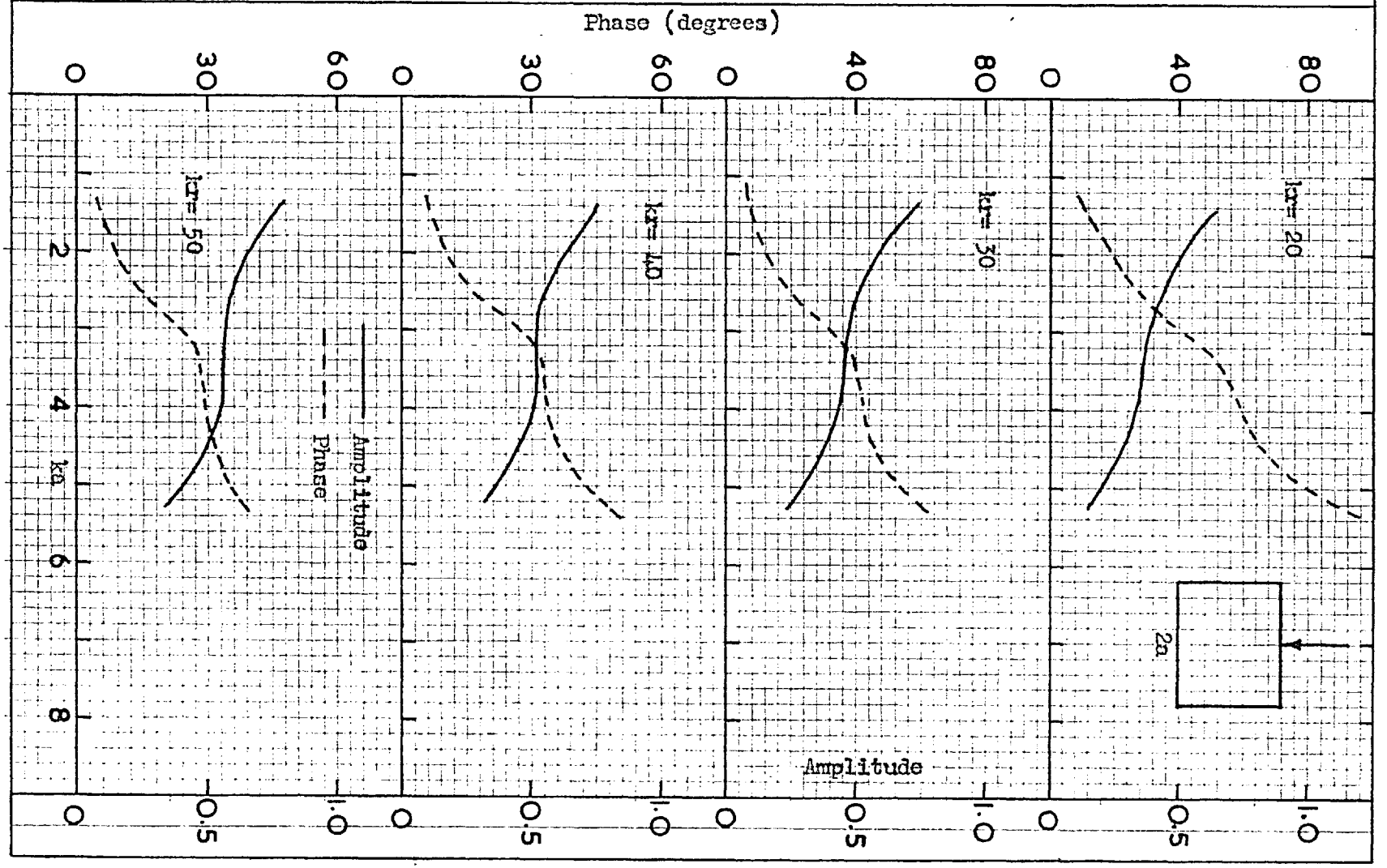

Artillery House, Artillery Row, Westminster, S.W.1

Fig. 8.2. Shadow field of metal squares. Diagonal incidence.

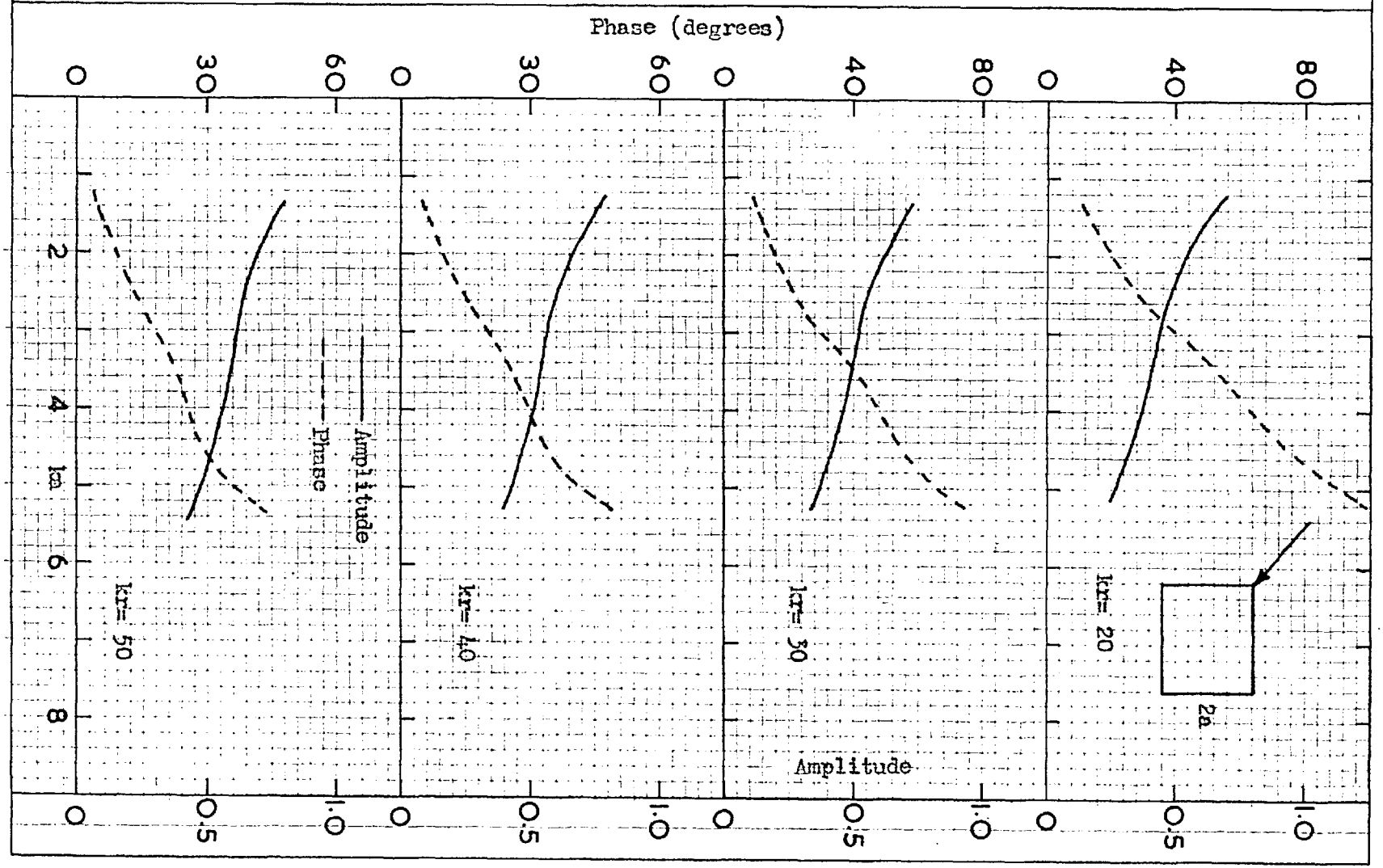

(a) The amplitude curves oscillate below those of the circular cylinder. For diagonal incidence the oscillations are about a curve which corresponds to a circular cylinder for which the ratio radius/half-side = 1.06. For normal incidence the ratio is 1.12.

(b) The phase curves oscillate above the circular cylinder curves. The ratios corresponding to those in (a) are 1.27 and 1.15 respectively.

The product of the ratios thus tends to be the same for both orientations, with the normal amplitudes and phases both being less than the corresponding diagonal ones.

One associates this circumstance that, if one shape of metal cylinder has the greater phase it has the lesser amplitude, with the opposite behaviour of the two features with respect to increasing k_1a- the amplitude decreasing and the phase increasing.

8.3. Polystyrene squares.

The corresponding curves for the polystyrene squares are given in Figs. 8.3 and 8.4. They were obtained from measurements on 10 squares in the k_1a range 2.18-6.43.

For both orientations there is a tendency- observed in the case of the circular cylinder- for the amplitude to have a zero value and the phase a change of form for a particular combination of k_1a and k_1r. The field complexity that can be encountered in the near region is well illustrated by Fig. 8.3 for $k_1r = 20$.

For normal incidence the detailed curves indicated that the critical radius-distance combination would be in the region of 4.2-4.3 and 50-60 respectively, and Fig. 8.3 indicated this tendency. The k_1r

value is thus much larger than for the circular cylinder, while the $k_1 a$ is a little smaller, the latter tendency indicating a higher effective permittivity.

For diagonal incidence the corresponding values are $k_1 a$ and $k_1 r$ in the region of 3.7 and 23 respectively.

Thus, just as for the metal squares, the polystyrene square with diagonal incidence seems to compare more closely with the circular cylinder than does that for normal incidence. This is perhaps understandable on the basis that the latter orientation presents a more abrupt discontinuity to the advancing wave.

The angles of Fig. 8.4 for the larger $k_1 r$ values were drawn in a different manner from that for the smaller, because of the large rise in phase after passing the critical $k_1 r$ value.

8.4. Metal rectangles.

Case A. For this case measurements were made on a family of 11 rectangles of dimensions 2a x 2b, with $k_1 b = 2.41$ and $k_1 a$ in the range of 1.63-6.42. The two orientations of incidence normal to each of a pair of adjacent sides were considered. The results for the orientation in which the dimension along the direction of incidence was varied are given in Fig. 8.5. As in Fig. 8.1 for the metal squares, the effect of the interaction between the front and back faces is apparent, with a sharp bend appearing in the polar diagram for $k_1 a$ in the region 3.0-4.0. Figs. 8.6 and 8.7 show the results for the amplitude and phase respectively for the other orientation. The effect of leaving constant the dim-

DATA SHEET NO. 2. 105 DIVISIONS × 45 DIVISIONS

IGHTMAN MOUNTAIN LTD.,
ARTILLERY HOUSE, ARTILLERY ROW, WESTMINSTER, S.W.1

Fig. 8.3. Shadow field of polystyrene squares. Normal incidenee.

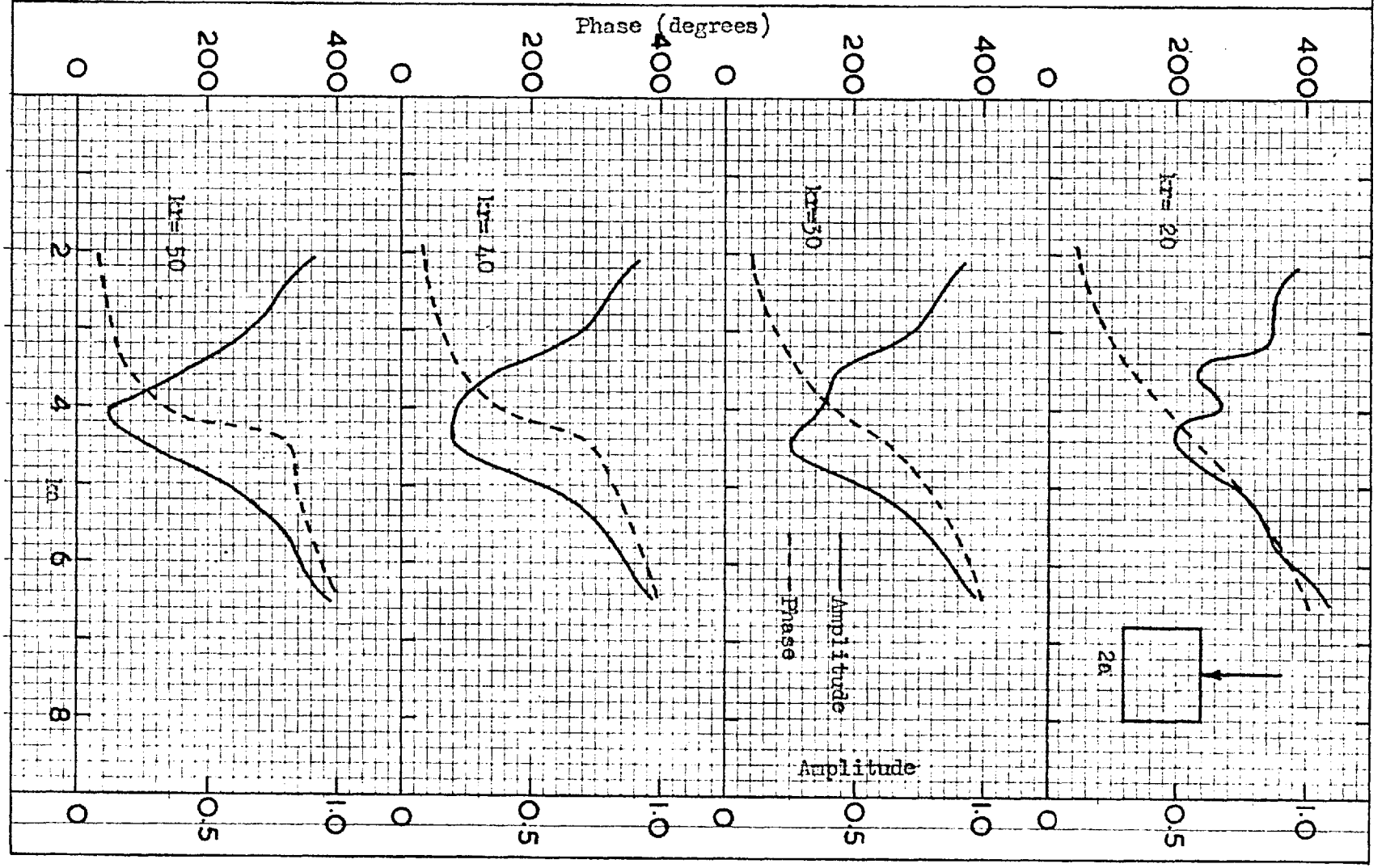

DATA SHEET NO. 2. 105 DIVISIONS × 45 DIVISIONS

IGHTMAN MOUNTAIN LTD.,
ARTILLERY HOUSE, ARTILLERY ROW, WESTMINSTER, S.W.1

Fig. 8.4. Shadow field of polystyrene squares. Diagonal incidence.

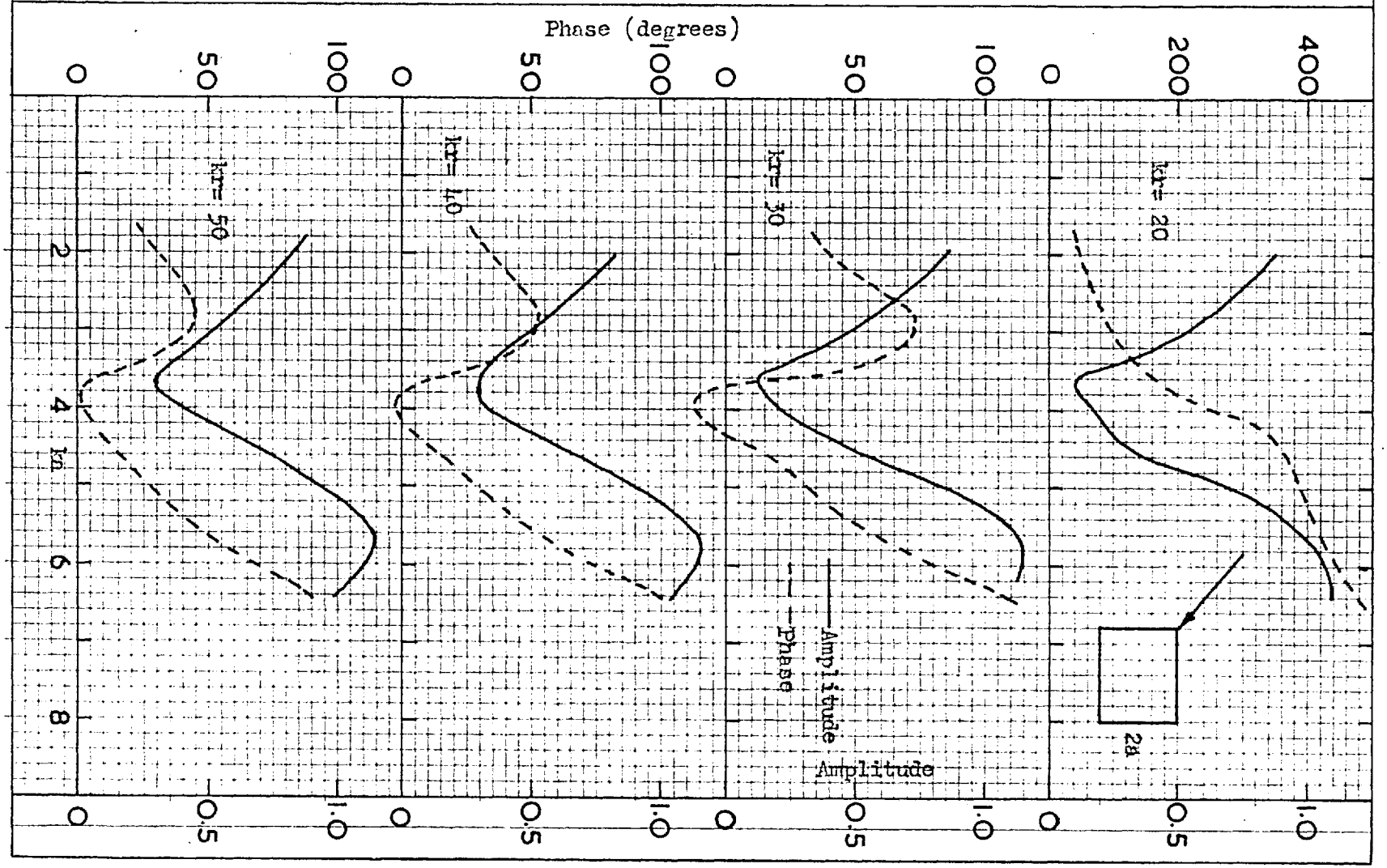

DATA SHEET No. 2. 105 DIVISIONS × 45 DIVISIONS

WIGHTMAN MOUNTAIN LTD.,
ARTILLERY HOUSE, ARTILLERY ROW, WESTMINSTER, S.W.1

Fig. 8.5. Shadow field of metal rectangles of kb= 2.41.

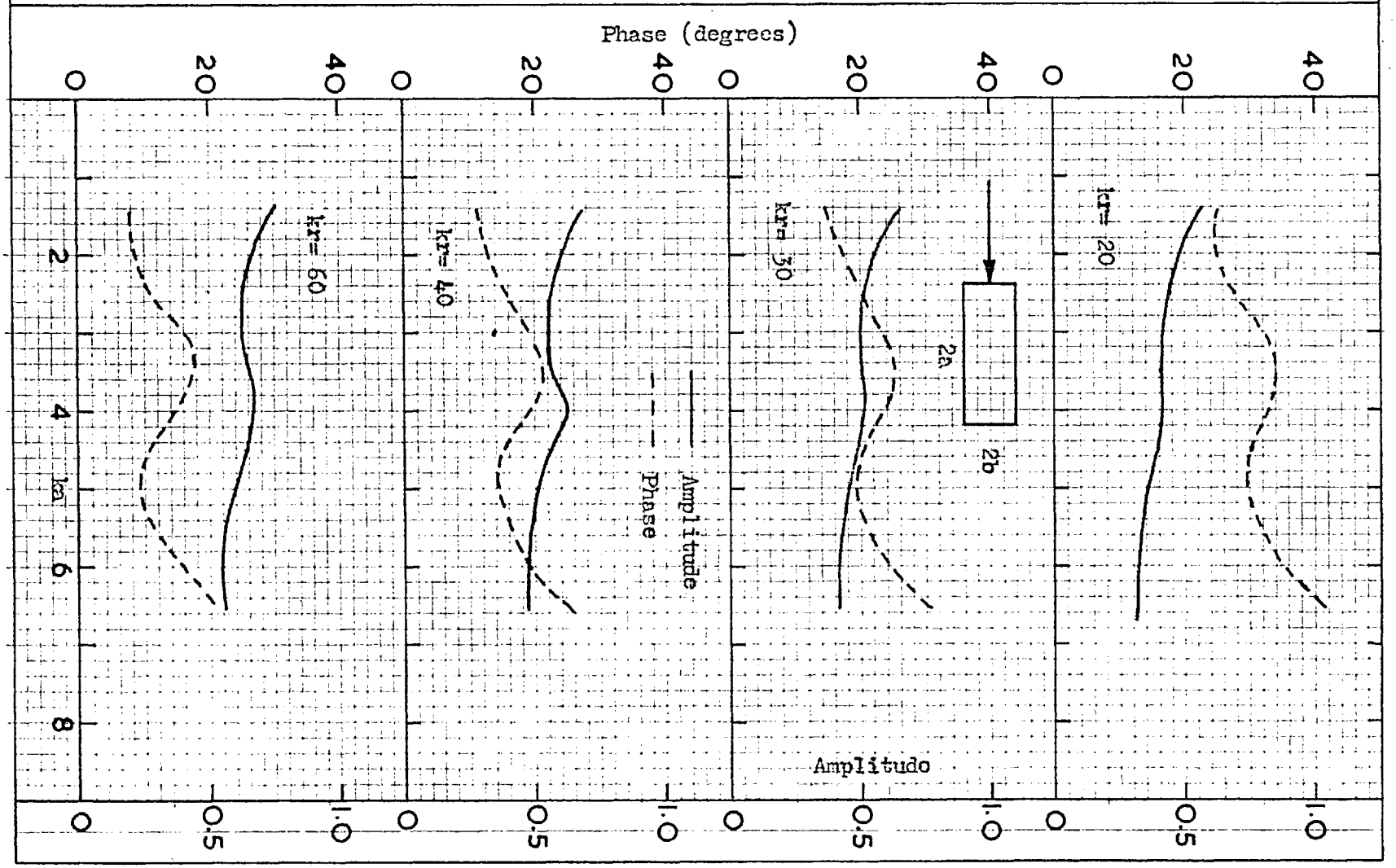

WIGHTMAN MOUNTAIN LTD.,
ARTILLERY HOUSE, ARTILLERY ROW, WESTMINSTER, S.W.1

Fig. 8.6. Shadow field amplitude of metal rectangles. kb= 2.41.

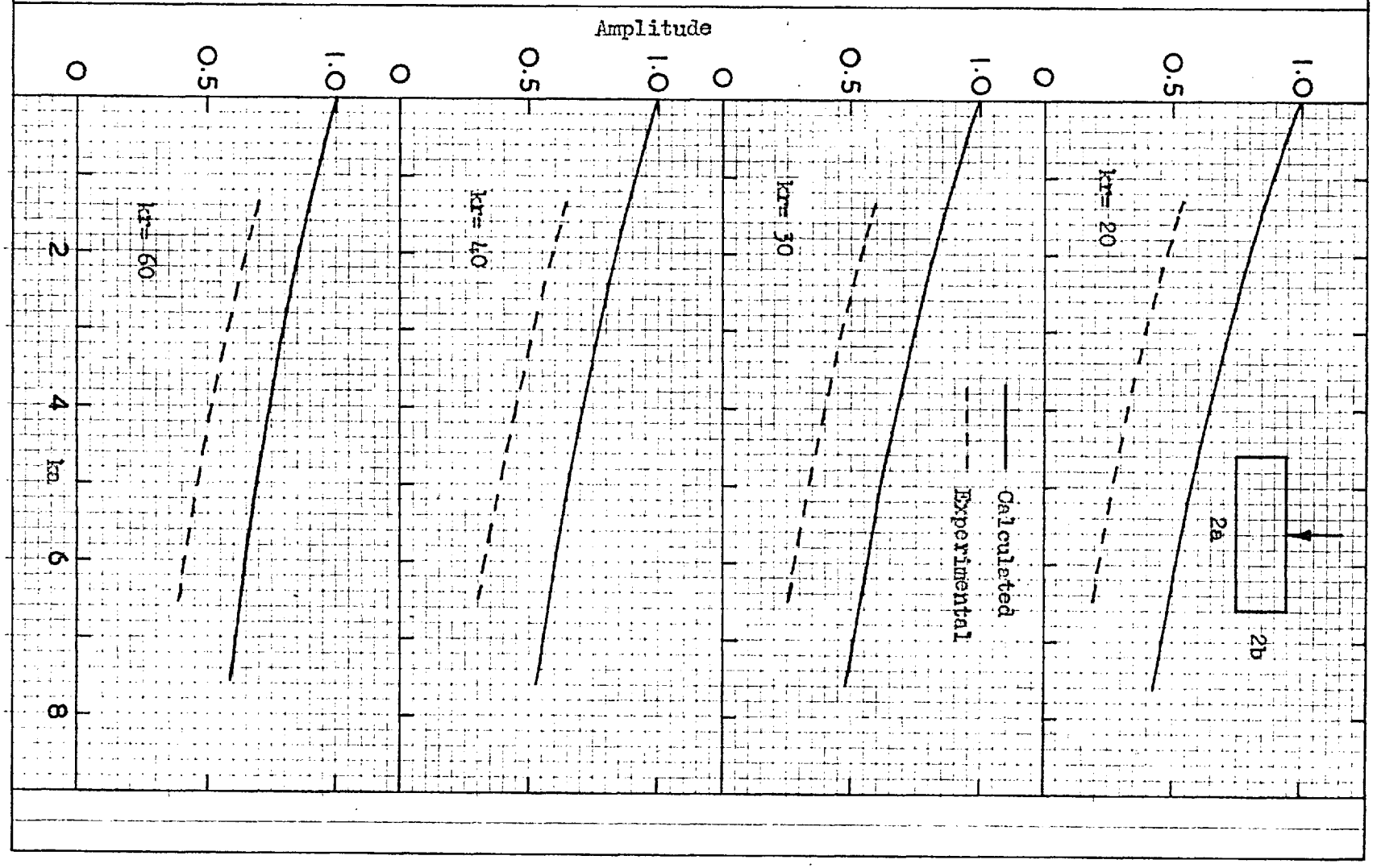

Data Sheet No. 2. 105 Divisions x 45 Divisions

Artillery House, Artillery Row, Westminster, S.W.1

Fig. 8.7. Shadow field phase of metal rectangles. kb= 2.41.

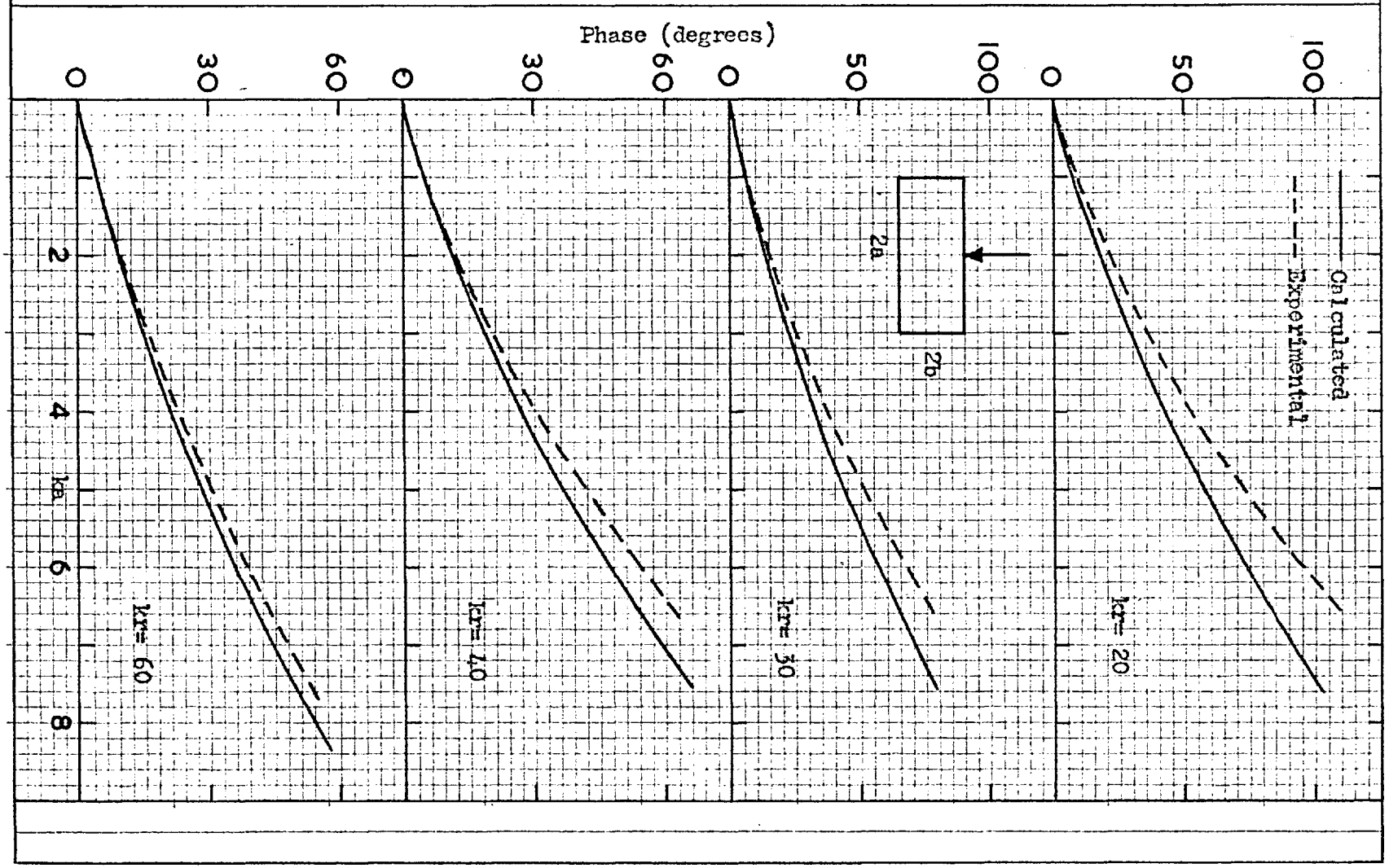

ension in the direction of incidence is shown by the absence of fluctuations. The results are again typical of metal obstacles.

For the latter orientation an attempt was made to obtain calculated results. A rigorous solution for this problem would undoubtedly be complex, but a rough approximation was made for the current distribution on the obstacle and used as a basis for the determination of the shadow field.

The approximation corresponds to that used by O'Neil and by Muller in studies of the acoustic pressure on and near metal obstacles. It involves replacing the obstacle by a current sheet in the plane occupied by the front face, with the current density the same as for an obstacle infinite in extent in the transverse direction. In the present case the induced current density is given by-

$$J = 2\, H_{tangential} = 2\, H_{inc} \qquad (8.1)$$

The scattered field resulting from this current distribution is determined with reference to Fig. 8.8-

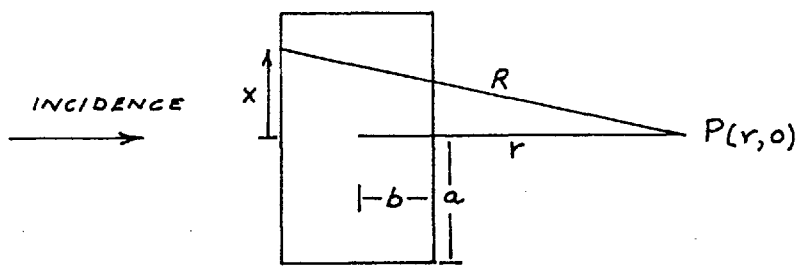

Fig. 8.8

Since the electric field, parallel to the obstacle axis and of amplitude unity, is given by-

$$E_{inc}(r,0) = \exp i k_1 r \quad ; \quad H_{inc}(r,0) = \frac{\kappa_1}{\omega\mu_1} \exp i k_1 r \qquad (8.2)$$

then, from (8.1), $$J = \frac{2\kappa_1}{\omega\mu_1} \exp i k_1 r \Big|_{r=-b} = \frac{2\kappa_1}{\omega\mu_1} \exp -i k_1 b \qquad (8.3)$$

The total scattered field then becomes(Stratton, p.595)-

$$E_{sc}(r,o) = -\frac{\kappa_1}{2}\int_{-a}^{a} H_o^{(1)}(\kappa_1 R)\, e^{-i\kappa_1 b}\, dx \qquad (8.4)$$

If now it is assumed that R is large enough for the use of the first term of the asymptotic expansion of the Hankel function to be valid, the integral can be put into a standard Fresnel form. As a result one obtains, omitting the details-

$$E_{sc}(r) = -\sqrt{2}\, \exp i(k_1 r - \pi/4)\, \left[C(t) + i\, S(t) \right] \qquad (8.5)$$

where

$$C(x) + i\, S(x) = \int_0^x e^{i\pi t^2/2}\, dt \qquad (8.6)$$

$$t = k_1 a \left(\frac{1}{\pi \kappa_1 (r+b)} \right)^{1/2} \qquad (8.7)$$

From (8.5) calculations were made for $k_1 b = 2.41$ and the results added to the incident field exp i $k_1 r$ to give the calculated curves of Figs. 8.6 and 8.7.

While the general form of the curves is in agreement with the experimental, the quantitative agreement is poor, particularly for the amplitude, although there is some improvement with increasing $k_1 r$.

In order to assess the effect of the ends of the obstacle on the experimental results, the measurements and calculations were repeated for another family of obstacles, with a different value of $k_1 b$.

Case B. The $k_1 b$ dimension was reduced to 1.20 and the resulting experimental and calculated fields plotted in Figs. 8.9- 8.11 for a family of 11 obstacles in the $k_1 a$ range 1.44-6.66.

DATA SHEET No. 2. 105 DIVISIONS × 45 DIVISIONS

WIGHTMAN MOUNTAIN LTD.,
ARTILLERY HOUSE, ARTILLERY ROW, WESTMINSTER, S.W.1

Fig. 8.9. Shadow field of metal rectangles. kb= 1.20.

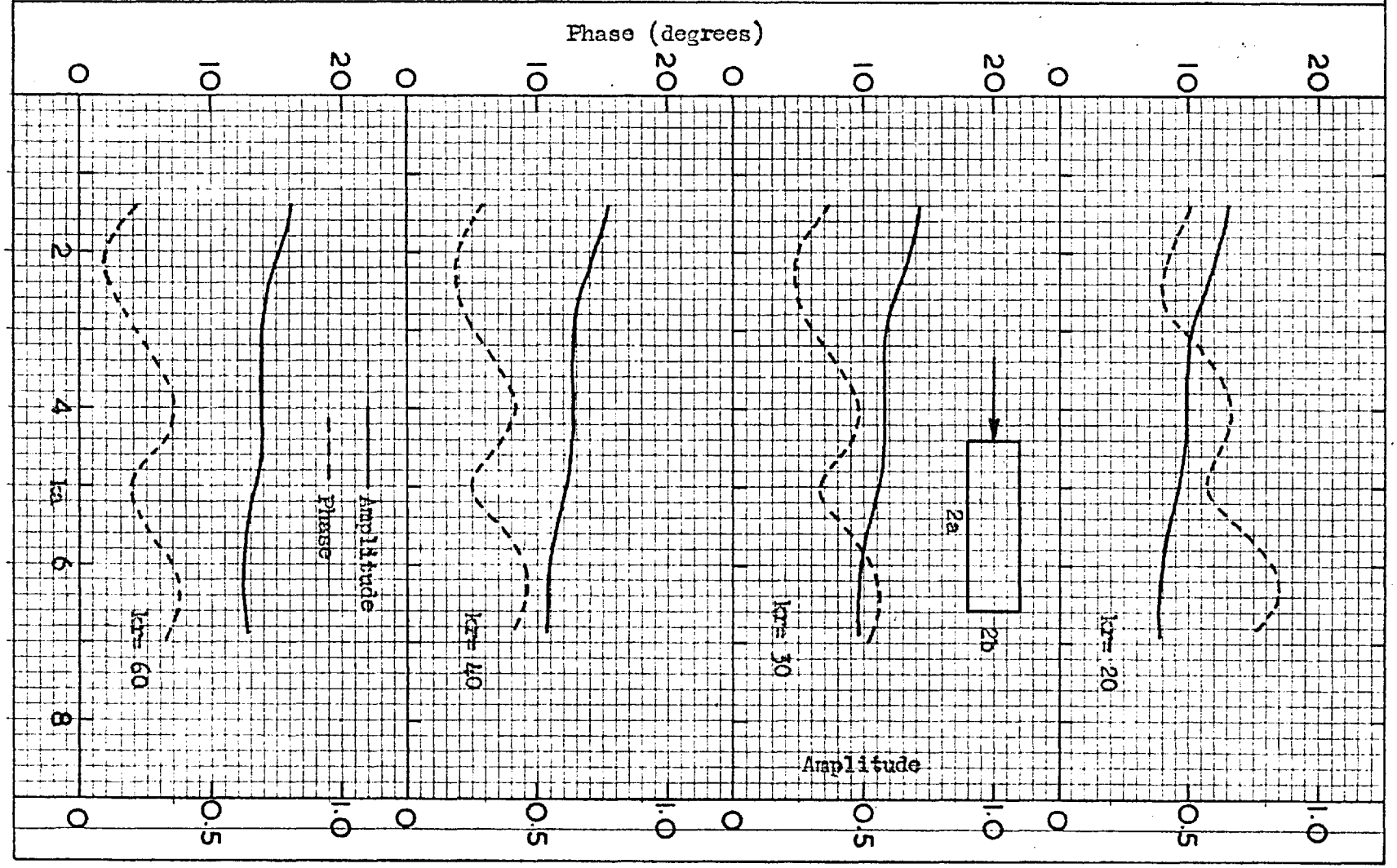

DATA SHEET NO. 2. 105 DIVISIONS × 45 DIVISIONS

WIGHTMAN MOUNTAIN LTD.,
ARTILLERY HOUSE, ARTILLERY ROW, WESTMINSTER, S.W.1

Fig. 8.10. Shadow field amplitude of metal rectangles. kb= 1.20.

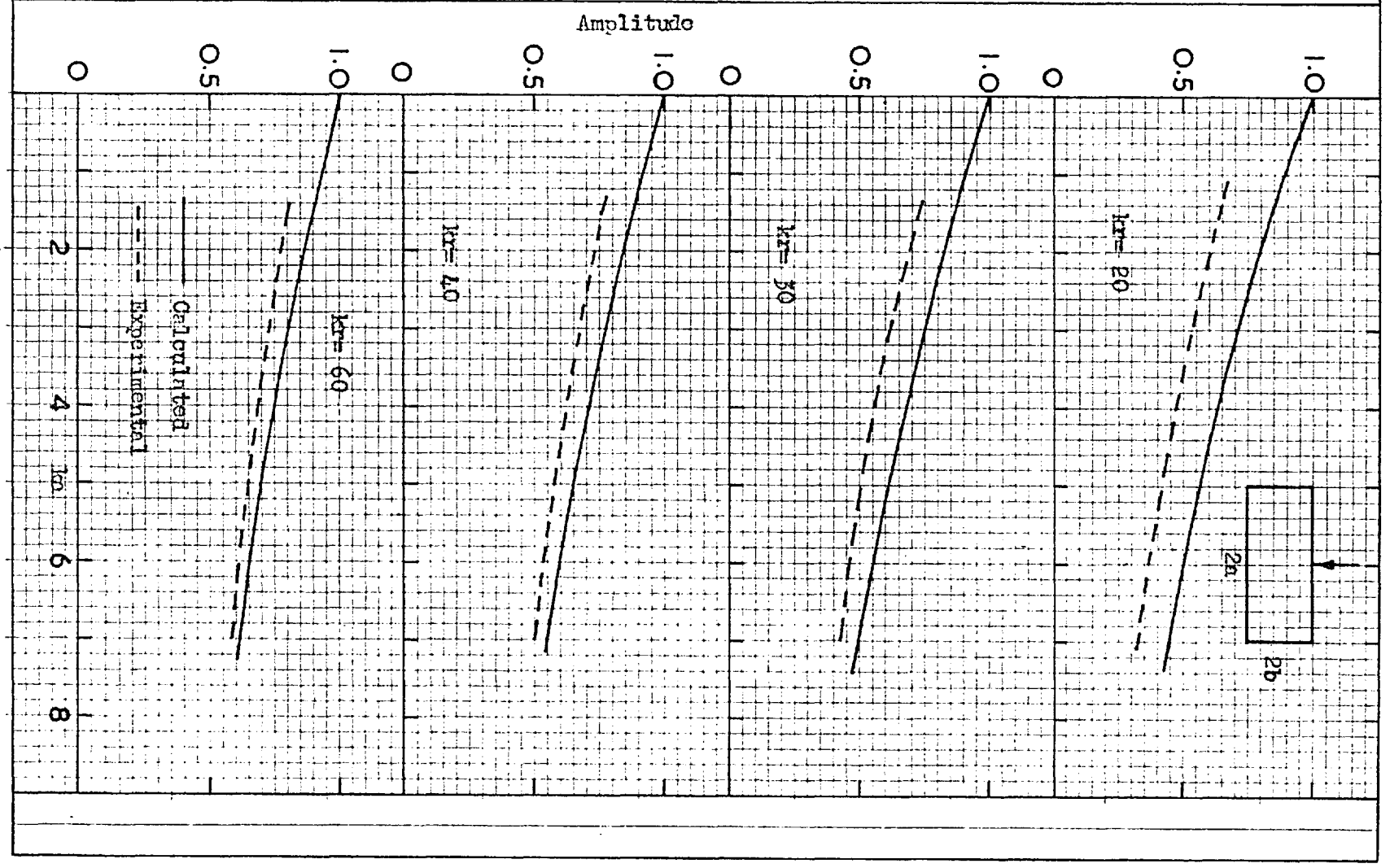

HIS A. . OON A N D.,
ARTILLERY HOUSE, ARTILLERY ROW, WESTMINSTER, S.W.1

Fig. 8.11. Shadow field phase of metal rectangles. kb= 1.20.

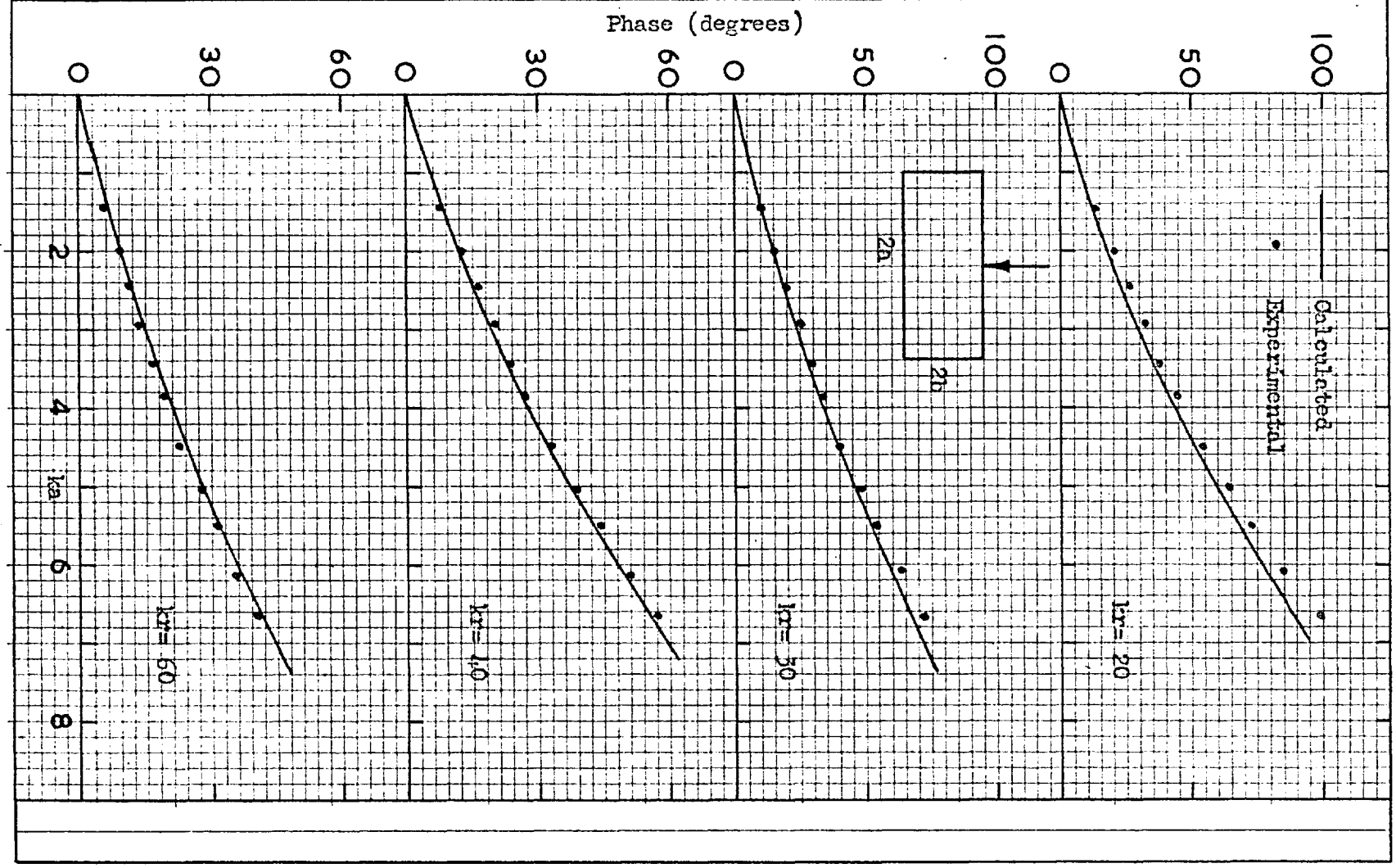

Fig. 8.9 shows the results when the dimension along the direction of incidence was varied. The back-front interaction is again apparent, with an additional cycle appearing in the curves, compared with those of Fig. 8.5. The polar curves again showed the cusps characteristic of a constant amplitude and an oscillating phase, for k_1a near 4 and 6.3. The phase results were getting a little less reliable here, because of the amplitude of the oscillations being of the order of the experimental error, but a repetition of the measurement on several of the obstacles showed no departure of the form of the curves from that shown.

Figs. 8.10 and 8.11 show the results for the other orientation. The agreement between measurement and calculation is seen to be much better. The difference in amplitude has decreased to about 7 percent at $k_1r = 60$, while for the phase the difference is well within experimental error by $k_1r = 40$ for the largest k_1a considered. The amplitude agreement is better for the larger values of k_1a, as might be anticipated from the nature of the current assumption, which corresponds to the Kirchhoff approximation.

The experience of this case has been, therefore, that the calculations based on the rough assumption used can serve as a basis for predicting the form of the shadow field of metal rectangles, provided the transverse dimension is of the order of a wavelength, the other dimension less than about 1/2 wavelength, and the minimum field distance of the order of 10 wavelengths.

There was obviously little use in making the calculations for the

other rectangle orientation, or for the metal squares.

8.5. Polystyrene rectangles.

These measurements were made on a family of 11 rectangles for $k_1 b = 2.37$ and in the $k_1 a$ range 1.52-6.44. The results are given in Figs. 8.12 and 8.13.

The results for a constant dimension in the direction of incidence are again fairly smooth, although less so than for the metal rectangles. One would expect the curves of both amplitude and phase to bend downward for the larger $k_1 a$ values, since, in the limit of very large $k_1 a$, the shadow field would approach the transmission coefficient for a polystyrene slab.

For the other orientation the trend of the curves is again similar to that for the circular cylinder and the square. From the detailed curves the critical combination of $k_1 a$ and $k_1 r$ appeared to be approximately 4.25 and 18 respectively. Thus, as for the polystyrene squares a higher value of effective permittivity is indicated than for the circular cylinder.

The subject of Fresnel zones has not been discussed previously as a possible factor in the results obtained since, for the largest transverse dimension considered, the field points were always in the first Fresnel zone.

Fig. 8.12. Shadow field of polystyrene rectangles of kb= 2.37.

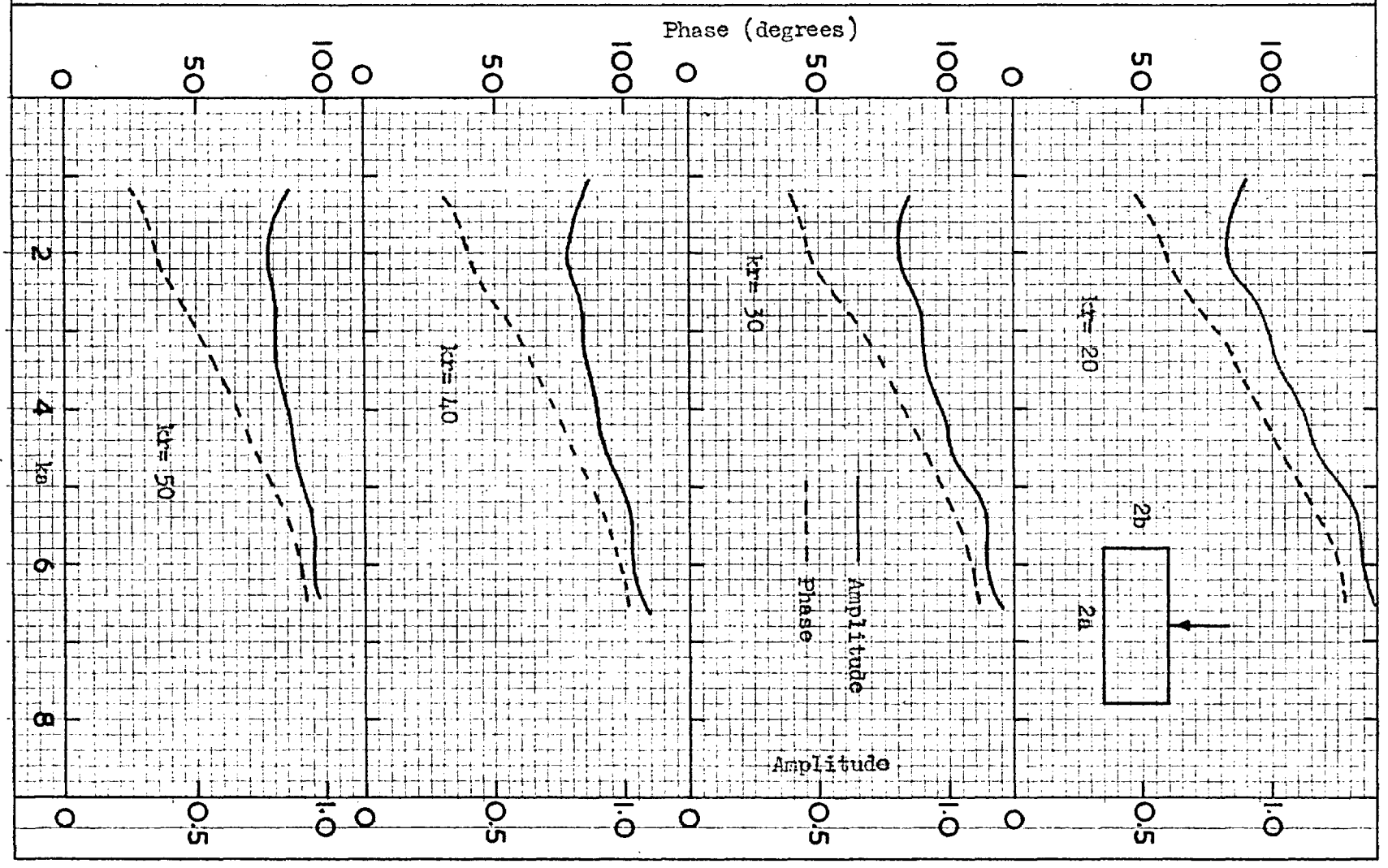

DATA SHEET NO. 2. 105 DIVISIONS × 45 DIVISIONS

ARTILLERY HOUSE, ARTILLERY ROW, WESTMINSTER, S.W.1

FIG. 8.13.

Shadow field of polystyrene rectangles of kb = 2.37.

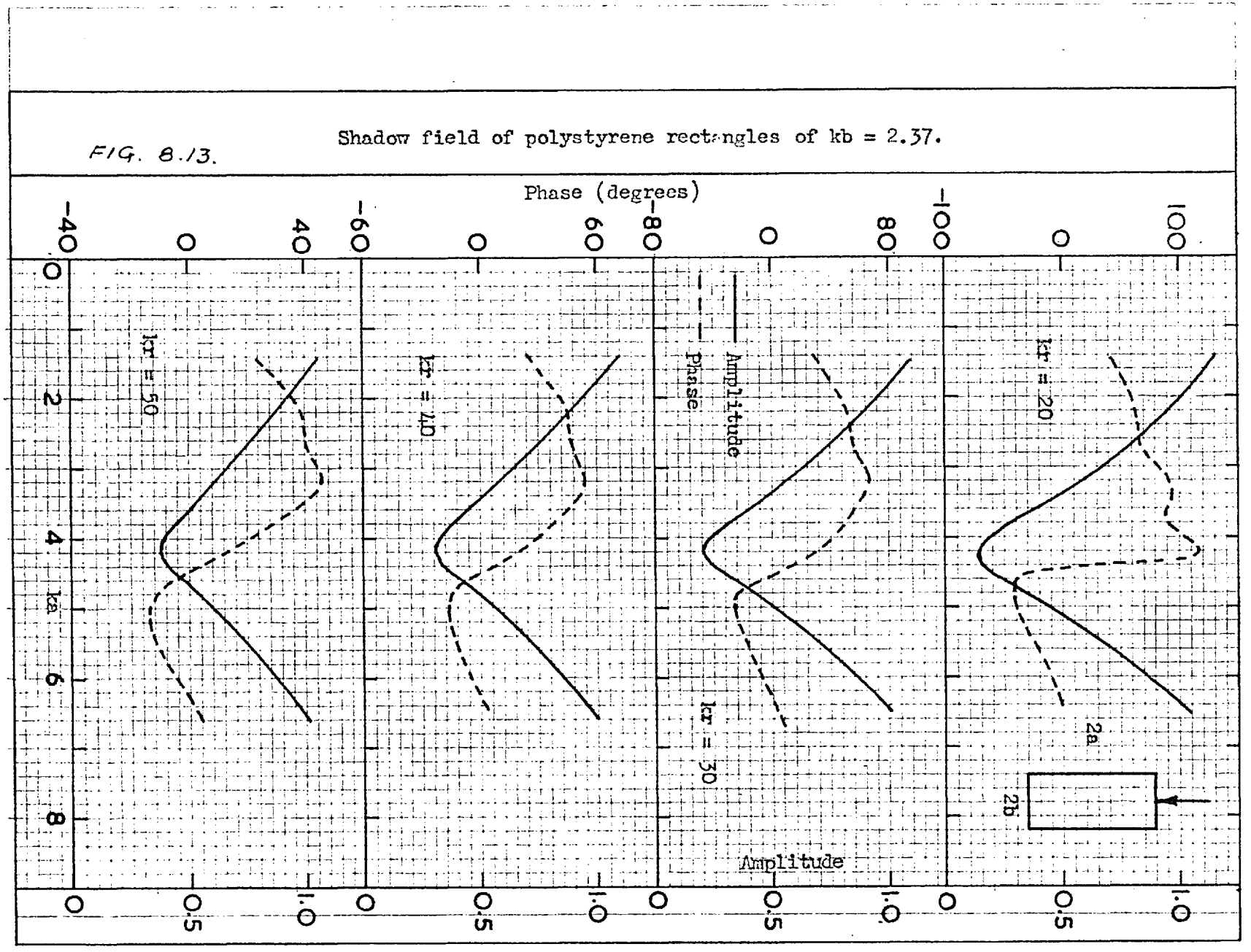

CONCLUSIONS.

A parallel-plate equipment has been described which has permitted measurements to be made, in the 3 cm. band, of the amplitude and phase of the near forward and back scattering by metal and dielectric cylinders of several cross-section forms and with lateral dimensions up to approximately two wavelengths. The accuracy achieved has been within 3 percent for amplitude and 3 degrees for phase.

The calculations and measurements on the dielectric, circular cylinders have shown them to be resonant structures, their scattering properties varying widely with the cylinder radius and material. This is in contrast with the scattering behaviour of metal obstacles, which is comparatively smooth. It has been found that the near fields are more complex than the far and that there may sometimes be very little similarity between their respective behaviours as a function of a parameter of the system. The main features of the near total shadow field, for the materials considered, have been the rapid rise in amplitude and phase on approaching the cylinder and the tendency for the amplitude to go to zero for some particular combination of cylinder radius and field distance. The scattering is shown to be predominantly forward. The effect of absorption on the results for lossy cylinders has been as might be anticipated from physical considerations.

The measurements on the cylinders of square cross-section have given results similar to those for the corresponding circular cylinder, as was also the case for the rectangles for the orientation for which the dimension in the direction of incidence was varied. For the other orientation

calculations based on a "Kirchhoff" type of approximation for the surface current density on the metal cylinder predicted the form of the shadow field, although the quantitative agreement was better, as might be expected, for the rectangles with the larger transverse dimensions and the smaller dimensions in the direction of incidence.

The main difficulty, in the case of the calculations, has been the necessity to use a larger number of terms of the series solution as the cylinder radius was increased. Montroll has given a closed-form solution in the case of the circular cylinder, but it applies only to materials of low index of refraction.

There is much scope for theoretical and experimental work on cylinders of dimensions comparable with the wavelength, with the parallel-plate equipment lending itself well to experimental work at microwaves, where structures are comparatively small and easy to form. No lossy structures of square or rectangular cross-section have yet been studied. Measurements and calculations on metal cylinders coated with dielectric might indicate the possibility of minimizing the shadow effect, as has been shown by the present measurements on coaxial cylinders. No measurements have been reported on arrays of dielectric cylinders of any cross-section, and the only ones for metal cylinders have been the recent ones by Row(1953) for two metal circular cylinders. The properties of cylinders periodic in the axial direction have not been investigated.

APPENDIX I.

TABLE OF VALUES OF THE FUNCTION-

$$C_n = J_n(k_2a)J_{n+1}(k_1a) - 1.6\, J_{n+1}(k_2a)J_n(k_1a)$$

$k_1 a$	n=0	n=1	n=2	n=3	n=4
0.00	0	0	0	0	0
0.50	-0.34880	-0.01810	-0.00031		
1.00	-0.49734	-0.11545	-0.00830	-0.00029	
1.50	-0.42460	-0.26401	-0.04730	-0.00394	-0.00019
1.75	-0.34926	-0.32297	-0.08440	-0.00998	-0.00067
2.00	-0.27828	-0.35398	-0.13132	-0.02129	-0.00194
2.25	-0.22748	-0.35164	-0.18210	-0.03962	-0.00473
2.50	-0.20253	-0.31907	-0.22814	-0.06569	-0.01011
2.75	-0.19905	-0.26656	-0.26030	-0.09854	-0.01929
3.00	-0.20572	-0.20806	-0.27150	-0.13472	-0.03333
3.25	-0.20932,	-0.15675	-0.25898	-0.16930	-0.05266
3.50	-0.19963	-0.12115	-0.22524	-0.19596	-0.07669
3.75	-0.17269	-0.10305	-0.17748	-0.20892	-0.10338
4.00	-0.13149	-0.09785	-0.12564	-0.20438	-0.12936
4.25	-0.08412	-0.09703	-0.07946	-0.18184	-0.15027
4.50	-0.04032	-0.09167	-0.04576	-0.14453	-0.16163
4.75	-0.00777	-0.07580	-0.02667	-0.09876	-0.15997
5.00	0.01045	-0.04829	-0.01953	-0.05240	-0.14480
5.25	0.01647	-0.01296	-0.01823	-0.01284	-0.11430
5.50	0.01628	0.02324	-0.01568	0.01498	-0.07532
5.75	0.01705	0.05305	-0.00639	0.02976	-0.03269
6.00	0.02419	0.07149	0.01164	0.03391	0.00713
6.25	0.03946	0.07759	0.03647	0.03251	0.03860
6.50	0.06052	0.07433	0.06308	0.03141	0.05848
6.75	0.08216	0.06727	0.08546	0.03526	0.06651

k_1a	n=0	n=1	n=2	n=3	n=4
7.00	0.09849	0.06216	0.09877	0.04595	0.06539
7.25	0.10533	0.06284	0.10105	0.06217	0.05973
7.50	0.10167	0.06983	0.09381	0.08000	0.05453
7.75	0.08994	0.08042	0.08124	0.09446	0.05363
8.00	0.07488	0.08997	0.06850	0.10132	0.05849
8.25	0.06155	0.09386	0.05987	0.09863	0.06790
8.50	0.05343	0.08936	0.05713	0.08729	0.07849
8.75	0.05125	0.07661	0.05919	0.07070	0.08608
9.00	0.05286	0.05851	0.06271	0.05344	0.08710
9.25	0.05439	0.03952	0.06350	0.03959	0.07992
9.50	0.05190	0.02388	0.05837	0.03138	0.06539
9.75	0.04303	0.01409	0.04627	0.02853	0.04647
10.00	0.02797	0.01007	0.02873	0.02856	0.02724

k_1a	n=5	n=6	n=7	n=8	n=9
2.00	-0.00011				
2.25	-0.00036				
2.50	-0.00097	-0.00006			
2.75	-0.00233	-0.00019			
3.00	-0.00498	-0.00050			
3.25	-0.00964	-0.00117	-0.00010		
3.50	-0.01714	-0.00250	-0.00026		
3.75	-0.02814	-0.00491	-0.00060		
4.00	-0.04292	-0.00892	-0.00129	-0.00013	

k_1a	n=5	n=6	n=7	n=8	n=9	n=10
4.25	-0.06103	-0.01507	-0.00254	-0.00030		
4.50	-0.08106	-0.02383	-0.00469	-0.00067		
4.75	-0.10067m	-0.03533	-0.00811	-0.00133	-0.00016	
5.00	-0.11670	-0.04920	-0.01318	-0.00249	-0.00035	
5.25	-0.12574	-0.06444	-0.02021	-0.00437	-0.00070	
5.50	-0.12485	-0.07930	-0.02925	-0.00728	-0.00133	-0.00018
5.75	-0.11236	-0.09143	-0.04001	-0.01148	-0.00237	-0.00038
6.00	-0.08849	-0.09822	-0.05169	-0.01715	-0.00403	-0.00071
6.25	-0.05554	-0.09727	-0.06296	-0.02431	-0.00650	-0.00129
6.50	-0.01775	-0.08702	-0.07205	-0.03271	-0.00996	-0.00223
6.75	0.01964	-0.06723	-0.07691	-0.04169	-0.01456	-0.00366
7.00	0.05143	-0.03934	-0.07562	-0.05025	-0.02026	-0.00574
7.25	0.07363	-0.00639	-0.06682	-0.05698	-0.02584	-0.00861
7.50	0.08452	0.02746	-0.05012	-0.06028	-0.03377	-0.01234
7.75	0.08492	0.05762	-0.02641	-0.05863	-0.04024	-0.01690
8.00	0.07788	0.08013	0.00211	-0.05086	-0.04513	-0.02205
8.25	0.06775	0.09252	0.03210	-0.03656	-0.04722	-0.02740
8.50	0.05883	0.09436	0.05970	-0.01629	-0.04525	-0.03226
8.75	0.05419	0.08737	0.08122	0.00828	-0.03828	-0.03578
9.00	0.05474	0.07492	0.09394	0.03451	-0.02592	-0.03693
9.25	0.05913	0.06106	0.09671	0.05916	-0.00854	-0.03473
9.50	0.06431	0.04949	0.09026	0.07894	0.01257	-0.02843
9.75	0.06666	0.04247	0.07700	0.09118	0.03531	-0.01767
10.00	0.06327	0.04035	0.06044	0.09434	0.05697	-0.00274

$k_1 a$	n=11	n=12	n=13	n=14	n=15	n=16
6.25	-0.00020					
6.50	-0.00039					
6.75	-0.00071					
7.00	-0.00123	-0.00021				
7.25	-0.00205	-0.00040				
7.50	-0.00330	-0.00069				
7.75	-0.00506	-0.00115	-0.00022			
8.00	-0.00743	-0.00189	-0.00038			
8.25	-0.01046	-0.00295	-0.00065			
8.50	-0.01408	-0.00443	-0.00108	-0.00021		
8.75	-0.01814	-0.00640	-0.00171	-0.00037		
9.00	-0.02225	-0.00885	-0.00262	-0.00062		
9.25	-0.02588	-0.01175	-0.00387	-0.00100	-0.00020	
9.50	-0.02833	-0.01493	-0.00549	-0.00155	-0.00035	
9.75	-0.02878	-0.01808	-0.00748	-0.00232	-0.00057	
10.00	-0.02646	-0.02075	-0.00980	-0.00336	-0.00090	-0.00020

APPENDIX II.

TABLE OF VALUES OF THE FUNCTION-

$$D_n = J_n(k_2a)Y_{n+1}(k_1a) - 1.6\, J_{n+1}(k_2a)Y_n(k_1a)$$

$k_1 a$	n=0	n=1	n=2	n=3	n=4
0.00					
0.50	-0.98296	-1.82848	-3.09971		
1.00	-0.43624	-0.61952	-1.30443	-2.27363	
1.50	-0.31934	-0.20060	-0.59816	-1.24511	-2.20045
1.75	-0.25816	-0.11553	-0.37410	-0.92007	-1.71731
2.00	-0.17914	-0.07855	-0.20642	-0.66070	-1.33810
2.25	-0.09009	-0.06669	-0.08784	-0.44902	-1.03005
2.50	-0.00532	-0.05983	-0.01283	-0.27644	-0.77389
2.75	0.06137	-0.04374	0.02599	-0.13942	-0.55812
3.00	0.10192	-0.01240	0.03893	-0.03661	-0.37609
3.25	0.11642	0.03193	0.03822	0.03335	-0.22447
3.50	0.11217	0.08090	0.03577	0.07350	-0.10185
3.75	0.10039	0.12382	0.04056	0.08934	-0.00782
4.00	0.09190	0.15183	0.05666	0.08867	0.05824
4.25	0.09342	0.16086	0.08269	0.08042	0.09809
4.50	0.10575	0.15269	0.11282	0.07297	0.11528
4.75	0.12423	0.13387	0.13920	0.07227	0.11529
5.00	0.14121	0.11300	0.15473	0.08060	0.10491
5.25	0.14933	0.09749	0.15554	0.09625	0.09131
5.50	0.14436	0.09113	0.14215	0.11442	0.08058
5.75	0.12672	0.09309	0.11904	0.12892	0.07656
6.00	0.10090	0.09873	0.09298	0.13429	0.08007
6.25	0.07368	0.10182	0.07053	0.12764	0.08892
6.50	0.05133	0.09712	0.05589	0.10953	0.09879
6.75	0.03743	0.08238	0.04966	0.08372	0.10465

k_1a	n=0	n=1	n=2	n=3	n=4
7.00	0.03179	0.05912	0.04897	0.05705	0.10238
7.25	0.03088	0.03189	0.04894	0.03157	0.09014
7.50	0.02958	0.00644	0.04464	0.01467	0.06894
7.75	0.02334	-0.01249	0.03308	0.00605	0.04233
8.00	0.01002	-0.02281	0.01432	0.00361	0.01524
8.25	-0.00932	-0.02568	-0.00872	0.00333	-0.00756
8.50	-0.03099	-0.02473	-0.03134	0.00082	-0.02289
8.75	-0.05019	-0.02448	-0.04896	-0.00695	-0.03010
9.00	-0.06288	-0.02848	-0.05870	-0.02054	-0.03104
9.25	-0.06735	-0.03788	-0.06041	-0.03795	-0.02932
9.50	-0.06463	-0.05118	-0.05647	-0.05540	-0.02883
9.75	-0.05801	-0.06480	-0.05080	-0.06877	-0.03239
10.00	-0.05160	-0.07472	-0.04721	-0.07514	-0.04077

k_1a	n=5	n=6	n=7	n=8	n=9
2.00	-2.38378				
2.25	-1.91774				
2.50	-1.53358	-2.74699			
2.75	-1.21112	-2.25068			
3.00	-0.93745	-1.83007			
3.25	-0.70354	-1.47067	-2.72995		
3.50	-0.50361	-1.16185	-2.24548		
3.75	-0.33387	-0.89601	-1.82724		
4.00	-0.19216	-0.66746	-1.46499	-2.81225	
4.25	-0.07740	-0.47200	-1.15160	-2.30983	

k_1a	n=5	n=6	n=7	n=8	n=9	n=10
4.50	0.01095	-0.30674	-0.88143	-1.87234		
4.75	0.07364	-0.16966	-0.64971	-1.49278	-2.95933	
5.00	0.11218	-0.05945	-0.45283	-1.16471	-2.41943	
5.25	0.12934	0.02506	-0.28781	-0.88296	-1.94985	
5.50	0.12939	0.08461	-0.15236	-0.64299	-1.54319	-3.15542
5.75	0.11778	0.12124	-0.04472	-0.44084	-1.19353	-2.56436
6.00	0.10062	0.13740	0.03674	-0.27336	-0.89502	-2.05203
6.25	0.08362	0.13675	0.09364	-0.13766	-0.64308	-1.61068
6.50	0.07114	0.12398	0.12801	-0.03136	-0.43307	-1.23355
6.75	0.06536	0.10438	0.14250	0.04782	-0.26123	-0.91429
7.00	0.06592	0.08320	0.14056	0.10213	-0.12399	-0.64739
7.25	0.07022	0.06485	0.12641	0.13401	-0.01818	-0.42747
7.50	0.07431	0.05219	0.10483	0.14635	0.05917	-0.24987
7.75	0.07407	0.04602	0.08064	0.14263	0.11092	-0.11014
8.00	0.06656	0.04510	0.05813	0.12684	0.14010	-0.00433
8.25	0.05090	0.04656	0.04043	0.10343	0.14992	0.07138
8.50	0.02863	0.04683	0.02906	0.07687	0.14403	0.12059
8.75	0.00320	0.04264	0.02373	0.05130	0.12632	0.14686
9.00	-0.02098	0.03206	0.02252	0.02994	0.10108	0.15384
9.25	-0.03994	0.01510	0.02250	0.01467	0.07253	0.14539
9.50	-0.05123	-0.00631	0.02054	0.00585	0.04455	0.12551
9.75	-0.05468	-0.02874	0.01421	0.00231	0.02057	0.09836
10.00	-0.05223	-0.04836	0.00246	0.00173	0.00243	0.06803

k_1a	n=11	n=12	n=13	n=14	n=15
6.25	-3.39305				
6.50	-2.73872				
6.75	-2.17452				
7.00	-1.69156	-3.66923			
7.25	-1.28201	-2.94000			
7.50	-0.93842	-2.31492			
7.75	-0.65407	-1.78382			
8.00	-0.42254	-1.33701	-3.16624		
8.25	-0.23806	-0.96573	-2.47149		
8.50	-0.09526	-0.66162	-1.88560		
8.75	0.01089	-0.41708	-1.39695	-3.41671	
9.00	0.08506	-0.22493	-0.99470	-2.64282	
9.25	0.13155	-0.07857	-0.66885	-1.99553	
9.50	0.15465	0.02807	-0.40997	-1.46030	-3.69026
9.75	0.15846	0.10057	-0.20945	-1.02395	-2.82786
10.00	0.14713	0.14416	-0.05931	-0.67442	-2.11214

APPENDIX III.

THE CROSS-SECTION THEOREM.

The relation between the total cross-section of a dielectric cylinder- absorption plus scattering - and the amplitude scattered forward will now be derived. It has been discussed by (a) Levine and Schwinger, (b) Lax, (c) Twersky and others.

The net power flow across the surface of a unit length of cylinder is given by-

$$-P_L \frac{2\omega\mu_1}{a} = Re\ i\int_0^{2\pi} E \frac{\partial}{\partial r} E^* d\phi \qquad (A3\text{-}1)$$

where P_L is the power loss per unit length of cylinder and the remainder of the notation is as before.

By use of the relations-

$$\text{(a)}\ E = E_{inc} + E_{sc}$$

$$\text{(b)}\ Re\ i\int_0^{2\pi} E_{INC} \frac{\partial}{\partial r} E_{INC}^* d\phi = 0 \qquad (A3\text{-}2)$$

$$\text{(c)}\ Re\ i\int_0^{2\pi} E_{SC} \frac{\partial}{\partial r} E_{SC}^* d\phi = \frac{2\omega\mu_1}{a} P_{SC}$$

where P_{sc} is the scattered power per unit length of cylinder, one obtains-

$$\frac{2\omega\mu_1}{a}(P_L + P_{SC}) = Im\left[\int_0^{2\pi} \left(E_{INC} \frac{\partial}{\partial r} E_{SC}^* + E_{SC} \frac{\partial}{\partial r} E_{INC}^*\right) d\phi\right] \qquad (A3\text{-}3)$$

If the far-scattered field is considered, the integral in (4.18) can be written as-

$$E_{sc}(r,\phi) = \frac{i}{4}\left(\frac{2}{\pi k_1 r}\right)^{1/2} e^{i(k_1 r - \pi/4)} \quad A(r,\phi) \tag{A3-4}$$

where $$A(r,\phi) = k_1^2(\varepsilon_r - 1)\int_S E(r')\, e^{-ik_1 r' \cos\phi'}\, ds'$$

$$= k_1^2(\varepsilon_r - 1)\int_S E(r')\, E_{INC}^{*}(r')\, ds' \tag{A3-5}$$

By a transformation given by Schwinger this can be changed to-

$$A(r,0) = -a\int_0^{2\pi}\left(E_{INC}^{*}(r')\frac{\partial}{\partial r'}E(r') - E(r')\frac{\partial}{\partial r'}E_{INC}^{*}(r')\right)d\phi' \tag{A3-6}$$

Again by use of (A3-2) (a) and (b) and, in addition,

$$Im\ E_{INC}^{*}\frac{\partial}{\partial r}E_{sc} = -\ Im\ E_{INC}\frac{\partial}{\partial r}E_{sc}^{*} \tag{A3-7}$$

there results-

$$Im\ A(r,0) = a\,Im\int_0^{2\pi}\left(E_{INC}\frac{\partial}{\partial r}E_{sc}^{*} + E_{sc}\frac{\partial}{\partial r}E_{INC}^{*}\right)d\phi \tag{A3-8}$$

Thus, from (A3-3)- $$2\omega\mu_1\,(P_L + P_{sc}) = Im\ A(r,0) \tag{A3-9}$$

and since the incident power density is given by $S_{INC} = \frac{k_1}{2\omega\mu_1}$, one obtains $$\sigma = \frac{1}{k_1} Im\ A(r,0) = -\frac{4}{k_1} Re \sum_0^{\infty} \varepsilon_n B_n \tag{A3-10}$$

from (4.17) and the definition of the cross-section. Or, more conveniently-

$$\frac{\sigma}{2a} = -\frac{2}{k_1 a}\, Re \sum_0^{\infty} \varepsilon_n B_n \tag{A3-11}$$

If the cylinder is lossless, (A3-11) represents the scattering cross-section alone.

BIBLIOGRAPHY

General References.

1. BARLOW, H.M. and CULLEN, A.L. — Microwave Measurements. Constable. 1950.
2. MARCUVITZ, N. — Waveguide Handbook. Radiation Laboratory Series, Vol. 10. McGraw-Hill.
3. MCLACHLAN, N.W. — Bessel Functions for Engineers. Oxford. 1941.
4. MONTGOMERY, C.G. — Technique of Microwave Measurements. Radiation Laboratory Series, Vol. 11. McGraw-Hill. 1947.
5. MOULLIN, E.B. — Radio Aerials. Oxford. 1949.
6. STRATTON, J.A. — Electromagnetic Theory. McGraw-Hill. 1941.

References.

1. BEZUSZKA, S.J. — Scattering of underwater plane ultrasonic waves by liquid cylindrical obstacles. J. Acoust. Soc. Amer., 25, 1090, 1953.
2. BREWITT-TAYLOR, E.G. — An improved form of cruciform directional coupler. RRDE Tech Note No. 83, 1952.
3. CARTER, P.S. — Antenna Arrays around cylinders. Proc. I.R.E., 31, 671, 1943.
4. EL-KHARADLY, M.Z. — An investigation of certain types of artificial dielectrics. Ph.D. Thesis, Univ. of London. 1953.
5. FARAN, J.J. — (a) Sound scattering by solid cylinders and spheres. J. Acoust. Soc. Amer., 23, 405, 1951.

(b) Scattering of cylindrical waves by a cylinder. J. Acoust. Soc. Amer., 25, 155, 1953.

6. FRANZ, W. and DEPPERMANN, K. Theory of diffraction at a cylinder, with consideration of the surface wave. Ann. d Phys., 10, 361, 1952.

7. GOLDBERG, B. New computations of the Mie scattering functions for spherical particles. J. Opt. Soc. Amer., 43, 1221, 1953.

8. HAMREN, S.D. Scattering from spheres. Univ. of Calif. Ant. Lab. Rprt. No. 171, June 15, 1950.

9. HAND, B.P. A wide-band rotary attenuator. Electronics, 27, 184, 1954.

10. IGNATOWSKI, W. Reflection of electric waves at a wire. Ann. d Phys., 18, 495, 1905.

11. JONES, D.S. Diffraction by a thick, semi-infinite plate. Proc. Roy. Soc. A, 217, 153, 1953.

12. KELLER, H.B. and KELLER, J.B. Reflection and transmission of EM waves by a spherical shell. J. Appl. Phys., 20, 393, 1949.

13. KOBAYASHI-IWAO Diffraction of electric waves at a dielectric cylinder. Ann d Phys., 43, 861, 1914.

14. KODIS, R. An experimental investigation of microwave diffraction. Cruft Lab. Rprt. No. 105, June 10, 1950. Also J. Appl. Phys., 23, 249, 1952.

15. LAX, M. On a well-known cross-section theorem. Phys. Rev., 78, 306, 1950.

16. LAX, M. and FESHBACH, H. Absorption and scattering for impedance boundary conditions on spheres and circular cylinders. J. Acoust. Soc. Amer., 20, 108, 1948.

17. LEVINE, H. and SCHWINGER, J. Diffraction by an aperture in an infinite plane screen. Phys. Rev., 74, 958, 1948; 75, 1423, 1949.

18. MILES, J. On radiation and scattering from a small cylinder. J. Acoust. Soc. Amer., 25, 1087, 1953.

19. MONTROLL, E.W. and HART, R.W. Scattering of plane waves by soft obstacles. J. Appl. Phys., 22, 1278, 1951.

20. MORSE, P.M. et al Scattering and radiation from circular cylinders and spheres. U.S. Navy Office of Research and Inventions, Washington, D.C. 1946.

21. MULLER, G.G. et al Diffraction by cylindrical and cubical obstacles and by circular and square plates. J. Acoust. Soc. Amer., 10, 6, 1938.

22. O'NEIL, H.T. and SIVIAN, L.J. Sound diffraction by various shaped screens. J. Acoust. Soc. Amer., 3, 483, 1932.

23. PAGE, L. The magnetic antenna. Phys. Rev., 69, 648, 1946.

24. PAPAS, C.H. Diffraction by a cylindrical obstacle. J. Appl. Phys., 21, 318, 1950.

25. RAYLEIGH, Lord (a) On the EM theory of light. Phil Mag., 12, 81, 1881. Also Sc. Papers, Vol. 1, p. 533.
(b) On the dispersal of light by a dielectric cylinder. Phil. Mag., 36, 365, 1918. Also Sc. Papers, Vol. 6, p.554.

26. RICE, S.O. Reflection of EM waves from slightly-rough surfaces.

Comm. Pure and Appl. Maths., 4, 351, 1951.

27. ROW, R.V. (a) Microwave diffraction measurements in a parallel-plate region. Cruft. Lab. Rprt. No.153, May 5, 1952. Also J. Appl. Phys., 24, 1448, 1953. (b) EM scattering from two parallel, conducting, circular cylinders. Cruft. Lab. Rprt. No. 170, May 1, 1953.

28. SCHAEFER, C.L. and GROSSMAN, F. Diffraction of EM waves by a dielectric cylinder. Ann. d Phys., 31, 455, 1910.

29. SCHWINGER, J. Notes on waveguide discontinuities. Ed. D. Saxon.

30. SEITZ, W. Infinite metal cylinder and Hertzian waves. Ann. d Phys., 16, 746, 1905; 19, 554, 1906.

31. SINCLAIR, G. Patterns of antennas located near elliptic cylinders. Proc. I.R.E., 39, 660, 1951.

32. SOUTHWORTH, G.C. Princ. and Applic. of Waveguide Transmission. Van Nostrand, 1950, p.374.

33. STERNS, W.G. Near-zone field studies of quasi-optical antennas. Univ. of Calif. Ant. Lab. Rprt. No. 153, June 15, 1949.

34. TAMARKIN, P. Scattering of an underwater ultrasonic beam by liquid, cylindrical obstacles. J. Acoust. Soc. Amer., 21, 612, 1949. Also 20, 858, 1948.

35. THILO, G. The radiation pressure at a circular cylinder of any material. Ann. d Phys., 62, 531, 1920.

36. THOMSON, J.J. Recent Researches in Electricity and Magnetism. Oxford. P. 428.

37. TWERSKY, V. Certain transmission and reflection theorems. J. Appl. Phys., 25, 859, 1954.

38. UNDERHILL, E.J.W. The effect of classical-shaped obstacles on the propagation of 3 cm. waves. Admir. Sig. and Rad. Estab. Tech Note No. R2/50/5, Aug. 31, 1950.

39. VAN de HULST, H.C. (a) Optics of spherical particles. Recherches Astronomiques de l'Observatoire d'Utrecht, Vol. XI, Part 1, 1946.

(b) The solid particles of inter-stellar space. Vol. XI, Part 2, 1949.

40. WILES S.T. and McLAY, A.B. Diffraction of 3.2 cm. waves by cylindrical objects. Canad. J. Phys., 32, 372, 1954.

41. ZAVISKA, F. Diffraction of electric waves at parallel cylinders. Ann. d Phys., 40, 1023, 1913.

TABLES.

1. Tables of $J_0(x)$ and $J_1(x)$ for $x = 0(0.001)16(0.01)25$ and auxiliary functions for high values of x.

Tables of $Y_0(x)$ and $Y_1(x)$ for $x = 0(0.01)25$.

British Assoc. Maths Tables, Vol. 6, Camb. Univ. Press, 1937.

2. Tables of $J_n(x)$ for $x = 0(0.1 \text{ or } 0.01)10(0.1)25$, $n = 2(1)20$, and for $x = 0(0.1)25$, $n = 0(1)20$.

Tables of $Y_n(x)$ or $y_n(x) = x^n Y_n(x)$ for $x = 0(0.1 \text{ or } 0.01)10(0.1)25$,

$n = 2(1)20$.

Tables of $Y_n(x)$ for $x = 0.1(0.1)25$, $n = 0(1)20$.

British Assoc. Maths. Tables, Vol. 10, 1952.

3. Extensive tables of $J_n(x)$ at small intervals. Computation Lab., Harvard University.

4. Tables of Sines and Cosines. Appl. Maths. Ser. 5, U.S. Nat. Bur. of Standards, Washington, D.C., May 1949.

5. Tables of Fresnel Integrals $C(x)$ and $S(x)$ for $x = 0(0.01)3$. Scientific Computing Service, London.